Universität Hamburg
DER FORSCHUNG | DER LEHRE | DER BILDUNG

Exploring the DREAM

Characterisation of the *Arabidopsis thaliana* DREAM Complex

Dissertation with the aim of achieving a doctoral degree at the faculty of Mathematics, Informatics and Natural Sciences

Department of Biology

University of Hamburg

submitted by

Lucas Lang

2023

Supervisor: **Prof. Dr. Arp Schnittger**

First Examiner: **Prof. Dr. Arp Schnittger**
Second Examiner: **Prof. Dr. Stefan Hoth**

Date of disputation: **01/03/2024**

“No me despiertes si duermo,
y si es verdad, no me duermas.
Mas sea verdad o sueño,
obrar bien es lo que importa
si fuere verdad, por serlo;
si no, por ganar amigos
para cuando despertemos.”

—— Segismundo, La vida es sueño,
de Pedro Calderón de la Barca

“Don’t awaken me if I’m asleep,
and, if this is reality, don’t put me to sleep.
But, whether it’s reality or a dream,
to do good is what matters;
if it should be reality, just because it is *good;*
if not, for the sake of winning friends
for the time when we awaken.”

—— Segismundo, Life is a Dream,
by Pedro Calderón de la Barca, edited and translated by Stanley Appelbaum

Table of contents

Acknowledgements

I want to express my sincere gratitude to Prof. Dr. Arp Schnittger for being my supervisor on this journey, for making things possible, for supporting my research both scientifically and financially, and for believing in a project that barely touched meiosis. *For all life is a DREAM*. Thank you, Arp.

I want to thank Prof. Dr. Stefan Hoth for agreeing to be my second examiner, and I hope you will enjoy the read. Thank you as well for the occasional healthy rivalry, be it at the kicker table or the table tennis table, that I much enjoyed.

A special mention goes to Franzi, Mariana, Stephan, and Susanne for critically reading and commenting on significant parts of this thesis. Your input was much appreciated, and I feel very grateful for your help.

Further, at a point in the middle of my thesis, I was able to welcome another lab member as a fellow DREAMer. Sharing and dividing your project is never easy, especially once your heart is already deep inside of it. I want to profoundly thank Hasibe for making this process not only easy but even enjoyable. *For even in DREAMs a good deed is not lost*.

Next, I want to voice my appreciation to all the past and current lab members that made my time in the Schnittger lab really special. In particular, I want to mention Franzi, Joke, Ankit, Stephan, Irenemaus, Mariana, Òscãr, Max, and Venesa for bringing much joy to my life out of the lab, for teaching me many lessons and making me a better person, as well as for being a significant part of this wonderful journey. Let's not end here.

I am grateful towards all the people who were not part of my scientific environment but contributed endlessly to my well-being. This includes the whole Ultimate Frisbee community, especially in Hamburg, with their unwavering spirit and positivity. We truly have something special here. Thank you to the EELECTRICs, who make me look forward every week to Friday eelvening and so much more.

A big thank you to Gazment, Erik, Deike, Julia, Sandra, Britta, Thorben, Stefan, Anabel, Katja, Lena, and Maike for making my life as fun as it is. My friendship with each of you is unique, and this is something I cherish. Long may it last!

The support and love I received from Paul and Doris are impossible to put into words. I won't even try. What you have done for me is more than anyone could ever wish for, and I appreciate having both of you in my life so, so much. Thank you from the bottom of my heart.

And lastly, there is Franzi. My pillar and my pillow. At my side, loving, caring, supportive, forever. I love what we have, and I vow to work every single day to make it even better. *Wherever you are, Whatever it takes, No matter how far, Through all that may come, And all that may go, I walk beside you.*

Publications

As an author

- **Lang L**, Schnittger A (2020) Endoreplication — a means to an end in cell growth and stress response. *Curr Opin Plant Biol* 54. doi:10.1016/j.pbi.2020.02.006.
- **Lang L**, Pettkó-Szandtner A, Tunçay Elbaşı H, Takatsuka H, Nomoto Y, Zaki A, Dorokhov S, De Jaeger G, Eeckhout D, Ito M, Magyar Z, Bögre L, Heese M, Schnittger A (2021) The DREAM complex represses growth in response to DNA damage in *Arabidopsis*. *Life Sci Alliance* 4. doi:10.26508/lsa.202101141.
- **Lang L**, Böwer F, Tunçay Elbaşı H, Eeckhout D, Marschlich N, de Jaeger G, Heese M, Schnittger A (2023) The two plant-specific DREAM components FLIC and FLAC repress floral transition in *Arabidopsis*. *bioRxiv*. doi:10.1101/2023.08.07.552284.
- **Lang L** et al (in preparation) FLIC and FLAC are suppressors of jasmonic acid biosynthesis in *Arabidopsis*.

As a supervisor

- Marschlich N (2019) Characterization of novel interacting partners of the DREAM complex in *Arabidopsis thaliana*. Bachelor's thesis.
- Krebs M (2022) DRC2A & DRC2B – Characterization of two homolog Proteins as prospective DREAM complex interactors under heat stress in *Arabidopsis thaliana*. Bachelor's thesis.

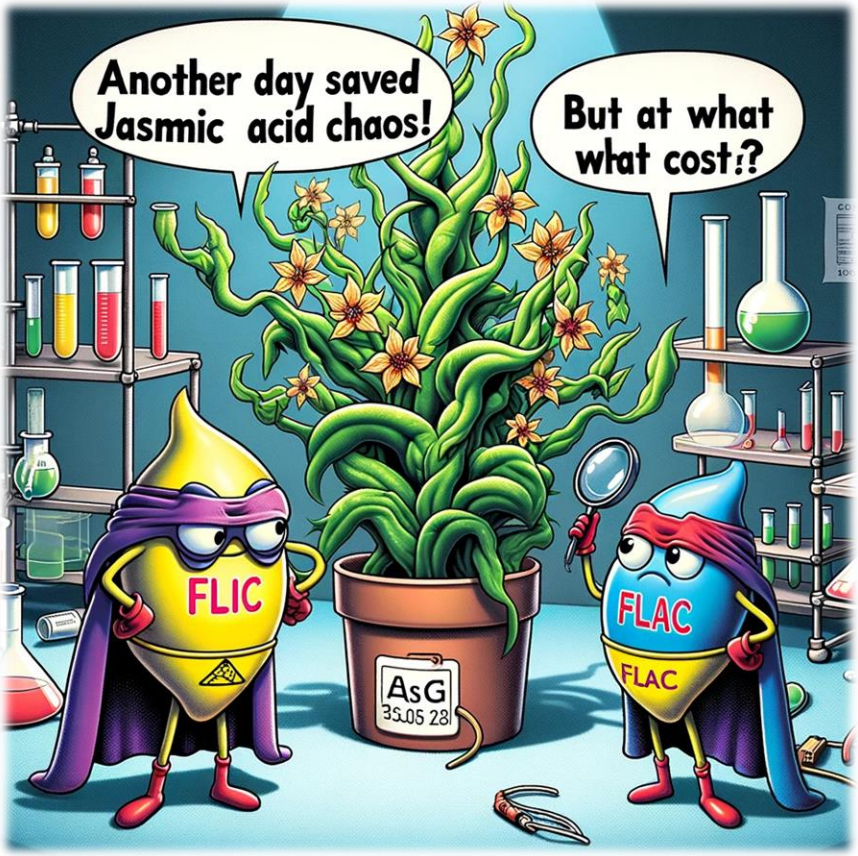

This meme was generated by OpenAI's ChatGPT 4 and DALLE·3 in November 2023

Abstract

The cell cycle is an essential mechanism ensuring that cells proliferate only when suitable. Besides its crucial developmentally programmed function, it is also an important means of reacting to stress, enabling a cell to properly repair any damage or temporarily or permanently exit the cell cycle altogether. Thus, it has to be under tight control. Failure to do so may result in genomic instability, uncontrolled cell growth, and in animals, even cancer. Given the estimates of tremendous population growth as well as climate change taking its toll in an ever-aggravating severity, comprehending the cell cycle in plants – especially in a stress context – is of paramount importance for optimising our food production capabilities.

In my doctoral thesis, I present my research on the plant DREAM complex, a key cell cycle master regulator, beginning with the identification of the complete complex orthologue in *Arabidopsis thaliana* and ending with a focus on two homologous plant-specific DREAM components, FLIC and FLAC.

The first chapter features our published results of investigating the plant DREAM complex within the scope of genotoxic stress. We identify the entirety of the canonical DREAM complex in *Arabidopsis thaliana*, including the previously unknown LIN37 and LIN52 orthologues, by pinpointing interactors of RBR1 under DNA-damaging conditions. There, we also discovered the transcription factor NAC044, which mediates cell cycle arrest in response to genotoxic insult, and we demonstrate its physical interaction with RBR1 and LIN37B. We show that mutants of *NAC044*, *LIN37A* and *LIN37B*, as well as *E2FB* all exhibit tolerance, i.e. a failure to appropriately arrest the cell cycle, towards DNA damage. These findings indicate a collaboration of the DREAM complex with NAC044 to properly respond to genotoxic challenges.

In our pre-print that comprises the second chapter, we characterise two novel plant-specific DREAM components, FLIC and FLAC. Absence of both leads to pleiotropic phenotypes, including dwarfism, early flowering, and severe fertility defects. To find out more about the cause behind this, we looked at the interactome of FLIC and FLAC, and we could detect the entire DREAM complex as well as the JMJ14/NAC050/NAC052 module, a known flowering repressor complex. We demonstrate early floral transition also in *lin37* mutants and a physical interaction

of FLIC, FLAC, and NAC050 with LIN37B. These results involve the DREAM complex in flowering time regulation while providing a mechanistic framework describing how it controls this process.

In the last chapter, I present a further analysis of the roles of FLIC and FLAC by elucidating a phytohormonal dys-regulation in their absence. I focus on the jasmonic acid pathway, since mRNA-seq data reveal what appears to be a constitutive up-regulation of jasmonate biosynthesis. We confirm this finding by direct measurement of methyl jasmonate levels, which are elevated in *flic flac* mutant seedlings. In this genetic background, I assess several jasmonate-affected phenotypes and show that they consistently contrast with *coi1* mutants, which are insensitive to jasmonic acid. Notably, mutants of Zm*Flac*, the only orthologue in *Zea mays*, exhibit developmental retardation, demonstrating that our results are relevant in crop species. These observations involve the DREAM components FLIC and FLAC in yet another highly important control mechanism.

In conclusion, this doctoral thesis presents significant insights into the workings of the cell cycle in plants, particularly under the lens of stress response and regulation, while focussing on the DREAM complex and its plant-specific components FLIC and FLAC. The findings presented here not only deepen our knowledge of plant cellular mechanisms but also have potential implications for agricultural practices.

Zusammenfassung

Der Zellzyklus ist ein wesentlicher Mechanismus, der sicherstellt, dass Zellen nur dann proliferieren, wenn geeignete Bedingungen herrschen. Neben seiner entscheidenden, entwicklungsgesteuerten Funktion ist er auch ein wichtiges Mittel zur Reaktion auf Stress und ermöglicht es einer Zelle, Schäden ordnungsgemäß zu reparieren oder vorübergehend oder dauerhaft aus dem Zellzyklus auszutreten. Daher muss er streng kontrolliert werden. Ein Versagen dabei kann zu genomischer Instabilität, unkontrolliertem Zellwachstum und bei Tieren sogar zu Krebs führen. Angesichts der Schätzungen über enormes Bevölkerungswachstum sowie der immer schwerwiegender werdenden Folgen des Klimawandels ist das Verständnis des Zellzyklus in Pflanzen – insbesondere im Stresskontext – von größter Bedeutung für unsere Nahrungsmittelproduktionskapazitätenoptimierung.

In meiner Doktorarbeit präsentiere ich meine Forschung am DREAM-Komplex in Pflanzen, einem Schlüsselregulator des Zellzyklus, beginnend mit der Identifizierung des vollständigen orthologen Komplexes in *Arabidopsis thaliana* und endend mit einem Fokus auf zwei homologe pflanzenspezifische DREAM-Komponenten, FLIC und FLAC.

Das erste Kapitel beinhaltet unsere veröffentlichten Ergebnisse zur Untersuchung des DREAM-Komplexes in Pflanzen im Rahmen von genotoxischem Stress. Wir identifizieren die Gesamtheit des kanonischen DREAM-Komplexes in *Arabidopsis thaliana*, einschließlich der zuvor unbekannten Orthologe LIN37 und LIN52, indem wir Interaktoren von RBR1 unter DNA-schädigenden Bedingungen ermitteln. Dort entdeckten wir auch den Transkriptionsfaktor NAC044, der den Zellzyklus in Reaktion auf genotoxische Beleidigungen arretiert, und wir weisen seine physische Interaktion mit RBR1 und LIN37B nach. Wir zeigen, dass Mutanten von NAC044, LIN37A und LIN37B sowie E2FB alle eine Toleranz, d. h. ein Versagen, den Zellzyklus bei DNA-Schäden angemessen zu stoppen, aufweisen. Diese Ergebnisse deuten auf eine Zusammenarbeit des DREAM-Komplexes mit NAC044 hin, um angemessen auf genotoxische Herausforderungen zu reagieren.

In unserem Preprint, das das zweite Kapitel umfasst, charakterisieren wir zwei neue pflanzenspezifische DREAM-Komponenten, FLIC und FLAC. Das Fehlen beider führt zu pleiotropen Phänotypen, einschließlich Zwergwuchs, früher Blüte und

schweren Fertilitätsdefekten. Um mehr über die Ursache dahinter herauszufinden, untersuchten wir das Interaktom von FLIC und FLAC, und wir konnten den gesamten DREAM-Komplex sowie das JMJ14/NAC050/NAC052-Modul, einen bekannten Blührepressor-Komplex, nachweisen. Wir demonstrieren einen frühen Blütenübergang auch bei *lin37*-Mutanten und eine physische Interaktion von FLIC, FLAC und NAC050 mit LIN37B. Diese Ergebnisse beziehen den DREAM-Komplex in die Regulation der Blütezeit ein und bieten einen mechanistischen Rahmen, der beschreibt, wie er diesen Prozess steuert.

Im letzten Kapitel präsentiere ich eine weitere Analyse der Rollen von FLIC und FLAC, indem ich eine Phytohormon-Dysregulation in ihrer Abwesenheit beleuchte. Ich konzentriere mich auf den Jasmonsäure-Weg, da mRNA-Seq-Daten auf eine scheinbar konstitutive Hochregulierung der Jasmonat-Biosynthese hindeuten. Wir bestätigen dieses Resultat durch direkte Messung des Methyljasmonat-Spiegels, der in *flic flac*-Mutantenkeimlingen erhöht ist. In diesem genetischen Hintergrund untersuche ich mehrere Jasmonat-beeinflusste Phänotypen und zeige, dass sie konsequent im Gegensatz zu *coi1*-Mutanten stehen, die gegenüber Jasmonsäure unempfindlich sind. Bemerkenswerterweise zeigen Mutanten von Zm*Flac*, dem einzigen Orthologen in *Zea mays*, eine Entwicklungsverzögerung, was demonstriert, dass unsere Ergebnisse auch in Nutzpflanzen relevant sind. Diese Beobachtungen beziehen die DREAM-Komponenten FLIC und FLAC in einen weiteren wichtigen Kontrollmechanismus ein.

Zusammenfassend präsentiert diese Doktorarbeit bedeutende Einblicke in die Funktionalität des Zellzyklus in Pflanzen, insbesondere unter dem Aspekt der Stressreaktion und -regulation, wobei der Fokus auf dem DREAM-Komplex und seinen pflanzenspezifischen Komponenten FLIC und FLAC liegt. Die hier vorgestellten Erkenntnisse vertiefen nicht nur unser Wissen über pflanzliche Zellmechanismen, sondern haben auch potenzielle Auswirkungen auf landwirtschaftliche Praktiken.

Introduction

Pivotally, plants possess a plethora of processes pertaining to providing them proficiency in preparing their proper proliferation and propagation, promoting their potential for persistence and population perpetuity. Examples include the tight regulation of the cell cycle, which consists of the precise sequence of gap 1 (G1), synthesis (S), G2, and mitosis (M) phases, the response to diverse stresses, such as DNA damage, or the decision to initiate floral transition. Defects in co-ordinating these essential mechanisms can lead to impaired development, diminished fitness, and even demise.

A master regulator involved in all of these processes is called DP, RB-like, E2F, and multi-vulval class B (MuvB)-core (DREAM) complex (Korenjak et al, 2004; Fischer & DeCaprio, 2015; Magyar et al, 2016; Fischer et al, 2022). It is conserved across eukaryotes and consists of a constant core sub-complex (MuvB) and a fluctuating combination of interactors, that depends on cell cycle state and phase, developmental stage, as well as environmental cues and stresses, to target different sets of genes (Korenjak et al, 2004; Litovchick et al, 2007; Schmit et al, 2007; Kobayashi et al, 2015; Magyar et al, 2016; Lang et al, 2021, 2023; Asthana et al, 2022; Koliopoulos et al, 2022).

In *Arabidopsis thaliana*, the MuvB-core is comprised of ALWAYS EARLY (ALY), LIN37, LIN52, TESMIN/TSO1-LIKE CXC (TCX), and MULTICOPY SUPPRESSOR OF IRA (MSI) homologues. Its flexible association with interactors, including RETINOBLASTOMA-RELATED 1 (RBR1), DIMERIZATION PARTNER (DP), E2 PROMOTER BINDING FACTOR (E2F), and MYELOBLASTOMA 3R (MYB3R), plays a crucial role in specifying the magnitude as well as the quality of transcriptional regulation, enabling the complex to appropriately initiate and maintain control over a varying array of target genes (as recently reviewed in the context of mammals in Fischer et al, 2022). Since naming of DREAM components varies wildly between organisms, I give an overview over their names in different species in Table 1.

Research on the DREAM complex in animals is far more advanced than in plants, where it only recently has been identified entirely (Ning et al, 2020; Lang et al, 2021). Thus, I will begin by briefly reviewing what has been described in the animal kingdom before presenting what is known in plants.

Table 1. Naming of MuvB-core and selected DREAM proteins in different organisms (Beall et al, 2007; Sadasivam & DeCaprio, 2013; Guiley et al, 2015; Kim et al, 2015; Kobayashi et al, 2015; Magyar et al, 2016; Laktionov et al, 2018; Lang et al, 2021, 2023; Goetsch & Strome, 2022). ALY, ALWAYS EARLY; B-MYB, B-Myeloblastoma; BTE, BARRIER OF TRANSCRIPTION ELONGATION; BTL, BTE1-LIKE; Caf, Chromatin assembly factor; DP, DIMERIZATION PARTNER; DPL, DP-like; EFL, E2F-like; E2F, E2 PROMOTER BINDING FACTOR; FLAC, FLORAL ANTICIPATION CONTROLLER; FLIC, FLORAL INDUCTION CONTROLLER; FOXM, Forkhead box protein M; LIN, ABNORMAL CELL LINEAGE PROTEIN; Mip, Myb-interacting protein; MSI, MULTICOPY SUPPRESSOR OF IRA; Myb, Myeloblastoma; MYB3R, MYELOBLASTOMA 3R; NAC, NAM, ATAF1, and CUC1/CUC2; RBBP, RB-binding protein; Rbf, Retinoblastoma family; RBR, RETINOBLASTOMA-RELATED; TCX, TESMIN/TSO1-LIKE CXC; Tomb, Tombola; Wuc, Wake-up-call.

Arabidopsis DREAM	Caenorhabditis DRM	Drosophila dREAM/tMAC	Homo DREAM
MuvB-core			
ALY	LIN-9	Mip130/Aly	LIN9
LIN37	LIN-37	Mip40/Mip40	LIN37
LIN52	LIN-52	Lin52/Wuc	LIN52
MSI	LIN-53	Caf1/Caf1	RBBP4
TCX	LIN-54	Mip120/Tomb	LIN54
Key MuvB interactors			
DP	DPL-1	Dp/–	DP
E2F	EFL-1	E2f2/–	E2F
RBR1	LIN-35	Rbf/–	p107/p130
MYB3R	–	Myb/–	B-MYB
–	–	–	FOXM1
FLIC/FLAC	–	–	–
NAC044	–	–	–
BTE1/BTL1	–	–	–

The DREAM complex in animals

The *RB1* and *E2F* genes were discovered long ago (Knudson, 1971; Yunis & Ramsay, 1978; Cavenee et al, 1983; Kovesdi et al, 1986; Yee et al, 1987; Weinberg, 1991). In the early 1990s, the interaction and behaviour of their corresponding proteins was characterised as controlled by as well as controlling the cell cycle (Chellappan et al, 1991; Nevins, 1992; Weintraub et al, 1992), but the discovery of the DREAM complex

only occurred more than a decade later. While individual members of the MuvB-core were identified in *Caenorhabditis elegans* before the exact nature of their interrelation had been unravelled (Beitel et al, 2000; Thomas et al, 2003), it soon became clear that they associate in a *Drosophila melanogaster* RBF, dE2F2, and dMyb-interacting proteins (dREAM) complex (Korenjak et al, 2004; Lewis et al, 2004). Not much later, this complex was also identified in *Caenorhabditis elegans*, however, Myb orthologues were notably absent as there exists no known orthologue in nematodes, and it was analogously named DP, Rb, and MuvB (DRM) complex (Harrison et al, 2006; Davidson et al, 2013). Identification in mammalian cells followed shortly after, where it was occasionally called Abnormal cell lineage protein complex (LINC) (Litovchick et al, 2007; Pilkinton et al, 2007; Schmit et al, 2007). Whereas RB itself could not be identified as a member of the DREAM complex, its homologous pocket proteins p130 and p107 could (Guiley et al, 2015). In the same year as the mammalian DREAM complex was discovered, a tissue-specific dREAM paralogue called testis-specific meiotic arrest complex (tMAC) was described in *Drosophila melanogaster*, which is crucial for cell differentiation and meiotic cell cycle progression (Beall et al, 2007; Lu & Fuller, 2015). The current model of DREAM compositions in different animal species is shown in Figure 1.

The canonical role of the DREAM complex is that of a transcriptional cell cycle master regulator, however, especially outside of mammals, such as in *Drosophila melanogaster* and *Caenorhabditis elegans*, DREAM-like complexes also target developmental, apoptosis-related, and reproductive genes (Georlette et al, 2007; Litovchick et al, 2007; Schmit et al, 2007; Tabuchi et al, 2011; Lee et al, 2012; Lewis et al, 2012; Rovani et al, 2012; Sadasivam et al, 2012; Chen et al, 2013; Esterlechner et al, 2013; Kudron et al, 2013; Latorre et al, 2015). While the DREAM complex has the ability to keep cells quiescent and exhibits largely, but not exclusively, repressive functions in G1/S phases, the recruitment of B-MYB and Forkhead box protein M1 (FOXM1) is required for timely activation and proper expression of G2/M genes (as reviewed in Fischer et al, 2022). Transcriptional specificity is fundamentally achieved by the presence or absence of promoter motifs. In human, LIN54 has been demonstrated to bind to cell cycle genes homology regions (CHRs) and CHR-like elements (CLEs), while the E2F/DP module binds to cell cycle-dependent elements (CDEs). These motifs can

occur solely or in tandem, offering a further level of regulation (Müller & Engeland, 2010; Tabuchi et al, 2011; Korenjak et al, 2012; Müller et al, 2012, 2014, 2017; Fischer & Müller, 2017). Thus, throughout the cell cycle, DREAM-like complexes have the ability to regulate genes on several levels and through various mechanisms.

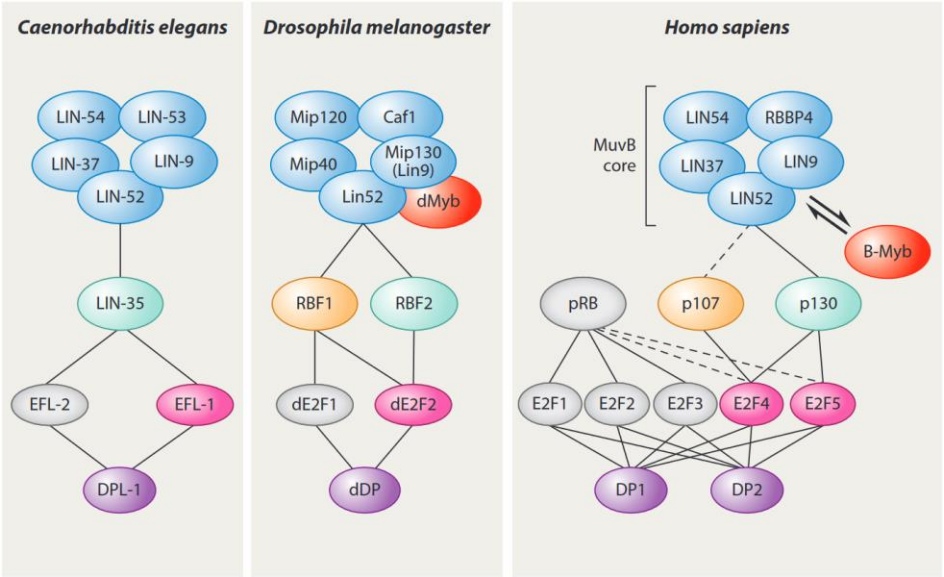

Figure 1. The composition of DREAM-like complexes in different animal species. Blue ovals represent MuvB-core members, grey ovals signify members of the Rb and E2F families that are not participating in DREAM-like complexes (Walston et al, 2021).

If cellular proliferation is warranted, the abolishment of DREAM-facilitated G1/S repression is initiated by cyclin D–cyclin-dependent kinase 4/6 (CDK4/6) phosphorylating p130, thereby occluding an LxCxE binding cleft within the pocket protein, which is bound by the LxSxExL motif of LIN52 when accessible. Dissociation of p130–E2F and subsequently of p130–LIN52 binding results in loss of DREAM association with G1/S gene promoters (Guiley et al, 2015; Schade et al, 2019b). Activity of RB-binding protein 4 (RBBP4), another MuvB-core member, has to be counteracted, since it has been described to interact with RB, Histone deacetylases (HDACs), histones H3 and H4, as well as chromatin-bound proteins to regulate histone acetylation status and in consequence E2F target gene repression (Qian et al, 1993; Hassig et al, 1997; Zhang et al, 1999, 2013; Nicolas et al, 2000, 2001; Taylor-Harding et al, 2004; Murzina et al, 2008; Saade et al, 2009; Millard et al, 2016). At the same time, the long-known and well-described process of RB phosphorylation takes

place, leading to a de-repression of activator E2Fs, an event which marks the commitment to cell division (Pardee, 1974; Weintraub et al, 1992; Yao et al, 2008; Dick & Rubin, 2013; Burke et al, 2014; Narasimha et al, 2014).

A hallmark of cell cycle progression past the S phase is the transformation of the DREAM complex into the B-MYB–MuvB (MMB) complex by binding B-MYB and subsequently, by addition of the transcription factor FOXM1, into the MMB–FOXM1 complex, substantially increasing its activating ability (Sadasivam et al, 2012). This assembly is tightly regulated to appropriate conditions, on the one hand transcriptionally through DREAM complex-facilitated repression itself and on the other hand by B-MYB and FOXM1 protein degradation (Litovchick et al, 2007; Laoukili et al, 2008; Park et al, 2008; Okumura et al, 2017). Once mitogenic signals are received, B-MYB and FOXM1 expression is promoted, which is sufficient to disrupt the DREAM complex (Eisinger-Mathason et al, 2015; Iness et al, 2019; Pattschull et al, 2019; Nilsson et al, 2020). At the same time, p130, E2F4, and DP dissociate from the complex (Litovchick et al, 2007; Pilkinton et al, 2007; Schmit et al, 2007; Sadasivam et al, 2012). B-MYB and FOXM1 are further phosphorylated by CDKs as well as Polo-like kinase 1 (Plk1), which is required for their activation (Johnson et al, 1999; Marceau et al, 2019; Werwein et al, 2019; Gallo et al, 2022). B-MYB as well as FOXM1 bind to CHR motifs through their association with the MuvB-core, and consequently, Myb binding sites are not enriched in promoters of G2/M genes as one might expect (Matsuo et al, 2012; Müller et al, 2012, 2014, 2017; Chen et al, 2013). This further explains an earlier finding that Myb's DNA-binding domain is dispensable in *Drosophila melanogaster* (Wen et al, 2008). Notably, whereas pocket proteins and B-MYB seem to never be integrated at the same time in mammalian complexes, Rbf and Myb can occur together in the same complex in *Drosophila melanogaster* (Sadasivam & DeCaprio, 2013), demonstrating that although such complexes are conserved across species, substantial differences have evolved.

Cells can respond to stress and/or differentiation signals by exiting the cell cycle into a phase called G0. The DREAM complex as well as RB are considered main regulators in maintaining this state, known as quiescence, senescence, or differentiation, temporarily or permanently (Mages et al, 2017; Schade et al, 2019b). While it is difficult to determine redundancy between these players due to partially

reciprocal as well as redundant control mechanisms (as reviewed in Fischer et al, 2022), concomitant loss of both abrogates the ability to arrest or exit the cell cycle completely (Uxa et al, 2019). In this, RB plays a crucial role in chromatin reorganisation, promoting a stable heterochromatin state which represses cell cycle gene expression (Narita et al, 2003; Grigoryev et al, 2006; Blais et al, 2007). Two important prerequisites for entering the G0 state are on the one hand the activation of Protein phosphatase 2A (PP2A) in the preceding G2 phase to counteract CDK-mediated phosphorylation of pocket proteins and on the other hand the phosphorylation of serine 28 (S28) on LIN52 by Dual specificity tyrosine-phosphorylation-regulated kinase 1A (DYRK1A) to facilitate DREAM complex assembly (Litovchick et al, 2011; Boichuk et al, 2013; Kolupaeva & Janssens, 2013; Naetar et al, 2014; Kurimchak & Graña, 2015; MacDonald et al, 2017). Subsequently, inhibition of CDKs and RB-dependent activation of the p53–p21 pathway enables cells to continuously suppress cell cycle progression by p53-mediated recruitment of E2F4, p130, and RB to promoters of cell cycle genes as well as stabilisation of repressive DREAM complexes (Harrington et al, 1998; Flatt et al, 2000; Gottifredi et al, 2001; Taylor et al, 2001; Polager & Ginsberg, 2003; Jackson & Pereira-Smith, 2006; Mannefeld et al, 2009; Calvisi et al, 2011; Quaas et al, 2012; Fischer et al, 2014, 2016a, 2016b; Schade et al, 2019a; Uxa et al, 2019).

Interestingly, still not much is known about the exact mechanism of how the DREAM complex represses gene expression (as reviewed in Fischer et al, 2022). In quiescent cells, p130, which is able to bind the repressive transcription factors E2F4 and E2F5, is the predominant pocket protein, whereas p107 is virtually undetectable (Takahashi et al, 2000; Litovchick et al, 2007). The selectivity for p130 is facilitated by the phosphorylation of S28 in LIN52 by DYRK1A, as p130 is only found with LIN52 phosphorylated at S28. Knockdown of p130 expression leads to elevated levels of p107, which could then be observed complementing the role of p130 to some degree (Litovchick et al, 2007). This being said, complete loss of p130 in BALB/c mice could be observed as embryonically lethal, whereas loss of p107 results in cell cycle and growth defects (LeCouter et al, 1998a, 1998b). Abolishment of both *p107* and *p130* led to neonatal lethality in knockout mice and promoted cell cycle re-entry of quiescent cells in mouse embryonic fibroblasts (MEFs) (Cobrinik et al, 1996; Hurford et al, 1997).

Similarly, inhibition of DYRK1A leads to impaired DREAM complex assembly as well as a diminished ability to enter quiescence, ultimately harbouring oncogenic potential (Litovchick et al, 2011). In contrast, *E2f4 E2f5* double-knockout MEFs show a normal cell cycle re-entry but an impaired ability for G1 arrest (Gaubatz et al, 2000).

Regarding MuvB-core components, depletion of LIN52 results in a G2/M arrest of gastrointestinal stromal tumour cells, while mutation of its crucial S28 to alanine hinders entry into quiescence due to impairment of DREAM complex formation in BJ skin fibroblasts (Litovchick et al, 2011; Boichuk et al, 2013). Interestingly, abolishment of LIN37 leads to a crucial loss of repressive ability, but the structural integrity of the DREAM complex is largely maintained (Mages et al, 2017). In mice, mutation of either *B-myb*, *Foxm1*, or *Lin9* results in embryonic lethality due to mitotic arrest, as they lack the required expression of essential mitotic genes, and loss of *Lin9* in adult mice is fatal within seven days (Tanaka et al, 1999; Krupczak-Hollis et al, 2004; Reichert et al, 2010). A similar mitotic arrest could be observed for *Lin9* and *B-myb* knockdown mutants in F9 murine embryonal carcinoma cells as well as in absence of LIN54 in HeLa cells (Kittler et al, 2007; Knight et al, 2009). Experiments in murine testicular GC-1 cells showed that abolishment of the *Lin54* DNA-binding domain was sufficient to cause these phenotypes, while mutation of *lin9* in *Danio rerio* revealed defects spread across mitotic entry, metaphase/anaphase transition, as well as cytokinesis (Kleinschmidt et al, 2009; Matsuo et al, 2012). Interestingly, *Foxm1* mutation in MEFs also leads to mitotic arrest but additionally incurs early senescence (Wang et al, 2005). These corresponding phenotypes make sense given the fact that *B-myb* mutant cells also exhibit almost complete abrogation of FoxM1 and Lin9 binding to promoters of late cell cycle genes with no additivity on further mutations, demonstrating a strong interdependability (Down et al, 2012; Sadasivam et al, 2012). However, FoxM1 knockdown does not affect the rest of the complex, indicating that the MuvB-core is the central connective element (Sadasivam et al, 2012).

The DREAM complex appears to also play a crucial role in stress responses, and they are being progressively elucidated. While its implication in most stress responses remains poorly understood, the role of LIN-35, the only *Caenorhabditis elegans* pocket protein, has been recently reviewed, and its attenuating role in temperature stress was illuminated not long ago (González-Rangel & Navarro, 2021;

Mikeworth et al, 2023). Revelatorily, the DREAM complex has recently been characterised as a master regulator of somatic DNA repair capacities in *Caenorhabditis elegans*, as it has been discovered to suppress an array of DNA repair genes involved in all major repair pathways (Bujarrabal-Dueso et al, 2023). Similar results could be obtained previously in human cells through DYRK1A inhibition (Göckler et al, 2009; Ogawa et al, 2010).

Naturally, mutation in DREAM components, being key cell cycle regulators, plays a frequent role in carcinogenesis. Since this dissertation is focused on plants, and plants can only develop tumours but not cancer, I want to refer the interested reader to some of the reviews that have been written about the role of the DREAM complex in cancer (Doonan & Sablowski, 2010; Sadasivam & DeCaprio, 2013; Fischer & Müller, 2017).

While a lot is known about the DREAM complex in animals, there are still many open points to address, and research questions are plenty. To highlight the fact that some essential modes of functionality are yet unclear, and since this has been reviewed extensively very recently, I want to mention some outstanding questions verbatim (Fischer et al, 2022):

- "How do DREAM and RB:E2F complexes coordinate their binding to E2F promoter motifs? From a biochemical and steric viewpoint, it is unlikely that they can bind together. Can both complexes reside at the chromatin, leading to an interchangeable binding? What factors affect their binding dynamics? In RB-mutated cancer, do activating E2F1–3 compete with the DREAM complex for binding to the E2F promoter site?"
- "Do the p130:DREAM and p107:DREAM complexes have distinct functions?"
- "What additional post-translational modifications and interaction partners regulate the functions and composition of MuvB complexes?"
- "How does FOXM1 get recruited to MMB and what exact role does B-MYB have in this?"

It will be captivating to follow future research tackling the important questions of how DREAM-like complexes assemble, compete, and function in detail as well as how many layers of regulatory potential are exactly available.

The DREAM complex in plants

While there exists a paucity of research on the DREAM complex in plants, several groups were able to elucidate this subject from different angles in recent years. Already decades ago, DREAM components were identified as controlling the cell cycle outside of a DREAM context. RBR1, the single pocket protein in *Arabidopsis thaliana*, has been shown to contribute to differentiation, promoting cell cycle exit (Wyrzykowska et al, 2006; Gutzat et al, 2011). In complex with E2FA, it stimulates proliferation as well as the post-mitotic endocycle, and MYB3Rs were characterised to activate late G2/M genes, just like their animal counterparts (Haga et al, 2011; Magyar et al, 2012; Kobayashi et al, 2015).

Arabidopsis thaliana MuvB-core components have only been discovered as such in 2015. While plant MYB3Rs use an alternative motif in their target promoters called M-specific activator (MSA) element (Ito et al, 1998, 2001), there was also an enrichment detected at E2F target sites, inspiring a search for a larger complex. After the discovery of the MuvB-core members ALY and TCX as part of such a complex, a model featuring two distinct DREAM complexes, one activating and one repressing, was developed. Surprisingly, both variants contained RBR1 as well as distinct MYB3R homologues, hence, a distinction between DREAM complex and MMB complex does not make sense in plants. In this model, the specifically bound E2F and MYB3R homologues crucially confer activating or repressing activity to the complex (Fischer & DeCaprio, 2015; Kobayashi et al, 2015). A switch between repressor and activator MYB3Rs occurs in the G2 phase, once G2/M genes are desired to be expressed. Notably, MYB3R1 in particular has been demonstrated to have a marked dual role, contributing significantly to both activating and repressive abilities (Kobayashi et al, 2015; Magyar et al, 2016).

Curiously, neither LIN37 nor LIN52 orthologues could be detected during the initial identification of MuvB-core members (Fischer & DeCaprio, 2015; Kobayashi et al, 2015; Magyar et al, 2016). It took until the early 2020s to finally identify these missing components and to establish a complete orthologous MuvB-core in plants. The plant DREAM complex was thereby characterised as having substantial roles in DNA damage repair as well as in DNA methylation (Ning et al, 2020; Lang et al, 2021).

Looking for novel regulators of methylation levels in a reverse genetics screen, TCX5 and TCX6 were identified as working partially redundantly to limit DNA methylation mainly in quiescent cells, and the missing DREAM components could be identified in a complex with them. In a *tcx5 tcx6* double mutant, the resulting hypermethylation causes excessive cell proliferation and consequently enlarged organ size through diminished suppression of methylation maintenance genes. Methylation levels in *aly2 aly3*, *lin37ab*, and *myb3r1* mutants could be detected as similarly increased, strongly indicating a functionality that is centred on the DREAM complex as a whole (Ning et al, 2020). These results provided a new perspective on DREAM functionality since research on the DREAM complex in conjunction with methylation maintenance in animals is only recent and scarce (Gal et al, 2021). Congruent with what has been discovered in animals two years later (Bujarrabal-Dueso et al, 2023), the DREAM complex has further been shown to govern plant growth in response to DNA damage. The entirety of the complex was identified in the RBR1 interactome under genotoxic stress conditions and was linked with the plant-specific NAM, ATAF1, and CUC1/CUC2 (NAC) type transcription factor NAC044. It was shown that mutants of *nac044*, *lin37ab*, as well as *e2fb* are tolerant to DNA damage, failing to properly initiate growth arrest (Lang et al, 2021). NAC044 is a close homologue of SUPPRESSOR OF GAMMA RESPONSE 1 (SOG1), which is thought to share a similar functionality with p53 that is absent in plants (Yoshiyama et al, 2014; Bourbousse et al, 2018), and binds to RBR1 canonically via its LxCxE motif (Lang et al, 2021). Without revealing any connection to the DREAM complex, it had been shown previously that *nac044* mutants fail to induce G2 arrest upon DNA damage through failure to accumulate repressor MYB3R3 (Takahashi et al, 2019).

More recently, the influence of the DREAM complex on the plant methylome has been further elucidated. While two homologous proteins, BARRIER OF TRANSCRIPTION ELONGATION 1 (BTE1) and its homologue BTE1-LIKE 1 (BTL1), have appeared in previous experiments, they were not characterised and their implication remained a mystery (Derkacheva et al, 2013; Ning et al, 2020; Lang et al, 2021). Eventually, they were described as plant-specific DREAM members that facilitate transcriptional repression by inhibiting WD40 REPEAT 5A (WDR5A), a member of the Complex Proteins Associated with Set1 (COMPASS)-like complex which catalyses

transcription-promoting DNA methylation. In this context, BTE1 recruitment to chromatin has been found as being dependent on E2F, where it, additionally to its inhibition of methylation, hinders RNA polymerase II (Pol II) elongation, thereby repressing transcription in a twofold way. Lastly, it was demonstrated that *bte1* mutation confers hypersensitivity to DNA damage, presenting another DREAM player involved in the response to genotoxic stress (Wang et al, 2022).

Defects in the transition to flowering upon mutation of MuvB-core members have been described occasionally. MSI1 has been researched as a floral transition regulator in-depth in the context of the Polycomb Repressive Complex 2 (PRC2), and *tcx5* and *tcx6* mutations have been associated with a late-flowering phenotype, albeit with limited detail (Bouveret et al, 2006; Ning et al, 2020). Most recently, the DREAM complex has been involved directly in this process unique to plants. This regulation appears to be facilitated by another set of homologous, plant-specific DREAM components, FLORAL INITIATION CONTROLLER (FLIC) and FLORAL ANTICIPATION CONTROLLER (FLAC), whose absence results in early flowering as well as severe vegetative phenotypes and fertility defects. Similar early floral transition could also be observed in *lin37b* mutants. In the FLIC/FLAC interactome, the histone demethylase JUMONJI 14 (JMJ14)–NAC050/NAC052 module could be detected, which themselves control flowering comparably. FLIC, FLAC, and NAC050 interact physically with LIN37B, so that either a separate complex or a DREAM complex extension seems likely (Lang et al, 2023).

Curiously, *Arabidopsis thaliana* LIN52 could not be shown to associate with RBR1, and it appears that rather TCXs are facilitating this interaction in plants. This is corroborated by the fact that neither the S28 nor the LxSxExL motif are conserved in the plant LIN52, making speculation about its role and remaining functionality interesting. Generally, no striking phenotypes could be observed so far in *lin52ab* mutants. In *lin37ab* mutant plants, early flowering and a tolerance to genotoxic insult could be observed (Lang et al, 2021, 2023). While absence of TCX5 and TCX6 only leads to hyperplasia and some mild phenotypic alterations, combined *aly1*, *aly2*, and *aly3* mutations are synthetically lethal (Ning et al, 2020). Although *Arabidopsis thaliana* possesses five homologues of MSI, there has been a strong bias towards finding MSI1 in the context of DREAM research (Ning et al, 2020; Lang et al, 2021). Homozygous *msi1*

mutation is gametophytically lethal, and reduction in MSI1 levels leads to dramatic defects, including methylation-dependent late floral transition and arrest of primary inflorescence shoots, but also tolerance to water stress (Hennig et al, 2003; Köhler et al, 2003; Schönrock et al, 2006; Alexandre et al, 2009; Xu et al, 2022).

Depending on the degree, disruption of *RBR1* leads to a plethora of vegetative and fertility defects up to gametophytic lethality, which has been well characterised (Ebel et al, 2004; Chen et al, 2009; Zhao et al, 2017). Together with MSI1, RBR1 controls methylation during gametogenesis (Jullien et al, 2008). Interestingly, it also plays multifaceted roles during genotoxic stress, with mutants having been characterised as hypersensitive (Biedermann et al, 2017; Horvath et al, 2017; Bouyer et al, 2018; Lang et al, 2021). During absence of all or some of its interactors E2FA, E2FB, and E2FC, cells fail to arrest the cell cycle upon biotic and abiotic challenges and show severe fertility defects (Leviczky et al, 2019; Lang et al, 2021). Surprisingly, *e2fabc* triple mutants exhibit a largely unaffected vegetative growth, featuring enlarged organs and disrupted cell cycle exit (Wang et al, 2014; Gombos et al, 2023), suggesting that E2Fs are required and regulated very specifically to control gene expression in certain developmental stages and environmental conditions. Another set of genes is controlled by MYB3Rs. A triple mutant of the redundant repressive *myb3r1*, *myb3r3*, and *myb3r5* transcription factors exhibits marked up-regulation of G2/M genes, comparable to their animal counterpart, also leading to hyperplasia (Kobayashi et al, 2015). In contrast, double mutants of the activating *myb3r1* and *myb3r4* homologues have a diminished G2/M gene expression and show pleiotropic vegetative as well as severe cytokinesis defects (Haga et al, 2007, 2011).

While the research of plant DREAM complexes might still be in its infancy, many interesting findings have already been made – some on plant-specific processes, such as regulation of floral transition, and some on mechanisms that have not been well investigated in animals yet, such as methylation maintenance. Ultimately, by harnessing the cell cycle in plants, we can significantly enhance agricultural yields. This advancement is crucial in meeting the rapidly increasing food demands of an ever-growing global population. It will be exciting to follow the discoveries of the coming years that hopefully will shed light on all the various processes the plant DREAM complex is involved in.

References

Alexandre C, Möller-Steinbach Y, Schönrock N, Gruissem W, Hennig L (2009) Arabidopsis MSI1 is required for negative regulation of the response to drought stress. *Mol Plant* 2: 675–687.

Asthana A, Ramanan P, Hirschi A, Guiley KZ, Wijeratne TU, Shelansky R, Doody MJ, Narasimhan H, Boeger H, Tripathi S *et al* (2022) The MuvB complex binds and stabilizes nucleosomes downstream of the transcription start site of cell-cycle dependent genes. *Nat Commun* 13: 526.

Beall EL, Lewis PW, Bell M, Rocha M, Jones DL, Botchan MR (2007) Discovery of tMAC: a Drosophila testis-specific meiotic arrest complex paralogous to Myb-Muv B. *Genes Dev* 21: 904–919.

Beitel GJ, Lambie EJ, Horvitz HR (2000) The C. elegans gene lin-9,which acts in an Rb-related pathway, is required for gonadal sheath cell development and encodes a novel protein. *Gene* 254: 253–263.

Biedermann S, Harashima H, Chen P, Heese M, Bouyer D, Sofroni K, Schnittger A (2017) The retinoblastoma homolog RBR1 mediates localization of the repair protein RAD51 to DNA lesions in. *EMBO J* 36: 1279–1297.

Blais A, van Oevelen CJC, Margueron R, Acosta-Alvear D, Dynlacht BD (2007) Retinoblastoma tumor suppressor protein-dependent methylation of histone H3 lysine 27 is associated with irreversible cell cycle exit. *J Cell Biol* 179: 1399–1412.

Boichuk S, Parry JA, Makielski KR, Litovchick L, Baron JL, Zewe JP, Wozniak A, Mehalek KR, Korzeniewski N, Seneviratne DS *et al* (2013) The DREAM complex mediates GIST cell quiescence and is a novel therapeutic target to enhance imatinib-induced apoptosis. *Cancer Res* 73: 5120–5129.

Bourbousse C, Vegesna N, Law JA (2018) SOG1 activator and MYB3R repressors regulate a complex DNA damage network in. *Proc Natl Acad Sci U S A* 115: E12453–E12462.

Bouveret R, Schönrock N, Gruissem W, Hennig L (2006) Regulation of flowering time by Arabidopsis MSI1. *Development* 133: 1693–1702.

Bouyer D, Heese M, Chen P, Harashima H, Roudier F, Grüttner C, Schnittger A (2018) Genome-wide identification of RETINOBLASTOMA RELATED 1 binding sites in Arabidopsis reveals novel DNA damage regulators. *PLoS Genet* 14: e1007797.

Bujarrabal-Dueso A, Sendtner G, Meyer DH, Chatzinikolaou G, Stratigi K, Garinis GA, Schumacher B (2023) The DREAM complex functions as conserved master regulator of somatic DNA-repair capacities. *Nat Struct Mol Biol* 30: 475–488.

Burke JR, Liban TJ, Restrepo T, Lee H-W, Rubin SM (2014) Multiple mechanisms for E2F binding inhibition by phosphorylation of the retinoblastoma protein C-terminal domain. *J Mol Biol* 426: 245–255.

Calvisi DF, Simile MM, Ladu S, Frau M, Evert M, Tomasi ML, Demartis MI, Daino L, Seddaiu MA, Brozzetti S *et al* (2011) Activation of v-Myb avian myeloblastosis viral oncogene homolog-like2 (MYBL2)-LIN9 complex contributes to human hepatocarcinogenesis and identifies a subset of hepatocellular carcinoma with mutant p53. *Hepatology* 53: 1226–1236.

Cavenee WK, Dryja TP, Phillips RA, Benedict WF, Godbout R, Gallie BL, Murphree AL, Strong LC, White RL (1983) Expression of recessive alleles by chromosomal mechanisms in retinoblastoma. *Nature* 305: 779–784.

Chellappan SP, Hiebert S, Mudryj M, Horowitz JM, Nevins JR (1991) The E2F transcription factor is a cellular target for the RB protein. *Cell* 65: 1053–1061.

Chen J-Y, Lin J-R, Tsai F-C, Meyer T (2013) Dosage of Dyrk1a shifts cells within a p21-cyclin D1 signaling map to control the decision to enter the cell cycle. *Mol Cell* 52: 87–100.

Chen Z, Hafidh S, Poh SH, Twell D, Berger F (2009) Proliferation and cell fate establishment during Arabidopsis male gametogenesis depends on the Retinoblastoma protein. *Proc Natl Acad Sci U S A* 106: 7257–7262.

Cobrinik D, Lee MH, Hannon G, Mulligan G, Bronson RT, Dyson N, Harlow E, Beach D, Weinberg RA, Jacks T (1996) Shared role of the pRB-related p130 and p107 proteins in limb development. *Genes Dev* 10: 1633–1644.

Davidson CJ, Guthrie EE, Lipsick JS (2013) Duplication and maintenance of the Myb genes of vertebrate animals. *Biol Open* 2: 101–110.

Derkacheva M, Steinbach Y, Wildhaber T, Mozgová I, Mahrez W, Nanni P, Bischof S, Gruissem W, Hennig L (2013) Arabidopsis MSI1 connects LHP1 to PRC2 complexes. *EMBO J* 32: 2073–2085.

Dick FA, Rubin SM (2013) Molecular mechanisms underlying RB protein function. *Nat Rev Mol Cell Biol* 14: 297–306.

Doonan JH, Sablowski R (2010) Walls around tumours - why plants do not develop cancer. *Nat Rev Cancer* 10: 794–802.

Down CF, Millour J, Lam EW-F, Watson RJ (2012) Binding of FoxM1 to G2/M gene promoters is dependent upon B-Myb. *Biochim Biophys Acta* 1819: 855–862.

Ebel C, Mariconti L, Gruissem W (2004) Plant retinoblastoma homologues control nuclear proliferation in the female gametophyte. *Nature* 429: 776–780.

Eisinger-Mathason TSK, Mucaj V, Biju KM, Nakazawa MS, Gohil M, Cash TP, Yoon SS, Skuli N, Park KM, Gerecht S *et al* (2015) Deregulation of the Hippo pathway in soft-tissue sarcoma promotes FOXM1 expression and tumorigenesis. *Proc Natl Acad Sci U S A* 112: E3402–E3411.

Esterlechner J, Reichert N, Iltzsche F, Krause M, Finkernagel F, Gaubatz S (2013) LIN9, a subunit of the DREAM complex, regulates mitotic gene expression and proliferation of embryonic stem cells. *PLoS One* 8: e62882.

Fischer M, DeCaprio JA (2015) Does Arabidopsis thaliana DREAM of cell cycle control? *EMBO J* 34: 1987–1989.

Fischer M, Grossmann P, Padi M, DeCaprio JA (2016a) Integration of TP53, DREAM, MMB-FOXM1 and RB-E2F target gene analyses identifies cell cycle gene regulatory networks. *Nucleic Acids Res* 44: 6070–6086.

Fischer M, Müller GA (2017) Cell cycle transcription control: DREAM/MuvB and RB-E2F complexes. *Crit Rev Biochem Mol Biol* 52: 638–662.

Fischer M, Quaas M, Steiner L, Engeland K (2016b) The p53-p21-DREAM-CDE/CHR pathway regulates G2/M cell cycle genes. *Nucleic Acids Res* 44: 164–174.

Fischer M, Schade AE, Branigan TB, Müller GA, DeCaprio JA (2022) Coordinating gene expression during the cell cycle. *Trends Biochem Sci* 47: 1009–1022.

Fischer M, Steiner L, Engeland K (2014) The transcription factor p53: not a repressor, solely an activator. *Cell Cycle* 13: 3037–3058.

Flatt PM, Tang LJ, Scatena CD, Szak ST, Pietenpol JA (2000) p53 regulation of G(2) checkpoint is retinoblastoma protein dependent. *Mol Cell Biol* 20: 4210–4223.

Gal C, Carelli FN, Appert A, Cerrato C, Huang N, Dong Y, Murphy J, Frapporti A, Ahringer J (2021) DREAM represses distinct targets by cooperating with different THAP domain proteins. *Cell Rep* 37: 109835.

Gallo D, Young JTF, Fourtounis J, Martino G, Álvarez-Quilón A, Bernier C, Duffy NM, Papp R, Roulston A, Stocco R *et al* (2022) CCNE1 amplification is synthetic lethal with PKMYT1 kinase inhibition. *Nature* 604: 749–756.

Gaubatz S, Lindeman GJ, Ishida S, Jakoi L, Nevins JR, Livingston DM, Rempel RE (2000) E2F4 and E2F5 play an essential role in pocket protein-mediated G1 control. *Mol Cell* 6: 729–735.

Georlette D, Ahn S, MacAlpine DM, Cheung E, Lewis PW, Beall EL, Bell SP, Speed T, Manak JR, Botchan MR (2007) Genomic profiling and expression studies reveal both positive and negative activities for the Drosophila Myb MuvB/dREAM complex in proliferating cells. *Genes Dev* 21: 2880–2896.

Göckler N, Jofre G, Papadopoulos C, Soppa U, Tejedor FJ, Becker W (2009) Harmine specifically inhibits protein kinase DYRK1A and interferes with neurite formation. *FEBS J* 276: 6324–6337.

Goetsch PD, Strome S (2022) DREAM interrupted: severing LIN-35-MuvB association in Caenorhabditis elegans impairs DREAM function but not its chromatin localization. *Genetics* 221. doi:10.1093/genetics/iyac073.

Gombos M, Raynaud C, Nomoto Y, Molnár E, Brik-Chaouche R, Takatsuka H, Zaki A, Bernula D, Latrasse D, Mineta K *et al* (2023) The canonical E2Fs together with RETINOBLASTOMA-RELATED are required to establish quiescence during plant development. *Commun Biol* 6: 903.

González-Rangel AA, Navarro RE (2021) LIN-35 beyond its classical roles: its function in the stress response. *Int J Dev Biol* 65: 377–382.

Gottifredi V, Karni-Schmidt O, Shieh SS, Prives C (2001) p53 down-regulates CHK1 through p21 and the retinoblastoma protein. *Mol Cell Biol* 21: 1066–1076.

Grigoryev SA, Bulynko YA, Popova EY (2006) The end adjusts the means: heterochromatin remodelling during terminal cell differentiation. *Chromosome Res* 14: 53–69.

Guiley KZ, Liban TJ, Felthousen JG, Ramanan P, Litovchick L, Rubin SM (2015) Structural mechanisms of DREAM complex assembly and regulation. *Genes Dev* 29: 961–974.

Gutzat R, Borghi L, Fütterer J, Bischof S, Laizet Y 'han, Hennig L, Feil R, Lunn J, Gruissem W (2011) RETINOBLASTOMA-RELATED PROTEIN controls the transition to autotrophic plant development. *Development* 138: 2977–2986.

Haga N, Kato K, Murase M, Araki S, Kubo M, Demura T, Suzuki K, Müller I, Voss U, Jürgens G *et al* (2007) R1R2R3-Myb proteins positively regulate cytokinesis through activation of KNOLLE transcription in Arabidopsis thaliana. *Development* 134: 1101–1110.

Haga N, Kobayashi K, Suzuki T, Maeo K, Kubo M, Ohtani M, Mitsuda N, Demura T, Nakamura K, Jürgens G *et al* (2011) Mutations in MYB3R1 and MYB3R4 cause pleiotropic developmental defects and preferential down-regulation of multiple G2/M-specific genes in Arabidopsis. *Plant Physiol* 157: 706–717.

Harrington EA, Bruce JL, Harlow E, Dyson N (1998) pRB plays an essential role in cell cycle arrest induced by DNA damage. *Proc Natl Acad Sci U S A* 95: 11945–11950.

Harrison MM, Ceol CJ, Lu X, Horvitz HR (2006) Some C. elegans class B synthetic multivulva proteins encode a conserved LIN-35 Rb-containing complex distinct from a NuRD-like complex. *Proc Natl Acad Sci U S A* 103: 16782–16787.

Hassig CA, Fleischer TC, Billin AN, Schreiber SL, Ayer DE (1997) Histone deacetylase activity is required for full transcriptional repression by mSin3A. *Cell* 89: 341–347.

Hennig L, Taranto P, Walser M, Schönrock N, Gruissem W (2003) Arabidopsis MSI1 is required for epigenetic maintenance of reproductive development. *Development* 130: 2555–2565.

Horvath BM, Kourova H, Nagy S, Nemeth E, Magyar Z, Papdi C, Ahmad Z, Sanchez-Perez GF, Perilli S, Blilou I *et al* (2017) RETINOBLASTOMA RELATED directly regulates DNA damage responses through functions beyond cell cycle control. *EMBO J* 36: 1261–1278.

Hurford RK Jr, Cobrinik D, Lee MH, Dyson N (1997) pRB and p107/p130 are required for the regulated expression of different sets of E2F responsive genes. *Genes Dev* 11: 1447–1463.

Iness AN, Felthousen J, Ananthapadmanabhan V, Sesay F, Saini S, Guiley KZ, Rubin SM, Dozmorov M, Litovchick L (2019) The cell cycle regulatory DREAM complex is disrupted by high expression of oncogenic B-Myb. *Oncogene* 38: 1080–1092.

Ito M, Araki S, Matsunaga S, Itoh T, Nishihama R, Machida Y, Doonan JH, Watanabe A (2001) G2/M-phase-specific transcription during the plant cell cycle is mediated by c-Myb-like transcription factors. *Plant Cell* 13: 1891–1905.

Ito M, Iwase M, Kodama H, Lavisse P, Komamine A, Nishihama R, Machida Y, Watanabe A (1998) A novel cis-acting element in promoters of plant B-type cyclin genes activates M phase-specific transcription. *Plant Cell* 10: 331–341.

Jackson JG, Pereira-Smith OM (2006) Primary and compensatory roles for RB family members at cell cycle gene promoters that are deacetylated and downregulated in doxorubicin-induced senescence of breast cancer cells. *Mol Cell Biol* 26: 2501–2510.

Johnson TK, Schweppe RE, Septer J, Lewis RE (1999) Phosphorylation of B-Myb regulates its transactivation potential and DNA binding. *J Biol Chem* 274: 36741–36749.

Jullien PE, Mosquna A, Ingouff M, Sakata T, Ohad N, Berger F (2008) Retinoblastoma and its binding partner MSI1 control imprinting in Arabidopsis. *PLoS Biol* 6: e194.

Kim S-H, Joshi K, Ezhilarasan R, Myers TR, Siu J, Gu C, Nakano-Okuno M, Taylor D, Minata M, Sulman EP *et al* (2015) EZH2 protects glioma stem cells from radiation-induced cell death in a MELK/FOXM1-dependent manner. *Stem Cell Reports* 4: 226–238.

Kittler R, Pelletier L, Heninger A-K, Slabicki M, Theis M, Miroslaw L, Poser I, Lawo S, Grabner H, Kozak K *et al* (2007) Genome-scale RNAi profiling of cell division in human tissue culture cells. *Nat Cell Biol* 9: 1401–1412.

Kleinschmidt MA, Wagner TU, Liedtke D, Spahr S, Samans B, Gaubatz S (2009) lin9 is required for mitosis and cell survival during early zebrafish development. *J Biol Chem* 284: 13119–13127.

Knight AS, Notaridou M, Watson RJ (2009) A Lin-9 complex is recruited by B-Myb to activate transcription of G2/M genes in undifferentiated embryonal carcinoma cells. *Oncogene* 28: 1737–1747.

Knudson AG Jr (1971) Mutation and cancer: statistical study of retinoblastoma. *Proc Natl Acad Sci U S A* 68: 820–823.

Kobayashi K, Suzuki T, Iwata E, Nakamichi N, Suzuki T, Chen P, Ohtani M, Ishida T, Hosoya H, Müller S *et al* (2015) Transcriptional repression by MYB3R proteins regulates plant organ growth. *EMBO J* 34: 1992–2007.

Köhler C, Hennig L, Bouveret R, Gheyselinck J, Grossniklaus U, Gruissem W (2003) Arabidopsis MSI1 is a component of the MEA/FIE Polycomb group complex and required for seed development. *EMBO J* 22: 4804–4814.

Koliopoulos MG, Muhammad R, Roumeliotis TI, Beuron F, Choudhary JS, Alfieri C (2022) Structure of a nucleosome-bound MuvB transcription factor complex reveals DNA remodelling. *Nat Commun* 13: 5075.

Kolupaeva V, Janssens V (2013) PP1 and PP2A phosphatases--cooperating partners in modulating retinoblastoma protein activation. *FEBS J* 280: 627–643.

Korenjak M, Anderssen E, Ramaswamy S, Whetstine JR, Dyson NJ (2012) RBF binding to both canonical E2F targets and noncanonical targets depends on functional dE2F/dDP complexes. *Mol Cell Biol* 32: 4375–4387.

Korenjak M, Taylor-Harding B, Binné UK, Satterlee JS, Stevaux O, Aasland R, White-Cooper H, Dyson N, Brehm A (2004) Native E2F/RBF complexes contain Myb-interacting proteins and repress transcription of developmentally controlled E2F target genes. *Cell* 119: 181–193.

Kovesdi I, Reichel R, Nevins JR (1986) Identification of a cellular transcription factor involved in E1A trans-activation. *Cell* 45: 219–228.

Krupczak-Hollis K, Wang X, Kalinichenko VV, Gusarova GA, Wang I-C, Dennewitz MB, Yoder HM, Kiyokawa H, Kaestner KH, Costa RH (2004) The mouse Forkhead Box m1 transcription factor is essential for hepatoblast mitosis and development of intrahepatic bile ducts and vessels during liver morphogenesis. *Dev Biol* 276: 74–88.

Kudron M, Niu W, Lu Z, Wang G, Gerstein M, Snyder M, Reinke V (2013) Tissue-specific direct targets of Caenorhabditis elegans Rb/E2F dictate distinct somatic and germline programs. *Genome Biol* 14: R5.

Kurimchak A, Graña X (2015) PP2A: more than a reset switch to activate pRB proteins during the cell cycle and in response to signaling cues. *Cell Cycle* 14: 18–30.

Laktionov PP, Maksimov DA, Romanov SE, Antoshina PA, Posukh OV, White-Cooper H, Koryakov DE, Belyakin SN (2018) Genome-wide analysis of gene regulation mechanisms during Drosophila spermatogenesis. *Epigenetics Chromatin* 11: 14.

Lang L, Böwer F, Tunçay Elbaşı H, Eeckhout D, Marschlich N, de Jaeger G, Heese M, Schnittger A (2023) The two plant-specific DREAM components FLIC and FLAC repress floral transition in *Arabidopsis*.

Lang L, Pettkó-Szandtner A, Tunçay Elbaşı H, Takatsuka H, Nomoto Y, Zaki A, Dorokhov S, De Jaeger G, Eeckhout D, Ito M *et al* (2021) The DREAM complex represses growth in response to DNA damage in. *Life Sci Alliance* 4. doi:10.26508/lsa.202101141.

Laoukili J, Alvarez-Fernandez M, Stahl M, Medema RH (2008) FoxM1 is degraded at mitotic exit in a Cdh1-dependent manner. *Cell Cycle* 7: 2720–2726.

Latorre I, Chesney MA, Garrigues JM, Stempor P, Appert A, Francesconi M, Strome S, Ahringer J (2015) The DREAM complex promotes gene body H2A.Z for target repression. *Genes Dev* 29: 495–500.

LeCouter JE, Kablar B, Hardy WR, Ying C, Megeney LA, May LL, Rudnicki MA (1998a) Strain-dependent myeloid hyperplasia, growth deficiency, and accelerated cell cycle in mice lacking the Rb-related *p107* gene. *Mol Cell Biol* 18: 7455–7465.

LeCouter JE, Kablar B, Whyte PF, Ying C, Rudnicki MA (1998b) Strain-dependent embryonic lethality in mice lacking the retinoblastoma-related p130 gene. *Development* 125: 4669–4679.

Lee H, Ragusano L, Martinez A, Gill J, Dimova DK (2012) A dual role for the dREAM/MMB complex in the regulation of differentiation-specific E2F/RB target genes. *Mol Cell Biol* 32: 2110–2120.

Leviczky T, Molnár E, Papdi C, Őszi E, Horváth GV, Vizler C, Nagy V, Pauk J, Bögre L, Magyar Z (2019) E2FA and E2FB transcription factors coordinate cell proliferation with seed maturation. *Development* 146. doi:10.1242/dev.179333.

Lewis PW, Beall EL, Fleischer TC, Georlette D, Link AJ, Botchan MR (2004) Identification of a Drosophila Myb-E2F2/RBF transcriptional repressor complex. *Genes Dev* 18: 2929–2940.

Lewis PW, Sahoo D, Geng C, Bell M, Lipsick JS, Botchan MR (2012) Drosophila lin-52 acts in opposition to repressive components of the Myb-MuvB/dREAM complex. *Mol Cell Biol* 32: 3218–3227.

Litovchick L, Florens LA, Swanson SK, Washburn MP, DeCaprio JA (2011) DYRK1A protein kinase promotes quiescence and senescence through DREAM complex assembly. *Genes Dev* 25: 801–813.

Litovchick L, Sadasivam S, Florens L, Zhu X, Swanson SK, Velmurugan S, Chen R, Washburn MP, Liu XS, DeCaprio JA (2007) Evolutionarily conserved multisubunit RBL2/p130 and E2F4 protein complex represses human cell cycle-dependent genes in quiescence. *Mol Cell* 26: 539–551.

Lu C, Fuller MT (2015) Recruitment of Mediator Complex by Cell Type and Stage-Specific Factors Required for Tissue-Specific TAF Dependent Gene Activation in an Adult Stem Cell Lineage. *PLoS Genet* 11: e1005701.

MacDonald J, Ramos-Valdes Y, Perampalam P, Litovchick L, DiMattia GE, Dick FA (2017) A Systematic Analysis of Negative Growth Control Implicates the DREAM Complex in Cancer Cell Dormancy. *Mol Cancer Res* 15: 371–381.

Mages CF, Wintsche A, Bernhart SH, Müller GA (2017) The DREAM complex through its subunit Lin37 cooperates with Rb to initiate quiescence. *Elife* 6. doi:10.7554/eLife.26876.

Magyar Z, Bögre L, Ito M (2016) DREAMs make plant cells to cycle or to become quiescent. *Curr Opin Plant Biol* 34: 100–106.

Magyar Z, Horváth B, Khan S, Mohammed B, Henriques R, De Veylder L, Bakó L, Scheres B, Bögre L (2012) Arabidopsis E2FA stimulates proliferation and endocycle separately through RBR-bound and RBR-free complexes. *EMBO J* 31: 1480–1493.

Mannefeld M, Klassen E, Gaubatz S (2009) B-MYB is required for recovery from the DNA damage-induced G2 checkpoint in p53 mutant cells. *Cancer Res* 69: 4073–4080.

Marceau AH, Brison CM, Nerli S, Arsenault HE, McShan AC, Chen E, Lee H-W, Benanti JA, Sgourakis NG, Rubin SM (2019) An order-to-disorder structural switch activates the FoxM1 transcription factor. *Elife* 8. doi:10.7554/eLife.46131.

Matsuo T, Kuramoto H, Kumazaki T, Mitsui Y, Takahashi T (2012) LIN54 harboring a mutation in CHC domain is localized to the cytoplasm and inhibits cell cycle progression. *Cell Cycle* 11: 3227–3236.

Mikeworth BP, Compere FV, Petrella LN (2023) LIN-35 is necessary in both the soma and germline for preserving fertility in Caenorhabditis elegans under moderate temperature stress. *PLoS One* 18: e0286926.

Millard CJ, Varma N, Saleh A, Morris K, Watson PJ, Bottrill AR, Fairall L, Smith CJ, Schwabe JWR (2016) The structure of the core NuRD repression complex provides insights into its interaction with chromatin. *Elife* 5: e13941.

Müller GA, Engeland K (2010) The central role of CDE/CHR promoter elements in the regulation of cell cycle-dependent gene transcription. *FEBS J* 277: 877–893.

Müller GA, Quaas M, Schümann M, Krause E, Padi M, Fischer M, Litovchick L, DeCaprio JA, Engeland K (2012) The CHR promoter element controls cell cycle-dependent gene transcription and binds the DREAM and MMB complexes. *Nucleic Acids Res* 40: 1561–1578.

Müller GA, Stangner K, Schmitt T, Wintsche A, Engeland K (2017) Timing of transcription during the cell cycle: Protein complexes binding to E2F, E2F/CLE, CDE/CHR, or CHR promoter elements define early and late cell cycle gene expression. *Oncotarget* 8: 97736–97748.

Müller GA, Wintsche A, Stangner K, Prohaska SJ, Stadler PF, Engeland K (2014) The CHR site: definition and genome-wide identification of a cell cycle transcriptional element. *Nucleic Acids Res* 42: 10331–10350.

Murzina NV, Pei X-Y, Zhang W, Sparkes M, Vicente-Garcia J, Pratap JV, McLaughlin SH, Ben-Shahar TR, Verreault A, Luisi BF *et al* (2008) Structural basis for the recognition of histone H4 by the histone-chaperone RbAp46. *Structure* 16: 1077–1085.

Naetar N, Soundarapandian V, Litovchick L, Goguen KL, Sablina AA, Bowman-Colin C, Sicinski P, Hahn WC, DeCaprio JA, Livingston DM (2014) PP2A-mediated regulation of Ras signaling in G2 is essential for stable quiescence and normal G1 length. *Mol Cell* 54: 932–945.

Narasimha AM, Kaulich M, Shapiro GS, Choi YJ, Sicinski P, Dowdy SF (2014) Cyclin D activates the Rb tumor suppressor by mono-phosphorylation. *Elife* 3. doi:10.7554/eLife.02872.

Narita M, Nũnez S, Heard E, Narita M, Lin AW, Hearn SA, Spector DL, Hannon GJ, Lowe SW (2003) Rb-mediated heterochromatin formation and silencing of E2F target genes during cellular senescence. *Cell* 113: 703–716.

Nevins JR (1992) E2F: a link between the Rb tumor suppressor protein and viral oncoproteins. *Science* 258: 424–429.

Nicolas E, Ait-Si-Ali S, Trouche D (2001) The histone deacetylase HDAC3 targets RbAp48 to the retinoblastoma protein. *Nucleic Acids Res* 29: 3131–3136.

Nicolas E, Morales V, Magnaghi-Jaulin L, Harel-Bellan A, Richard-Foy H, Trouche D (2000) RbAp48 belongs to the histone deacetylase complex that associates with the retinoblastoma protein. *J Biol Chem* 275: 9797–9804.

Nilsson MB, Sun H, Robichaux J, Pfeifer M, McDermott U, Travers J, Diao L, Xi Y, Tong P, Shen L *et al* (2020) A YAP/FOXM1 axis mediates EMT-associated EGFR inhibitor resistance and increased expression of spindle assembly checkpoint components. *Sci Transl Med* 12. doi:10.1126/scitranslmed.aaz4589.

Ning Y-Q, Liu N, Lan K-K, Su Y-N, Li L, Chen S, He X-J (2020) DREAM complex suppresses DNA methylation maintenance genes and precludes DNA hypermethylation. *Nat Plants* 6: 942–956.

Ogawa Y, Nonaka Y, Goto T, Ohnishi E, Hiramatsu T, Kii I, Yoshida M, Ikura T, Onogi H, Shibuya H *et al* (2010) Development of a novel selective inhibitor of the Down syndrome-related kinase Dyrk1A. *Nat Commun* 1: 86.

Okumura F, Joo-Okumura A, Nakatsukasa K, Kamura T (2017) Hypoxia-inducible factor-2α stabilizes the von Hippel-Lindau (VHL) disease suppressor, Myb-related protein 2. *PLoS One* 12: e0175593.

Pardee AB (1974) A restriction point for control of normal animal cell proliferation. *Proc Natl Acad Sci U S A* 71: 1286–1290.

Park HJ, Costa RH, Lau LF, Tyner AL, Raychaudhuri P (2008) Anaphase-promoting complex/cyclosome-CDH1-mediated proteolysis of the forkhead box M1 transcription factor is critical for regulated entry into S phase. *Mol Cell Biol* 28: 5162–5171.

Pattschull G, Walz S, Gründl M, Schwab M, Rühl E, Baluapuri A, Cindric-Vranesic A, Kneitz S, Wolf E, Ade CP *et al* (2019) The Myb-MuvB Complex Is Required for YAP-Dependent Transcription of Mitotic Genes. *Cell Rep* 27: 3533–3546.e7.

Pilkinton M, Sandoval R, Colamonici OR (2007) Mammalian Mip/LIN-9 interacts with either the p107, p130/E2F4 repressor complex or B-Myb in a cell cycle-phase-dependent context distinct from the Drosophila dREAM complex. *Oncogene* 26: 7535–7543.

Polager S, Ginsberg D (2003) E2F mediates sustained G2 arrest and down-regulation of Stathmin and AIM-1 expression in response to genotoxic stress. *J Biol Chem* 278: 1443–1449.

Qian YW, Wang YC, Hollingsworth RE Jr, Jones D, Ling N, Lee EY (1993) A retinoblastoma-binding protein related to a negative regulator of Ras in yeast. *Nature* 364: 648–652.

Quaas M, Müller GA, Engeland K (2012) p53 can repress transcription of cell cycle genes through a p21(WAF1/CIP1)-dependent switch from MMB to DREAM protein complex binding at CHR promoter elements. *Cell Cycle* 11: 4661–4672.

Reichert N, Wurster S, Ulrich T, Schmitt K, Hauser S, Probst L, Götz R, Ceteci F, Moll R, Rapp U *et al* (2010) Lin9, a subunit of the mammalian DREAM complex, is essential for embryonic development, for survival of adult mice, and for tumor suppression. *Mol Cell Biol* 30: 2896–2908.

Rovani MK, Brachmann CB, Ramsay G, Katzen AL (2012) The dREAM/Myb-MuvB complex and Grim are key regulators of the programmed death of neural precursor cells at the Drosophila posterior wing margin. *Dev Biol* 372: 88–102.

Saade E, Mechold U, Kulyyassov A, Vertut D, Lipinski M, Ogryzko V (2009) Analysis of interaction partners of H4 histone by a new proteomics approach. *Proteomics* 9: 4934–4943.

Sadasivam S, DeCaprio JA (2013) The DREAM complex: master coordinator of cell cycle-dependent gene expression. *Nat Rev Cancer* 13: 585–595.

Sadasivam S, Duan S, DeCaprio JA (2012) The MuvB complex sequentially recruits B-Myb and FoxM1 to promote mitotic gene expression. *Genes Dev* 26: 474–489.

Schade AE, Fischer M, DeCaprio JA (2019a) RB, p130 and p107 differentially repress G1/S and G2/M genes after p53 activation. *Nucleic Acids Res* 47: 11197–11208.

Schade AE, Oser MG, Nicholson HE, DeCaprio JA (2019b) Cyclin D-CDK4 relieves cooperative repression of proliferation and cell cycle gene expression by DREAM and RB. *Oncogene* 38: 4962–4976.

Schmit F, Korenjak M, Mannefeld M, Schmitt K, Franke C, von Eyss B, Gagrica S, Hänel F, Brehm A, Gaubatz S (2007) LINC, a human complex that is related to pRB-containing complexes in invertebrates regulates the expression of G2/M genes. *Cell Cycle* 6: 1903–1913.

Schönrock N, Bouveret R, Leroy O, Borghi L, Köhler C, Gruissem W, Hennig L (2006) Polycomb-group proteins repress the floral activator AGL19 in the FLC-independent vernalization pathway. *Genes Dev* 20: 1667–1678.

Tabuchi TM, Deplancke B, Osato N, Zhu LJ, Barrasa MI, Harrison MM, Horvitz HR, Walhout AJM, Hagstrom KA (2011) Chromosome-biased binding and gene regulation by the Caenorhabditis elegans DRM complex. *PLoS Genet* 7: e1002074.

Takahashi N, Ogita N, Takahashi T, Taniguchi S, Tanaka M, Seki M, Umeda M (2019) A regulatory module controlling stress-induced cell cycle arrest in. *Elife* 8. doi:10.7554/eLife.43944.

Takahashi Y, Rayman JB, Dynlacht BD (2000) Analysis of promoter binding by the E2F and pRB families in vivo: distinct E2F proteins mediate activation and repression. *Genes Dev* 14: 804–816.

Tanaka Y, Patestos NP, Maekawa T, Ishii S (1999) B-myb is required for inner cell mass formation at an early stage of development. *J Biol Chem* 274: 28067–28070.

Taylor-Harding B, Binné UK, Korenjak M, Brehm A, Dyson NJ (2004) p55, the Drosophila ortholog of RbAp46/RbAp48, is required for the repression of dE2F2/RBF-regulated genes. *Mol Cell Biol* 24: 9124–9136.

Taylor WR, Schonthal AH, Galante J, Stark GR (2001) p130/E2F4 binds to and represses the cdc2 promoter in response to p53. *J Biol Chem* 276: 1998–2006.

Thomas JH, Ceol CJ, Schwartz HT, Horvitz HR (2003) New genes that interact with lin-35 Rb to negatively regulate the let-60 ras pathway in Caenorhabditis elegans. *Genetics* 164: 135–151.

Uxa S, Bernhart SH, Mages CFS, Fischer M, Kohler R, Hoffmann S, Stadler PF, Engeland K, Müller GA (2019) DREAM and RB cooperate to induce gene repression and cell-cycle arrest in response to p53 activation. *Nucleic Acids Res* 47: 9087–9103.

Walston H, Iness AN, Litovchick L (2021) DREAM On: Cell Cycle Control in Development and Disease. *Annu Rev Genet* 55: 309–329.

Wang I-C, Chen Y-J, Hughes D, Petrovic V, Major ML, Park HJ, Tan Y, Ackerson T, Costa RH (2005) Forkhead box M1 regulates the transcriptional network of genes essential for mitotic progression and genes encoding the SCF (Skp2-Cks1) ubiquitin ligase. *Mol Cell Biol* 25: 10875–10894.

Wang S, Gu Y, Zebell SG, Anderson LK, Wang W, Mohan R, Dong X (2014) A noncanonical role for the CKI-RB-E2F cell-cycle signaling pathway in plant effector-triggered immunity. *Cell Host Microbe* 16: 787–794.

Wang Y, Fan Y, Fan D, Zhang Y, Zhou X, Zhang R, Wang Y, Sun Y, Zhang W, He Y *et al* (2022) The DREAM complex antagonizes WDR5A to modulate histone H3K4me2/3 deposition for a subset of genome repression. *Proc Natl Acad Sci U S A* 119: e2206075119.

Weinberg RA (1991) Tumor suppressor genes. *Science* 254: 1138–1146.

Weintraub SJ, Prater CA, Dean DC (1992) Retinoblastoma protein switches the E2F site from positive to negative element. *Nature* 358: 259–261.

Wen H, Andrejka L, Ashton J, Karess R, Lipsick JS (2008) Epigenetic regulation of gene expression by Drosophila Myb and E2F2-RBF via the Myb-MuvB/dREAM complex. *Genes Dev* 22: 601–614.

Werwein E, Cibis H, Hess D, Klempnauer K-H (2019) Activation of the oncogenic transcription factor B-Myb via multisite phosphorylation and prolyl cis/trans isomerization. *Nucleic Acids Res* 47: 103–121.

Wyrzykowska J, Schorderet M, Pien S, Gruissem W, Fleming AJ (2006) Induction of differentiation in the shoot apical meristem by transient overexpression of a retinoblastoma-related protein. *Plant Physiol* 141: 1338–1348.

Xu Y, Li Q, Yuan L, Huang Y, Hung F-Y, Wu K, Yang S (2022) MSI1 and HDA6 function interdependently to control flowering time via chromatin modifications. *Plant J* 109: 831–843.

Yao G, Lee TJ, Mori S, Nevins JR, You L (2008) A bistable Rb-E2F switch underlies the restriction point. *Nat Cell Biol* 10: 476–482.

Yee AS, Reichel R, Kovesdi I, Nevins JR (1987) Promoter interaction of the E1A-inducible factor E2F and its potential role in the formation of a multi-component complex. *EMBO J* 6: 2061–2068.

Yoshiyama KO, Kimura S, Maki H, Britt AB, Umeda M (2014) The role of SOG1, a plant-specific transcriptional regulator, in the DNA damage response. *Plant Signal Behav* 9: e28889.

Yunis JJ, Ramsay N (1978) Retinoblastoma and subband deletion of chromosome 13. *Am J Dis Child* 132: 161–163.

Zhang P, Wong C, Liu D, Finegold M, Harper JW, Elledge SJ (1999) p21(CIP1) and p57(KIP2) control muscle differentiation at the myogenin step. *Genes Dev* 13: 213–224.

Zhang W, Tyl M, Ward R, Sobott F, Maman J, Murthy AS, Watson AA, Fedorov O, Bowman A, Owen-Hughes T *et al* (2013) Structural plasticity of histones H3-H4 facilitates their allosteric exchange between RbAp48 and ASF1. *Nat Struct Mol Biol* 20: 29–35.

Zhao X 'ai, Bramsiepe J, Van Durme M, Komaki S, Prusicki MA, Maruyama D, Forner J, Medzihradszky A, Wijnker E, Harashima H *et al* (2017) RETINOBLASTOMA RELATED1 mediates germline entry in Arabidopsis. *Science* 356. doi:10.1126/science.aaf6532.

CHAPTER 1

The DREAM complex represses growth in response to DNA damage in Arabidopsis

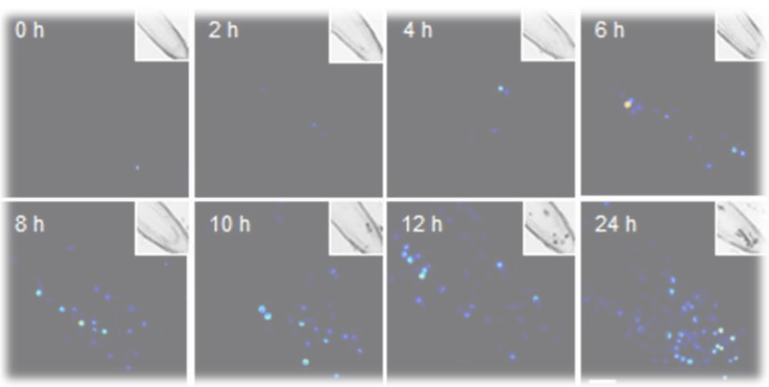

This chapter presents a study published in the journal Life Science Alliance on 28/09/2021. It can be accessed using the doi: 10.26508/lsa.202101141.

The following page shows the cover of Life Science Alliance: Volume 4, No. 12, featuring an image I generated and submitted. I want to further acknowledge contributions to the cover design by F Böwer.

The image description, as featured on the journal's website (www.life-science-alliance.org/content/4/12.cover-expansion, accessed 21/11/2023): "Upregulation of mEGFP-NAC044 (coloured in blue to red) in the tip of an *Arabidopsis thaliana* root that has been treated with a genotoxin. Cell walls as well as cells dying due to excessive DNA damage are stained by propidium iodide and are coloured in magenta (Lang et al.)"

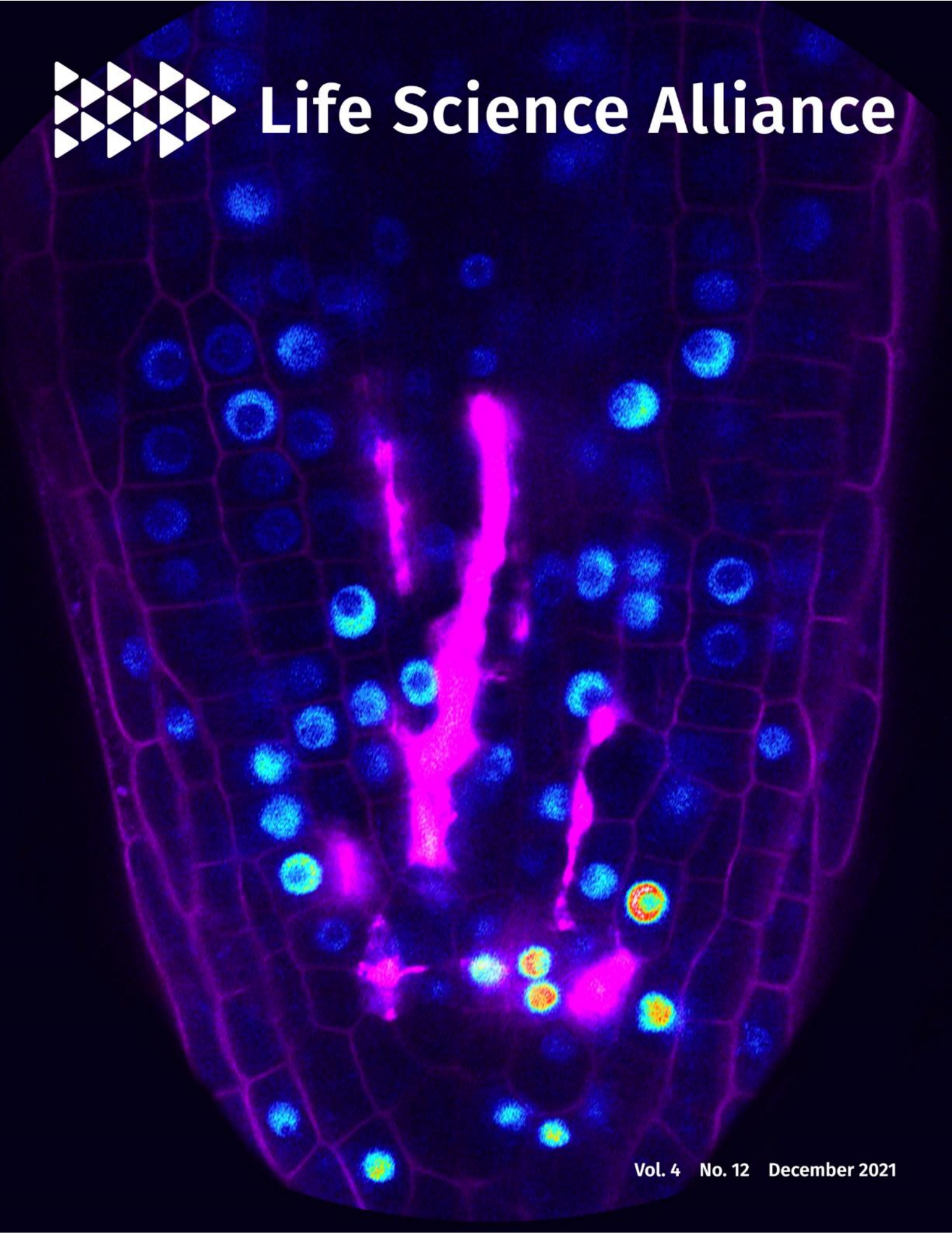

Life Science Alliance

Vol. 4 No. 12 December 2021

Published Online: 28 September, 2021 | Supp Info: http://doi.org/10.26508/lsa.202101141

Research Article

TRANSPARENT PROCESS OPEN ACCESS Life Science Alliance

The DREAM complex represses growth in response to DNA damage in *Arabidopsis*

Lucas Lang[1,*], Aladár Pettkó-Szandtner[2,3,*], Hasibe Tunçay Elbaşı[1], Hirotomo Takatsuka[7], Yuji Nomoto[7], Ahmad Zaki[4,8], Stefan Dorokhov[4], Geert De Jaeger[5,6], Dominique Eeckhout[5,6], Masaki Ito[7], Zoltán Magyar[3], László Bögre[6], Maren Heese[1], Arp Schnittger[1]

The DNA of all organisms is constantly damaged by physiological processes and environmental conditions. Upon persistent damage, plant growth and cell proliferation are reduced. Based on previous findings that RBR1, the only Arabidopsis homolog of the mammalian tumor suppressor gene retinoblastoma, plays a key role in the DNA damage response in plants, we unravel here the network of RBR1 interactors under DNA stress conditions. This led to the identification of homologs of every DREAM component in Arabidopsis, including previously not recognized homologs of LIN52. Interestingly, we also discovered NAC044, a mediator of DNA damage response in plants and close homolog of the major DNA damage regulator SOG1, to directly interact with RBR1 and the DREAM component LIN37B. Consistently, not only mutants in *NAC044* but also the double mutant of the two *LIN37* homologs and mutants for the DREAM component *E2FB* showed reduced sensitivities to DNA-damaging conditions. Our work indicates the existence of multiple DREAM complexes that work in conjunction with NAC044 to mediate growth arrest after DNA damage.

DOI 10.26508/lsa.202101141 | Received 23 June 2021 | Revised 17 September 2021 | Accepted 17 September 2021 | Published online 28 September 2021

Introduction

The DNA of any organism is constantly damaged by intrinsic factors, such as reactive oxygen species and failures in DNA replication, as well as extrinsic conditions, for example, high energy radiation and the uptake of toxic compounds such as aluminum. Common cellular responses to DNA damage ranging from humans to plants include cell cycle arrest, transcriptional induction of DNA repair genes, and cell death to erase damaged cells. Whereas homologous genes between animals and plants are readily found at the level of the repair machinery itself, damage signaling and transcriptional regulation display fundamental differences between these kingdoms (Nisa et al, 2019).

A key DNA damage regulator in humans is the transcription factor p53, which is phosphorylated and thus stabilized after DNA damage, leading to the induction of many DNA repair genes and the repression of cell cycle-promoting genes. Whereas in many cases transcriptional activation by p53 is direct, down-regulation of cell cycle regulators is rather indirect. According to a current model (Hafner et al, 2019), repression is achieved by p53 promoting the transcription of p21, a CDK inhibitor, that leads to a reduction of CDK activity and thus, less phosphorylation of the retinoblastoma protein (pRb)-like proteins p107 and p130. Hypophosphorylated p107/p130 are then incorporated into the transcriptional repressor complex DREAM, composed of DP, pRb-like (p130 or p107), E2F, and the Multivulval class B (MuvB)-core, comprising five additional proteins, LIN9, LIN37, LIN52, LIN54, and RBBP4. In unperturbed cellular conditions, differential MuvB-core interactions are regulated in a cell cycle-specific manner, and the transcription-repressing DREAM complex is restricted to G0 and early G1 cells. In contrast to its homologs, the tumor suppressor pRb itself is not found as part of a DREAM complex but exerts its repressive function independently (Fischer & Müller, 2017). Thus, p53-mediated down-regulation of cell cycle genes after DNA damage can be separated into the repression of G1/S genes by mainly pRb, with some contribution of p130 and p107, and the repression of G2/M genes by p130 and p107 (Schade et al, 2019). In addition, the atypical E2F and transcriptional repressor E2F7, which is under direct transcriptional control of p53, is thought to function in conjunction with pRb and DREAM to mediate repression of cell cycle-related genes (Carvajal et al, 2012).

Notably, p53 is not conserved in all eukaryotes and a p53 homolog has not been identified in plants. Instead, the transcriptional regulator SOG1 is central to signal transduction after DNA damage (Yoshiyama et al, 2009; Yoshiyama, 2016). Upon DNA stress, SOG1 is

[1]Department of Developmental Biology, University of Hamburg, Institute for Plant Sciences and Microbiology, Hamburg, Germany [2]Laboratory of Proteomic Research, Biological Research Centre, Szeged, Hungary [3]Institute of Plant Biology, Biological Research Centre, Szeged, Hungary [4]Department of Biological Sciences, Centre for Systems and Synthetic Biology, Royal Holloway University of London, Egham, UK [5]Department of Plant Biotechnology and Bioinformatics, Ghent University, Ghent, Belgium [6]Vlaams Instituut voor Biotechnologie (VIB) Center for Plant Systems Biology, Ghent, Belgium [7]School of Biological Science and Technology, College of Science and Engineering, Kanazawa University, Kanazawa, Japan [8]School of Life Sciences, University of Warwick, Coventry, UK

Correspondence: maren.heese@uni-hamburg.de; arp.schnittger@uni-hamburg.de
*Lucas Lang and Aladár Pettkó-Szandtner contributed equally to this work

Life Science Alliance

phosphorylated and thus activated by the stress sensor kinases ATM/ATR (Yoshiyama et al, 2014). Similar to p53, SOG1 is upstream of a broad transcriptional program eventually leading to DNA repair, cell cycle arrest, cell differentiation, and/or cell death (Yoshiyama, 2016). SOG1 is, for example, a direct positive regulator of DNA repair genes as well as of the CDK inhibitors SMR5 and SMR7 and two closely related SOG1 homologs, NAC044 and NAC085 (Bourbousse et al, 2018). Although transcriptional targets of NAC044 and NAC085 are currently unknown, they have been hypothesized to indirectly control the stability of MYB3R3, a repressive transcription factor, shown to act on mitotic genes (Takahashi et al, 2019).

In contrast to p53, pRb-like proteins are greatly conserved between plants and animals. Previous work indicated that the only Arabidopsis pRb homolog RETINOBLASTOMA-RELATED 1 (RBR1) is another key regulator of the DNA damage response (DDR). On the one hand, RBR1 was found to accumulate in foci in the nucleus, to work together with the BREAST AND OVARIAN CANCER TYPE 1 SUSCEPTIBILITY PROTEIN (BRCA1) (Horvath et al, 2017), and to be necessary for the recruitment of the DNA repair machinery, such as RAD51, to DNA lesions (Biedermann et al, 2017). On the other hand, RBR1 was found to associate with promoters of many DDR genes and to regulate their expression in a SOG1-independent manner (Biedermann et al, 2017; Horvath et al, 2017; Bouyer et al, 2018), an interaction that likely represents a priming mechanism and couples DNA repair genes with cell proliferation.

Apart from its DNA damage targets, RBR1 has been shown to bind promoters of genes related to different cell cycle phases (Bouyer et al, 2018), and DREAM-like complexes have been identified to differentially regulate cell division activity also in plants (Kobayashi et al, 2015; Fischer & Müller, 2017). Interestingly, in this context, the existence of not only repressing but also activating DREAM complexes, depending on the type of MYB3R and E2F homologs involved, has been postulated. The complex activating mitotic genes was found to at least contain ALY3 (LIN9 homolog), TCX5 (LIN54 homolog), CDKA1, RBR1, MYB3R4, E2FB, and DPA/B, whereas for a presumptive repressive complex ALY2, ALY3, TCX5, RBR1, MYB3R3, and E2FC have been shown to interact. However, homologs of the MuvB-core components LIN37, LIN52, and RBBP4 have not been detected in this study (Kobayashi et al, 2015). Recently, TCX5/6-containing multi-subunit complexes were found to promote DNA demethylation in Arabidopsis by repressing DNA methylation genes. In addition to the previously described DREAM components these complexes also included the RBBP4 homolog MSI1, two LIN37 homologs as well as two uncharacterized proteins termed DREAM COMPONENT 1 (DRC1) and DREAM COMPONENT 2 (DRC2) (Ning et al, 2020). In addition, different plant homologs of LIN54, namely, TSO1, TCX2 (SOL2), TCX3 (SOL1), and TCX8, have been shown to be involved in different developmental processes, for example, in reproductive development (Liu et al, 1997; Hauser et al, 2000; Song et al, 2000; Andersen et al, 2007; Sijacic et al, 2011), the formation of stomata (Simmons et al, 2019) and tracheary elements (Clark et al, 2019), as well as senescence (Noh et al, 2021). However, the formation of a DREAM complex remained hypothetical in these contexts. Moreover, our knowledge on plant DREAM composition is still patchy and for instance, pairwise interaction assays among the identified components have only been performed to a limited extent (Ning et al, 2020).

Unraveling the RBR1 interactome upon DNA damage, we have identified here homologs of all core DREAM complex components known from humans and animals. By analyzing the composition of the DREAM complex under DNA damage as well as several other growth-modifying conditions, we have obtained a robust atlas of DREAM complex composition in Arabidopsis and have systematically mapped the interaction network of its constituents by binary interaction assays. Furthermore, we show that the SOG1 homolog NAC044 interacts with RBR1 in an LxCxE motif-dependent manner and functions in conjunction with the DREAM complex to suppress growth upon DNA damage.

Results

Identification of a plant complement of the animal DREAM complex proteins

To explore the RBR1 interactome upon DNA damage, we performed tandem affinity purification (TAP) assays (Van Leene et al, 2015) using cell cultures expressing N-terminally tagged RBR1 as bait. For DNA damage induction, we added the genotoxin cisplatin, a DNA cross-linker, 16 h before harvest. The experiment was performed in duplicate and resulted in the identification of 16 interactors, 15 of which passed the background threshold in both assays (Fig 1 and Tables S1 and S2). Notably, homologs of most components of the animal DREAM complex were found, including a protein with homology to LIN52, a DREAM component previously not recognized as such in plants (Kobayashi et al, 2015; Ning et al, 2020), and that we therefore named LIN52A (AT2G45250; Fig S1). To verify these interactions, reciprocal TAPs were performed in duplicates, again after 16 h of cisplatin treatment, taking N- and C-terminal fusions of TCX5 and LIN52A as bait proteins. This approach led to the identification of additional DREAM components, such as LIN37 and MYB3R proteins, as well as a second homolog of LIN52 (AT4G38280), named LIN52B, thus resulting in an entire equivalent of the mammalian DREAM complex (Fig 1 and Tables 1, S1, and S2).

Except for RBR1, Arabidopsis contains more than one homolog of each DREAM component, and for some components different family members were identified in our TAP experiments suggesting the existence of several versions of the DREAM complex after DNA damage treatment. However, our data also indicate specificity because only two of the eight Arabidopsis LIN54 homologs were identified, that is, TCX5 and TCX6. Whereas TCX5 was detected in all five experimental setups, TCX6 was found only in the one using N-terminally tagged LIN52A as a bait. For RBBP4, there are five homologs in Arabidopsis, called MSI1 to MSI5, but only MSI1 was identified in our experiments, yet consistently in all five assays. For LIN52, two homologs were co-purified, also here with a clear bias for one member, LIN52A, which was detected in five of five assays, whereas LIN52B was only found when N-terminally tagged TCX5 was used as bait. Whereas the Arabidopsis LIN9 homologs ALY1 and ALY2 were only present in the RBR1 and TCX5 TAP experiments, ALY3 was additionally found in both LIN52A experiments. We also found MYB3R3, which was previously shown to act as a repressive transcription factor, as well as MYB3R1, which has both activating and repressive functions, in the TCX5 TAP experiments. In addition, we

Life Science Alliance

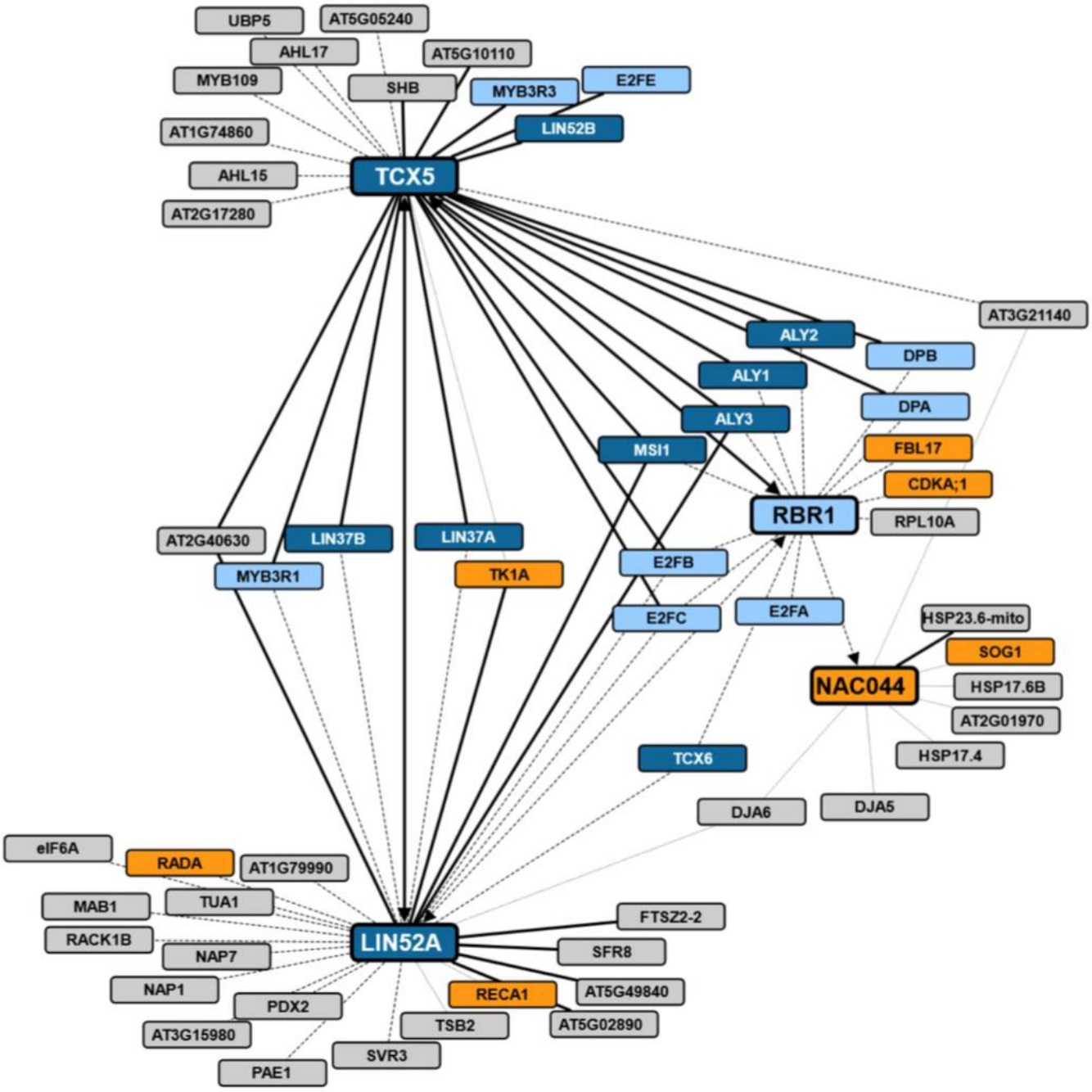

Figure 1. Overview of tandem affinity purification (TAP) results from cisplatin-treated cell cultures.
Cytoscape representation of all TAP experiments from cisplatin-treated cell culture. Proteins taken as baits are shown in large rectangles, proteins only found as prey are represented by small rectangles. TAPs with NAC044, LIN52A, and TCX5 as bait were performed with both N-terminally and C-terminally tagged proteins. Thick black edges indicate that the corresponding prey was detected with both tags, whereas dashed and dotted edges denote detection only with N-terminal and C-terminal tagging, respectively. For RBR1, only an N-terminally tagged version was used. If an edge connects two proteins which both served as bait in different experiments, arrowheads indicate which proteins have been found as prey. Dark blue: MuvB-core proteins; light blue: other DREAM components; orange: known DNA damage regulators; grey: other interactors.

observed apparent specificity in the family of E2F transcription factors. Whereas E2FB and E2FC were found in complex with RBR1, TCX5, and LIN52A as bait, E2FA was only found with RBR1 and the atypical E2FE (DEL1) only with TCX5.

In previously performed GFP-pulldown experiments using MYB3R proteins as baits, the key cell cycle kinase CDKA;1 was co-purified and thus suggested to be part of plant DREAM-like complexes (Kobayashi et al, 2015). Consistently, we also found CDKA;1 when we used RBR1 as

Life Science Alliance

Table 1. Arabidopsis sequence homologs of DREAM components and their presence in different affinity purifications.

Human DREAM	Arabidopsis homologs		TAP results from cisplatin-treated cell culture					FP-IP results from seedlings					
Type	AGI	Alias	TAG-RBR1	TAG-LIN54A	LIN54A-TAG	TAG-LIN52A	LIN52A-TAG	E2FA-GFP	E2FB-GFP	E2FC-GFP	RBR1-GFP	DPA-GFP	DPB-3xCFP
MYBL2	AT4G32730	MYB3R1		x	x	x							
	AT5G00540	MYB3R2											
	AT3G09370	MYB3R3		x	x								
	AT5G11510	MYB3R4											
	AT5G02320	MYB3R5											
E2F	AT2G36010	E2FA	X					x			x	x	x
	AT5G22220	E2FB	X	x	x	x			x		x	x	x
	AT1G47870	E2FC	X	x	x	x				x	x	x	x
	AT5G14960	E2FD/DEL2											
	AT3G48160	E2FE/DEL1		x	x								
	AT3G01330	E2FF/DEL3											
DP	AT5G02470	DPA	X	x				x	x	x	x	x	
	AT5G03415	DPB	X	x	x			x	x	x	x		x
RBL	AT3G12280	RBR1	X	x	x	x		x	x	x	x	x	x
LIN9	*AT5G27610*	*ALY1*	*X*	*x*	*x*				*x*	*x*	*x*		*x*
	AT3G05380	*ALY2*	*X*	*x*	*x*				*x*	*x*			*x*
	AT3G21430	*ALY3*	*X*	*x*	*x*	*x*	*x*		*x*	*x*	*x*	*x*	*x*
LIN54	*AT3G22780*	*TSO1*											
	AT4G14770	*TCX2/SOL2*											
	AT3G22760	*TCX3/SOL1*											
	AT3G04850	*TCX4*											
	AT4G29000	*TCX5/LIN54A*	*X*	*x*	*x*	*x*	*x*		*x*	*x*	*x*	*x*	*x*
	AT2G20110	*TCX6/LIN54B*				*x*							
	AT5G25790	*TCX7*											
	AT3G16160	*TCX8*											
LIN37	*AT1G04930*	*LIN37A*		*x*	*x*	*x*			*x*	*x*	*x*		*x*
	AT2G32840	*LIN37B*		*x*	*x*	*x*				*x*			*x*
LIN52	*AT2G45250*	*LIN52A/DRC1*	*X*	*x*	*x*	*x*	*x*		*x*	*x*	*x*	*x*	*x*
	AT4G38280	*LIN52B*		*x*									
RBBP4	*AT5G58230*	*MSI1*	*X*	*x*	*x*	*x*	*x*		*x*	*x*	*x*	*x*	*x*
	AT2G16780	*MSI2*											
	AT4G35050	*MSI3*											
	AT2G19520	*MSI4*									*x*		
	AT4G29730	*MSI5*											

This table summarizes which Arabidopsis sequence homologs of known DREAM components have been identified by different complex purification approaches from different biological materials. For quantitative information, see Tables S2–S4. MuvB-core candidates are written in italics. Homologs which have not been significantly enriched in any of our experiments are written in grey.

Life Science Alliance

a bait. However, CDKA;1 was not identified when we performed the experiment with one of the MuvB-core components tagged, that is, TCX5 or LIN52A. It was previously found that CDKB1 kinases have partially overlapping functions with CDKA;1, with CDKB1 playing a specific role during DNA damage (Nowack et al, 2012; Weimer et al, 2016). However, besides CDKA;1, we never retrieved any of the other 12 CDK proteins in our TAP experiments.

To corroborate our findings on the composition of the DREAM complex in plants, we performed pulldown experiments using young seedlings of Arabidopsis plants, where either RBR1 or one of the three E2F proteins tagged with GFP at their C-termini were expressed under the control of their own promoters (Kobayashi et al, 2015; Horvath et al, 2017). We identified and quantified proteins associating with E2FA-GFP, E2FB-GFP, E2FC-GFP, and RBR1-GFP against proteins interacting with the control GFP alone in six replicates each using label-free mass spectrometry (Lokdarshi et al, 2020). To certify interactors with statistical confidence, we computed the false discovery rate (FDR) and the amount ratio between proteins identified with the relevant baits versus GFP-only pulldowns and established thresholds as visualised in volcano plots (Fig S2A–D). The results show that among the proteins that co-precipitated with RBR1, E2FB, and E2FC from seedling extracts, we indeed found MuvB-core proteins, whereas these were completely absent from the E2FA pulldown experiments. Besides the DREAM components, we could also identify other interactors specific to RBR1 and the different E2F family members, suggesting functions linked to RNA binding and translational control (Lokdarshi et al, 2020) as well as chromatin organization (Table S3). Although our results are in accordance with previous experiments showing that homologs of the MuvB-core components LIN54 and LIN9 can be co-precipitated with E2FB-GFP and E2FC-GFP but not E2FA-GFP (Kobayashi et al, 2015), we additionally find homologs of LIN52 and RBBP4 in complex with E2FB and E2FC, indicating the presence of a complete set of DREAM proteins not only in our cisplatin-treated cell culture but also in untreated seedlings.

With the aim to comprehensively identify recurring interactors of RBR1 and the E2F/DP modules in seedlings, we performed a meta-analysis on a large set of pulldown mass spectrometry data generated from C-terminally GFP or CFP-tagged RBR1, E2FA, E2FB, E2FC, DPA, and DPB lines under a variety of growth-promoting and growth-restricting environmental conditions. In total, 182 IPs were performed and analyzed (50 GFP, 35 E2FA, 39 E2FB, 20 E2FC, 32 RBR1, 3 DPA, and 3 DPB). EdgeR statistical analyses were used on the spectral counts of all pulldown data and 217 preys passed a threshold of eight fold change (FC) and a p of 0.05 (Table S4). Fig 2 displays a reduced dataset as only prey proteins which were enriched in at least one-third of the IPs of one bait are shown (105 proteins). The vast size of the interactome likely reflects the multiple functions of RBR1 and E2F/DP. For example WIN2, PDF2.2, RIN4, and MOS1 (Table S4) might provide a molecular link to pathogen response, which is interesting in the light of the finding that the RBR1/E2F pathway has been shown to control programmed cell death in plant immunity (Wang et al, 2014). In the following, we focus on interactions relating to the DREAM complex.

The set of potential DREAM complex subunits found in seedlings under varying conditions largely matched what we observed in the cisplatin-treated cell culture (Tables S1 and S4). While LIN52A, TCX5, LIN37A/B, ALY1/2/3, MSI1, DPA/B, E2FA/B/C, and RBR1 were identified in both approaches, only LIN52B and E2FE (DEL1) were found specifically in the cisplatin-treated cell culture. However, these proteins were not present in the RBR1 TAP experiment but only when the MuvB-core components were used as bait. With respect to the Arabidopsis LIN9 homologs, there is a clear bias in the frequency of experiments by which ALY3 was found with respect to the other two ALYs, with ALY3 clearly being the most prominent. Apart from what is shown in Fig 2 and Table S4, CDKA;1, MSI4, TCX6, as well as MYB3R3 and MYB3R1 were also present in some pulldown experiments from seedlings, but did not pass the more stringent selection criteria applied for the meta-analysis. With respect to E2FA, our data consistently showed that this E2F homolog is never found in complex with MuvB-core components in vivo, neither in the cisplatin-treated cell culture nor in seedlings grown under different conditions, whereas it could be readily co-purified with DP and RBR1.

Interestingly, a couple of proteins which appear to be unrelated to the animal DREAM complex were found in the TAPs of the MuvB-core components as well as in our FP-pulldown approaches, that is, the uncharacterized protein AT2G40630 (DRC2), which was found previously in complex with MSI1, LIN37B, and ALY3 (Derkacheva et al, 2013; Ning et al, 2020) and seems plant-specific, the EUKARYOTIC INITIATION FACTOR 6A (eIF6A), as well as a protein involved in pyridoxine biosynthesis (PDX2) (Fig 1 and Tables S1 and S4). Although beyond the scope of this investigation, it will be interesting to see whether and if so how they relate to DREAM function.

A binary interaction atlas of the plant DREAM complex and implications of the LxCxE motif

To complement our data derived from the different complex isolation approaches, we performed yeast two-hybrid (Y2H) assays to establish an atlas of binary interactions for all of the here-identified Arabidopsis DREAM components (Fig 3A and B). In general, we see differences for a given protein pair depending on which interaction partner is fused to the activation (AD) or DNA-binding domain (BD), most likely due to folding differences of the different fusion proteins and 3D assembly of the reconstituted transcription factor. Interestingly, we also see differences in the interaction matrix between the different homologs, which might indicate the preferential formation of certain complex variants, although we cannot exclude a Y2H bias. In the following, we interpret our matrix as showing binding potential and describe the maximally observed interactions for each DREAM component. For more detailed, homolog-specific information, please refer to Fig 3A and B.

Considering the five members of the MuvB-core complex (ALY, LIN37, LIN52, TCX, and MSI), we found that LIN37 interacts with every component except ALY, whereas TCX binds RBR1, LIN37, and ALY in our Y2H system. Further, ALY associates with LIN52 and MSI, adding to an intricate interaction network among the plant MuvB-core members. Consistent with previous experiments, we found that the typical E2F transcription factors directly bind DP and RBR1 (Kosugi & Ohashi, 2002; del Pozo et al, 2006; Boruc et al, 2010; Magyar et al, 2012, 2005). In addition, our Y2H data indicate that contact of typical E2Fs to the MuvB-core occurs likely via LIN37, whereas the only MuvB-core RBR1 interaction interface seems to be on TCX. Notably,

Life Science Alliance

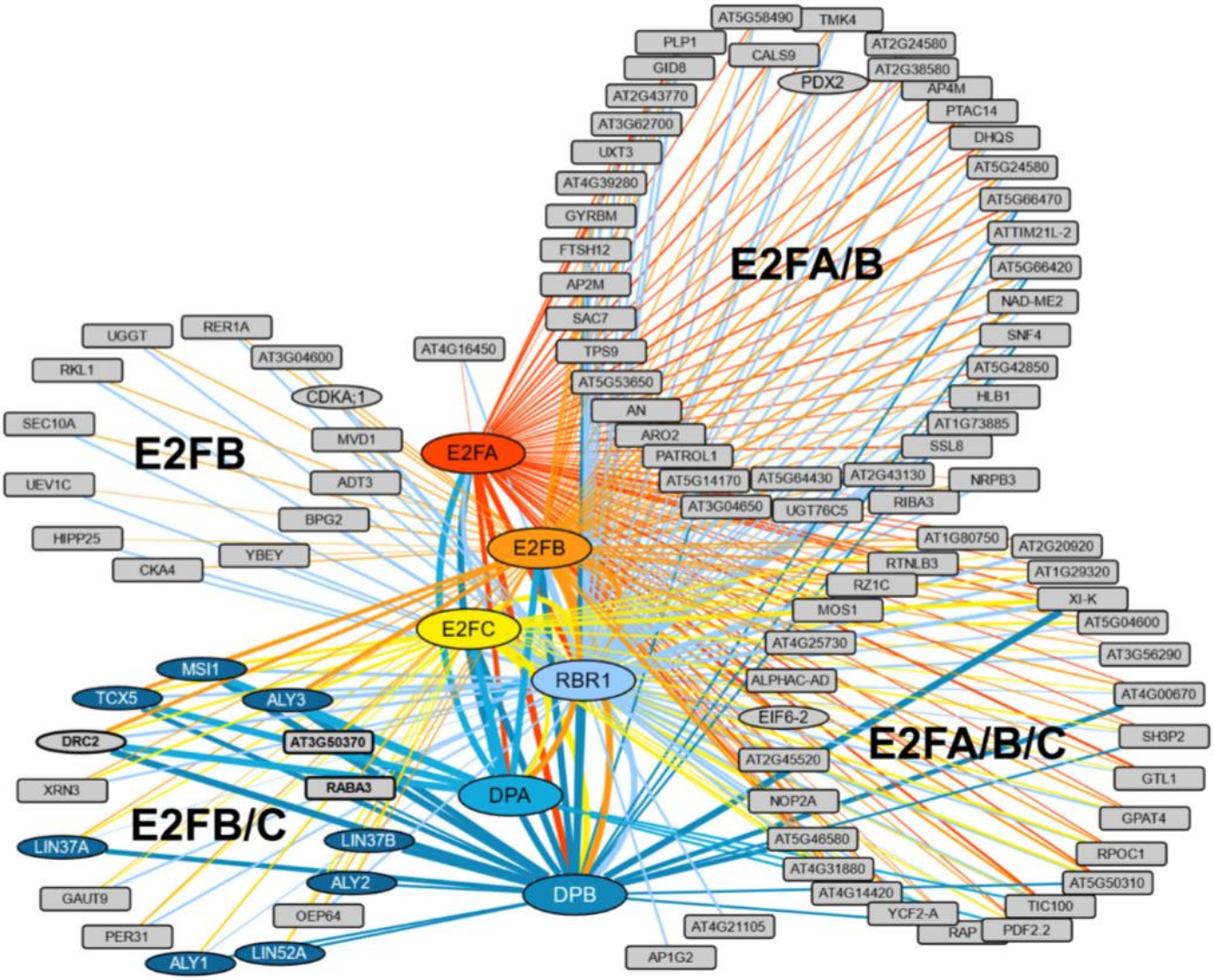

Figure 2. Meta-Analysis of FP-IP results from seedlings.
Cytoscape representation of a meta-analysis of 182 FP-IPs using different bait proteins (35 × E2FA-GFP [blue], 39 × E2FB-GFP [red], 20 × E2FC-GFP [green], 32 × RBR1-GFP [yellow], 3 × DPA-GFP [orange], and 3 × DPB-CFP [pale-orange], 50 × GFP [control]). To reduce complexity, only prey proteins which were enriched in at least one third of the IPs of one bait are shown. For the more comprehensive dataset, see Table S4. The thickness of the edges corresponds to the frequency of positive IPs by which a bait/prey interaction was found. Proteins that were also identified in the tandem affinity purification experiments are represented by an ellipse. Prey proteins are grouped according to their occurences in different E2F-IPs. DREAM complex homologs are shown in dark blue. Additional proteins that display an interaction pattern like the DREAM component homologs, that is, do not interact with E2FA, but interact with E2FB/C and the DPs, are shown in bold with a thick outline.

the E2F dimerization partner DP is capable of binding both TCX and LIN37. As expected, the atypical E2F transcription factor E2FE (DEL1) does neither bind DP nor RBR1 but it is capable of interacting with three MuvB-core components, that is, LIN37, TCX, and LIN52. In contrast to the rather distinct association of the E2F/DP-RBR1 module with the MuvB-core, interaction of the latter with the MYB3R proteins seems to occur via multiple interfaces because we see interaction of MYB3R with all five core proteins, albeit of different strength, in the Y2H analyses. Finally, dimerization seems to be frequent among plant DREAM members, as found it not only for MYB3R3, but also for LIN37, LIN52, and TCX. In addition dimerization is also seen for the atypical E2FE.

While our pulldown data clearly show the existence of complete DREAM complexes in Arabidopsis when compared to the human version, protein–protein contact points within these complexes likely have shifted, as exemplified by the RBR1 MuvB-core interface. Pocket proteins like pRb contain a region called LxCxE binding cleft, which is bound by proteins displaying a signature similar or identical to the so-called LxCxE motif. In the human DREAM complex, the LxCxE binding cleft of p107 is bound by LIN52 (Guiley et al, 2015). However, the LxSxExL motif in HsLIN52, which is responsible for this interaction, is not conserved in the Arabidopsis LIN52 homologs (Fig S1), and when tested by Y2H assay, no direct interaction between RBR1 and LIN52A or LIN52B could be found

Life Science Alliance

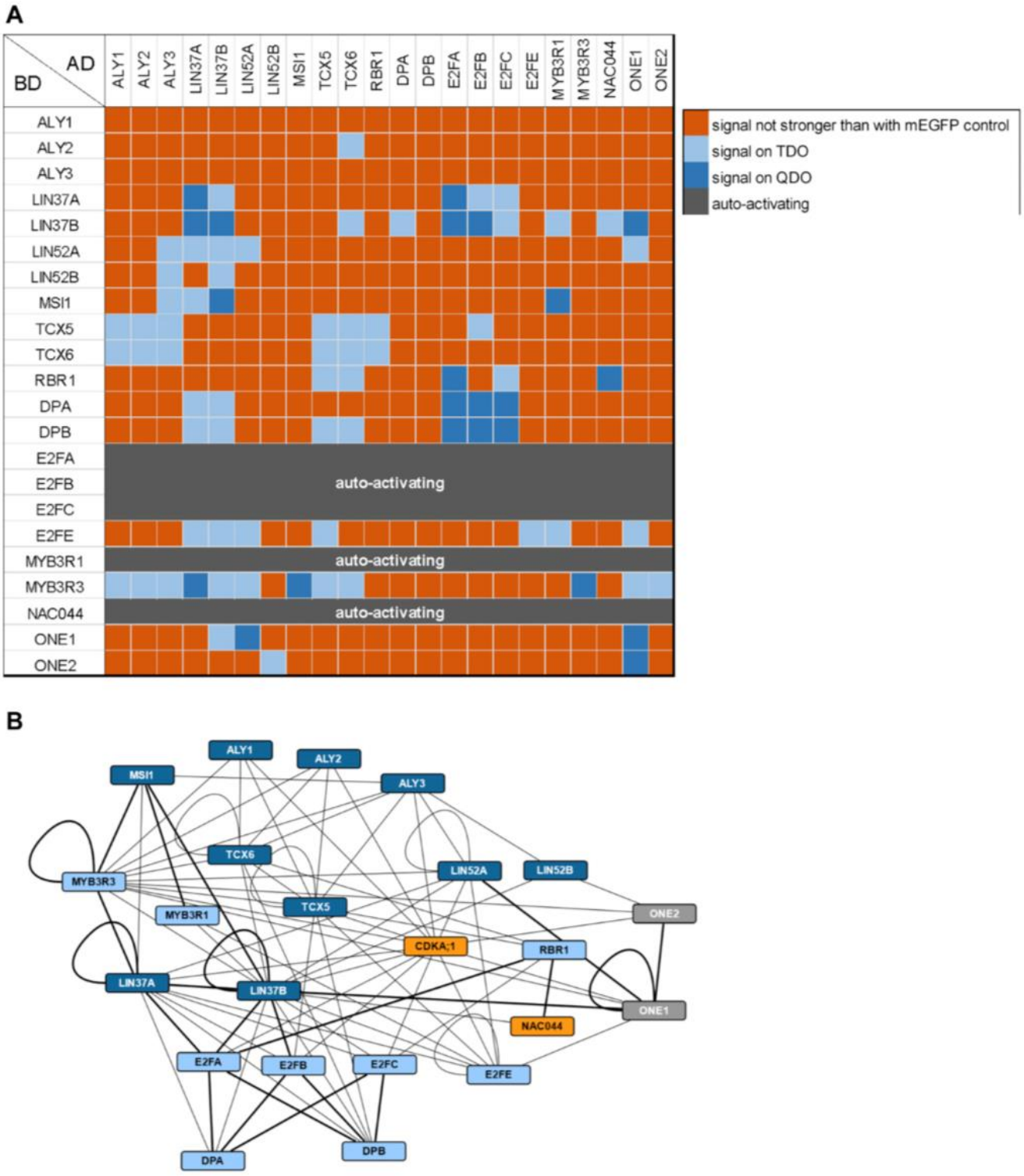

Figure 3. Binary interactions of DREAM complex components and additional proteins.
Results of Y2H assays testing the here-identified DREAM complex components and selected additional proteins for binary interactions. AD, activating domain; BD, DNA-binding domain. **(A)** Interaction matrix. Signal strength was classified according to yeast growth on different dropout media in two categories and is indicated by shades of blue. Dark blue, signal on QDO; light blue, signal on TDO but not on QDO; orange, signal not stronger than with mEGFP control; dark grey, strong auto-activation observed using the BD construct and an AD-mEGFP control. **(B)** Cytoscape representation of the observed interaction network. Interactions are indicated by an edge between two protein nodes and were classified according to yeast growth in two categories. If yeast growth was observed with a pair of proteins in both AD/BD combinations, the stronger signal is shown. Thick line, growth on QDO; thin line, growth on TDO but not on QDO. Dark blue, MuvB-core proteins; light blue, other DREAM components; orange, known DNA damage regulators; grey, other interactors.

Life Science Alliance

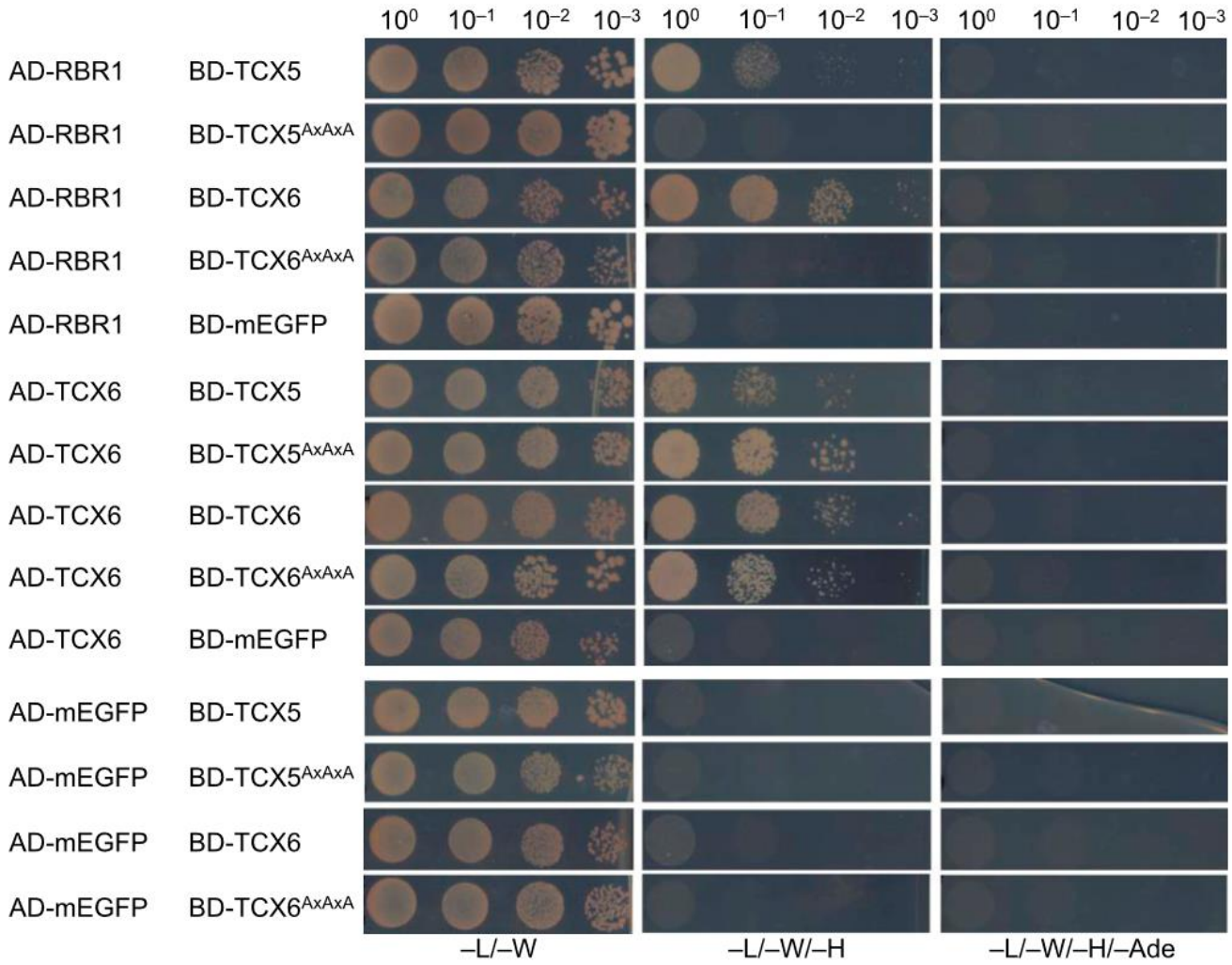

Figure 4. The LxCxE motif of TCX5 and TCX6 is essential for interaction with RBR1.
Y2H interaction assays to test for binary interaction of wild type as well as mutant TCX5 and TCX6 with RBR1, TCX6, and mEGFP as auto-activation control. AxAxA replaces the LxCxE motif in the mutant proteins. AD, activating domain; BD, DNA-binding domain. Yeast cells were diluted as shown on top and spotted on different dropout media as indicated below. Growth on TDO and QDO indicates interaction.

(Fig 3A). Supporting this notion, Arabidopsis TCX5 and TCX6, the two LIN54 homologs identified in our pulldown experiments and interactors of RBR1 in the Y2H assays, both contain an LxCxE motif, which is not present in their human counterpart (Fig S3). When we mutated this motif in TCX to AxAxA, the interaction with RBR1 was abolished, whereas dimerization with TCX6 was still possible (Fig 4), indicating that loss of RBR1 binding was not due to complete misfolding of the TCX proteins but dependent on a functional LxCxE motif.

Interestingly, not all LIN54 homologs in Arabidopsis carry an LxCxE motif and the region surrounding the motif in TCX5 is only conserved in TCX6 and TCX7 (Fig S3) (Andersen et al, 2007). Consistently, when testing non-LxCxE-bearing homologs, for example, TCX2 (SOL2), TCX3 (SOL1), and TSO1 in combination with RBR1 in the Y2H system, we could not detect any interaction while binding assays with the MYB3R3 transcription factor were positive, indicating that lack of yeast growth in combination with RBR1 was not due to a technical problem with the TCX2, TCX3, and TSO1 constructs per se (Fig S4). Furthermore, none of the LIN54 homologs without LxCxE were found in any of our pulldown experiments although, according to publicly available transcriptome data, at least some of them are well expressed in seedlings and cell culture (Andersen et al, 2007) (Fig S5A and B).

NAC044 links the RBR1 interactome to DNA damage

Apart from DREAM complex components, we also found the transcriptional regulator NAC044 in our RBR1 TAPs performed with cisplatin-treated cell culture (Fig 1 and Tables S1 and S2). NAC044 is a close homolog and transcriptional target of the major DNA damage regulator SOG1 and has recently been shown to limit root growth after DNA damage (Takahashi et al, 2019). However, how the latter is achieved molecularly is still unknown.

When we performed reciprocal TAP experiments using N- and C-terminally tagged versions of NAC044 as bait, we identified SOG1

Life Science Alliance

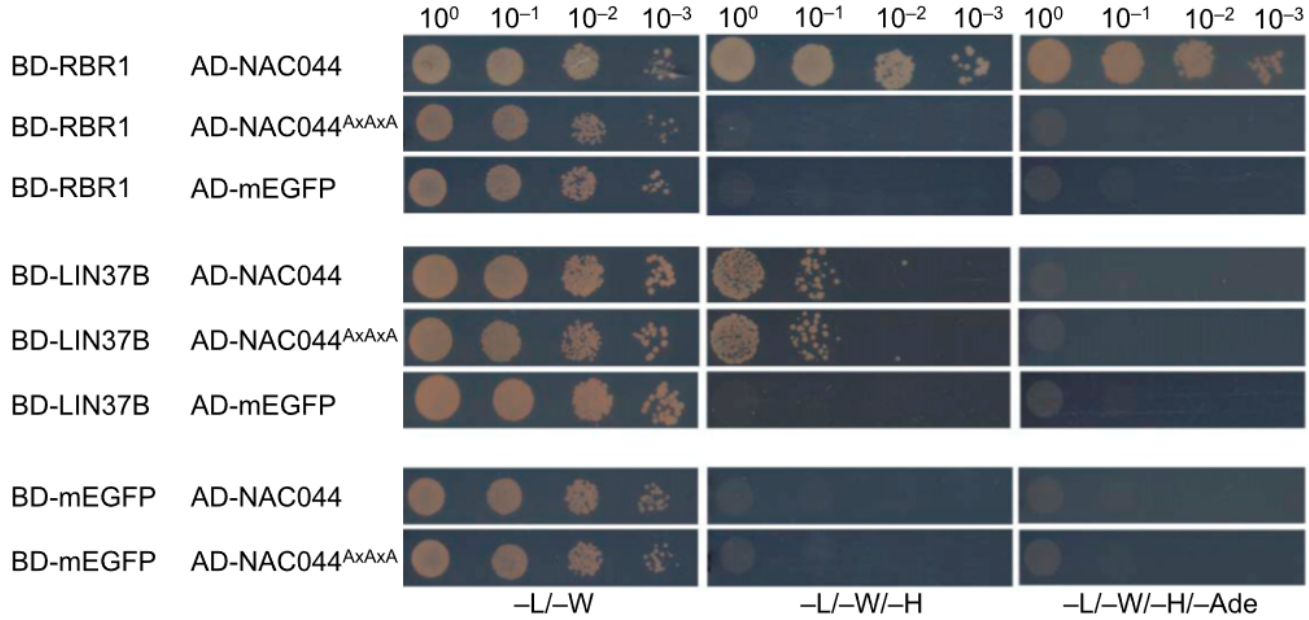

Figure 5. The LxCxE domain of NAC044 is essential for interaction with RBR1.
Y2H interaction assays to test for binary interaction of wild type as well as mutant NAC044 with RBR1, LIN37B, and mEGFP as auto-activation control. AxAxA replaces the LxCxE motif in the mutant NAC044. AD, activating domain; BD, DNA-binding domain. Yeast cells were diluted as shown on top and spotted on different dropout media as indicated below. Growth on TDO and QDO indicates interaction.

as an interactor of C-terminally tagged NAC044, whereas none of the DREAM components were co-precipitated at a significant level. However, RBR1 could be identified in the background when using C-terminally tagged NAC044 as bait corroborating their interaction (Table S2). In addition, common interactors of NAC044 and LIN52A as well as NAC044 and TCX5 were found in the affinity purifications, that is, AT2G22360 (DJA6) and AT3G21140, respectively (Tables S1 and S2 and Fig 1). Since AT3G21140 has been so far uncharacterized, we named it ONEIRIC 1 (ONE1; oneiric meaning "relating to dreams or dreaming"), reflecting its potential relation to the DREAM complex.

To more directly assay if NAC044 might be part of an extended DREAM complex, we performed Y2H interaction assays between NAC044 and all DREAM components identified in this project as well as the common interactor ONE1 and its close homolog ONE2 (AT1G51560) (Fig 3A and B). Whereas NAC044 fused to the Gal4 DNA-binding domain (BD-NAC044) was auto-activating and could not be analyzed in the Y2H assays, NAC044 fused to the activation domain (AD-NAC044) strongly interacted with RBR1 and at moderate strength with LIN37B. The interaction with SOG1 could not be tested in Y2H, because SOG1 was also auto-activating when fused to the DNA-binding domain. Intriguingly, NAC044 also contains an LxCxE motif located at amino acids 303–307 and we wondered if this was relevant for RBR1 interaction. Therefore, we generated a NAC044 version in which the LxCxE motif was changed to AxAxA and re-tested the respective mutant for interaction with RBR1 as well as LIN37B (Fig 5). Whereas RBR1 interaction was clearly abolished in the mutant, the interaction with LIN37 remained, indicating that the induced mutation did not lead to a completely misfolded protein but specifically abolished RBR1 binding.

In the Y2H system, ONE1 showed interactions with LIN37B, LIN52A, E2FE, MYB3R3, and the ability to homodimerize as well as heterodimerize with its homolog ONE2. ONE2 on the other hand is bound weakly by LIN52A and MYB3R3 as well. Although these results are in favor of an in vivo involvement of ONE1 and ONE2 with DREAM complex components, a direct interaction with NAC044 could not be demonstrated by Y2H.

Dynamics of NAC044 and selected DREAM components after DNA damage

NAC044 has been shown to be a transcriptional target of SOG1 and its mRNA accumulates upon DNA damage (Bourbousse et al, 2018; Takahashi et al, 2019). To monitor protein amount and localization with and without DNA damage, we generated a genomic reporter where the coding sequence of *mEGFP* was inserted right before the start codon of *NAC044*. This construct was considered functional as it complemented the *nac044-1* growth phenotype upon cisplatin treatment (Fig S6A–D). When we analyzed root tips of the reporter line grown on control plates for protein expression, we did not find any mEGFP signal in most of the cells. However, occasionally we saw strong nuclear accumulation of mEGFP-NAC044 in isolated cells in different tissue layers of the root. Next, we monitored NAC044 abundance upon treatment with 50 μM cisplatin. Time point zero corresponds to what we observed in untreated roots, that is, very few, apparently randomly located cells with clear nuclear fluorescence signal (Fig 6A). Beginning at 6–8 h after treatment onset, we saw enhanced nuclear mEGFP accumulation that reached a maximum after 24 h and could be observed in nearly all cells of the root tip. However, the fluorescence intensity was very different between different cells, resulting in a salt-and-pepper-like pattern (Fig 6A). Consistent with the observation that NAC044 protein is largely absent from roots in non-stressed conditions, we never found NAC044 in any of the pulldown experiments from seedlings (Table S4).

Life Science Alliance

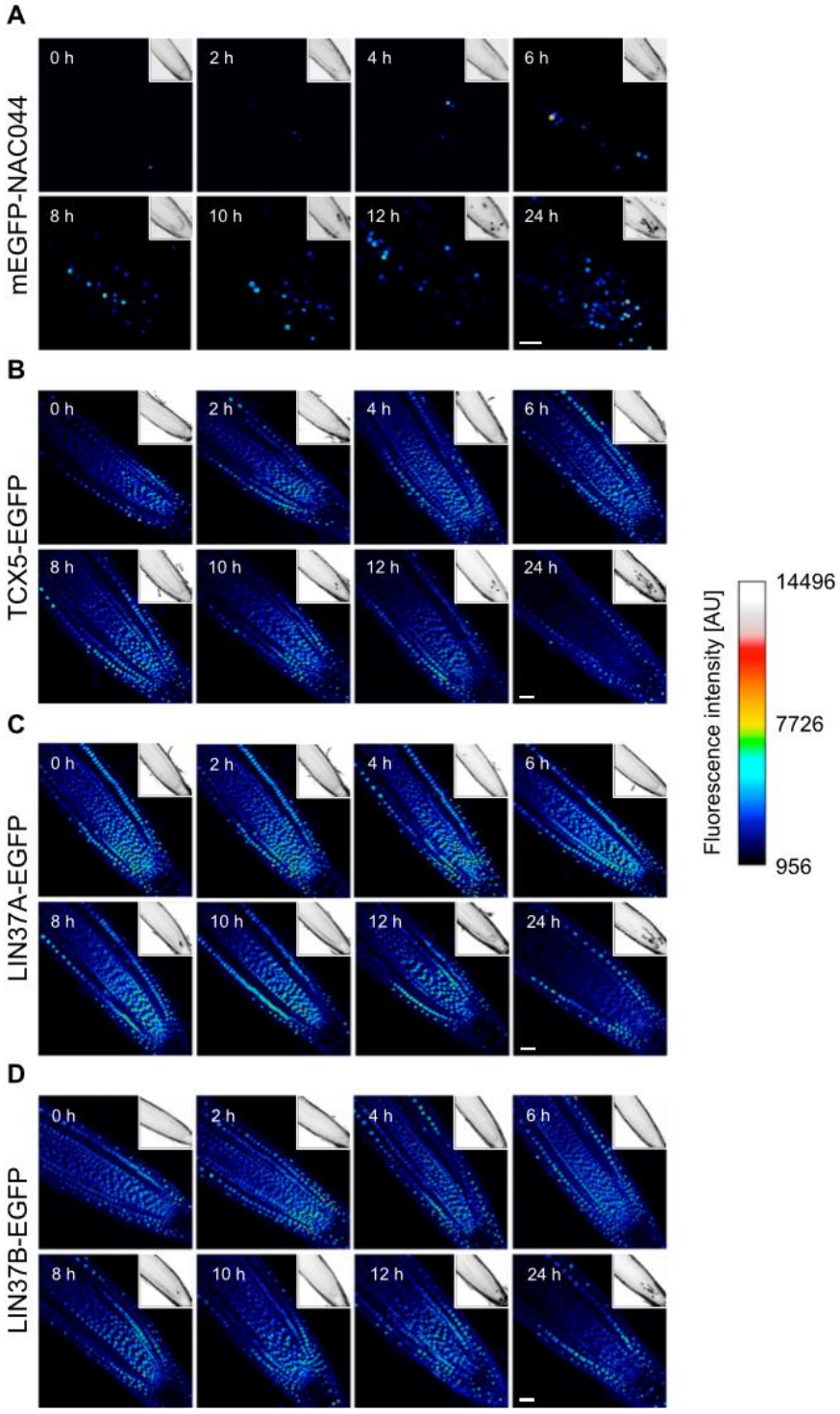

Figure 6. Time course of NAC044, TCX5, LIN37A, and LIN37B protein expression after cisplatin treatment.
(A, B, C, D) Using genomic reporter lines to include the native regulatory sequences, expression of mEGFP-NAC044 (A), TCX5-EGFP (B), LIN37A-EGFP (C), and LIN37B-EGFP (D) was followed for 24 h after transfer of 6-d-old seedlings to 50 μM cisplatin-containing plates. Representative images of root tips at different time points, as indicated in the upper left corner of each panel, are shown here using the royal LUT in ImageJ. PI staining of the corresponding part of the root tip is shown as inset in the upper right corner of each panel. Scale bar = 30 μm. Microscopic settings were kept constant for each line, but not necessarily between lines.

Regarding the dynamic pattern of NAC044 after DNA damage, we wondered if also other components of the RBR1 interactome, specifically the DREAM core components, would change expression after DNA damage. We therefore generated genomic TCX5-EGFP, LIN37A-EGFP, and LIN37B-EGFP reporter lines and analyzed the expression of these reporters after treatment with 50 μM cisplatin. For the first 12 h, TCX5 as well as LIN37A and LIN37B showed clear nuclear signals in most cell files of the root tip, without obvious dynamics (Fig 6B–D). At 24 h, expression in the central cylinder appears slightly decreased, however, is still present. Thus, we

Life Science Alliance

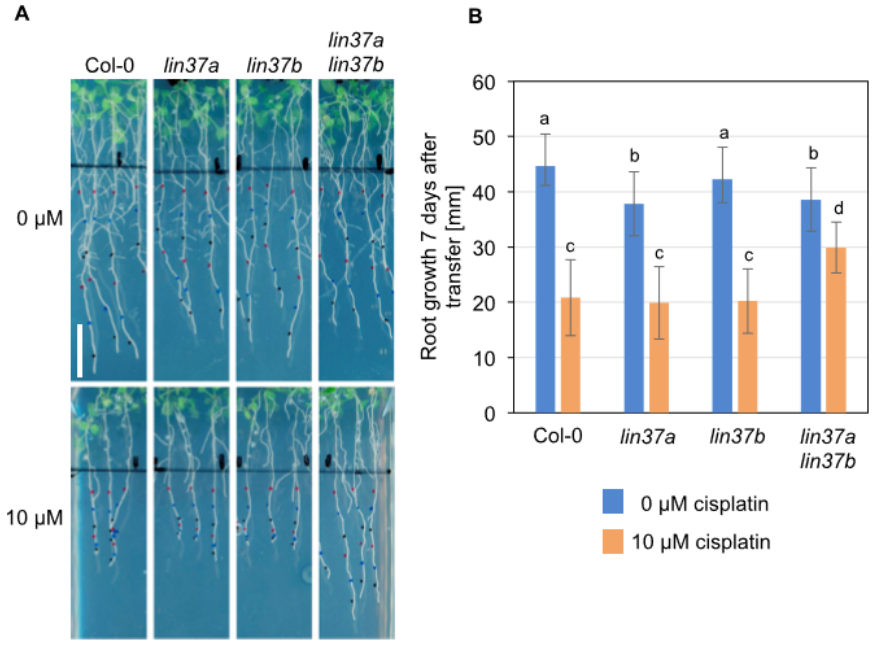

Figure 7. Double mutants for *LIN37A* and *LIN37B* display less repression of root growth under DNA-damaging conditions than the wild type.
(A, B) Root growth of the wild type, *lin37a*, *lin37b*, and *lin37a lin37b* double mutants on control plates and in the presence of cisplatin (A: representative pictures; B: quantification). Plants grown for 5 d in the absence of cisplatin were transferred to medium containing 0 or 10 μM cisplatin, and grown for further 7 d. Data are presented as mean ± SD (n = 10). Significant differences as determined by two-way ANOVA and Tukey–Kramer post hoc test ($P < 0.05$) are indicated by differing letters over the bars.

conclude that, although the expression dynamics of NAC044 and MuvB-core components differ upon DNA damage, they are expressed in overlapping patterns and therefore, likely engage with the same pool of RBR1 in a cell type- and/or cell cycle phase-specific manner.

Loss of DREAM components compromises growth arrest under DNA-damaging conditions

Because *nac044* mutants have been shown to grow better under DNA-damaging conditions than the wild type (Takahashi et al, 2019) (Figs S6 and S8), we wondered if the same would hold true for mutants in other components of the RBR1 DNA stress interactome, in particular the DREAM complex. Therefore, we first isolated T-DNA insertion mutants for several components of the MuvB-core and tested for gene expression. No full-length transcript was found in homozygous mutants of *ALY1* (*aly1-1*, *aly1-2*, *aly1-3*), *ALY2* (*aly2-2*, *aly2-3*, *aly2-4*), *ALY3* (*aly3-1*, *aly3-3*, *aly3-4*), *LIN37A* (*lin37a-2*), *LIN37B* (*lin37b-3*), *TCX5* (*tcx5-1*, *tcx5-2*), *TCX6* (*tcx6-1*), and *LIN52B* (*lin52b-1*) (Fig S7A–D). On the other hand, all T-DNA insertion lines tested for *LIN52A* showed full-length transcripts. Thus, we generated a CRISPR allele, *lin52a-c1*, to be used in our analysis (Fig S7C).

When root growth was analyzed under DNA-damaging conditions, the results between biological replicates were considerably variable, with some genotypes showing repeatedly better growth than the wild type upon cisplatin or mitomycin C (MMC) treatment, however not consistent enough to always yield statistically significant results (see Fig S8A–D for examples). The source of this variation is currently unknown. Because the *lin37* single mutants frequently showed better growth than the wild type on DNA-damaging media, we generated a *lin37a-2 lin37b-3* double mutant, aiming at an enhanced phenotype. Indeed, when we analyzed its root growth (Fig 7A and B), the double mutant consistently grew significantly ($P < 0.05$) better than the wild type and the respective single mutants on 10 μM cisplatin-containing plates, even though on control plates, the double as well as the *lin37a* single mutant occasionally even displayed slightly shorter roots than the wild type. Because we previously identified ALY1 as an RBR1 target gene which is up-regulated under DNA-damaging conditions (Bouyer et al, 2018), we also aimed at a comprehensive mutant analysis of the ALY family. However, in this case, none of the double mutants showed significant growth difference on DNA-damaging media when compared with the wild type (Fig S8D), whereas the triple mutant could not be analyzed because of lethality (Ning et al, 2020).

In summary, by mutant analysis, we show that in *Arabidopsis thaliana*, the MuvB-core component LIN37 is functionally relevant to restrict root growth after DNA damage.

E2FB is required for DNA damage-induced cell cycle arrest

In addition to the MuvB-core, we decided to also follow up the typical E2F transcription factors. Whereas E2FA (Horvath et al, 2017) and E2FC (Gómez et al, 2019) have previously been shown to be part of the DDR network, the role of E2FB has not yet been explored in detail. When we analyzed seedling roots expressing *pgE2FA-3xvYFP* or *pgE2FB-3xvYFP* by confocal microscopy after 24 h growth on cisplatin-containing or control plates, respectively, we observed that the overall E2FB signal seemed slightly enhanced after 24 h growth on genotoxin, whereas the E2FA signal was very similar to the signal in roots grown on control plates (Fig 8A).

For a more quantitative analysis of all three typical E2F transcription factors, we made use of our well-established E2F pulldown system from seedlings, that is, 6-d-old seedlings were incubated with and without 50 μM cisplatin for 24 h and subsequently analyzed by GFP-IP and mass spectroscopy. Fig 8B–D show the ratio of peptides found in cisplatin-treated versus

Life Science Alliance

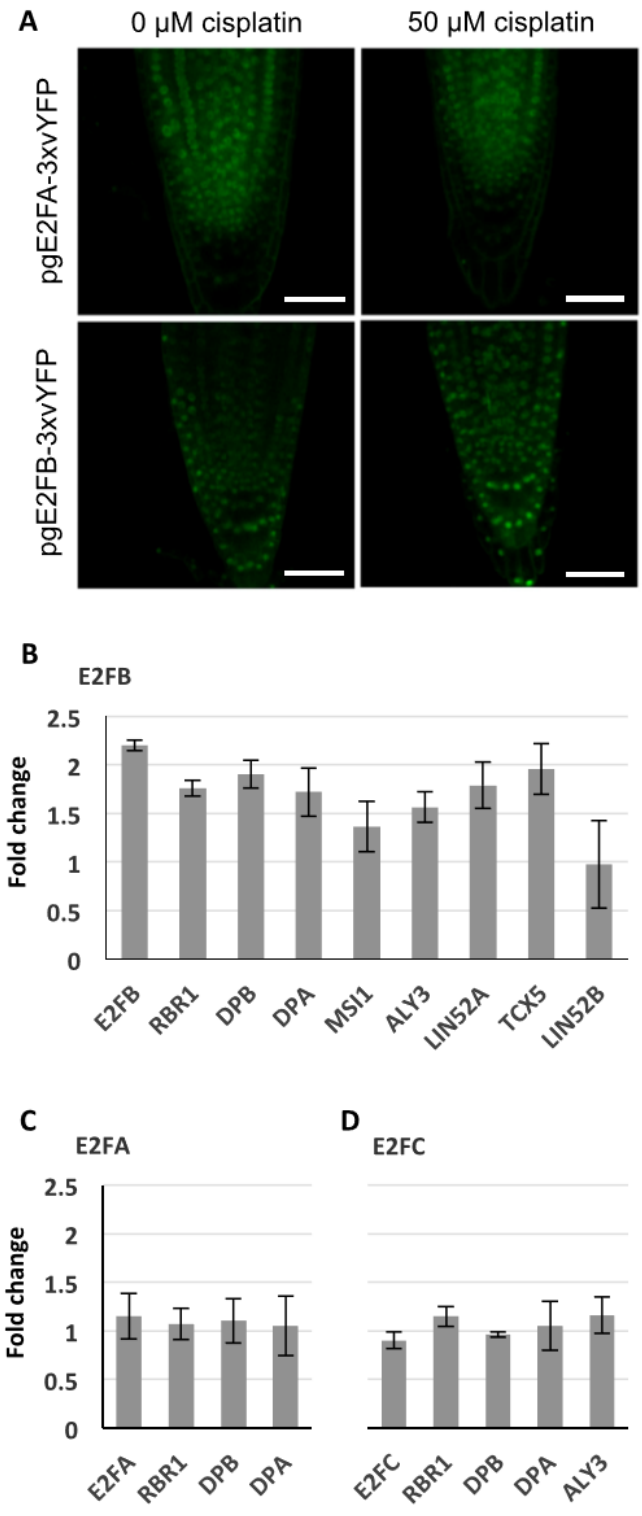

Figure 8. An E2FB-containing DREAM complex is enriched under DNA damage conditions.
(A) Confocal analysis of seedling roots expressing *pgE2FA-3xvYFP* or *pgE2FB-3xvYFP* indicates an overall increase in E2FB-3xvYFP but not E2FA-3xvYFP fluorescence after 24 h treatment with 50 µM cisplatin. Scale bar = 50 µm. **(B, C, D)** Quantification by FP-IP. **(B, C, D)** 1 d of cisplatin treatment (50 µM) of 6-d-old E2F-GFP-expressing seedlings increases the quantity of DREAM components specifically in the protein complexes containing E2FB (B) but not E2FA (C) or E2FC (D). Interacting protein partners were immunopurified from the corresponding E2F-GFP translational lines by using anti-GFP-containing magnetic beads, and components were identified with mass spectrometry. Graphs show fold change calculated as a ratio of immunoprecipitated components after cisplatin treatment relative to untreated conditions. Values represent the mean of three biological replicates ± SE.

untreated plants. On a whole seedling level, the amount of E2FA was not significantly changed after DNA damage treatment, and also, we still did not find MuvB-core components in association with E2FA after incubation with cisplatin. Likewise, the amount of E2FC stayed constant after DNA stress treatment as did the load of co-precipitated RBR1, DP, and ALY3. In contrast, for E2FB and most of its interacting DREAM components, we saw an up to two-fold enrichment after 24 h of cisplatin treatment. Although these results indicate a global enrichment in E2FB-containing complexes after cisplatin treatment, we cannot exclude that different tissues of the seedling behave differently and some cell type-specific enrichment or depletion of the different complexes might not be revealed at this level of analysis. In addition, we would like to point out that most cells in a seedling are post-mitotic so that changes taking place in actively dividing cells are likely only reflected by rather minor changes in total protein amount.

To further zoom in on E2FB functionality, we analyzed *e2fb* mutants of different allelic strengths, *e2fb-1* and *e2fb-2* (Leviczky et al, 2019), by measuring root growth, cell cycle parameters, and cell death upon cisplatin treatment. As a first step, we monitored root growth after transfer to 15 µM cisplatin-containing plates or control plates. The two *e2fb* alleles have been shown to differ in phenotypic strength, such as embryo size and seed maturation, which could be related to the site of T-DNA insertion, resulting in the inclusion (*e2fb-1*) or exclusion (*e2fb-2*) of the dimerization domain within the truncated E2FB protein (Leviczky et al, 2019). As in seed maturation, the two mutant alleles showed a differential response to DNA damage, with the more severely affected *e2fb-2* mutants showing a significantly longer root ($P < 0.05$) than the wild type 6 d after transfer onto 15 µM cisplatin plates (Figs 9A and B and S9A for time course). This suggests that like the RBR1 interactor NAC044 and the MuvB-core component LIN37, E2FB is required for maximum inhibition of root growth upon DNA damage.

A cellular response to DNA damage is cell cycle arrest to allow time for repair of damaged DNA regions (Nisa et al, 2019). Thus, we asked whether E2FB plays a role to control G1-to-S transition. To this end, we transferred seedlings for 3 h onto 50 µM cisplatin plates and then carried out a 30 min EdU labelling of root tips to quantify meristematic cells in S phase as a percentage of the total number of nuclei stained with DAPI. Whereas in wild-type plants and *e2fb-1* mutants S phase count was reduced by 30–40%, the stronger *e2fb-2* allele did not show any significant change (Fig 9C and D). The DAPI staining also allowed us to count cells that undergo mitosis, which in our conditions were seen at a frequency of on average three to six in an optical section of the untreated root tip. Although none of the differences in mitotic cell count was statistically significant applying an ANOVA test, we still saw a trend (Fig S9B and C). As expected from previous publications (Weingartner et al, 2003) we observed a reduction in mitotic cells upon cisplatin treatment in

Life Science Alliance

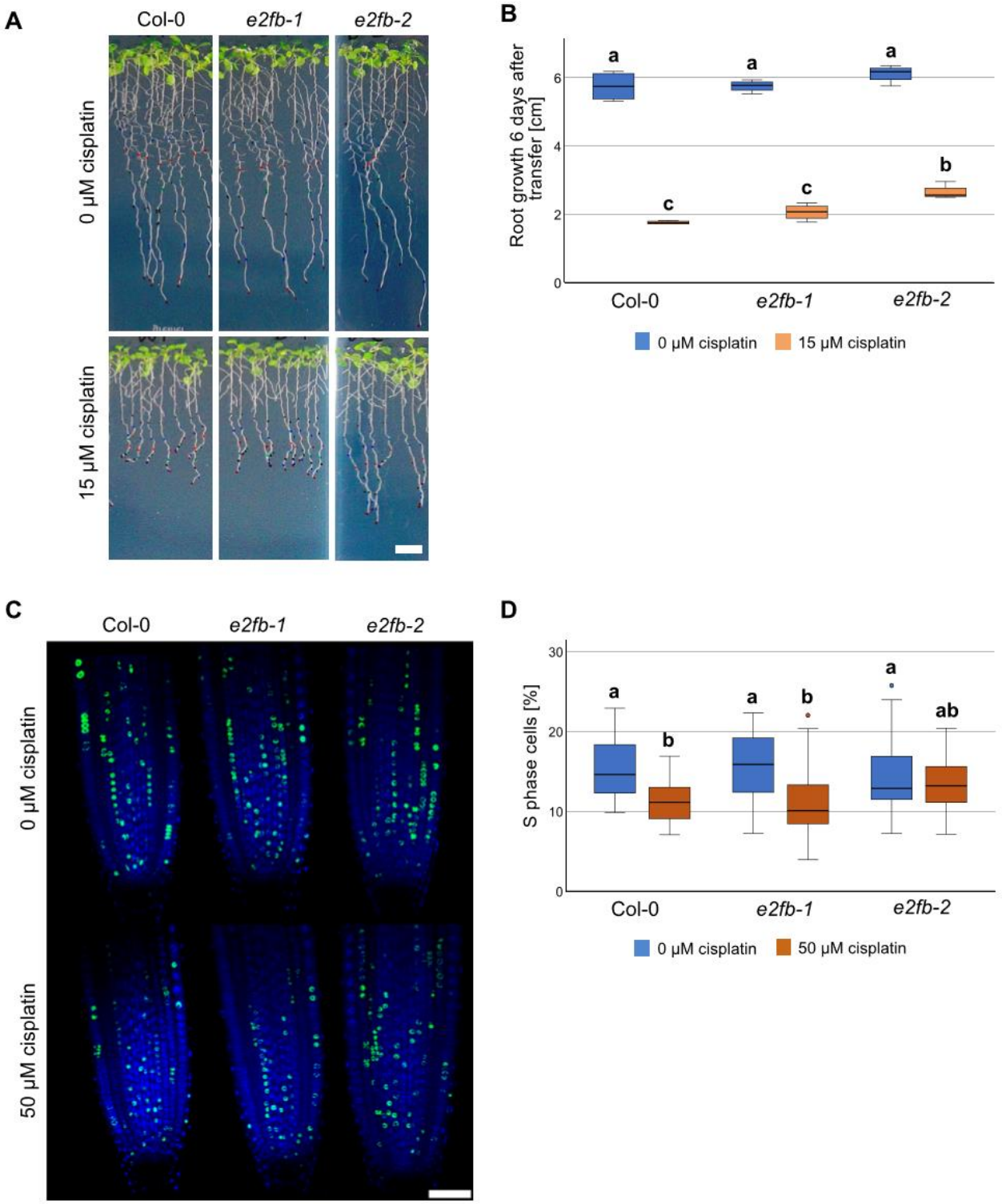

Figure 9. DNA damage-induced cell cycle arrest requires E2FB.
(A) Whole-plant photographs of Col-0, *e2fb-1*, and *e2fb-2* treated with 0.05% vol/vol DMF (mock) or 15 μM cisplatin. Scale bar = 10 mm. **(B)** Primary root length Col-0, *e2fb-1*, and *e2fb-2* seedlings after 6 d of 15 μM cisplatin or mock treatment. An average of 20 roots were measured for each genotype and condition. A box plot of the replicate means is shown. Significant differences were determined by ANOVA and Tukey post hoc test ($P < 0.05$). **(C)** Representative confocal images of EdU-labelled root tips of Col-0, *e2fb-1*, and *e2fb-2* treated with 50 μM cisplatin or 0.16% vol/vol DMF (mock) for 3 h. Scale bar = 50 μm. **(D)** Percentage of EdU-positive S phase cells relative to DAPI-stained nuclei in the root meristems of Col-0, *e2fb-1*, and *e2fb-2* treated with 50 μM cisplatin or 0.16% DMF (mock) for 3 h. An average of 25 roots were imaged for each genotype and condition. A box plot of the replicate means is shown, outlier values are shown as circles. Significant differences were determined by ANOVA and Tukey post hoc test ($P < 0.05$).

Life Science Alliance

the wild type, indicating a G2/M cell cycle arrest because of checkpoint activation. In contrast, both the *e2fb-1* and *e2fb-2* mutants had an increased number of mitotic cells upon cisplatin treatment compared with the untreated control (Fig S9B). Thus, *e2fb* mutant cells either enter mitosis more readily than the wild type under DNA-damaging conditions and/or stay in this cell cycle phase for a prolonged time.

Irreparable DNA damage frequently results in cell death of rapidly dividing tissues to prevent damaged DNA being passed on to the daughter cells. To assess this cellular response, we carried out propidium iodide (PI) staining and quantified cell death area in the root tip 1 d after transfer to 50 μM cisplatin. Because cell death in the vasculature or in columella and lateral root cap initial cells (stem cells and their immediate daughters) is known to evolve differently in response to DNA damage, we quantitated these areas separately as described before (Horvath et al, 2017). Compared with the wild type, both *e2fb* mutants showed reduced cell death areas; however, the reduction was only statistically significant for columella and lateral root cap initial cells but not in the vasculature (Fig S10A–C).

Taken together, our data show that E2FB is needed to restrict root growth after DNA damage which is in part due to a function at G1/S transition and likely includes additional functions in the control of cell death and entry into mitosis.

Discussion

The adjustment of gene expression is a key instrument in the DDR of cells and organisms. On the one hand, DNA repair genes have to be induced or cell death is triggered to eliminate excessively damaged cells. On the other hand, the expression of genes involved in cell proliferation and growth is reduced to provide time for repair.

Here, we have focussed on the Arabidopsis pocket protein RBR1 and its role in DNA damage control by elucidating RBR1's protein interaction network. A previous genome wide analysis of DNA sites occupied by RBR1 has revealed many cell cycle-related targets, reflecting its role in S- and M-phase control, but also sets of proteins involved in chromatin organization and DNA damage repair (Bouyer et al, 2018). However, in which protein assemblies RBR1 fulfills its multiple functions is only starting to be explored (for a recent review see Desvoyes and Gutierrez [2020]). To reveal with which proteins RBR1 cooperates upon DNA damage, we have identified here the RBR1 interactome of a cisplatin-treated cell culture. First of all, we found a whole-plant equivalent of the human DREAM complex, including two proteins which have sequence similarity to LIN52 and have therefore been named LIN52A (formerly called DRC1, Ning et al, 2020) and LIN52B. However, according to our Y2H data, the arrangement of the components in the Arabidopsis complex(es) seems different from the one in humans because the contact of the MuvB-core to RBR1 depends on an LxCxE motif in the plant LIN54 orthologs TCX5/TCX6 and not on a LIN52 LxSxExL motif as in humans. Remarkably, the RBR1-binding LxCxE motif in TCX5/TCX6 is not found in all members of the TCX family, but is part of a conserved region termed ALM motif (due to its amino acid sequence) that is characteristic for type 2 TCX proteins (Andersen et al, 2007) including TCX5, TCX6, and TCX7 from Arabidopsis. Interestingly, the ALM motif with the consensus sequence SPxTxA**LMCDE** includes a conserved SP site preceding the LxCxE motif, i.e., a potential phosphorylation site for proline-directed kinases, such as CDKA;1, which was also present in the RBR1 TAP. For TCX6 and TCX7, this site has already been detected to be phosphorylated in vivo as documented in the Arabidopsis protein phosphorylation site database PhosPhAt4.0 (http://phosphat.uni-hohenheim.de) (Durek et al, 2010). It will thus be interesting to see in future if such a phosphorylation impacts DREAM complex assembly and if so, which kinase is involved. Furthermore, to our knowledge, only TCX proteins with the ALM motif have been found to interact with other MuvB-core proteins in planta (Kobayashi et al, 2015; Ning et al, 2020), although recently TCX8 has been found to bind to ALY3 in the Y2H system (Noh et al, 2021). So either the non-ALM motif-bearing LIN54 homologs of Arabidopsis are part of less stable or less abundant versions of the DREAM complex, making complex precipitation from plant material difficult or they do not build a DREAM complex at all but rather function as transcriptional regulators in different assemblies.

For mammalian cells, it has been shown that the MuvB-core forms different complexes depending on the cell cycle phase. In plants, the existence of activating and repressing DREAM complexes, depending on the MYB3R and E2F version involved, has been postulated (Fischer & Müller, 2017). Thus, it is well possible that an even larger variety, depending on the cellular context, of related complexes exists. For example, under DNA-damaging conditions, we have not only found DREAM components but also the transcription factor NAC044 to be part of the RBR1 interactome, and in Y2H assays, NAC044 directly binds to RBR1 and to the MuvB-core component LIN37. Because TCX5 and TCX6 as well as NAC044 interact with RBR1 in an LxCxE motif-dependent manner and thus, likely target the same site in RBR1, they are probably not part of the same complex unless this complex contains several copies of RBR1. It is also possible that NAC044 recruits the DREAM complex to certain promoters under DNA damage with its position in the complex being subsequently replaced by TCX5/TCX6. The exact composition and the dynamics of the one or multiple DREAM complexes need to be resolved in the future. However, our results already provide evidence that DREAM and NAC044-containing complexes are both involved in restricting growth after DNA damage and likely are functionally interdependent because both were found as part of the RBR1 DNA stress interactome in cell culture.

A dynamic composition of RBR1-containing complexes is also suggested by the different accumulation patterns of NAC044 versus DREAM components. In root tips, the expression pattern of LIN37B and TCX5 appears to be not altered upon DNA damage, with the exception of a reduction in protein amount in the vasculature after 24 h. In contrast, NAC044 shows a patchy pattern reminiscent of cell cycle-dependent regulation, and accumulates after DNA damage treatment over time, peaking at 24 h after exposure to cisplatin. Interestingly, it has been shown that NAC044 positively feeds back on the amount of MYB3R3, that is, whereas MYB3R3 mRNA levels remain stable, MYB3R3 protein accumulates in an NAC044/NAC085-dependent manner after DNA damage and results in a reduced expression of mitotic genes (Takahashi et al, 2019). This led to the hypothesis that the transcription factor NAC044 controls

Life Science Alliance

protein abundance of MYB3R3 leading to the repression of mitotic genes, which, in addition to a direct interaction with RBR1 and LIN37, would represent a second route by which NAC044 impinges on DREAM function after DNA damage.

In animal cells, it has been shown that G1/S and G2/M genes are differentially regulated by different pocket proteins, that is, the non-DREAM complex-forming pRb and the DREAM-compatible p130 and p107, in response to DNA damage. According to a current model, G1/S genes are mainly repressed by pRb, with a contribution of p130 and p107, whereas p130 and p107 repress G2/M genes (Schade et al, 2019). In Arabidopsis, there is only one pocket protein, RBR1, by which we could co-precipitate an almost complete set of DREAM proteins after DNA damage. However, consistent with previous results (Horvath et al, 2017), we found that, in contrast to E2FB and E2FC, E2FA never seems to be incorporated in a DREAM complex in vivo, neither under DNA-damaging nor under control conditions. Considering that in our Y2H assays E2FA interacted not only with RBR1 but also with the DREAM core component LIN37, we suspect plant-specific posttranslational modifications or the binding of inhibitors to be responsible to prevent incorporation into a DREAM complex under in vivo conditions. Although not present in a DREAM complex, E2FA was still part of the RBR1 interactome upon DNA damage. Thus, we conclude that DREAM and non-DREAM pocket protein complexes are also present in plants after DNA damage.

Interestingly, we could also precipitate the atypical, repressive E2FE (DEL1) from DNA-stressed cells using TCX5 as a bait, suggesting the presence of yet another complex variety. In humans, the atypical, non-pocket protein-binding E2F7 is also involved in DDR as it mediates, for example, the transcriptional repression of indirect p53/TP53 target genes involved in DNA replication (Carvajal et al, 2012) and on the other hand negatively regulates genes involved in DNA damage repair (Mitxelena et al, 2018).

As it is well known in yeast and animal cells, upon DNA damage, cell cycle checkpoints are activated at the G1-to-S and G2-to-M transitions to allow time for DNA repair. This has also been shown to be the case in plants (Carballo et al, 2006). To zoom in on the DREAM function after DNA damage, we focussed here on E2FB because we found an E2FB-containing DREAM complex to be slightly but significantly enriched upon DNA damage and root growth was less reduced in *e2fb* mutants than in the wild type when treated with DNA-damaging agents. This indicates that E2FB is required for DNA damage-induced cell cycle checkpoints. We showed by visualising S-phase cells and mitotic cells within the root meristem after a short 3 h treatment with DNA-damaging drugs that these checkpoints operate at the G1-to-S and potentially also at the G2-to-M phase transition. This is consistent with E2FB's function to control both cell cycle transitions in cultured tobacco cells (Magyar et al, 2005). Furthermore, RBR1 repression on E2FA was shown to regulate the DNA damage–induced cell death (Horvath et al, 2017). Our data now indicate that E2FB is also required for this process. Interestingly, a mutant phenotype similar to *e2fb*'s with less cell death and impaired G2 arrest after DNA damage treatment was seen for *nac044 nac085* double mutants (Takahashi et al, 2019). Albeit E2FB was originally described as an activator of cell cycle progression (Magyar et al, 2005) and also hypothesized to be part of activating DREAM complexes in plants (Kobayashi et al, 2015), we recently found that E2FB in association with RBR acts as a repressor of cell proliferation during leaf development (Őszi et al, 2020). Consistently, it has been shown that many transcription factors are able to fulfill activating as well as repressive functions depending on the molecular context (Bauer et al, 2010; Boyle & Després, 2010).

In summary, our data indicate the existence of multiple routes of transcriptional control after DNA damage, that is, via E2FA-RBR1, E2FE-TCX5, and various DREAM complexes likely involving different homologs. The functional relevance of DREAM-like complexes in DNA damage is shown by the compromised root growth arrest of *lin37* and *e2fb* mutants after damage, resembling the derepressed growth of *nac044* mutants on genotoxic media. We propose that by direct interaction with RBR1 and LIN37B, NAC044 cooperates with the DREAM complex to suppress root growth after DNA damage by controlling cell cycle progression. Identifying NAC044 target genes and analyzing complex composition at tissue or cellular level will shed light on the molecular nature of this cooperation in the future.

Materials and Methods

TAP

Cloning of transgenes encoding N- or C-terminal GS^{rhino} tag (Van Leene et al, 2015) fusions under control of the constitutive cauliflower tobacco mosaic virus *35S* promoter and transformation of Arabidopsis cell suspension cultures (PSB-D) with direct selection in liquid medium was carried out as previously described (Van Leene et al, 2011). Cisplatin was added to a final concentration of 30 μM 16 h before harvest of the cell culture. TAP experiments were performed with 100 mg of total protein extract as input as described in Van Leene et al (2015). Bound proteins were digested on-bead after a final wash with 500 μl 50 mM NH_4HCO_3 (pH 8.0). Beads were incubated with 1 μg Trypsin/Lys-C in 50 μl 50 mM NH_4OH and incubated at 37°C for 4 h in a thermomixer at 800 rpm. Next, the digest was separated from the beads, an extra 0.5 μg Trypsin/Lys-C was added and the digest was further incubated overnight at 37°C. Finally, the digest was centrifuged at 20,800 rcf in an Eppendorf centrifuge for 5 min, the supernatant was transferred to a new 1.5 ml Eppendorf tube, and the peptides were dried in a Speedvac and stored at −20°C until mass spectrometry (MS) analysis. Co-purified proteins were identified by mass spectrometry using an Orbitrap Elite (Thermo Fisher Scientific) or Q Exactive mass spectrometer (Thermo Fisher Scientific) using the procedures as described below. Proteins with at least two matched high confident peptides in at least two experiments in the dataset were retained. Background proteins were filtered out based on frequency of occurrence of the co-purified proteins in a large dataset containing 543 TAP experiments using 115 different baits (Van Leene et al, 2015). True interactors that might have been filtered out because of their presence in the list of nonspecific proteins were retained by means of semi-quantitative analysis using the average normalized spectral abundance factors of the identified proteins (Van Leene et al, 2015).

Ultimate 3000 RSLC nano–Orbitrap Elite system (analysis of TAP data)

The obtained peptide mixtures were introduced into an LC–MS/MS system, the Ultimate 3000 RSLC nano (Dionex) in-line connected to an Orbitrap Elite Hybrid Ion Trap-Orbitrap Mass Spectrometer

Life Science Alliance

(Thermo Fisher Scientific). The sample mixture was loaded on a trapping column (made in-house, 100 μm internal diameter [I.D.] × 20 mm [length], 5 μm C18 Reprosil-HD beads, Dr. Maisch GmbH). After back-flushing from the trapping column, the sample was loaded on a reverse-phase column (made in-house, 75 mm I.D. × 150 mm, 5 μm C18 Reprosil-HD beads, Dr. Maisch). Peptides were loaded with solvent A (0.1% trifluoroacetic acid and 2% acetonitrile) and separated with a 30-min linear gradient from 98% solvent A′ (0.1% formic acid) to 50% solvent B′ (0.1% formic acid and 80% acetonitrile) at a flow rate of 300 nl/min, followed by a wash step reaching 100% solvent B′. The mass spectrometer was operated in data-dependent, positive ionization mode, automatically switching between MS and MS/MS acquisition for the 20 most abundant peaks in a given MS spectrum. In the Orbitrap Elite, full scan MS spectra were acquired in the Orbitrap at a target value of 3×10^6 with a resolution of 60,000. The 20 most intense ions were then isolated for fragmentation in the linear ion trap, with a dynamic exclusion of 20 s. Peptides were fragmented after filling the ion trap at a target value of 3×10^4 ion counts.

Ultimate 3000 RSLCnano–Q exactive (analysis of TAP data)

The obtained peptide mixtures were introduced into an LC–MS/MS system, the Ultimate 3000 RSLC nano (Dionex) in-line connected to a Q Exactive Mass Spectrometer (Thermo Fisher Scientific). The sample mixture was loaded on a trapping column (made in-house, 100 μm I.D. × 20 mm (length), 5 μm C18 Reprosil-HD beads, Dr. Maisch GmbH). After back-flushing from the trapping column, the sample was loaded on a reverse-phase column (made in-house, 75 mm I.D. × 150 mm, 5 μm C18 Reprosil-HD beads, Dr. Maisch). Peptides were loaded with solvent A (0.1% trifluoro-acetic acid and 2% acetonitrile) and separated with a 30-min linear gradient from 98% solvent A′ (0.1% formic acid) to 50% solvent B′ (0.1% formic acid and 80% acetonitrile) at a flow rate of 300 nl/min, followed by a wash step reaching 100% solvent B′. The mass spectrometer was operated in data-dependent, positive ionization mode, automatically switching between MS and MS/MS acquisition for the five most abundant peaks in a given MS spectrum. The source voltage was 3.6 kV and the capillary temperature was 275° C. One MS1 scan (m/z 400–2,000, AGC target 3×10^6 ions, maximum ion injection time 80 ms), acquired at a resolution of 70,000 (at 200 m/z), was followed by up to five tandem MS scans (resolution 17,500 at 200 m/z) of the most intense ions fulfilling predefined selection criteria (AGC target 5×10^4 ions, maximum ion injection time 80 ms, isolation window 2 D, fixed first mass 140 m/z, spectrum data type: centroid, intensity threshold 1.3×10^4, exclusion of unassigned, 1, 5–8, >8 positively charged precursors, peptide match preferred, exclude isotopes on, dynamic exclusion time 12 s). The higher energy collisional dissociation (HCD) collision energy was set to 25% Normalized Collision Energy and the polydimethylcyclosiloxane background ion at 445.120025 D was used for internal calibration (lock mass).

Fluorescent protein-immunoprecipitation (FP-IP)

Sterilized seeds were germinated on ½ Murashige and Skoog (MS) medium. For standard conditions, plants were grown for 7 d under continuous light at 22°C. For cisplatin treatment, seedlings were grown on ½ MS medium for 6 d (6 dag). Then, they were transferred to ½ MS plates supplemented either with or without 50 μM cisplatin and were grown for another day. For the different growth regimes and treatments used in the meta-analysis, see Table S4, sheet1. 150–200 seedlings were harvested, frozen in liquid nitrogen and ground with a TissueLyser (QIAGEN) (30 Hz, 4 × 30 s). Total proteins were extracted as described in Henriques et al (2010). Total protein extracts (4 mg/IP) were immunopurified using anti-GFP antibody coupled to 50 nm size magnetic beads (MACS Technology, Miltenyi) with a method from Hubner et al (2010) and Horvath et al (2017) and digested in column with trypsin (Promega). The resulting peptide mixture was desalted before LC–MS/MS analysis (Omix C18 100 μl tips; Varian) and the purified peptide mixture was analyzed by LC–MS/MS using a nanoflow RP-HPLC (Lc program: linear gradient of 3–40% B in 100 min, solvent A: 0.1% formic acid in water, solvent B: 0.1% formic acid in acetonitrile) on-line coupled to a linear ion trap-Orbitrap (Orbitrap-Elite or Fusion-Lumos; Thermo Fisher Scientific) mass spectrometer operating in positive ion mode. Data acquisition was carried out in a data-dependent fashion, the 20 most abundant, multiply charged ions were selected from each MS survey for MS/MS analysis (MS and HCD spectra were acquired in the Orbitrap, and collision-induced dissociation spectra in the linear ion trap).

Data analysis FP-IP (Fig S2)

To identify potential bait-specific interactors, MaxQuant proteomics software version 1.6.6.0 (Cox & Mann, 2008) was used to perform label-free quantification analysis on the corresponding MS files (.raw) and *A. thaliana* database. Recommended default parameters were used with the minimum ratio count set to 1. Given the label-free approach, multiplicity was also set to 1. False discovery rate threshold for peptide and protein identification was kept at 1%. The resulting non-normalised data were extracted for downstream analysis in R statistical software environment (version 4.0.0: "Arbor Day") interacting with RStudio v1.2.5033 (RStudio).

Quantified proteins were first segregated by bait and filtered for identification by site, matched to the reverse decoy database or common laboratory contaminants. The filtered list of proteins was then further trimmed to allow for a maximum of up to two missing values in each bait experimental condition. The raw intensities for the remaining proteins were normalized using variance-stabilizing normalization approach, and the missing values statistically imputed by randomly drawing from a left shifted Gaussian distribution (shift = 1.8; width = 0.2) via the DEP package (Zhang et al, 2018). As part of quality control, all samples were assessed for technical artefacts and outliers using principal component analysis and agglomerative hierarchical clustering performed on the top 500 most variable proteins. Hierarchical clustering was performed using complete linkage method with Euclidian distance as a proximity measure. In addition, Pearson's correlation coefficients were calculated to further access the reproducibility across samples.

Differential protein expression analysis was performed using limma as part of the DEP package. To correct for multiple hypothesis testing, *P*-values were adjusted by the Benjamini–Hochberg procedure. For each bait, significant interactors were determined based on appropriate logarithmic FC and adjusted *P*-value thresholds. Results were visualised via volcano plots using R.

Data analysis FP-IP (meta-analysis and cisplatin treatment)

Raw data were converted into peak lists using the in-house Proteome Discoverer (v 1.4) (Guan et al, 2011) and searched against the

Life Science Alliance

Swissprot database (downloaded 2019/6/12, 560,292 proteins) using the Protein Prospector search engine (v5.15.1) with the following parameters: enzyme: trypsin with maximum one missed cleavage; mass accuracies: 5 ppm for precursor ions and 0.6 D for fragment ions (both monoisotopic); fixed modification: carbamidomethylation of Cys residues; variable modifications: acetylation of protein N-termini; Met oxidation; cyclization of N-terminal Gln residues allowing maximum two variable modifications per peptide. Acceptance criteria: minimum scores: 22 and 15; maximum E values: 0.01 and 0.05 for protein and peptide identifications, respectively. Another database search was also performed using the same search and acceptance parameters except that Uniprot.random.concat database (downloaded 2019/6/12) was searched with *A. thaliana* species restriction (89,229 proteins) including additional proteins identified from the previous Swissprot search (protein score > 50).

FCs of the proteins upon cisplatin treatment were determined by using the Proteome Discoverer (v 2.4.1.1) (Thermo Fisher Scientific) software using MS1 quantitation.

For the meta-analysis, 182 IPs (50 GFP, 35 E2FA, 39 E2FB, 20 E2FC, 32 RBR1, 3 DPA and 3 DPB) were used. The statistical analyses were performed by edgeR (Robinson et al, 2010) using spectral counting (Branson & Freitas, 2016) to determine relative abundance of individual proteins (label-free quantitation). As cut-offs, we used a *P*-value of 0.05 and a FC of eight relative to the negative controls.

Plant materials

The *A. thaliana* accession Columbia-0 (Col-0) was used as the wild type reference. All mutants and transgenic lines used in this study were in the Col-0 background. The mutant lines *aly1-1* (SALK_073108), *aly1-2* (SALK_114476), *aly1-3* (SAIL_409_B01), *aly2-2* (SALK_118765C), *aly2-3* (GK_083C03), *aly2-4* (SALK_056946), *aly3-1* (SALK_40756), *aly3-3* (SALK_49711), *aly3-4* (SALK_125138C), *lin37a-2* (SALK_057175), *lin37b-3* (SALK_103139C), *lin52b-1* (GK_854A11), *tcx5-1* (SALK_047165), *tcx5-2* (SALK_144605C), and *tcx6-1* (GK_453H07) were identified from the GABI-KAT, SAIL, and SALK T-DNA collections (Sessions et al, 2002; Alonso et al, 2003; Kleinboelting et al, 2012) and provided by the Nottingham Arabidopsis Stock Centre (NASC) (Scholl et al, 2000). The mutant line *nac044-1* was kindly provided by Prof. Masaaki Umeda (Nara Institute of Science and Technology) and was described previously (Takahashi et al, 2019). It was used as the genetic background for the PRO_{NAC044}*:mEGFP:NAC044* line as described below. The *lin52a-c1* mutant was generated by CRISPR/Cas9 (Fauser et al, 2014) using the protospacer-containing oligonucleotides listed in Table S5. For the FP-IP experiments, we used Col-0 plants expressing translational GFP- or CFP-fusions, that is, *E2FA:GFP* (Magyar et al, 2012), *E2FB:GFP* (Kállai et al, 2020), *E2FC:GFP* (Kállai et al, 2020), *DPA:GFP* (see below), and *DPB:3xCFP* (see below) under the control of their own promoter, as well as PRO_{35S}*:GFP* (Magyar et al, 2012) as control. Construction of the PRO_{TCX5}*:TCX5:EGFP*, PRO_{LIN37A}*:LIN37A:EGFP*, and PRO_{LIN37B}*:LIN37B:EGFP* reporter lines is described below. For confocal analysis, plants expressing *pgE2FA-3xvYFP* and *pgE2FB-3xvYFP* were used (Leviczky et al, 2019; Őszi et al, 2020).

Plasmid construction and plant transformation

For generation of the PRO_{NAC044}*:mEGFP:NAC044* reporter, a 3,936-bp genomic sequence of *NAC044* was amplified by PCR and subsequently integrated into the *pENTR2B* vector by SLiCE reaction (Zhang et al, 2014). After introducing a *SmaI* restriction site in front of the start codon, the obtained construct was sequenced and an *mEGFP* fragment was introduced into the *SmaI* site. For generating PRO_{TCX5}*:TCX5:EGFP*, PRO_{LIN37A}*:LIN37A:EGFP*, and PRO_{LIN37B}*:LIN37B:EGFP* reporter constructs, genomic fragments of *TCX5* (5,650 bp), *LIN37A* (4,381 bp), and *LIN37B* (3,862 bp) were amplified by PCR and cloned into *pDONR201* vector by Gateway BP reaction. The resulting plasmids were sequenced and used for creating C-terminal EGFP fusions, by inserting *EGFP* fragments in frame at the position corresponding to the C-terminus of the protein encoded by each gene. All fusion constructs were then transferred into the binary destination vector *pGWB501* (Nakagawa et al, 2007) by Gateway LR reaction. To construct the PRO_{DPA}*:DPA:GFP* and PRO_{DPB}*:DPB:3xCFP* translational fusions, the promoter regions and the genomic clones including exons and introns were amplified from genomic DNA (Col-0) using the primer combinations described in Table S5. The coding sequence of a single GFP or a triple CFP was added as a C-terminal fusion to the genomic sequence of *DPA* and *DPB*, respectively, in the *pGreenII*-based *pGII0125* destination vector (Galinha et al, 2007) by using the Invitrogen 3 way gateway system (Invitrogen). Transgenic plants were generated by *Agrobacterium*-mediated transformation (Zhang et al, 2006).

To generate constructs for yeast two-hybrid assays, the coding sequences of the respective genes were amplified from cDNA and attB-recombination sites were added in two consecutive PCRs. By Gateway BP reactions, these sequences were subcloned into the *pDONR223* entry vector. The corresponding N-terminally fused *pGAD424-GW*, *pGADT7-GW*, *pGBKT7-GW*, and *pGBT9-GW* destination clones as well as the C-terminally fused *pGADCg* and *pGBKCg* destination clones were generated by Gateway LR reactions. Primers used for construct generation are shown in Table S5.

Root growth assay

Plants were germinated and grown on vertical plates containing $\frac{1}{2}$ MS medium under long day conditions (16 h light, 8 h dark) at 22°C for 5 d. Seedlings were then transferred to $\frac{1}{2}$ MS medium containing cisplatin (Sigma-Aldrich) or MMC (Sigma-Aldrich) in the indicated concentrations and were grown for further 6 or 7 d. It is to note that the optimal cisplatin concentration required a new adjustment for every new batch of cisplatin, being in our hands around 10–15 μM. After 5 d, the position of the root tip was marked. Plates were scanned and root length was measured digitally using the Simple Neurite Tracer plugin (Longair et al, 2011) for ImageJ.

Yeast two-hybrid assay

Yeast two-hybrid assays were performed according to the Yeastmaker Yeast Transformation System 2 manual (Clontech). The yeast strain AH109 was co-transformed with an AD-fused and a BD-fused construct using the lithium acetate method. Yeast cells harbouring both constructs were grown on DDO, TDO, and QDO medium (−L/−W, −L/−W/−H, and −L/−W/−H/−Ade, respectively) to assess protein/protein interactions. Co-transformation of a construct with the corresponding mEGFP construct was used as an auto-activation control.

Microscopy

Plants were germinated and grown on vertical plates containing $\frac{1}{2}$ MS medium under continuous light at 22°C for 5 d. Seedlings were

Life Science Alliance

then transferred to ½ MS medium containing cisplatin (Sigma-Aldrich) or MMC (Sigma-Aldrich) in the indicated concentrations and were imaged at different time points for time course experiments. For this, roots were placed in 0.1 mg ml^{-1} propidium iodide (PI) solution and fluorescence was imaged by confocal laser scanning microscopy using an LSM780 (Zeiss) with a 40× water immersion C-Apochromat 1.2 NA objective (Zeiss). The microscope was controlled using the Zen black software (Zeiss). GFP variants and PI were exited with a 488-nm argon laser and a 561-nm DPSS laser, respectively. GFP variant fluorescence was detected at 498–550 nm and PI fluorescence was detected at 568–690 nm.

Expression analysis

Total RNA was extracted from 7-d-old Arabidopsis seedlings using the innuPREP Plant RNA kit (Analytik Jena BioSolutions) according to the instructions of the manufacturer. cDNA synthesis was performed using a QuantiTect Reverse Transcription Kit (QIAGEN) following the manufacturer's instructions. The cDNA was used for semi-quantitative PCR experiments to test for the presence of mRNA in respective T-DNA insertion lines. Primers used for semi-quantitative PCR experiments are listed in Table S5.

EdU labelling of arabidopsis root tip

To detect S phase cells, a commercially available 5-ethynyl-2′-deoxyuridine (EdU) kit was used (Click-iTTM EdU Alexa FluorTM 488 Imaging Kit; Thermo Fisher Scientific). Stocks of EdU and reaction mixture components were prepared in accordance with manufacturer's instructions. Seedlings were incubated in 5 μM EdU-containing liquid MS medium for 30 min.

After the incubation period, seedlings were placed on a glass microscope slide containing a drop of 3.7% vol/vol formaldehyde (Sigma-Aldrich) and shoots were excised. The cut roots were transferred to a 1.5 ml microcentrifuge tube containing 1 ml of fixation solution consisting of 3.7% vol/vol formaldehyde + 0.1% vol/vol Triton X-100 (Sigma-Aldrich) in microtubule-stabilizing buffer (MTSB) for 1 h under vacuum at RT. The fixation solution was removed, and the roots were washed three times with MTSB. Samples were permeabilized in 1 ml 0.5% vol/vol Triton X-100 in PBS for 15 min at RT. Permeabilization solution was discarded and roots were washed three times with PBS. Samples were then incubated in Click-iT reaction mixture for 40 min at RT, protected from light. Samples were washed three times with PBS. For counter-staining of the nuclei, samples were incubated in 500 μl 25% vol/vol Sysmex CyStain UV Precise P staining buffer in PBS for 15 min at RT, protected from light. Samples were then washed three times with PBS. Samples were kept in PBS after the final wash until imaging.

In silico analysis

Proteins sequence alignments were carried out using the MUSCLE algorithm from the European Molecular Biology Laboratory-European Bioinformatics Institute toolkit with default settings (Madeira et al, 2019). Alignments were formatted at http://www.bioinformatics.org/sms/multi_align.html setting the coloring option to 50%. Gene expression analysis of publicly available mRNA seq data from wild-type *Arabidopsis* samples was performed using the GENEVESTIGATOR software (Hruz et al, 2008).

Data Availability

Supporting data for Fig 1 (TAP results) can be found in Tables S1 and S2. Enrichment data for the GST-pulldown experiments, graphically represented by the volcano plots in Fig S2, are listed in Table S3. Fig 2 presents a reduced dataset of the GST-pulldown meta-analysis detailed in Table S4.

Supplementary Information

Supplementary Information is available at https://doi.org/10.26508/lsa.202101141.

Acknowledgements

We thank the Single Cell Omics Advanced Core Facility staff of the Hungarian Centre of Excellence for Molecular Medicine (HCEMM) and Biological Research Center for help with their resources and their support. HCEMM has received funding from the EU's Horizon 2020 research and innovation program (739593). This work was supported through a fellowship of the University of Hamburg to L Lang, a grant by the Development and Innovation Office of Hungary (GINOP-2.3.2-15-2016-00032) to A Pettkó-Szandtner, a grant from the Japan Society for the Promotion of Science KAKENHI (20H05408 and 18H04833) to M Ito, a grant from the Hungarian National Research Funding (NKFIH-K132486) to Z Magyar, a BBSRC-NSF grant (BB/M025047/1) to L Bögre, and a DFG grant (SCHN 736/16-1) to A Schnittger.

Author Contributions

L Lang: formal analysis, investigation, and visualization.
A Pettkó-Szandtner: conceptualization, formal analysis, investigation, and visualization.
H Tunçay Elbaşi: formal analysis, investigation, and visualization.
H Takatsuka: formal analysis, investigation, and visualization.
Y Nomoto: formal analysis, investigation, and visualization.
A Zaki: formal analysis, investigation, and visualization.
S Dorokhov: formal analysis, investigation, and visualization.
G De Jaeger: resources, data curation, supervision, funding acquisition, and project administration.
D Eeckhout: data curation, formal analysis, and investigation.
M Ito: resources, supervision, funding acquisition, project administration, and writing—review and editing.
Z Magyar: conceptualization, formal analysis, supervision, funding acquisition, investigation, visualization, and writing—review and editing.
L Bogre: conceptualization, supervision, funding acquisition, writing—original draft, and project administration.
M Heese: conceptualization, formal analysis, supervision, visualization, writing—original draft, and project administration.
A Schnittger: conceptualization, formal analysis, supervision, funding acquisition, writing—original draft, and project administration.

Life Science Alliance

Conflict of Interest Statement

The authors declare that they have no conflict of interest.

References

Alonso JM, Stepanova AN, Leisse TJ, Kim CJ, Chen H, Shinn P, Stevenson DK, Zimmerman J, Barajas P, Cheuk R, et al (2003) Genome-wide insertional mutagenesis of Arabidopsis thaliana. *Science* 301: 653–657. doi:10.1126/science.1086391

Andersen SU, Algreen-Petersen RG, Hoedl M, Jurkiewicz A, Cvitanich C, Braunschweig U, Schauser L, Oh SA, Twell D, Jensen EØ (2007) The conserved cysteine-rich domain of a tesmin/TSO1-like protein binds zinc in vitro and TSO1 is required for both male and female fertility in Arabidopsis thaliana. *J Exp Bot* 58: 3657–3670. doi:10.1093/jxb/erm215

Bauer DC, Buske FA, Bailey TL (2010) Dual-functioning transcription factors in the developmental gene network of Drosophila melanogaster. *BMC Bioinformatics* 11: 366. doi:10.1186/1471-2105-11-366

Biedermann S, Harashima H, Chen P, Heese M, Bouyer D, Sofroni K, Schnittger A (2017) The retinoblastoma homolog RBR1 mediates localization of the repair protein RAD51 to DNA lesions in Arabidopsis. *EMBO J* 36: 1279–1297. doi:10.15252/embj.201694571

Boruc J, Mylle E, Duda M, De Clercq R, Rombauts S, Geelen D, Hilson P, Inzé D, Van Damme D, Russinova E (2010) Systematic localization of the Arabidopsis core cell cycle proteins reveals novel cell division complexes. *Plant Physiol* 152: 553–565. doi:10.1104/pp.109.148643

Bourbousse C, Vegesna N, Law JA (2018) SOG1 activator and MYB3R repressors regulate a complex DNA damage network in Arabidopsis. *Proc Natl Acad Sci U S A* 115: E12453–E12462. doi:10.1073/pnas.1810582115

Bouyer D, Heese M, Chen P, Harashima H, Roudier F, Grüttner C, Schnittger A (2018) Genome-wide identification of RETINOBLASTOMA RELATED 1 binding sites in Arabidopsis reveals novel DNA damage regulators. *PLoS Genet* 14: e1007797. doi:10.1371/journal.pgen.1007797

Boyle P, Després C (2010) Dual-function transcription factors and their entourage: Unique and unifying themes governing two pathogenesis-related genes. *Plant Signal Behav* 5: 629–634. doi:10.4161/psb.5.6.11570

Branson OE, Freitas MA (2016) A multi-model statistical approach for proteomic spectral count quantitation. *J Proteomics* 144: 23–32. doi:10.1016/j.jprot.2016.05.032

Carballo JA, Pincheira J, de la Torre C (2006) The G2 checkpoint activated by DNA damage does not prevent genome instability in plant cells. *Biol Res* 39: 331–340. doi:10.4067/s0716-97602006000200015

Carvajal LA, Hamard PJ, Tonnessen C, Manfredi JJ (2012) E2F7, a novel target, is up-regulated by p53 and mediates DNA damage-dependent transcriptional repression. *Genes Dev* 26: 1533–1545. doi:10.1101/gad.184911.111

Clark NM, Buckner E, Fisher AP, Nelson EC, Nguyen TT, Simmons AR, de Luis Balaguer MA, Butler-Smith T, Sheldon PJ, Bergmann DC, et al (2019) Stem-cell-ubiquitous genes spatiotemporally coordinate division through regulation of stem-cell-specific gene networks. *Nat Commun* 10: 5574. doi:10.1038/s41467-019-13132-2

Cox J, Mann M (2008) MaxQuant enables high peptide identification rates, individualized p.p.b.-range mass accuracies and proteome-wide protein quantification. *Nat Biotechnol* 26: 1367–1372. doi:10.1038/nbt.1511

del Pozo JC, Diaz-Trivino S, Cisneros N, Gutierrez C (2006) The balance between cell division and endoreplication depends on E2FC-DPB, transcription factors regulated by the ubiquitin-SCFSKP2A pathway in Arabidopsis. *Plant Cell* 18: 2224–2235. doi:10.1105/tpc.105.039651

Derkacheva M, Steinbach Y, Wildhaber T, Mozgová I, Mahrez W, Nanni P, Bischof S, Gruissem W, Hennig L (2013) Arabidopsis MSI1 connects LHP1 to PRC2 complexes. *EMBO J* 32: 2073–2085. doi:10.1038/emboj.2013.145

Desvoyes B, Gutierrez C (2020) Roles of plant retinoblastoma protein: Cell cycle and beyond. *EMBO J* 39: e105802. doi:10.15252/embj.2020105802

Durek P, Schmidt R, Heazlewood JL, Jones A, MacLean D, Nagel A, Kersten B, Schulze WX (2010) PhosPhAt: The Arabidopsis thaliana phosphorylation site database. An update. *Nucleic Acids Res* 38: D828–D834. doi:10.1093/nar/gkp810

Fauser F, Schiml S, Puchta H (2014) Both CRISPR/Cas-based nucleases and nickases can be used efficiently for genome engineering in Arabidopsis thaliana. *Plant J* 79: 348–359. doi:10.1111/tpj.12554

Fischer M, Müller GA (2017) Cell cycle transcription control: DREAM/MuvB and RB-E2F complexes. *Crit Rev Biochem Mol Biol* 52: 638–662. doi:10.1080/10409238.2017.1360836

Galinha C, Hofhuis H, Luijten M, Willemsen V, Blilou I, Heidstra R, Scheres B (2007) PLETHORA proteins as dose-dependent master regulators of Arabidopsis root development. *Nature* 449: 1053–1057. doi:10.1038/nature06206

Gómez MS, Falcone Ferreyra ML, Sheridan ML, Casati P (2019) Arabidopsis E2Fc is required for the DNA damage response under UV-B radiation epistatically over the microRNA396 and independently of E2Fe. *Plant J* 97: 749–764. doi:10.1111/tpj.14158

Guan S, Price JC, Prusiner SB, Ghaemmaghami S, Burlingame AL (2011) A data processing pipeline for mammalian proteome dynamics studies using stable isotope metabolic labeling. *Mol Cell Proteomics* 10: M111.010728. doi:10.1074/mcp.M111.010728

Guiley KZ, Liban TJ, Felthousen JG, Ramanan P, Litovchick L, Rubin SM (2015) Structural mechanisms of DREAM complex assembly and regulation. *Genes Dev* 29: 961–974. doi:10.1101/gad.257568.114

Hafner A, Bulyk ML, Jambhekar A, Lahav G (2019) The multiple mechanisms that regulate p53 activity and cell fate. *Nat Rev Mol Cell Biol* 20: 199–210. doi:10.1038/s41580-019-0110-x

Hauser BA, He JQ, Park SO, Gasser CS (2000) TSO1 is a novel protein that modulates cytokinesis and cell expansion in Arabidopsis. *Development* 127: 2219–2226. doi:10.1242/dev.127.10.2219

Henriques R, Magyar Z, Monardes A, Khan S, Zalejski C, Orellana J, Szabados L, de la Torre C, Koncz C, Bögre L (2010) Arabidopsis S6 kinase mutants display chromosome instability and altered RBR1-E2F pathway activity. *EMBO J* 29: 2979–2993. doi:10.1038/emboj.2010.164

Horvath BM, Kourova H, Nagy S, Nemeth E, Magyar Z, Papdi C, Ahmad Z, Sanchez-Perez GF, Perilli S, Blilou I, et al (2017) Arabidopsis RETINOBLASTOMA RELATED directly regulates DNA damage responses through functions beyond cell cycle control. *EMBO J* 36: 1261–1278. doi:10.15252/embj.201694561

Hruz T, Laule O, Szabo G, Wessendorp F, Bleuler S, Oertle L, Widmayer P, Gruissem W, Zimmermann P (2008) Genevestigator v3: A reference expression database for the meta-analysis of transcriptomes. *Adv Bioinformatics* 2008: 420747. doi:10.1155/2008/420747

Hubner NC, Bird AW, Cox J, Splettstoesser B, Bandilla P, Poser I, Hyman A, Mann M (2010) Quantitative proteomics combined with BAC TransgeneOmics reveals in vivo protein interactions. *J Cell Biol* 189: 739–754. doi:10.1083/jcb.200911091

Kállai BM, Kourová H, Chumová J, Papdi C, Trögelová L, Kofroňová O, Hozák P, Filimonenko V, Mészáros T, Magyar Z, et al (2020) γ-Tubulin interacts with E2F transcription factors to regulate proliferation and endocycling in Arabidopsis. *J Exp Bot* 71: 1265–1277. doi:10.1093/jxb/erz498

Kleinboelting N, Huep G, Kloetgen A, Viehoever P, Weisshaar B (2012) GABI-Kat SimpleSearch: New features of the Arabidopsis thaliana T-DNA mutant database. *Nucleic Acids Res* 40: D1211–D1215. doi:10.1093/nar/gkr1047

Kobayashi K, Suzuki T, Iwata E, Nakamichi N, Suzuki T, Chen P, Ohtani M, Ishida T, Hosoya H, Müller S, et al (2015) Transcriptional repression by MYB3R proteins regulates plant organ growth. *EMBO J* 34: 1992–2007. doi:10.15252/embj.201490899

Life Science Alliance

Kosugi S, Ohashi Y (2002) E2Ls, E2F-like repressors of Arabidopsis that bind to E2F sites in a monomeric form. *J Biol Chem* 277: 16553–16558. doi:10.1074/jbc.m200913200

Leviczky T, Molnár E, Papdi C, Őszi E, Horváth GV, Vizler C, Nagy V, Pauk J, Bögre L, Magyar Z (2019) E2FA and E2FB transcription factors coordinate cell proliferation with seed maturation. *Development* 146: dev179333. doi:10.1242/dev.179333

Liu Z, Running MP, Meyerowitz EM (1997) TSO1 functions in cell division during Arabidopsis flower development. *Development* 124: 665–672. doi:10.1242/dev.124.3.665

Lokdarshi A, Papdi C, Pettkó-Szandtner A, Dorokhov S, Scheres B, Magyar Z, von Arnim AG, Bögre L, Horváth BM (2020) ErbB-3 BINDING PROTEIN 1 regulates translation and counteracts RETINOBLASTOMA RELATED to maintain the root meristem. *Plant Physiol* 182: 919–932. doi:10.1104/pp.19.00805

Longair MH, Baker DA, Armstrong JD (2011) Simple neurite tracer: Open source software for reconstruction, visualization and analysis of neuronal processes. *Bioinformatics* 27: 2453–2454. doi:10.1093/bioinformatics/btr390

Madeira F, Park YM, Lee J, Buso N, Gur T, Madhusoodanan N, Basutkar P, Tivey ARN, Potter SC, Finn RD, et al (2019) The EMBL-EBI search and sequence analysis tools APIs in 2019. *Nucleic Acids Res* 47: W636–W641. doi:10.1093/nar/gkz268

Magyar Z, De Veylder L, Atanassova A, Bakó L, Inzé D, Bögre L (2005) The role of the Arabidopsis E2FB transcription factor in regulating auxin-dependent cell division. *Plant Cell* 17: 2527–2541. doi:10.1105/tpc.105.033761

Magyar Z, Horváth B, Khan S, Mohammed B, Henriques R, De Veylder L, Bakó L, Scheres B, Bögre L (2012) Arabidopsis E2FA stimulates proliferation and endocycle separately through RBR-bound and RBR-free complexes. *EMBO J* 31: 1480–1493. doi:10.1038/emboj.2012.13

Mitxelena J, Apraiz A, Vallejo-Rodríguez J, García-Santisteban I, Fullaondo A, Alvarez-Fernández M, Malumbres M, Zubiaga AM (2018) An E2F7-dependent transcriptional program modulates DNA damage repair and genomic stability. *Nucleic Acids Res* 46: 4546–4559. doi:10.1093/nar/gky218

Nakagawa T, Suzuki T, Murata S, Nakamura S, Hino T, Maeo K, Tabata R, Kawai T, Tanaka K, Niwa Y, et al (2007) Improved gateway binary vectors: High-performance vectors for creation of fusion constructs in transgenic analysis of plants. *Biosci Biotechnol Biochem* 71: 2095–2100. doi:10.1271/bbb.70216

Ning YQ, Liu N, Lan KK, Su YN, Li L, Chen S, He XJ (2020) DREAM complex suppresses DNA methylation maintenance genes and precludes DNA hypermethylation. *Nat Plants* 6: 942–956. doi:10.1038/s41477-020-0710-7

Nisa MU, Huang Y, Benhamed M, Raynaud C (2019) The plant DNA damage response: Signaling pathways leading to growth inhibition and putative role in response to stress conditions. *Front Plant Sci* 10: 653. doi:10.3389/fpls.2019.00653

Noh M, Shin JS, Hong JC, Kim SY, Shin JS (2021) Arabidopsis TCX8 functions as a senescence modulator by regulating LOX2 expression. *Plant Cell Rep* 40: 677–689. doi:10.1007/s00299-021-02663-y

Nowack MK, Harashima H, Dissmeyer N, Zhao X, Bouyer D, Weimer AK, De Winter F, Yang F, Schnittger A (2012) Genetic framework of cyclin-dependent kinase function in Arabidopsis. *Dev Cell* 22: 1030–1040. doi:10.1016/j.devcel.2012.02.015

Őszi E, Papdi C, Mohammed B, Petkó-Szandtner A, Leviczky T, Molnár E, Galvan-Ampudia C, Khan S, Juez EL, Horváth B, et al (2020) E2FB interacts with RETINOBLASTOMA RELATED and regulates cell proliferation during leaf development. *Plant Physiol* 182: 518–533. doi:10.1104/pp.19.00212

Robinson MD, McCarthy DJ, Smyth GK (2010) edgeR: A bioconductor package for differential expression analysis of digital gene expression data. *Bioinformatics* 26: 139–140. doi:10.1093/bioinformatics/btp616

Schade AE, Fischer M, DeCaprio JA (2019) RB, p130 and p107 differentially repress G1/S and G2/M genes after p53 activation. *Nucleic Acids Res* 47: 11197–11208. doi:10.1093/nar/gkz961

Scholl RL, May ST, Ware DH (2000) Seed and molecular resources for Arabidopsis. *Plant Physiol* 124: 1477–1480. doi:10.1104/pp.124.4.1477

Sessions A, Burke E, Presting G, Aux G, McElver J, Patton D, Dietrich B, Ho P, Bacwaden J, Ko C, et al (2002) A high-throughput Arabidopsis reverse genetics system. *Plant Cell* 14: 2985–2994. doi:10.1105/tpc.004630

Sijacic P, Wang W, Liu Z (2011) Recessive antimorphic alleles overcome functionally redundant loci to reveal TSO1 function in Arabidopsis flowers and meristems. *PLoS Genet* 7: e1002352. doi:10.1371/journal.pgen.1002352

Simmons AR, Davies KA, Wang W, Liu Z, Bergmann DC (2019) SOL1 and SOL2 regulate fate transition and cell divisions in the Arabidopsis stomatal lineage. *Development* 146: dev171066. doi:10.1242/dev.171066

Song JY, Leung T, Ehler LK, Wang C, Liu Z (2000) Regulation of meristem organization and cell division by TSO1, an Arabidopsis gene with cysteine-rich repeats. *Development* 127: 2207–2217. doi:10.1242/dev.127.10.2207

Takahashi N, Ogita N, Takahashi T, Taniguchi S, Tanaka M, Seki M, Umeda M (2019) A regulatory module controlling stress-induced cell cycle arrest in Arabidopsis. *Elife* 8: 2177. doi:10.7554/eLife.43944

Van Leene J, Eeckhout D, Cannoot B, De Winne N, Persiau G, Van De Slijke E, Vercruysse L, Dedecker M, Verkest A, Vandepoele K, et al (2015) An improved toolbox to unravel the plant cellular machinery by tandem affinity purification of Arabidopsis protein complexes. *Nat Protoc* 10: 169–187. doi:10.1038/nprot.2014.199

Van Leene J, Eeckhout D, Persiau G, Van De Slijke E, Geerinck J, Van Isterdael G, Witters E, De Jaeger G (2011) Isolation of transcription factor complexes from Arabidopsis cell suspension cultures by tandem affinity purification. *Methods Mol Biol* 754: 195–218. doi:10.1007/978-1-61779-154-3_11

Wang S, Gu Y, Zebell SG, Anderson LK, Wang W, Mohan R, Dong X (2014) A noncanonical role for the CKI-RB-E2F cell-cycle signaling pathway in plant effector-triggered immunity. *Cell Host Microbe* 16: 787–794. doi:10.1016/j.chom.2014.10.005

Weimer AK, Biedermann S, Harashima H, Roodbarkelari F, Takahashi N, Foreman J, Guan Y, Pochon G, Heese M, Van Damme D, et al (2016) The plant-specific CDKB1-CYCB1 complex mediates homologous recombination repair in Arabidopsis. *EMBO J* 35: 2068–2086. doi:10.15252/embj.201593083

Weingartner M, Pelayo HR, Binarova P, Zwerger K, Melikant B, de la Torre C, Heberle-Bors E, Bögre L (2003) A plant cyclin B2 is degraded early in mitosis and its ectopic expression shortens G2-phase and alleviates the DNA-damage checkpoint. *J Cell Sci* 116: 487–498. doi:10.1242/jcs.00250

Yoshiyama K, Conklin PA, Huefner ND, Britt AB (2009) Suppressor of gamma response 1 (SOG1) encodes a putative transcription factor governing multiple responses to DNA damage. *Proc Natl Acad Sci U S A* 106: 12843–12848. doi:10.1073/pnas.0810304106

Yoshiyama KO (2016) SOG1: A master regulator of the DNA damage response in plants. *Genes Genet Syst* 90: 209–216. doi:10.1266/ggs.15-00011

Yoshiyama KO, Kimura S, Maki H, Britt AB, Umeda M (2014) The role of SOG1, a plant-specific transcriptional regulator, in the DNA damage response. *Plant Signal Behav* 9: e28889. doi:10.4161/psb.28889

Zhang X, Henriques R, Lin SS, Niu QW, Chua NH (2006) Agrobacterium-mediated transformation of Arabidopsis thaliana using the floral dip method. *Nat Protoc* 1: 641–646. doi:10.1038/nprot.2006.97

Zhang X, Smits AH, van Tilburg GB, Ovaa H, Huber W, Vermeulen M (2018) Proteome-wide identification of ubiquitin interactions using UbIA-MS. *Nat Protoc* 13: 530–550. doi:10.1038/nprot.2017.147

Zhang Y, Werling U, Edelmann W (2014) Seamless ligation cloning extract (SLiCE) cloning method. *Methods Mol Biol* 1116: 235–244. doi:10.1007/978-1-62703-764-8_16

CHAPTER 2

The two plant-specific DREAM components FLIC and FLAC repress floral transition in *Arabidopsis*

This chapter contains a pre-print submitted to bioRxiv on 07/08/2023. It can currently be accessed using the doi: 10.1101/2023.08.07.552284.

Since some statistical descriptions are missing from the manuscript in its current form, I want to provide the following clarifications:

- In Fig 3C, significant differences were determined by ANOVA and Tukey post hoc test ($P < 0.05$).
- Fig 4A and B shows a quantification of the same two replicates with 10 plants in each replicate per genotype. Significant differences were determined by Welch test and Dunnett T3 post hoc test ($P < 0.05$) in the case of bolting time and by ANOVA and Tukey post hoc test ($P < 0.05$) in the case of leaf number at bolting.
- Fig 4C shows a quantification of two replicates with 9–10 plants in each replicate per genotype. Significant differences were determined by Welch test and Dunnett T3 post hoc test ($P < 0.05$).
- Fig 4D and E shows a quantification of the same two replicates with 8–10 plants in each replicate per genotype. Significant differences were determined by ANOVA and Tukey post hoc test ($P < 0.05$).

Further, I want to highlight the following corrigenda:

- Lines 363 ff. wrongly state that phosphorylation of LIN52 at its serine residue 28 facilitates the switch from repressive to activating DREAM complex. This should read: “Moreover, in other organisms, LIN52 has the crucial function of facilitating DREAM assembly after being phosphorylated at its serine residue 28 (Litovchick et al, 2011).”

- Lines 445 ff. wrongly state that the mutant lines *flic*-2 and *flic*-4 were used in this study. This should read: “The mutant lines *flic*-1 (GK-612E12) and *flac*-1 (GK-327D05) were identified from the GABI-KAT (Kleinboelting et al, 2012) T-DNA collections and provided by the Nottingham Arabidopsis Stock Centre (NASC) (Scholl et al, 2000).”

These points will also be amended in the manuscript before proper publication in a journal.

The two plant-specific DREAM components FLIC and FLAC repress floral transition in *Arabidopsis*

Lucas Lang[1], Franziska Böwer[1], Hasibe Tunçay Elbaşı[1], Dominique Eeckhout[2,3], Nick Marschlich[1], Geert de Jaeger[2,3], Maren Heese[1], Arp Schnittger[1]

[1]*Department of Developmental Biology, University of Hamburg, Institute for Plant Sciences and Microbiology, Hamburg, Germany*
[2]*Department of Plant Biotechnology and Bioinformatics, Ghent University, Ghent, Belgium*
[3]*Vlaams Instituut voor Biotechnologie (VIB) Center for Plant Systems Biology, Ghent, Belgium*
Correspondence: arp.schnittger@uni-hamburg.de

Running title

Control of flowering by DREAM complex components

Keywords

Arabidopsis, DREAM complex, flowering, FLIC, FLAC, LIN37

Summary blurb

This study identifies two plant-specific members of the DREAM complex, explores their roles by mutant analysis and protein interaction investigation, and links them and additional DREAM complex components to the regulation of floral transition.

Abstract

The DREAM complex is a key transcriptional regulator especially involved in the control of the cell cycle and development. Here, we characterise two novel plant-specific DREAM components, FLIC and FLAC, which we identified through tandem affinity purification experiments as interactors of conserved core DREAM constituents. We demonstrate that plants lacking both FLIC and FLAC exhibit pleiotropic phenotypes, including stunted growth and reduced fertility. Notably, *flic flac* double mutants show an early-flowering phenotype, an aspect that we found to be shared with mutants of the core DREAM component LIN37, with which FLIC and FLAC interact in binary protein-protein interaction assays. Performing reverse affinity purification experiments, we detected the JMJ14/NAC050/NAC052 module, known for its involvement in flowering repression, in the interactome of both FLIC and FLAC. Subsequent binary interaction studies then link the JMJ14/NAC050/NAC052 module via LIN37 to the DREAM complex providing a mechanistic framework on how flowering time could be transcriptionally controlled by the DREAM complex.

Introduction

Proper timing of the transition from vegetative growth to flowering is of crucial importance for a plant to maximise its reproductive success. Reflecting the importance and complexity of this transition, an intricate genetic network gauges both the endogenous state of a plant as well as the environmental conditions and promotes flowering at the optimal moment (Koornneef et al, 1998; Amasino & Michaels, 2010; Srikanth & Schmid, 2011).

During the extensive research of flowering time genes that has been performed in Arabidopsis, two major networks have been identified (Simpson & Dean, 2002; Kinoshita & Richter, 2020). First, internal factors, such as plant age and phytohormones, regulate initiation of flowering (partly) independently of environmental cues (Huijser & Schmid, 2011; Hyun et al, 2017). Secondly, floral transition can be controlled externally by factors such as vernalisation, photoperiod, and temperature (Yanovsky & Kay, 2002; Andrés & Coupland, 2012).

Many floral effector signals become integrated at the *FLOWERING LOCUS T* (*FT*) gene which is required for induction of floral meristem identity (Wigge et al, 2005; Hayama et al, 2017). To initiate floral transition, FT gets relocated to the shoot apical meristem by florigen transporters (Abe et al, 2005; Corbesier et al, 2007; Jaeger & Wigge, 2007), where it then forms the florigen activation complex (FAC) to regulate floral meristem identity genes, such as *APETALA1* (*AP1*), *FRUITFULL* (*FUL*), *SUPPRESSOR OF OVEREXPRESSION OF CONSTANS1* (*SOC1*), and *SEPALLATA3* (*SEP3*) (Abe et al, 2005; Kawamoto et al, 2015; Collani et al, 2019).

FT expression is also subject to epigenetic regulation. Several Jumonji C (JmjC) domain-containing histone demethylases have been demonstrated to regulate *FT* in different ways. The H3K27 demethylase RELATIVE OF EARLY FLOWERING 6 (REF6)/JUMONJI 12 (JMJ12) activates *FT* transcription when overexpressed, whereas its close homologue EARLY FLOWERING 6 (ELF6) is an upstream repressor of photoperiodic floral induction (Noh et al, 2004; Lu et al, 2011). Additionally, there are H3K4-specific members of the JMJ demethylase group that either repress *FT*, such as JMJ14, or activate *FT*, such as JMJ15 and JMJ18 (Lu et al, 2010; Yang et al, 2012a, 2012b).

One central regulator of florigen expression is the well-described MADS-box transcription factor FLOWERING LOCUS C (FLC) (Wang et al, 2014). Recently, it has been

demonstrated that the floral repression through FLC can be counteracted by absence of JMJ14 through increased H3K4me3 levels, emphasising its role as an important epigenetic flowering time regulator (Richter et al, 2019). JMJ14 physically associates with the plant-specific NAM, ATAF1, and CUC1/CUC2 (NAC) type transcription factors NAC050 and NAC052, and it has been demonstrated that a similar set of genes is deregulated in *jmj14* and *nac050 nac052* mutants leading to an early-flowering phenotype in both mutants (Ning et al, 2015; Zhang et al, 2015). Further, an interaction of JMJ14 with TELOMERE REPEAT BINDING FACTOR (TRB) proteins has been shown recently, together with hyper-methylation of a common set of genes in the respective mutants as well as an impact on flowering time regulation via the naturally silenced transcription factor FLOWERING WAGENINGEN (FWA) (Soppe et al, 2000; Wang et al, 2023).

Developmental transitions, such as the induction of flowering, also usually involve a fine-tuned cell proliferation control (Jacqmard et al, 2003). The DP, RB-like, E2F, and multi-vulval class B (MuvB)-core (DREAM) complex is a multi-protein complex with a canonical role in transcriptional cell cycle regulation (Korenjak et al, 2004; Litovchick et al, 2007; Schmit et al, 2007; Asthana et al, 2022; Koliopoulos et al, 2022). Notably, mutants in several components of the DREAM complex have been previously linked to control of floral transition (Bouveret et al, 2006; Ning et al, 2020). However, this complex has only recently been fully identified in plants and how this complex and/or subcomplexes control flowering is largely not understood (Ning et al, 2020; Lang et al, 2021).

The MuvB-core is considered to be the constant part that is present in every variation of the DREAM complex and is comprised of the different homologues of ALWAYS EARLY (ALY, a homologue of the *C. elegans* DREAM component LIN9), ABNORMAL CELL LINEAGE PROTEIN 37 (LIN37), LIN52, TESMIN/TSO1-LIKE CXC (TCX, a LIN54 homologue), and MULTICOPY SUPPRESSOR OF IRA (MSI, a RBBP4 homologue). This core complex is able to recruit other proteins, such as RETINOBLASTOMA-RELATED 1 (RBR1), DIMERIZATION PARTNER (DP), E2 PROMOTER BINDING FACTOR (E2F), and MYELOBLASTOMA 3R (MYB3R), enabling the DREAM complex to control and maintain the appropriate transcriptional program (Kobayashi et al, 2015; Fischer & Müller, 2017). It has been postulated that depending on the exact homologues being

105 incorporated in a certain variant of the DREAM complex, it can facilitate either
106 activation or repression (or both for different subsets of genes) (Magyar et al, 2016;
107 Fischer & Müller, 2017).

108 Recent research on the plant DREAM complex has focused on DNA methylation
109 maintenance, developmental control, and the DNA damage stress response (Ning et
110 al, 2020; Lang et al, 2021; Wang et al, 2022b). Late-flowering phenotypes have been
111 described for mutants of the MuvB-core components *MSI1*, which also constitutes a
112 subunit of the Polycomb Repressive Complex 2 (PRC2), as well as for *TCX5* and *TCX6*
113 (Bouveret et al, 2006; Ning et al, 2020). MSI1 is responsible for gene silencing by
114 controlling histone methylation and acetylation levels, and mutation leads to
115 reduced expression of CO. This results in the inability of proper *FT* and *SOC1*
116 activation, thereby inhibiting the photoperiod pathway of floral initiation (Steinbach
117 & Hennig, 2014). Furthermore, it has recently been shown that MSI1 is needed
118 interdependently with HISTONE DEACETYLASE 6 (HDA6) for repression of the flowering
119 repressor genes *FLC*, *MADS AFFECTING FLOWERING* 4 (*MAF4*), and *MAF5* (Xu et al, 2022).

120 Here, we have identified a homologous pair of uncharacterised, plant-specific
121 interactors of the DREAM complex, FLORAL INDUCTION CONTROLLER (FLIC) and
122 FLORAL ANTICIPATION CONTROLLER (FLAC). By performing different interaction
123 assays, we show how they integrate into the complex, and we characterise them as
124 novel DREAM components in plants. Observing the phenotypes of the *flic flac* double
125 mutant, we describe its pleiotropic effects, ranging from severe vegetative defects to
126 strongly affected fertility, indicating a role in a wide range of developmental
127 processes. We further demonstrate a photoperiodically independent early floral
128 transition in the absence of FLIC and FLAC as well as for mutants of the MuvB-core
129 component LIN37 and connect them to the JMJ14/NAC050/NAC052 module.

Results

FLIC and FLAC are novel components of the plant DREAM complex

Previously, we have identified several uncharacterised proteins as potential DREAM complex interactors by tandem affinity purification (TAP) analyses conducted with TCX5, LIN52, and RBR1 serving as baits (Lang et al, 2021). Amongst those, AT5G10110, which we have here named FLORAL INDUCTION CONTROLLER (FLIC), co-purified as a prey of TCX5. A similarity search using BLAST identified no homologues outside of the plant kingdom, while one homologous protein, AT5G65120 (FLORAL ANTICIPATION CONTROLLER, FLAC), was identified in *Arabidopsis thaliana*. Aligning the sequences of FLIC and FLAC reveals a sequence identity of 47.2% (Fig S1), indicating an overlapping function (Pearson, 2013).

To explore their interaction network, we first performed reciprocal affinity purification coupled to mass spectrometry (AP-MS) analyses using N- and C-terminal fusions of these two proteins as baits. For each experiment, three replicates were conducted. A total of 37 interacting proteins were identified in at least two replicates (Tables S1 and S2). Notably, homologues of the entire MuvB-core were found (Fig 1, Tables S1 and S2). Furthermore, the atypical E2F transcription factors E2FE/DEL1 and E2FF/DEL3 could be retrieved with both FLIC and FLAC baits expanding the previous finding that E2FE/DEL1 can be co-purified with the DREAM component TCX5 (Lang et al, 2021). Interestingly, we also saw the co-purification of the recently described, plant-specific transcriptional repressors BARRIER OF TRANSCRIPTIONAL ELONGATION 1 (BTE1)/DREAM COMPONENT 2 (DRC2) and BTE1-LIKE 1 (BTL1) which have been previously identified as DREAM interactors (Derkacheva et al, 2013; Ning et al, 2020; Lang et al, 2021; Wang et al, 2022b). A single MYELOBLASTOMA 3R (MYB3R) transcription factor could be detected, i.e. MYB3R1 appeared as a prey of FLIC.

Interestingly, amongst a group of 24 proteins that have so far not been linked to the DREAM complex, we noted the presence of the histone demethylase JUMONJI 14 (JMJ14) as well as the NAC type transcription factor NAC052 as preys for both FLIC and FLAC. JMJ14, NAC052, and its close homologue NAC050 have been shown to form a complex that is involved in flowering time regulation (Ning et al, 2015; Zhang et al, 2015; Rodrigues et al, 2021). Other hits include proteins involved in various processes,

e.g. translational control and protein degradation. This suggests that FLIC and FLAC might be relevant in several additional pathways that may or may not be connected to DREAM function.

FLIC and FLAC bind to the MuvB-core

To further investigate the relationship between FLIC, FLAC, and the Arabidopsis DREAM complex, we investigated binary interactions by performing yeast two-hybrid (Y2H) assays, including BTE1 and BTL1, that have been identified in previous TAP experiments. Noticeably, FLIC exhibited a strong auto-activational activity when fused to the DNA-binding domain (BD), so that interactions could not be checked with the BD-FLIC fusion protein.

FLIC and FLAC both interacted with LIN37, LIN52, BTE1, and MYB3R3 (Fig 2A and B). This finding also confirms an interaction between FLIC and BTE1 that has been shown before (Arabidopsis Interactome Mapping Consortium, 2011). Whereas FLIC showed no interactions specific to a certain homologue and interacted with all of LIN37A, LIN37B, LIN52A, LIN52B, BTE1, and BTL1, FLAC appears to have a more defined interaction activity with a single homologue of each protein group, i.e. only with LIN37B, LIN52A, and BTE1. Additionally, we could see BD-FLAC binding to CDKA;1, which has previously been suggested to be part of plant DREAM complexes (Kobayashi et al, 2015; Lang et al, 2021). Although both FLIC and FLAC showed interactions with MYB3R3, which co-purified with TCX5 as a TAP bait, interactions could not be observed with MYB3R1, which we identified in DREAM-related TAP experiments before (Lang et al, 2021).

Since we could see strong interactions of FLIC and FLAC with BTE1 in the Y2H, as well as with both BTE1 and BTL1 in the AP-MS experiments (Fig 2A and B, Table S1), we also investigated how BTE1 and BTL1 bind to the DREAM complex (Fig S2) and found that they appear to only connect to the MuvB-core via LIN37B. Apart from that, both BTE1 and BTL1 show an interaction with MYB3R3. Additionally, BTE1 appears to be binding DPA and E2FE, whereas BTL1 binds MYB3R1.

Taken together, these results suggest that FLIC and FLAC can act as part of a plant DREAM complex and bind to the MuvB-core via a specific subset of its components, namely LIN37 and LIN52.

Concomitant loss of *FLIC* and *FLAC* leads to defects in vegetative growth and reduced fertility

To address the function of *FLIC* and *FLAC*, we characterised T-DNA insertion mutants for both genes. One transcriptional null mutant for each gene could be identified, *flic*-1 and *flac*-1 (Fig S3), and we refer to them in the following simply as *flic* and *flac*.

Since both single mutants did not exhibit any striking mutant phenotype by themselves, we generated a *flic flac* double mutant. Notably, we only detected 15% double homozygous mutants (N = 184) with an excess of wild-type plants (34%) when the progeny $flic^{-/-}$ $flac^{+/-}$ was analysed.

Homozygous double mutant plants exhibit several differences in vegetative growth when compared to the wildtype and the single mutants (Fig 3A and B). First, rosette leaf size is generally reduced and a serrated leaf shape is observable. Next, flowering starts early with the formation of multiple shoots that are thinner than in the wildtype, indicating a loss of apical dominance. This results in a bushy appearance of adult plants with reduced stem height. Furthermore, silique size and pollen amount are drastically reduced in the double mutant.

An analysis of seed viability revealed that only 7.5±2.5% ($P < 0.001$) of *flic flac* seeds are viable, whereas there was no significant reduction of viability in the single mutants (*flic*: 93.5±3.1%; *flac*: 99.0±0.7%) in comparison with the wildtype (96.5±1.2%) (Fig 3C and D). This reduction is consistent with the above-described strong reduction of viable seeds in double mutant siliques.

To test whether FLIC and FLAC are also required for gametophyte development, we performed reciprocal crossing between wild-type and *flic* $flac^{+/-}$ plants and quantified the proportion of $FLAC^{+/-}$ progeny. We could detect that loss of *FLAC* in either of the gametophytes resulted in a reduced number of heterozygous *FLAC* F1 plants (34% and 36%, respectively; N = 152–183), demonstrating that at least one functional copy of *FLIC* or *FLAC* is required for faithful female and male gamete transmission. Consistent with a requirement of FLIC and FLAC for male gametophyte development, we found that pollen viability in the double mutant is reduced (Fig 3C and E). Whereas viable pollen grains made up 99.6±0.2% of all pollen in the wildtype (*flic*: 99.7±0.1%; *flac*: 99.8±0.2%), this proportion is reduced to 89.1±0.9% in *flic flac* ($P < 0.001$).

These mutant phenotypes indicate that FLIC and FLAC are redundantly required for various aspects of sporophyte and gametophyte development.

FLIC and FLAC control flowering time

As indicated by our AP-MS analyses, FLIC and FLAC appeared to be possible interactors of the floral transition regulators JMJ14 and NAC052. Since early flowering was one of the strongest and most obvious mutant phenotypes of the *flic flac* double mutant, we focussed next on the description of this defect. We first compared the bolting time as well as the number of rosette leaves at bolting of the *flic* and *flac* single mutants as well as the *flic flac* double mutant under long-day (LD) conditions in a 16 h light/8 h dark cycle. For this purpose, days after sowing (das) were tracked and leaves were counted as soon as the shoot of a plant reached a length of 1 cm.

Our results show that whereas the *flic* single mutant (31.2±0.5 das; 19.0±0.9 leaves) does not differ significantly from the wildtype (31.2±0.5 das; 21.4±1.2 leaves), *flac* single mutant plants bolt already slightly earlier (29.0±0.6 das; $P = 0.022$) and have fewer rosette leaves at this point (16.9±1.0 leaves; $P = 0.036$) (Fig 4A and B). In the *flic flac* double mutant, this early-flowering phenotype is strongly enhanced as bolting occurs already at 23.5±0.5 das (compared to the wildtype and *flac*: $P < 0.001$) and double mutant plants possess an average of 10.8±0.3 leaves (compared to the wildtype and *flac*: $P < 0.001$).

Next, we wanted to determine whether FLIC and FLAC control flowering in a photoperiod-dependent manner and measured the time to bolting in short-day (SD) conditions, for which plants were grown in an 8 h light/16 h dark cycle (Fig 4C). While we could not observe a significant early-flowering phenotype for the *flac* single mutant in these conditions (77.5±2.1 das), barely differing from the wildtype (78.3±2.1 das), the *flic flac* double mutant again showed significantly early floral initiation (69.8±0.4 das; $P = 0.004$). These results demonstrate that FLIC and FLAC are general regulators of flowering, independent of the light regime.

Since we could identify LIN37 and LIN52 as direct interactors of FLIC and FLAC, we assessed whether these MuvB-core components were also involved in flowering time control. To this end, we performed the same LD assay as before for all *lin37* and *lin52* single and double mutants (Fig 4D and E). Whereas *lin52* mutant (*lin52a-c1*:

31.8±0.7 das; 16.8±1.0 leaves; *lin52b-1*: 30.4±0.8 das; 14.8±1.1 leaves; *lin52ab*: 29.7±0.6 das; 14.3±0.8 leaves) and *lin37a* single mutant (29.7±0.4 das; 12.9±0.3 leaves) bolting times appeared to be similar to the wildtype (31.2±0.6 das; 15.2±1.4 leaves), we found a significant difference when abolishing *LIN37B*. Both *lin37b* single mutants (28.5±0.5 das, P = 0.048; 12.2±0.3 leaves) and *lin37ab* double mutants (28.5±0.6 das, P = 0.040; 12.5±0.4 leaves) were bolting early, however, not to the degree that we could observe for the *flic flac* double mutant (25.2±0.7 das, compared to *lin37b* and *lin37ab*: $P < 0.01$; 10.9±0.6 leaves).

These findings demonstrate that the DREAM complex not only plays a role in the promotion of floral transition as suggested previously, but is also repressing it via the MuvB-core component LIN37B.

LIN37B appears to facilitate a ternary interaction connecting JMJ14/NAC050/NAC052 and FLIC/FLAC

Our above-presented finding that FLIC and FLAC are in one protein interaction network with the flowering time regulators JMJ14 and NAC052 suggested that they possibly directly interact to control flowering. To test this, we generated split-YFP fusion constructs to perform BiFC assays by transient tobacco transformation. Since a flowering time phenotype could be seen for *lin37* mutants, we decided to assess the interactions of FLIC, FLAC, and both LIN37 homologues each with JMJ14, NAC050, as well as NAC052 (Fig 5A). In our BiFC experiments, we were able to detect a YFP signal for almost all of the combinations tested (except for the three pairs of cYFP-FLAC/nYFP-NAC050, cYFP-LIN37A/nYFP-JMJ14, and cYFP-LIN37A/nYFP-NAC052).

To corroborate our BiFC data, we next tested the same combinations in Y2H assays with N- and C-terminally tagged fusions. When fused to the BD, FLIC showed a strong auto-activating activity in both variants. We could determine that while FLIC, FLAC, and the JMJ14/NAC050/NAC052 module show no binary interactions, FLIC, FLAC, and NAC050 share LIN37B as a common interactor (Fig 5B and C). Taken together, our findings open up the possibility of a ternary interaction linking FLIC/FLAC and the JMJ14/NAC050/NAC052 module indirectly.

Discussion

The repression of premature floral transition and its subsequent onset at the optimal time requires tight regulation to ensure maximal reproductive fitness. This intricate process is governed by multiple pathways influenced by a plethora of internal and external factors that collectively determine the timing of floral meristem identity establishment. Here, we demonstrate a role of the DREAM complex and its novel plant-specific components FLIC and FLAC in proper maintenance of floral repression likely working in conjunction with JMJ14, NAC050, and NAC052.

When performing AP-MS experiments with FLIC and FLAC as baits, we were able to co-purify a large part of the DREAM complex, including at least one homologue of each MuvB-core component (Fig 1, Tables S1 and S2), placing these proteins as novel plant DREAM components. However, whether and to what degree the mutant phenotypes observed for *flic* and *flac* are due to their function within a DREAM complex versus an independent role remains to be investigated.

Evidence for a repressive nature of a FLIC/FLAC-containing DREAM complex comes with the observation that both proteins interact with BTE1/BTL1. It has recently been published that BTE1 is required for transcriptional repression by the DREAM complex through binding of WD REPEAT DOMAIN 5A (WDR5A) and denying its binding to chromatin. Thereby, H3K4me2 deposition is facilitated, whereas H3K4me3 deposition is inhibited (Wang et al, 2022b). Interestingly, it has already been demonstrated that WDR5A is repressing the floral transition, with mutants exhibiting an early-flowering phenotype, by regulating methylation levels of the floral repressor genes *FLC* and *MAF4* (Jiang et al, 2009; Zhao et al, 2018). The recent identification of WDR5A in Co-IPs with TRB protein baits, while TRBs could be shown to interact with JMJ14, hints at the possible existence of a complex network (Fig 6) (Wang et al, 2023).

Regarding the DREAM-related BTE1/BTL1 interactome besides FLIC and FLAC, we could establish that their only anchor point to the MuvB-core is LIN37B. Apart from this, BTE1 and BTL1 rather appear to interact with other cell cycle regulatory proteins of the DREAM complex as we could detect interactions with DPA, E2FE, and MYB3R1 (Fig S2).

Interestingly, we also identified the histone demethylase JMJ14 in our pull-downs. Outside of the plant kingdom, JmjC domain-containing histone demethylases

316 have been extensively characterised. Functions in a range of nuclear processes, such
317 as transcriptional control, cell cycle transitions, and DNA repair have been shown,
318 and they are involved in a diverse set of diseases, including cancer, cardiac disease,
319 and obesity (Franci et al, 2014; Dimitrova et al, 2015). The roles of this class of proteins
320 in plants are being progressively elucidated (Crevillén, 2020; He et al, 2021; Ma et al,
321 2022; Wang et al, 2022a).
322 Mutants for another JmjC domain-containing histone demethylase INCREASE
323 IN BONSAI METHYLATION 1 (IBM1) exhibit developmental defects similar to *flic flac*
324 mutants (Saze et al, 2008). Remarkably, it has been demonstrated that a mutation of
325 the chromatin remodeler *DECREASED DNA METHYLATION 1* (*DDM1*), which in turn leads
326 to hypomethylation, results in a similar dwarfism phenotype by the constitutive
327 overexpression of pathogenesis-related (PR) genes. This happens via deregulation of
328 the SA-dependent defence response pathway and is therefore striking the link to
329 phytohormonal imbalance (Stokes et al, 2002; Li et al, 2010; Zhu et al, 2010). Further,
330 DDM1 plays an important role in flowering time regulation via maintaining
331 methylation levels of FWA (Kakutani, 1997; Soppe et al, 2000). As the deregulated
332 methylation patterns in *ibm1* and *ddm1* mutants differ, an additive phenotype can be
333 observed in *ddm1 ibm1* double mutants (Saze et al, 2008). Since the DREAM complex
334 has recently been linked to methylation maintenance in several ways (Ning et al,
335 2020; Wang et al, 2022b), FLIC and FLAC might be involved in this process as well, and
336 it will be interesting to explore this possibility in future.
337 JMJ14 itself has been shown to associate with a diverse set of partners to
338 regulate floral transition, such as EMF1 (Wang et al, 2014), the NAC transcription
339 factors NAC050 and NAC052, and most recently TRBs. In this study, we unveil a novel
340 regulatory mechanism of flowering time involving the DREAM complex and in
341 particular its subunits FLIC and FLAC, as well as the core subunit LIN37B as novel
342 interactors of the JMJ14/NAC050/NAC052 module. Ultimately, we could demonstrate
343 that FLAC alone and FLIC in combination with its homologue are indispensable for
344 proper regulation of floral transition in LD and SD conditions (Fig 4). The early-
345 flowering phenotype we observed is very reminiscent of what has been described for
346 plants lacking JMJ14 or NAC052, both of which we could identify in our pull-downs. A
347 milder dysregulation of flowering time could be seen in mutants of *LIN37B*, a shared

MuvB-core interactor of FLIC, FLAC, and the JMJ14/NAC050/NAC052 module via NAC050. These observations strongly point towards a co-operative repression of floral transition independent of photoperiod by JMJ14/NAC050/NAC052 and FLIC/FLAC facilitated via the DREAM complex.

Noteworthily, the DREAM complex seems to fulfil opposing roles of activating and repressing floral initiation through its different subunits. Whereas FLIC/FLAC and LIN37B delay flowering until appropriate, TCX5/6 and MSI1 are required for the timely activation of this process. This can be explained by the observation of the DREAM complex being able to change its functionality depending on its bound subunits and interactors (Fischer & DeCaprio, 2015; Engeland, 2018). However, at least MSI1 seems to also control flowering in the context of being incorporated into another complex, the PRC2 (Bouveret et al, 2006). While no research has been done on how TCX5 and TCX6 are promoting floral transition, we could not establish any function of LIN52 in flowering control. So far, we could not determine any mutant phenotype in *lin52ab* double mutants, and, in contrast to humans (Guiley et al, 2015), LIN52 does not bind RBR1 in Arabidopsis (Lang et al, 2021). Moreover, in other organisms, LIN52 has the crucial function of switching the complex from its repressive to an activating state after being phosphorylated at its serine residue 28 (Litovchick et al, 2011). This serine is not conserved in plants (Fig S4). Therefore, it is interesting to consider that LIN52 might have lost its functionality in plants at least partially.

Our observations lead us to hypothesise about at least three different modes of DREAM action that could reconcile its dual function in flowering time regulation (Fig 6A). Firstly, the composition of the DREAM complex might change depending on whether flowering should be repressed or activated. This could be realised through incorporation of different component homologues with separate sets of target genes, e.g. whereas TCX5 and TCX6 promote flowering, TCX8 is able to bind to ALY3 and represses LIPOXYGENASE 2 (LOX2) expression (Noh et al, 2021). Interestingly, it has been demonstrated that LOX2 is up-regulated upon floral transition, and there are hints at a delayed-flowering phenotype in the corresponding mutants (Bañuelos et al, 2008; Wang et al, 2017). Thus, TCX5 and TCX6 might even have opposing roles to other TCX homologues, such as TCX8. Such homologue-specific behaviour could also be the case for other DREAM components.

Secondly, regulatory modifications could govern the ability of individual DREAM components to control transcription. This possibly includes post-translational modifications of distinct subunits as well as epigenetic marks on specific genes to regulate chromatin access. Lastly, flowering regulation by DREAM components might be achieved through different (largely) independent (sub-)complexes. Just as MSI1 works in conjunction with the PRC2, LIN37 might act in an independent FLIC/FLAC–LIN37B–JMJ14/NAC050/NAC052 complex. Of course, it is possible that these regulational options overlap and apply at the same time. Further research will elucidate the true nature of DREAM action on flowering initiation and to what degree FLIC and FLAC are involved in this process.

Taking into account what has been discussed, it seems possible that these regulatory complexes extend to include BTE1/BTL1, WDR5A, and/or TRB proteins and that JMJ14 is recruited to multiple subsets of genes by different transcription factor interactors (Fig 6B). Thus, we are still beginning to unravel the stunning complexity of DREAM functionality in plants. It is already clear that the composition of the complex and the cross-talk with other complexes, such as the PRC2, will be decisive for its action in different developmental and environmental contexts.

Material and Methods

AP-MS and filtering of the data

Cloning of FLIC and FLAC encoding C- and N-terminal GS^{rhino} tag (Van Leene et al, 2015) fusions under control of the constitutive cauliflower tobacco mosaic virus 35S promoter and transformation of Arabidopsis cell suspension cultures (PSB-D) with direct selection in liquid medium was carried out as previously described (Van Leene et al, 2022).

Pull-downs were performed in triplicate, using in-house prepared magnetic IgG beads and 25 mg of total protein extract per pull-down as described (Van Leene et al, 2022). On-bead digested samples were analysed on a Q Exactive (ThermoFisher Scientific) and co-purified proteins were identified with Mascot (Matrix Science) using standard procedures (Van Leene et al, 2022).

After identification, the protein list was filtered versus a large dataset of similar experiments with non-related baits using calculated average Normalised Spectral Abundance Factors (NSAFs) (Van Leene et al, 2022). Proteins identified with at least two matched high confident peptides in at least two experiments, showing high and significant enrichment compared to the large dataset, either at least a 10-fold enrichment with a $-\log_{10}(p\text{-value(T-test)})\geq 10$, or at least 20-fold enrichment with a $-\log_{10}(p\text{-value(T-test)})\geq 8$, were retained. Furthermore, proteins appearing with only very few bait groups in the large dataset were retained when they met the following criteria: present with not more than two bait groups in the large dataset, and identified with at least two matched high confident peptide sequences in at least two experiments. Or present with no more than four bait groups in the large dataset and identified with one high confident peptide sequence in all three replicates and showing high (at least 10-fold) and significant [$-\log_{10}(p\text{-value(T-test)})\geq 10$] enrichment compared to the large dataset.

Multiple sequence alignments

Alignments were generated using the MUSCLE algorithm using default settings (Edgar, 2004). Structural predictions were generated by AlphaFold (Varadi et al, 2022). Data visualisation was done using ESPript 3 (Robert & Gouet, 2014).

Yeast two-hybrid assay

To generate constructs for yeast two-hybrid assays, the coding sequences of the respective genes were amplified from cDNA and attB-recombination sites were added in two consecutive PCRs. By Gateway BP reactions, these sequences were subcloned into the *pDONR223* entry vector. The corresponding N-terminally fused *pGAD424-GW* and *pGBT9-GW* expression clones as well as the C-terminally fused *pGADCg* and *pGBKCg* expression clones were generated by Gateway LR reactions. Primers used for construct generation are shown in Table S2.

Yeast two-hybrid assays were performed according to the Yeastmaker Yeast Transformation System 2 manual (Clontech). The yeast strain AH109 was co-transformed with an AD-fused and a BD-fused construct using the lithium acetate method. Yeast cells harbouring both constructs were grown on 2DO, 3DO, and 4DO medium (–L/–W, –L/–W/–H, and –L/–W/–H/–Ade, respectively) to assess protein/protein interactions. Co-transformation of a construct with the corresponding mEGFP construct was used as an auto-activation control.

Plant materials and growth conditions

The *Arabidopsis thaliana* accession Columbia-0 (Col-0) was used as the wild-type reference. All mutants and transgenic lines used in this study were in the Col-0 background. The mutant lines *flic-2* (SAIL_893_B04), *flic-4* (GK-612E12), and *flac-1* (GK-327D05) were identified from the GABI-KAT (Kleinboelting et al, 2012) or SAIL (Sessions et al, 2002) T-DNA collections and provided by the Nottingham Arabidopsis Stock Centre (NASC) (Scholl et al, 2000). The mutant lines *lin37a-2*, *lin37b-3*, *lin52a-c1*, and *lin52b-1* have been described previously (Lang et al, 2021).

Plants were germinated and grown on vertical plates containing ½ Murashige and Skoog (MS) medium under long-day conditions (16 h light, 8 h dark) at 22°C for 7 d.

Seedlings were then transplanted into soil and grown under the same conditions for all experiments using adult plants, and additionally under short-day conditions (8 h light, 16 h dark) for the examination of bolting.

Bimolecular fluorescence complementation assay

To generate constructs for bimolecular fluorescence complementation assays, the coding sequences of the respective genes were amplified from cDNA and attB-recombination sites were added in two consecutive PCRs. By Gateway BP reactions, these sequences were subcloned into *pDONR221-P1P4* and *pDONR221-P3P2* entry vectors. The corresponding *pBiFC-2in1-NN* expression clones were generated by Gateway LR reactions. Primers used for construct generation are shown in Table S2. The relevant proteins were transiently expressed in *Nicotiana benthamiana* leaves after *Agrobacterium tumefaciens* infiltration and the fluorescence of YFP was imaged 2 d after infiltration using a Leica SP8 laser-scanning confocal microscope.

Pollen and seed viability assays

The Peterson staining method was used to analyse the pollen viability (Peterson et al, 2010). For counting of pollen, three mature flower buds containing dehiscent anthers (or five in the case of *flic flac*) were collected and dipped in 13 µL Peterson staining solution (25% glycerol, 10% ethanol, 4% glacial acetic acid, 0.05% acid fuchsin, 0.01% malachite green, 0.005% orange G) for 10 s on a microscope slide, which was then covered by a coverslip. Subsequently, slides were heated on a hotplate at 80°C for 10 min to distinguish aborted and non-aborted pollen grains. Slides were analysed and imaged using a light microscope. Seed sets were determined by quantifying viable and aborted seeds of mature siliques; 5 siliques of 5 plants per genotype were analysed.

Data Availability

Supporting data for Fig 1 (AP-MS results) can be found in Tables S1 and S2.

Acknowledgements

We are grateful to Masaki Ito (School of Biological Science and Technology, Kanazawa University) and Claudio Alfieri (The Institute of Cancer Research, London) for critical reading and helpful comments on the manuscript. We thank the VIB Proteomics Core Facility (VIB, University of Gent, Belgium) for performing the LC-MS/MS analyses. This work was supported through a fellowship of the University of Hamburg to LL, a fellowship of the Friedrich-Ebert-Stiftung to FB, and a DFG grant (SCHN 736/16-1) to AS.

Author contributions

L Lang: conceptualisation, formal analysis, supervision, visualisation, writing—original draft.
F Böwer: formal analysis, investigation, and visualisation.
H Tunçay Elbaşı: investigation and visualisation.
D Eeckhout: data curation, formal analysis, and investigation.
N Marschlich: investigation and visualisation.
G De Jaeger: resources, data curation, supervision, funding acquisition, and project administration.
M Heese: conceptualisation and formal analysis.
A Schnittger: conceptualisation, formal analysis, supervision, funding acquisition, writing—original draft, and project administration.

Competing interests

No competing interests declared.

References

Abe M, Kobayashi Y, Yamamoto S, Daimon Y, Yamaguchi A, Ikeda Y, Ichinoki H, Notaguchi M, Goto K, Araki T (2005) FD, a bZIP protein mediating signals from the floral pathway integrator FT at the shoot apex. *Science* 309: 1052–1056.

Amasino RM, Michaels SD (2010) The timing of flowering. *Plant Physiol* 154: 516–520.

Andrés F, Coupland G (2012) The genetic basis of flowering responses to seasonal cues. *Nat Rev Genet* 13: 627–639.

Arabidopsis Interactome Mapping Consortium (2011) Evidence for network evolution in an Arabidopsis interactome map. *Science* 333: 601–607.

Asthana A, Ramanan P, Hirschi A, Guiley KZ, Wijeratne TU, Shelansky R, Doody MJ, Narasimhan H, Boeger H, Tripathi S *et al* (2022) The MuvB complex binds and stabilizes nucleosomes downstream of the transcription start site of cell-cycle dependent genes. *Nat Commun* 13: 526.

Bañuelos GR, Argumedo R, Patel K, Ng V, Zhou F, Vellanoweth RL (2008) The developmental transition to flowering in Arabidopsis is associated with an increase in leaf chloroplastic lipoxygenase activity. *Plant Sci* 174: 366–373.

Bouveret R, Schönrock N, Gruissem W, Hennig L (2006) Regulation of flowering time by Arabidopsis MSI1. *Development* 133: 1693–1702.

Collani S, Neumann M, Yant L, Schmid M (2019) FT Modulates Genome-Wide DNA-Binding of the bZIP Transcription Factor FD. *Plant Physiol* 180: 367–380.

Corbesier L, Vincent C, Jang S, Fornara F, Fan Q, Searle I, Giakountis A, Farrona S, Gissot L, Turnbull C *et al* (2007) FT protein movement contributes to long-distance signaling in floral induction of Arabidopsis. *Science* 316: 1030–1033.

Crevillén P (2020) Histone Demethylases as Counterbalance to H3K27me3 Silencing in Plants. *iScience* 23: 101715.

Derkacheva M, Steinbach Y, Wildhaber T, Mozgová I, Mahrez W, Nanni P, Bischof S, Gruissem W, Hennig L (2013) Arabidopsis MSI1 connects LHP1 to PRC2 complexes. *EMBO J* 32: 2073–2085.

Dimitrova E, Turberfield AH, Klose RJ (2015) Histone demethylases in chromatin biology and beyond. *EMBO Rep* 16: 1620–1639.

Edgar RC (2004) MUSCLE: multiple sequence alignment with high accuracy and high throughput. *Nucleic Acids Res* 32: 1792–1797.

Engeland K (2018) Cell cycle arrest through indirect transcriptional repression by p53: I have a DREAM. *Cell Death Differ* 25: 114–132.

Fischer M, DeCaprio JA (2015) Does Arabidopsis thaliana DREAM of cell cycle control? *EMBO J* 34: 1987–1989.

Fischer M, Müller GA (2017) Cell cycle transcription control: DREAM/MuvB and RB-E2F complexes. *Crit Rev Biochem Mol Biol* 52: 638–662.

538 Franci G, Ciotta A, Altucci L (2014) The Jumonji family: past, present and future of histone
539 demethylases in cancer. *Biomol Concepts* 5: 209–224.

540 Guiley KZ, Liban TJ, Felthousen JG, Ramanan P, Litovchick L, Rubin SM (2015) Structural
541 mechanisms of DREAM complex assembly and regulation. *Genes Dev* 29: 961–974.

542 Hayama R, Sarid-Krebs L, Richter R, Fernández V, Jang S, Coupland G (2017) PSEUDO
543 RESPONSE REGULATORs stabilize CONSTANS protein to promote flowering in response to
544 day length. *EMBO J* 36: 904–918.

545 He X, Wang Q, Pan J, Liu B, Ruan Y, Huang Y (2021) Systematic analysis of JmjC gene family
546 and stress--response expression of KDM5 subfamily genes in. *PeerJ* 9: e11137.

547 Huijser P, Schmid M (2011) The control of developmental phase transitions in plants.
548 *Development* 138: 4117–4129.

549 Hyun Y, Richter R, Coupland G (2017) Competence to Flower: Age-Controlled Sensitivity to
550 Environmental Cues. *Plant Physiol* 173: 36–46.

551 Jacqmard A, Gadisseur I, Bernier G (2003) Cell division and morphological changes in the
552 shoot apex of Arabidopsis thaliana during floral transition. *Ann Bot* 91: 571–576.

553 Jaeger KE, Wigge PA (2007) FT protein acts as a long-range signal in Arabidopsis. *Curr Biol* 17:
554 1050–1054.

555 Jiang D, Gu X, He Y (2009) Establishment of the winter-annual growth habit via FRIGIDA-
556 mediated histone methylation at FLOWERING LOCUS C in Arabidopsis. *Plant Cell* 21: 1733–
557 1746.

558 Kakutani T (1997) Genetic characterization of late-flowering traits induced by DNA
559 hypomethylation mutation in Arabidopsis thaliana. *Plant J* 12: 1447–1451.

560 Kawamoto N, Sasabe M, Endo M, Machida Y, Araki T (2015) Calcium-dependent protein
561 kinases responsible for the phosphorylation of a bZIP transcription factor FD crucial for the
562 florigen complex formation. *Sci Rep* 5: 8341.

563 Kinoshita A, Richter R (2020) Genetic and molecular basis of floral induction in Arabidopsis
564 thaliana. *J Exp Bot* 71: 2490–2504.

565 Kleinboelting N, Huep G, Kloetgen A, Viehoever P, Weisshaar B (2012) GABI-Kat
566 SimpleSearch: new features of the Arabidopsis thaliana T-DNA mutant database. *Nucleic*
567 *Acids Res* 40: D1211–D1215.

568 Kobayashi K, Suzuki T, Iwata E, Nakamichi N, Suzuki T, Chen P, Ohtani M, Ishida T, Hosoya H,
569 Müller S *et al* (2015) Transcriptional repression by MYB3R proteins regulates plant organ
570 growth. *EMBO J* 34: 1992–2007.

571 Koliopoulos MG, Muhammad R, Roumeliotis TI, Beuron F, Choudhary JS, Alfieri C (2022)
572 Structure of a nucleosome-bound MuvB transcription factor complex reveals DNA
573 remodelling. *Nat Commun* 13: 5075.

574 Koornneef M, Alonso-Blanco C, Peeters AJM, Soppe W (1998) GENETIC CONTROL OF
575 FLOWERING TIME IN ARABIDOPSIS. *Annu Rev Plant Physiol Plant Mol Biol* 49: 345–370.

576 Korenjak M, Taylor-Harding B, Binné UK, Satterlee JS, Stevaux O, Aasland R, White-Cooper H,

577 Dyson N, Brehm A (2004) Native E2F/RBF complexes contain Myb-interacting proteins and
578 repress transcription of developmentally controlled E2F target genes. *Cell* 119: 181–193.

579 Lang L, Pettkó-Szandtner A, Tunçay Elbaşı H, Takatsuka H, Nomoto Y, Zaki A, Dorokhov S, De
580 Jaeger G, Eeckhout D, Ito M *et al* (2021) The DREAM complex represses growth in response to
581 DNA damage in. *Life Sci Alliance* 4. doi:10.26508/lsa.202101141.

582 Litovchick L, Florens LA, Swanson SK, Washburn MP, DeCaprio JA (2011) DYRK1A protein
583 kinase promotes quiescence and senescence through DREAM complex assembly. *Genes Dev*
584 25: 801–813.

585 Litovchick L, Sadasivam S, Florens L, Zhu X, Swanson SK, Velmurugan S, Chen R, Washburn
586 MP, Liu XS, DeCaprio JA (2007) Evolutionarily conserved multisubunit RBL2/p130 and E2F4
587 protein complex represses human cell cycle-dependent genes in quiescence. *Mol Cell* 26:
588 539–551.

589 Li Y, Tessaro MJ, Li X, Zhang Y (2010) Regulation of the expression of plant resistance gene
590 SNC1 by a protein with a conserved BAT2 domain. *Plant Physiol* 153: 1425–1434.

591 Lu F, Cui X, Zhang S, Jenuwein T, Cao X (2011) Arabidopsis REF6 is a histone H3 lysine 27
592 demethylase. *Nat Genet* 43: 715–719.

593 Lu F, Cui X, Zhang S, Liu C, Cao X (2010) JMJ14 is an H3K4 demethylase regulating flowering
594 time in Arabidopsis. *Cell Res* 20: 387–390.

595 Magyar Z, Bögre L, Ito M (2016) DREAMs make plant cells to cycle or to become quiescent.
596 *Curr Opin Plant Biol* 34: 100–106.

597 Ma S, Zhang Z, Long Y, Huo W, Zhang Y, Yang X, Zhang J, Li X, Du Q, Liu W *et al* (2022)
598 Evolutionary History and Functional Diversification of the Domain-Containing Histone
599 Demethylase Gene Family in Plants. *Plants* 11. doi:10.3390/plants11081041.

600 Ning Y-Q, Liu N, Lan K-K, Su Y-N, Li L, Chen S, He X-J (2020) DREAM complex suppresses DNA
601 methylation maintenance genes and precludes DNA hypermethylation. *Nat Plants* 6: 942–
602 956.

603 Ning Y-Q, Ma Z-Y, Huang H-W, Mo H, Zhao T-T, Li L, Cai T, Chen S, Ma L, He X-J (2015) Two
604 novel NAC transcription factors regulate gene expression and flowering time by associating
605 with the histone demethylase JMJ14. *Nucleic Acids Res* 43: 1469–1484.

606 Noh B, Lee S-H, Kim H-J, Yi G, Shin E-A, Lee M, Jung K-J, Doyle MR, Amasino RM, Noh Y-S
607 (2004) Divergent roles of a pair of homologous jumonji/zinc-finger-class transcription
608 factor proteins in the regulation of Arabidopsis flowering time. *Plant Cell* 16: 2601–2613.

609 Noh M, Shin JS, Hong JC, Kim SY, Shin JS (2021) Arabidopsis TCX8 functions as a senescence
610 modulator by regulating LOX2 expression. *Plant Cell Rep* 40: 677–689.

611 Pearson WR (2013) An introduction to sequence similarity ('homology') searching. *Curr*
612 *Protoc Bioinformatics* Chapter 3: 3.1.1–3.1.8.

613 Peterson R, Slovin JP, Chen C (2010) A simplified method for differential staining of aborted
614 and non-aborted pollen grains. *Int J Plant Biol* 1: e13.

615 Richter R, Kinoshita A, Vincent C, Martinez-Gallegos R, Gao H, van Driel AD, Hyun Y, Mateos
616 JL, Coupland G (2019) Floral regulators FLC and SOC1 directly regulate expression of the B3-

617 type transcription factor TARGET OF FLC AND SVP 1 at the Arabidopsis shoot apex via
618 antagonistic chromatin modifications. *PLoS Genet* 15: e1008065.

619 Robert X, Gouet P (2014) Deciphering key features in protein structures with the new
620 ENDscript server. *Nucleic Acids Res* 42: W320–W324.

621 Rodrigues VL, Dolde U, Sun B, Blaakmeer A, Straub D, Eguen T, Botterweg-Paredes E, Hong S,
622 Graeff M, Li M-W *et al* (2021) A microProtein repressor complex in the shoot meristem
623 controls the transition to flowering. *Plant Physiol* 187: 187–202.

624 Saze H, Shiraishi A, Miura A, Kakutani T (2008) Control of genic DNA methylation by a jmjC
625 domain-containing protein in Arabidopsis thaliana. *Science* 319: 462–465.

626 Schmit F, Korenjak M, Mannefeld M, Schmitt K, Franke C, von Eyss B, Gagrica S, Hänel F,
627 Brehm A, Gaubatz S (2007) LINC, a human complex that is related to pRB-containing
628 complexes in invertebrates regulates the expression of G2/M genes. *Cell Cycle* 6: 1903–1913.

629 Scholl RL, May ST, Ware DH (2000) Seed and molecular resources for Arabidopsis. *Plant*
630 *Physiol* 124: 1477–1480.

631 Sessions A, Burke E, Presting G, Aux G, McElver J, Patton D, Dietrich B, Ho P, Bacwaden J, Ko C
632 *et al* (2002) A high-throughput Arabidopsis reverse genetics system. *Plant Cell* 14: 2985–
633 2994.

634 Simpson GG, Dean C (2002) Arabidopsis, the Rosetta stone of flowering time? *Science* 296:
635 285–289.

636 Soppe WJ, Jacobsen SE, Alonso-Blanco C, Jackson JP, Kakutani T, Koornneef M, Peeters AJ
637 (2000) The late flowering phenotype of fwa mutants is caused by gain-of-function
638 epigenetic alleles of a homeodomain gene. *Mol Cell* 6: 791–802.

639 Srikanth A, Schmid M (2011) Regulation of flowering time: all roads lead to Rome. *Cell Mol*
640 *Life Sci* 68: 2013–2037.

641 Steinbach Y, Hennig L (2014) Arabidopsis MSI1 functions in photoperiodic flowering time
642 control. *Front Plant Sci* 5: 77.

643 Stokes TL, Kunkel BN, Richards EJ (2002) Epigenetic variation in Arabidopsis disease
644 resistance. *Genes Dev* 16: 171–182.

645 Van Leene J, Eeckhout D, Cannoot B, De Winne N, Persiau G, Van De Slijke E, Vercruysse L,
646 Dedecker M, Verkest A, Vandepoele K *et al* (2015) An improved toolbox to unravel the plant
647 cellular machinery by tandem affinity purification of Arabidopsis protein complexes. *Nat*
648 *Protoc* 10: 169–187.

649 Van Leene J, Eeckhout D, Gadeyne A, Matthijs C, Han C, De Winne N, Persiau G, Van De Slijke
650 E, Persyn F, Mertens T *et al* (2022) Mapping of the plant SnRK1 kinase signalling network
651 reveals a key regulatory role for the class II T6P synthase-like proteins. *Nat Plants* 8: 1245–
652 1261.

653 Varadi M, Anyango S, Deshpande M, Nair S, Natassia C, Yordanova G, Yuan D, Stroe O, Wood
654 G, Laydon A *et al* (2022) AlphaFold Protein Structure Database: massively expanding the
655 structural coverage of protein-sequence space with high-accuracy models. *Nucleic Acids*
656 *Res* 50: D439–D444.

Wang H, Li Y, Pan J, Lou D, Hu Y, Yu D (2017) The bHLH Transcription Factors MYC2, MYC3, and MYC4 Are Required for Jasmonate-Mediated Inhibition of Flowering in Arabidopsis. *Mol Plant* 10: 1461–1464.

Wang J, Jiang X, Bai H, Liu C (2022a) Genome-wide identification, classification and expression analysis of the JmjC domain-containing histone demethylase gene family in Jatropha curcas L. *Sci Rep* 12: 6543.

Wang M, Zhong Z, Gallego-Bartolomé J, Feng S, Shih Y-H, Liu M, Zhou J, Richey JC, Ng C, Jami-Alahmadi Y *et al* (2023) Arabidopsis TRB proteins function in H3K4me3 demethylation by recruiting JMJ14. *Nat Commun* 14: 1736.

Wang Y, Fan Y, Fan D, Zhang Y, Zhou X, Zhang R, Wang Y, Sun Y, Zhang W, He Y *et al* (2022b) The DREAM complex antagonizes WDR5A to modulate histone H3K4me2/3 deposition for a subset of genome repression. *Proc Natl Acad Sci U S A* 119: e2206075119.

Wang Y, Gu X, Yuan W, Schmitz RJ, He Y (2014) Photoperiodic control of the floral transition through a distinct polycomb repressive complex. *Dev Cell* 28: 727–736.

Wigge PA, Kim MC, Jaeger KE, Busch W, Schmid M, Lohmann JU, Weigel D (2005) Integration of spatial and temporal information during floral induction in Arabidopsis. *Science* 309: 1056–1059.

Xu Y, Li Q, Yuan L, Huang Y, Hung F-Y, Wu K, Yang S (2022) MSI1 and HDA6 function interdependently to control flowering time via chromatin modifications. *Plant J* 109: 831–843.

Yang H, Han Z, Cao Y, Fan D, Li H, Mo H, Feng Y, Liu L, Wang Z, Yue Y *et al* (2012a) A companion cell-dominant and developmentally regulated H3K4 demethylase controls flowering time in Arabidopsis via the repression of FLC expression. *PLoS Genet* 8: e1002664.

Yang H, Mo H, Fan D, Cao Y, Cui S, Ma L (2012b) Overexpression of a histone H3K4 demethylase, JMJ15, accelerates flowering time in Arabidopsis. *Plant Cell Rep* 31: 1297–1308.

Yanovsky MJ, Kay SA (2002) Molecular basis of seasonal time measurement in Arabidopsis. *Nature* 419: 308–312.

Zhang S, Zhou B, Kang Y, Cui X, Liu A, Deleris A, Greenberg MVC, Cui X, Qiu Q, Lu F *et al* (2015) C-terminal domains of a histone demethylase interact with a pair of transcription factors and mediate specific chromatin association. *Cell Discov* 1: 15003 – .

Zhao X, Li J, Lian B, Gu H, Li Y, Qi Y (2018) Global identification of Arabidopsis lncRNAs reveals the regulation of MAF4 by a natural antisense RNA. *Nat Commun* 9: 5056.

Zhu Z, Xu F, Zhang Y, Cheng YT, Wiermer M, Li X, Zhang Y (2010) Arabidopsis resistance protein SNC1 activates immune responses through association with a transcriptional corepressor. *Proc Natl Acad Sci U S A* 107: 13960–13965.

Figures

Figure 1. Overview of AP-MS results using FLIC and FLAC as baits.

FLIC and FLAC were used as baits, N- as well as C-terminally tagged, in three replicates per fusion. All prey proteins that were found in at least two experiments and passed the filtering thresholds specified in the method section are connected to the respective bait by an edge. Solid edges represent prey found with both N- and C-terminally tagged bait, while prey connected by dashed edges were only detected above the threshold with either tag position. Gold, FLIC/FLAC; light blue, MuvB-core protein; dark cyan, other DREAM protein; pink, DREAM-related proteins; grey, other proteins.

Figure 2. Binary interactions of FLIC and FLAC with the DREAM complex and associated proteins as determined by Y2H.

Combinations for FLIC were only tested using the AD-FLIC fusion, as BD-FLIC showed strong auto-activation as observed with an AD-mEGFP control. FLAC was tested using both variants and only the strongest interaction is shown. Signal strength was classified according to yeast growth on different dropout media in three categories. **(A)** Dark pink, growth on 4DO; red, growth on 3DO but not on 4DO; cyan: growth not stronger than with mEGFP control. **(B)** Schematic representation of the observed interactions of FLIC and FLAC indicated by edges. Thick line, growth on 4DO; thin line, growth on 3DO but not on 4DO. Gold, FLIC/FLAC; blue, MuvB-core protein; pink, DREAM-related proteins.

Figure 3. Phenotypical analysis of *flic flac* mutant plants.

(A) Wildtype (WT, left) and *flic flac* mutant (right) grown under long-day conditions. An early-bolting phenotype can be observed in *flic flac* mutants. **(B)** Adult wildtype (left) and *flic flac* mutant (right) grown under long-day conditions. The *flic flac* double mutants show a loss of apical dominance resulting in a bushy phenotype and dramatically reduced height. **(C)** Quantification of seed and pollen viability in wildtype, *flic*, *flac*, and *flic flac* mutants. Seed viability analysis was conducted with 5 siliques from 5 plants per genotype. For assessing pollen viability, 9 flowers were

analysed for wildtype, *flic*, and *flac* mutants, and 15 flowers were analysed for *flic flac* mutants. **(D)** Representative open siliques of wildtype, *flic*, *flac*, and *flic flac* mutants. White arrowheads show viable seeds in the *flic flac* silique. Scale bars, 1 mm. **(E)** Representative Peterson staining of wildtype, *flic*, *flac*, and *flic flac* pollen. Golden arrowheads show aborted pollen grains. Scale bars, 100 µm.

Figure 4. Flowering time analysis of *flic*, *flac*, *flic flac*, and their MuvB-core interactor (*lin37* and *lin52*) mutant plants.

Floral transition was compared for mutants of *FLIC*, *FLAC*, and their MuvB-core interactors *LIN37* and *LIN52* by quantifying bolting as the time point when the shoot of a plant reached a height of 1 cm as well as the number of rosette leaves at that time point. Blue and pink boxes indicate LD and SD conditions, respectively. **(A)** Assessment of bolting time for wildtype, *flic*, *flac*, and *flic flac* mutants grown under LD conditions in days after sowing (das). **(B)** Number of rosette leaves at the time point of bolting for wildtype, *flic*, *flac*, and *flic flac* mutants grown under LD conditions. **(C)** Assessment of bolting time for wildtype, *flic*, *flac*, and *flic flac* mutants grown under SD conditions. **(D)** Assessment of bolting time for wildtype, *flic flac*, and their MuvB-core interactor (*lin37* and *lin52*) mutants grown under LD conditions. **(E)** Number of rosette leaves at the time point of bolting for wildtype, *flic flac*, and their MuvB-core interactor (*lin37* and *lin52*) mutants grown under LD conditions.

Figure 5. Interaction assays of FLIC, FLAC, LIN37 and the JMJ14/NAC050/NAC052 module.

Interactions between FLIC, FLAC, their early-flowering MuvB-core interactors LIN37A and LIN37B, as well as JMJ14, NAC050, and NAC052 were determined via BiFC and Y2H assays. **(A)** BiFC interaction matrix. Cyan, no YFP signal could be detected; pink, YFP signal could be detected; black, not determined. **(B)** Y2H interaction matrix. Interactions of FLIC, FLAC, and LIN37 with JMJ14, NAC050, and NAC052 were tested with N- and C-terminal fusion proteins. Only the strongest signal obtained is shown for each combination. *, interaction determined previously (Lang et al, 2021). †, interaction determined previously (Ning et al, 2015). Dark pink, signal on 4DO; red, signal on 3DO but not on 4DO; cyan: signal not stronger than with mEGFP control;

grey, strong auto-activation observable; black, not determined. **(C)** Schematic representation of the interactions observed in the Y2H assays (self-interactions were omitted). Thick line, signal on 4DO; thin solid line, signal on 3DO but not on 4DO; thin dashed line, as determined previously (Ning et al, 2015). Gold, FLIC/FLAC; blue, MuvB-core protein; dark cyan, other DREAM protein.

Figure 6. Model of DREAM involvement in flowering time regulation.

(A) Possible modes of action of the DREAM complex to control flowering. Compositional changes could establish separate variants of the complex to either repress or promote flowering at different time points. Regulatory modifications, such as post-translational modifications (PTMs) or histone marks (green circles), might govern the ability of individual subunits to regulate transcription, even if they are part of the same complex. Lastly, DREAM components possibly form independent (sub-)complexes. Note, that the presented options are not mutually exclusive. **(B)** A variant or subcomplex of the DREAM complex (as presented in (A)) including FLIC, FLAC, LIN37B, and the JMJ14/NAC050/NAC052 module is repressing flowering when appropriate. Additionally, JMJ14 seems to be recruited by different transcription factors, both repressing and promoting flowering, possibly depending on environmental cues or developmental requirements. Other components of the DREAM complex, i.e. MSI1, TCX5, and TCX6, have been shown to promote flowering. BTE1 and BTL1, which are directly binding to components of the flowering-repressive complex, appear to indirectly promote floral transitioning by binding to and blocking of WDR5A action. WDR5A has recently been identified in Co-IPs using TRB baits indicating a possible connection, however if so, the nature of it is still unclear.

Supplementary Figures

Figure S1. Pairwise sequence alignment of FLIC and FLAC protein sequences.

Structural predictions for FLIC and FLAC are indicated above and below the sequences, respectively.

Figure S2. Binary interactions of BTE1 and BTL1 with the DREAM complex and associated proteins by Y2H.

All proteins were tested using both AD- and BD-variants and only the strongest interaction is shown. Signal strength was classified according to yeast growth on different dropout media in three categories. **(A)** Dark pink, growth on 4DO; red, growth on 3DO but not on 4DO; cyan: growth not stronger than with mEGFP control. **(B)** Schematic representation of the observed interactions of BTE1 and BTL1 as indicated by edges. Thick line, growth on 4DO; thin line, growth on 3DO but not on 4DO. Gold, FLIC/FLAC; blue, MuvB-core protein; dark cyan, other DREAM protein; pink, DREAM-related proteins.

Figure S3. Scheme of the *FLIC* and *FLAC* genes and Arabidopsis mutants isolated in this study.

T-DNA insertion positions were confirmed by sequencing of PCR products. The line GK-612E12 (*flic-1*) has its T-DNA insertion in the third exon of *FLIC*. An insertion line for *FLAC*, GK-327D05 (*flac-1*), shows an insertion in the first exon. **(A)** The T-DNA insertion sites of the mutant alleles as well as the location of primers used for expression analysis are indicated. Blue rectangles indicate exons, whereas black lines in between the rectangles show introns. Grey rectangles and pentagon arrows represent 5′ UTRs and 3′ UTRs, respectively. **(B)** The presence of full-length transcripts in the different insertion lines was checked by RT-PCR using H2A10 as a control for the generated cDNA. WT, Wildtype; M, GeneRuler DNA Ladder Mix.

799 **Figure S4. Multiple sequence alignment of HsLIN52 and Arabidopsis orthologue**
800 **protein sequences.**

801 Structural predictions for HsLIN52 and AtLIN52B are indicated above and below the
802 sequences, respectively. HsLIN52's serine residue 28 and its proline substitutions in
803 the Arabidopsis orthologues are surrounded by a red rectangle.

Supplementary Tables

Table S1.

Overview of AP-MS results using FLIC and FLAC as baits (for details refer to Table S2). Numbers in columns C–F indicate the number of times the interactor was identified above threshold in the corresponding AP-MS replicates; only interactors that were found in at least 2 replicates of one experiment are considered reliable positives and are listed here.

Table S2.

Protein Identification details obtained with the Q Exactive (Thermo Fisher Scientific) and Mascot Distiller software (version 2.5.0, Matrix Science) combined with the Mascot search engine (version 2.6.2, Matrix Science) using the Mascot Daemon interface and database Araport11plus_DE2020 (database available from Pride repository project PXD029833) (Van Leene et al, 2022).

Table S3.

List of primers used in this study.

Figure 1

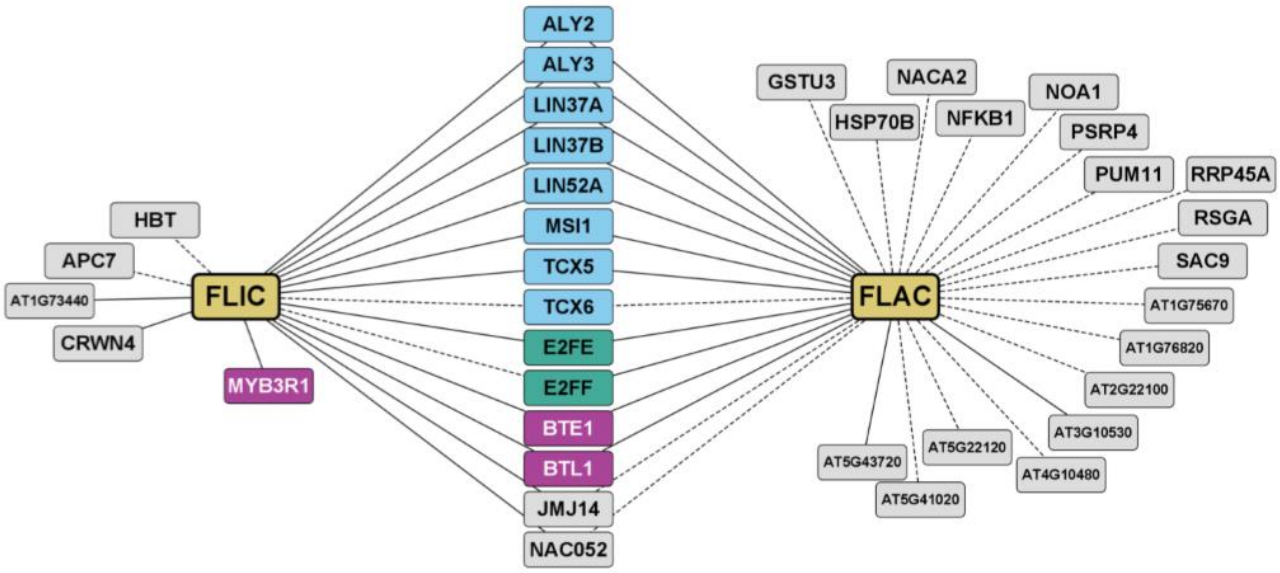
ALY2
ALY3
LIN37A
LIN37B
LIN52A
MSI1
TCX5
TCX6
E2FE
E2FF
BTE1
BTL1
JMJ14
NAC052
HBT
APC7
AT1G73440
CRWN4
FLIC
MYB3R1
GSTU3
NACA2
NOA1
HSP70B
NFKB1
PSRP4
PUM11
RRP45A
RSGA
SAC9
AT1G75670
AT1G76820
AT2G22100
AT3G10530
AT4G10480
AT5G22120
AT5G43720
AT5G41020
FLAC

Figure 2

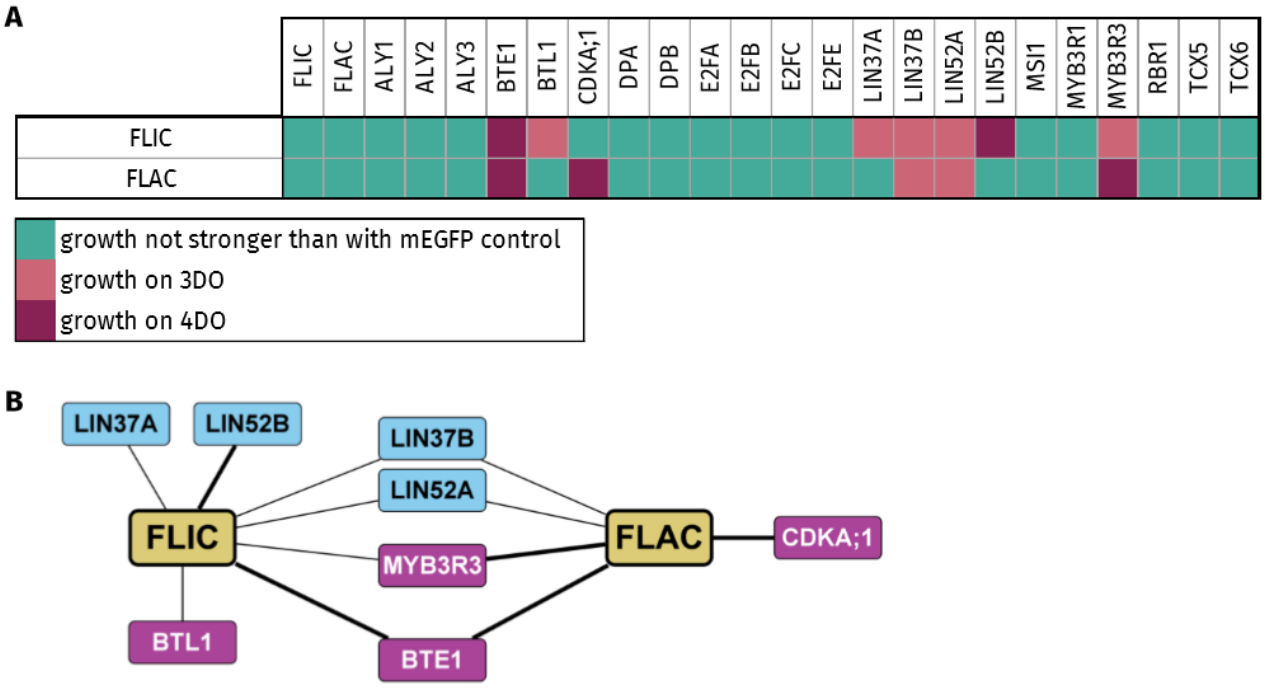
A
FLIC
FLAC
ALY1
ALY2
ALY3
BTE1
BTL1
CDKA;1
DPA
DPB
E2FA
E2FB
E2FC
E2FE
LIN37A
LIN37B
LIN52A
LIN52B
MSI1
MYB3R1
MYB3R3
RBR1
TCX5
TCX6
FLIC
FLAC
growth not stronger than with mEGFP control
growth on 3DO
growth on 4DO

B
LIN37A
LIN52B
LIN37B
LIN52A
FLIC
FLAC
CDKA;1
MYB3R3
BTL1
BTE1

Figure 3

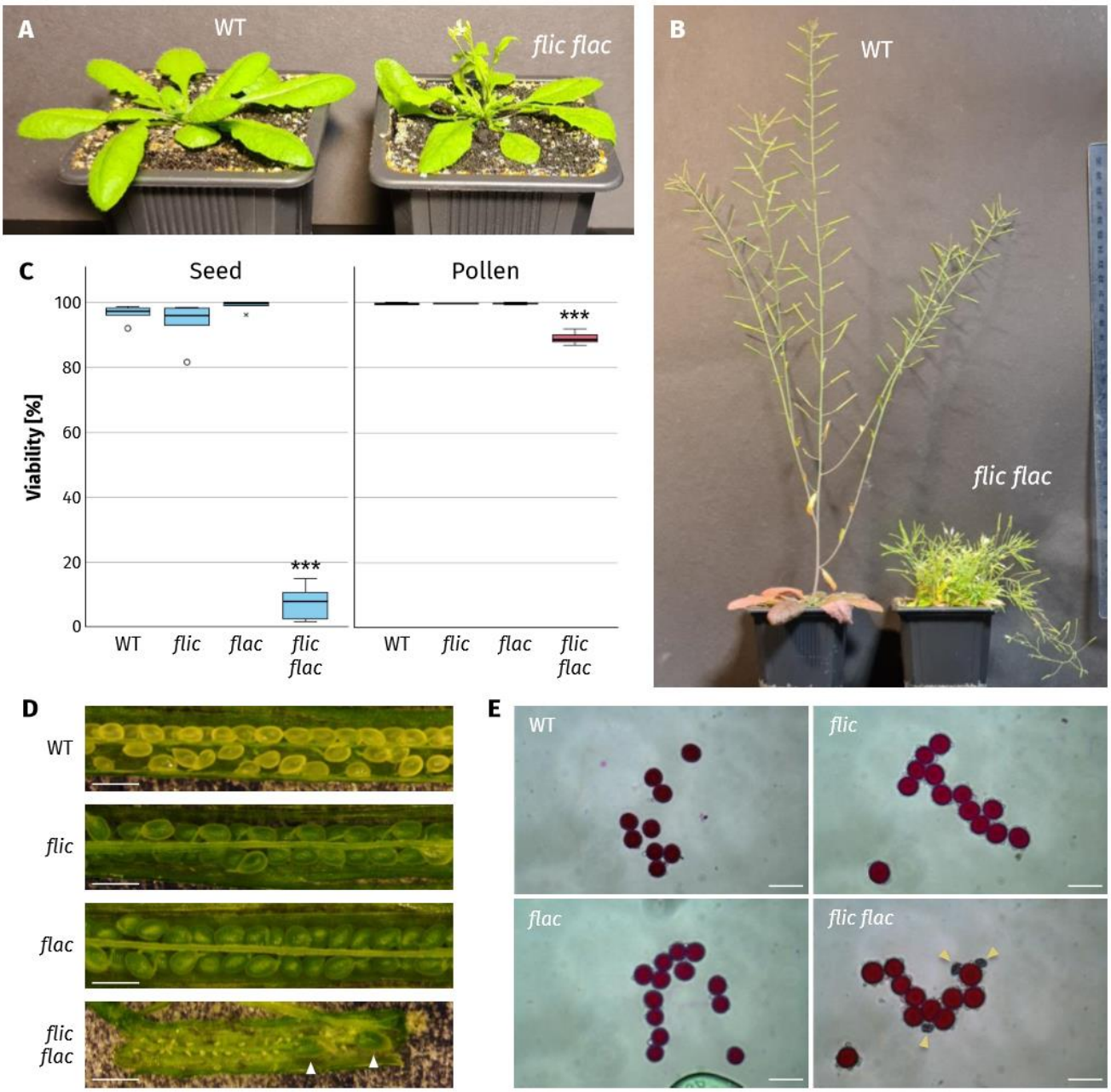
A
WT
flic flac
B
WT
flic flac
C
Seed
Pollen
Viability [%]
100
80
60
40
20
0
***
***
WT
flic
flac
flic flac
WT
flic
flac
flic flac
D
WT
flic
flac
flic flac
E
WT
flic
flac
flic flac

Figure 4

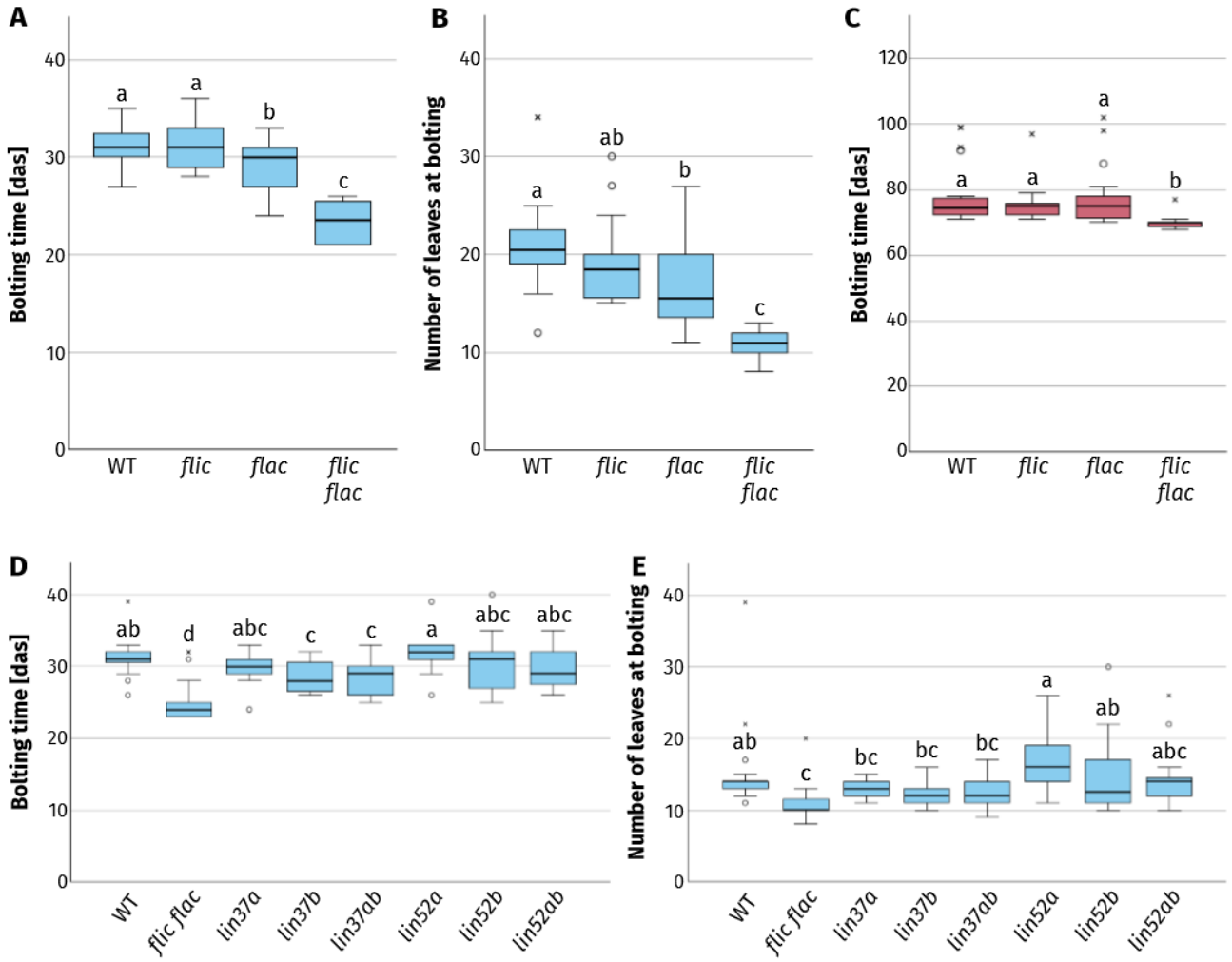
A
Bolting time [das]
40
30
20
10
0
a
a
b
c
WT
flic
flac
flic flac
B
Number of leaves at bolting
40
30
20
10
0
a
ab
b
c
WT
flic
flac
flic flac
C
Bolting time [das]
120
100
80
60
40
20
0
a
a
a
b
WT
flic
flac
flic flac
D
Bolting time [das]
40
30
20
10
0
ab
d
abc
c
c
a
abc
abc
WT
flic flac
lin37a
lin37b
lin37ab
lin52a
lin52b
lin52ab
E
Number of leaves at bolting
40
30
20
10
0
ab
c
bc
bc
bc
a
ab
abc
WT
flic flac
lin37a
lin37b
lin37ab
lin52a
lin52b
lin52ab

Figure 5

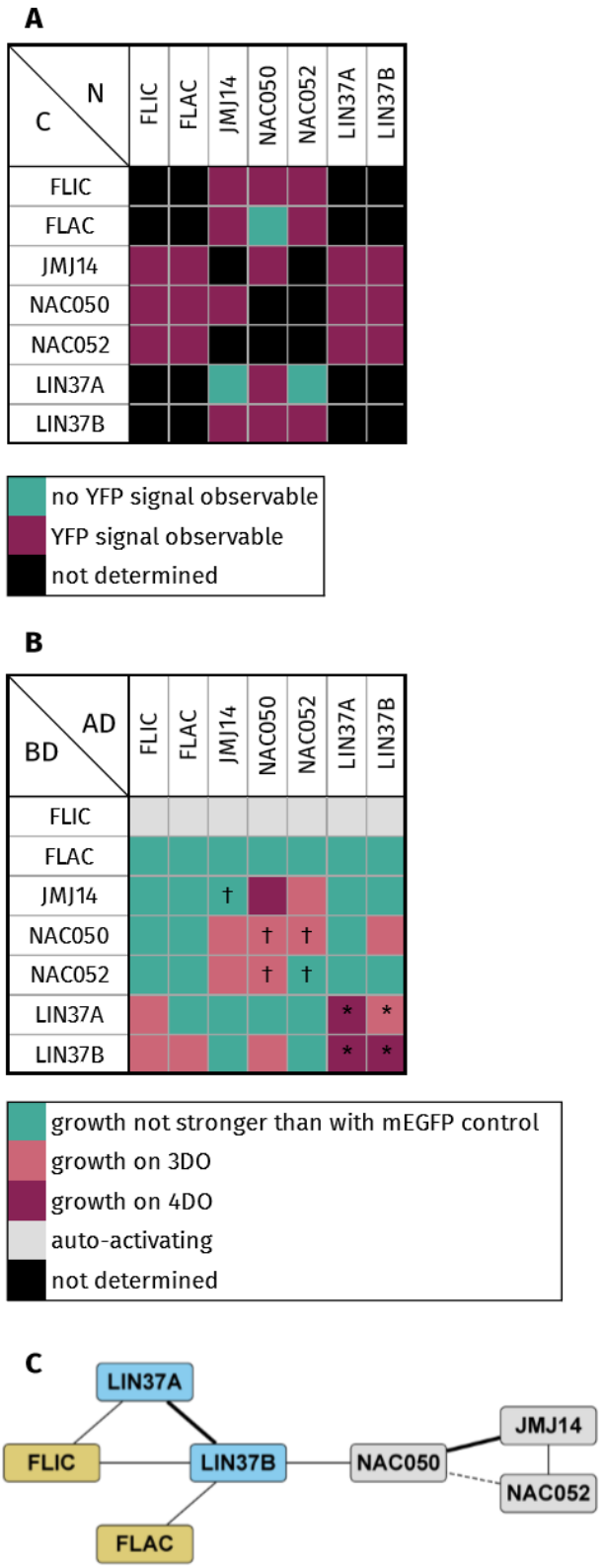
A
C
N
FLIC
FLAC
JMJ14
NAC050
NAC052
LIN37A
LIN37B
no YFP signal observable
YFP signal observable
not determined
B
BD
AD
growth not stronger than with mEGFP control
growth on 3DO
growth on 4DO
auto-activating
not determined
C
LIN37A
FLIC
LIN37B
FLAC
NAC050
JMJ14
NAC052

Figure 6

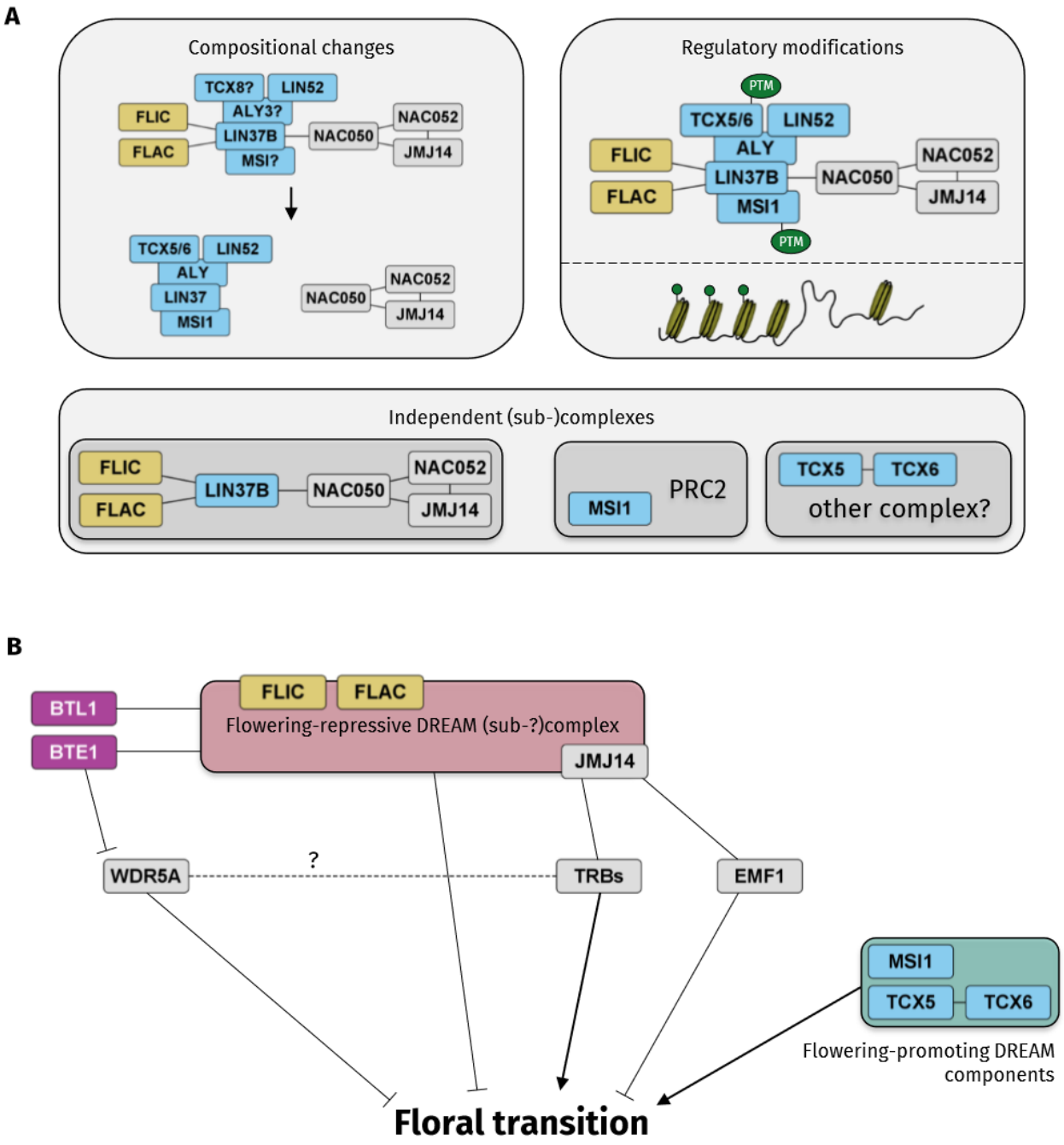
A
Compositional changes
TCX8?
LIN52
ALY3?
FLIC
FLAC
LIN37B
MSI?
NAC050
NAC052
JMJ14
TCX5/6
LIN52
ALY
LIN37
MSI1
NAC050
NAC052
JMJ14
Regulatory modifications
PTM
TCX5/6
LIN52
ALY
FLIC
FLAC
LIN37B
MSI1
NAC050
NAC052
JMJ14
PTM
Independent (sub-)complexes
FLIC
FLAC
LIN37B
NAC050
NAC052
JMJ14
MSI1
PRC2
TCX5
TCX6
other complex?
B
BTL1
BTE1
FLIC
FLAC
Flowering-repressive DREAM (sub-?)complex
JMJ14
WDR5A
?
TRBs
EMF1
MSI1
TCX5
TCX6
Flowering-promoting DREAM components
Floral transition

Figure S1

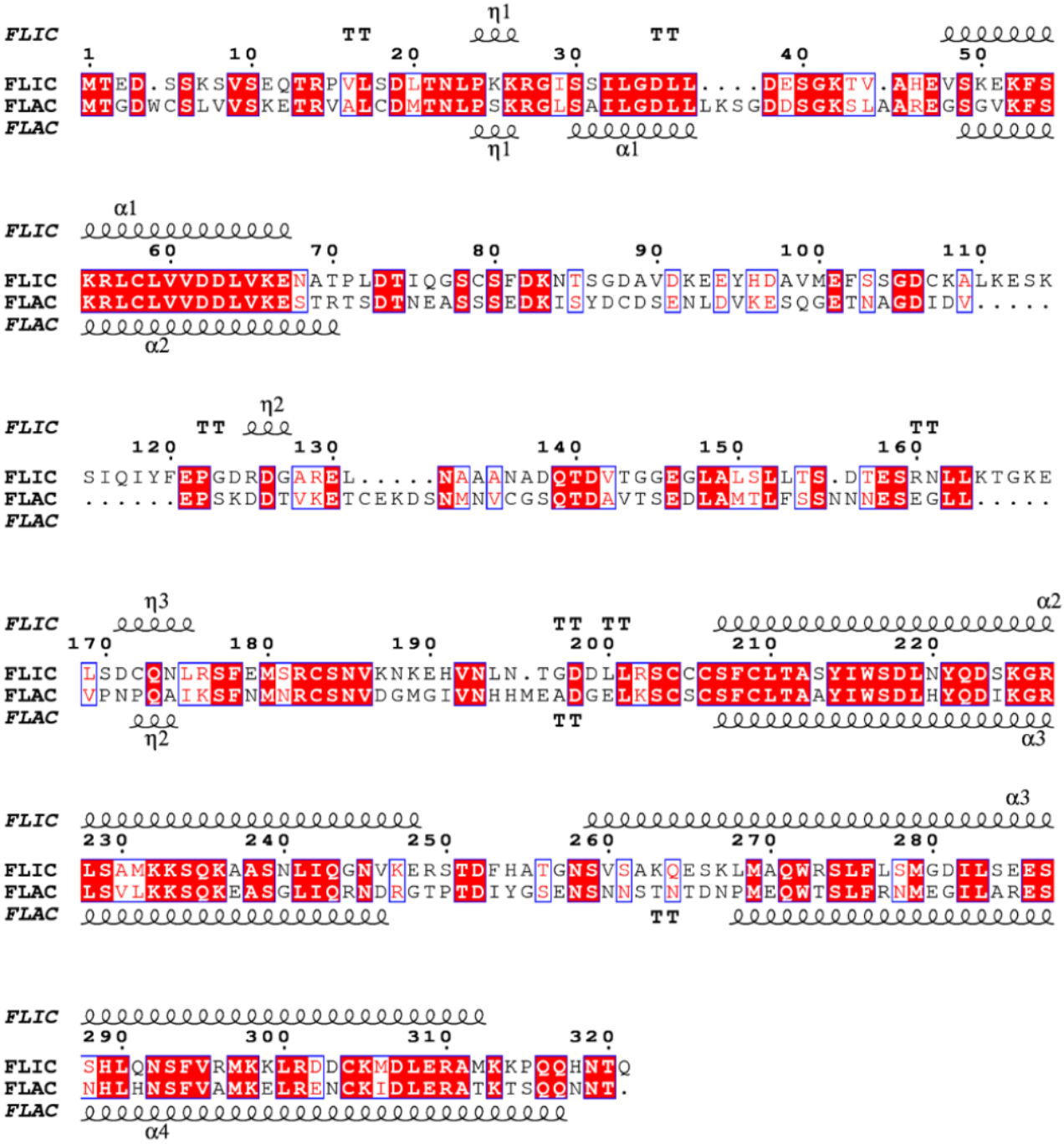

Figure S2

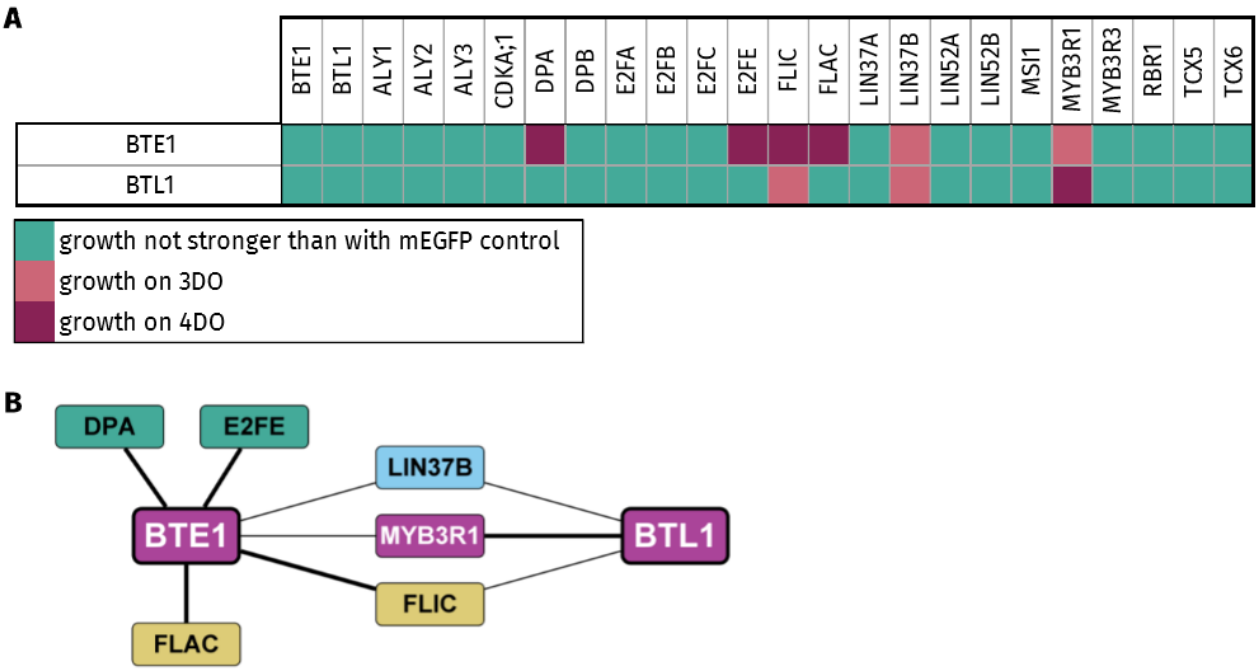
A
BTE1
BTL1
ALY1
ALY2
ALY3
CDKA;1
DPA
DPB
E2FA
E2FB
E2FC
E2FE
FLIC
FLAC
LIN37A
LIN37B
LIN52A
LIN52B
MSI1
MYB3R1
MYB3R3
RBR1
TCX5
TCX6
BTE1
BTL1
growth not stronger than with mEGFP control
growth on 3DO
growth on 4DO

B
DPA
E2FE
LIN37B
BTE1
MYB3R1
BTL1
FLIC
FLAC

Figure S3

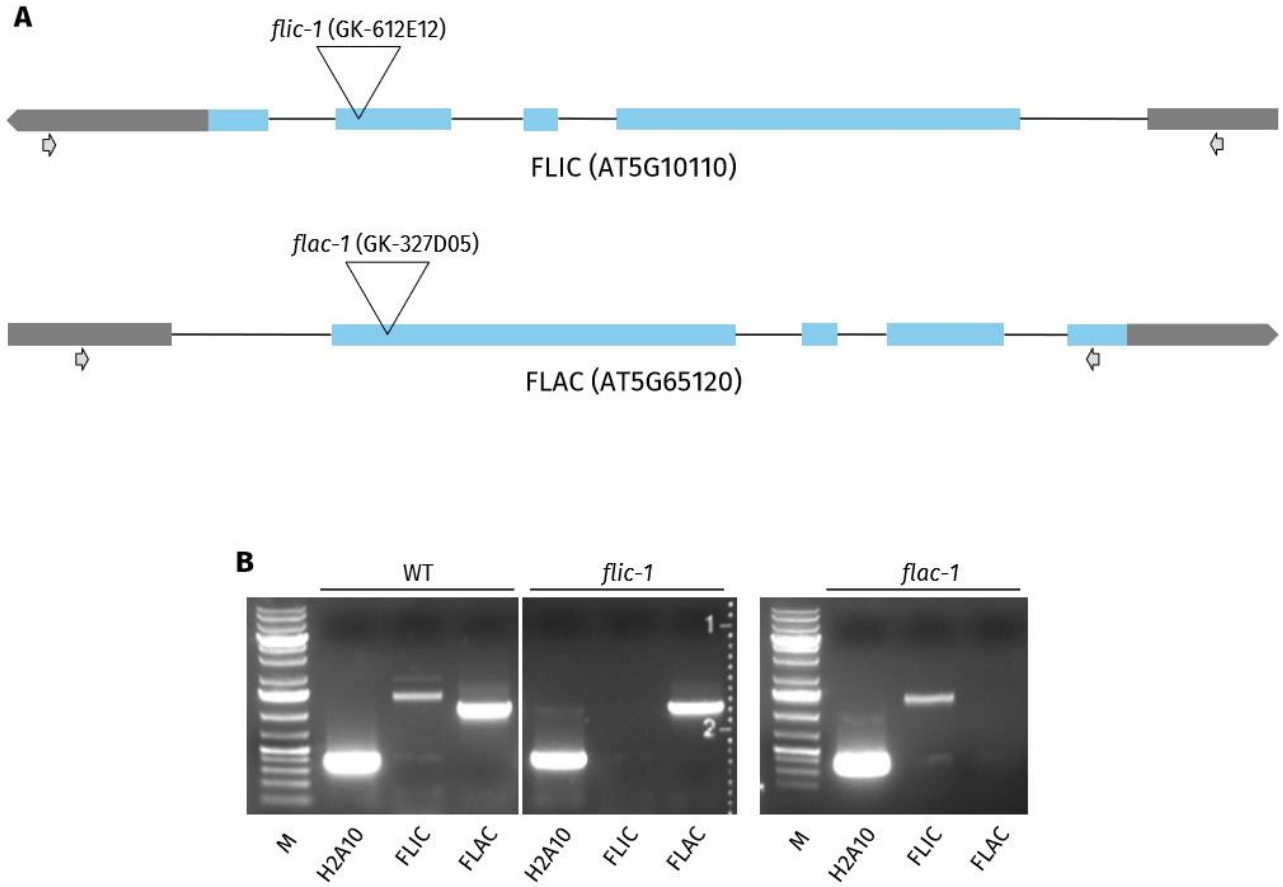
A
flic-1 (GK-612E12)
FLIC (AT5G10110)
flac-1 (GK-327D05)
FLAC (AT5G65120)
B
WT
flic-1
flac-1
1
2
M
H2A10
FLIC
FLAC
H2A10
FLIC
FLAC
M
H2A10
FLIC
FLAC

Figure S4

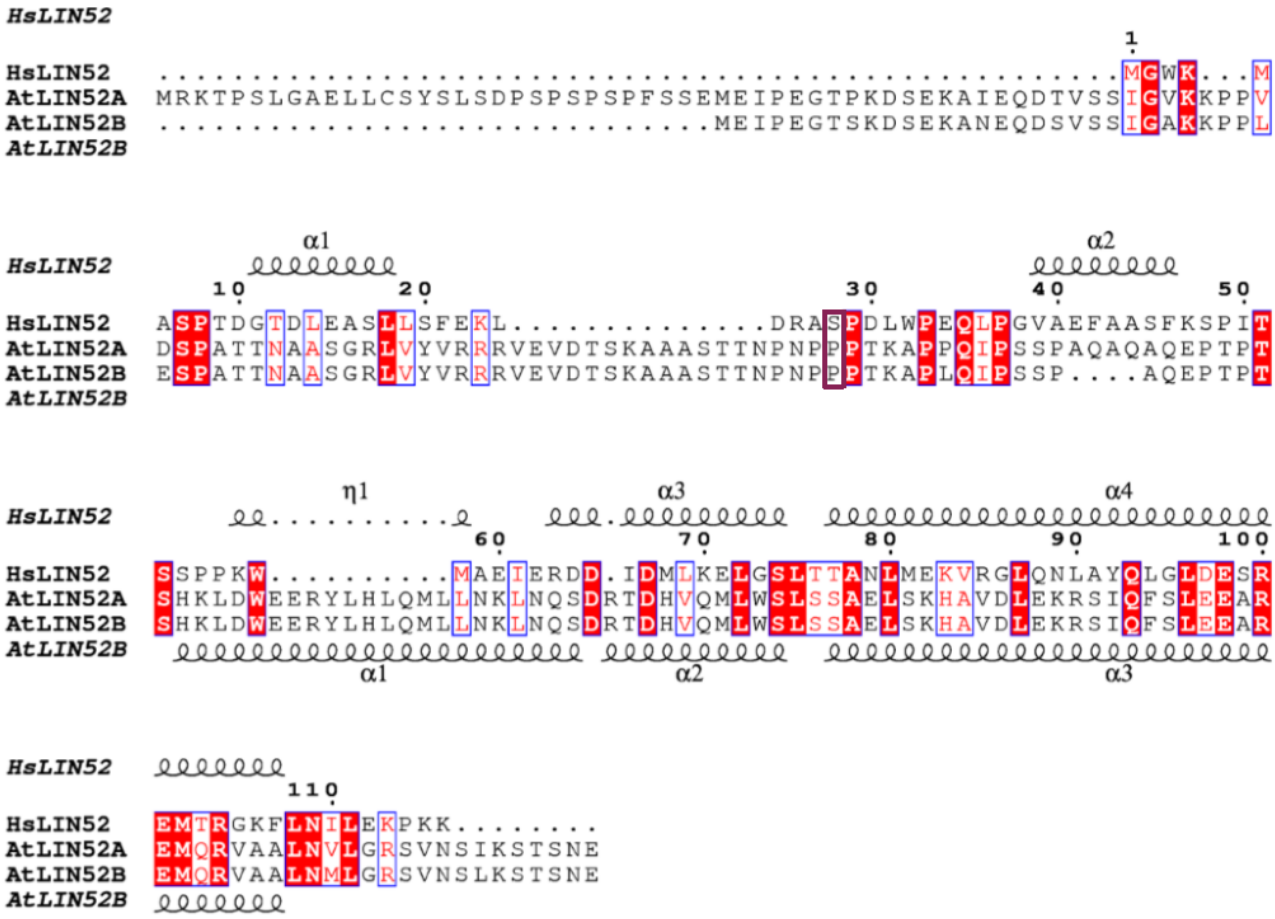

CHAPTER 3

FLIC and FLAC are suppressors of jasmonic acid biosynthesis in *Arabidopsis*

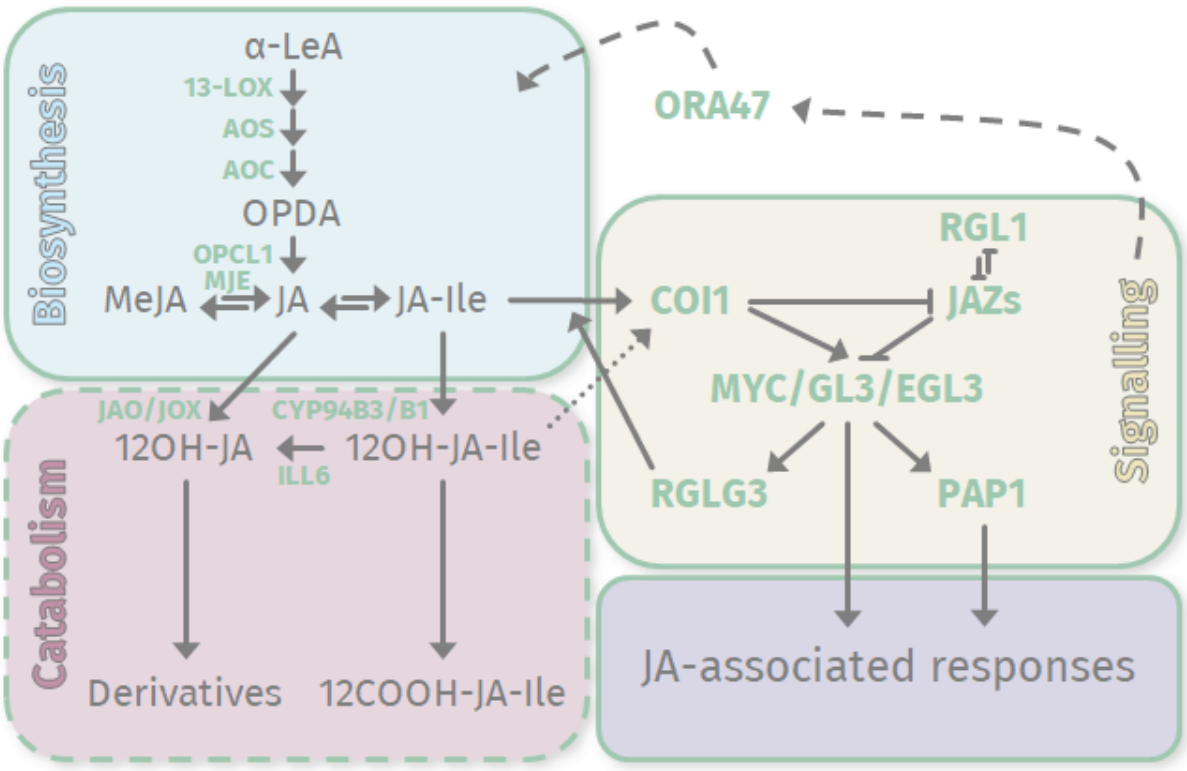

Since publication of the data provided in this chapter will be pursued in the future, they are given in a publication format. Despite presentation in this manner, please note that this is explicitly work in progress; sample sizes and replicate numbers in some cases are still small, and further experiments will be completed prior to submission to a journal.

The following manuscript has not been shared with any of the (current) collaborators prior to submission of this doctoral thesis, hence, no author list is given. Foreign contributions can be found listed in the section “Declaration of contributions”. Since they are not available online yet, Sup Tables are available in the appendix section.

FLIC and FLAC are suppressors of jasmonic acid biosynthesis in *Arabidopsis*

Running title

Control of jasmonic acid biosynthesis by FLIC and FLAC

Keywords

Arabidopsis, FLIC, FLAC, jasmonic acid, phytohormones, stress response

Summary blurb

This study identifies FLIC and FLAC as suppressors of jasmonic acid biosynthesis by exploring the altered transcriptome as well as phytohormone levels in *flic flac* mutants, puts the reactions of these plants towards different stresses in contrast to *coi1* mutants, and finally developmentally analyses an orthologous mutant in *Zea mays*.

Abstract

FLIC and FLAC are two homologous proteins that have been described as repressors of floral transition, and mutation results in severe vegetative defects, most strikingly stunted, bushy growth, as well as drastically reduced fertility. This study illuminates a disrupted phytohormonal homeostasis in *flic flac* mutants and reveals by transcriptomic analyses that the jasmonic acid pathway appears constitutively activated through hyper-activity of its biosynthetic genes. Direct quantification confirms elevated methyl jasmonate levels in the absence of FLIC and FLAC. By characterising their responses to exogenous jasmonate supplementation, boron deficiency, as well as microtubule destabilisation, we demonstrate that *flic flac* mutants consistently contrast with *coi1* mutants, which are insensitive to jasmonic acid. Notably, we extend our findings to *Zea mays* by mutating the only orthologue in this species, leading to developmental retardation and highlighting the importance of FLIC and FLAC across clades.

Introduction

Being sessile organisms, plants are unable to evade their environmental conditions and have developed an elaborate signalling network to provide the best possible response to abiotic and biotic threats. An important part of this network are phytohormones, with jasmonic acid (JA) and its derivatives, collectively called jasmonates, being major players in co-ordinating stress responses. In particular, JA levels govern the trade-off between plant growth and defensive capabilities (Sembdner & Parthier, 1993; Chini et al, 2007; Thines et al, 2007; Yan et al, 2007; Browse, 2009; Yang et al, 2012; Frerigmann et al, 2021; Hewedy et al, 2023).

JA biosynthesis has been a major target of JA research in the past decades and has been reviewed extensively (Wasternack & Hause, 2013; Wasternack & Song, 2017; Shi et al, 2023). JA is derived from galactolipids released from the chloroplast with α-linolenic acid (α-LeA) being its precursor molecule (Nilsson et al, 2012; Lin et al, 2016; Zhai et al, 2017; Wasternack & Strnad, 2018; Yu et al, 2020). Subsequently, α-LeA goes through oxidative processes of the lipoxygenase (LOX) pathway, including ALLENE OXIDE SYNTHASEs (AOSs) and ALLENE OXIDE CYCLASEs (AOCs), with a major intermediate being 12-oxophytodienoic acid (OPDA) (Vick & Zimmerman, 1983; Feussner & Wasternack, 2002; Taki et al, 2005; Kombrink, 2012; Wasternack & Hause, 2013; Arnold et al, 2016; Floková et al, 2016; Wasternack & Strnad, 2018). OPDA derivatives largely replace the functions of JA in bryophytes, however, their influence has diminished to involvement in stress responses throughout evolution in tracheophytes (Pratiwi et al, 2017; Monte et al, 2020, 2022; Jimenez Aleman et al, 2022). OPDA can subsequently be further converted into JA by multiple iterations of β-oxidation, requiring the action of several enzymes, such as 12-OPDA REDUCTASE 3 (OPR3) and (1*R*,2*S*)-3-OXO-2-[(*Z*)PENT-2'-ENYL]-CYCLOPENTAN-1-OCTANOIC ACID-8:0 CoA LIGASE 1 (OPCL1) (Koo et al, 2006; Kienow et al, 2008; Schaller & Stintzi, 2009; Wasternack & Hause, 2013). Further conjugation of JA with isoleucine, yielding jasmonoyl-isoleucine (JA-Ile), is required to confer (most of the) bioactivity (Fonseca et al, 2009; Yan et al, 2009; Wasternack & Strnad, 2016). A plethora of further JA derivatives has been characterised in the last decade (as reviewed in Zhai et al, 2017). Notably, methyl jasmonate (MeJA) serves as a suggested transport form of JA, being easily converted into JA and vice-versa in a single step (Seo et al, 2001; Woldemariam et al, 2012; Koo et al, 2013).

While there is a certain minimal basal expression of JA biosynthesis genes, JA levels in leaves are virtually undetectable (Stenzel et al, 2003; Chung et al, 2008; Glauser et al, 2008; Koo et al, 2009; Schaller & Stintzi, 2009; Heitz et al, 2012). JA-responsive genes are largely repressed by a highly redundant group of transcriptional repressors called JASMONATE-ZIM-DOMAIN PROTEINs (JAZs) that, besides dimerising, work in conjunction with several co-repressors, notably NOVEL INTERACTOR OF JAZ (NINJA) and TOPLESS (TPL) (Chini et al, 2007, 2009; Thines et al, 2007; Yan et al, 2007; Pauwels et al, 2010; Zhang et al, 2015b; Campos et al, 2016). The F-box protein CORONATINE-INSENSITIVE 1 (COI1) functions as a JA-Ile receptor that, as soon as JA levels rise above a certain threshold, targets JAZs for proteasomal degradation (Xie et al, 1998; Devoto et al, 2002; Xu et al, 2002; Ren et al, 2005). Strikingly, *coi1* mutants are insensitive to JA and exhibit defects in all JA-dependent mechanisms (Feys et al, 1994; Xu et al, 2002; Zhai et al, 2017; Bömer et al, 2018). Once JAZs are degraded, a central regulator of the JA response, MYELOCYTOMATOSIS 2 (MYC2), is de-repressed. MYC2 is an activator of a large set of tightly controlled JA-responsive genes and additionally activates a positive feedback loop amplifying JA biosynthesis (Van Moerkercke et al, 2019). Further JAZ-repressed transcription factors include basic helix–loop–helix (bHLH) proteins, such as GLABRA 3 (GL3) and ENHANCER OF GL3 (EGL3), as well as MYELOBLASTOMA (MYB) transcription factors, such as PRODUCTION OF ANTHOCYANIN PIGMENT 1 (PAP1) (as reviewed in Wasternack & Hause, 2013; Zhai et al, 2017). While active, the JA pathway governs the diversion of resources from plant growth into resistance against biotic and abiotic stressors and influences several developmental processes, such as seed germination, root growth, and flowering time (Kombrink, 2012; Zhang et al, 2015a; Wasternack & Song, 2017; Zhai et al, 2017; Heitz et al, 2019; Delgado et al, 2021; Li et al, 2022; Zhao et al, 2022).

JA catabolism offers an additional convoluted layer of control. The highly redundant CYTOCHROME P450 94 (CYP94) family is able to either hydroxylate JA-Ile to 12OH-JA-Ile or to oxidise it to 12COOH-JA-Ile, the former retaining a significantly diminished bioactivity and the latter becoming fully inactive (Koo et al, 2011, 2014; Heitz et al, 2012; Aubert et al, 2015; Bruckhoff et al, 2016). Counterintuitively, higher order *cyp94* mutants display phenotypes that are similar to those caused by JA-Ile deficiency (Poudel et al, 2016). This could recently be related to the presence of a known second catabolic pathway, prominently featuring INDOLE-3-ACETIC ACID-ALANINE RESISTANT 3 (IAR3) and

INDOLE-3-ACETIC ACID-LEUCINE RESISTANT-LIKE GENE 6 (ILL6), both exhibiting amidohydrolase activities that deconjugate the isoleucyl moiety from both JA and tuberonic acid (12OH-JA) (Widemann et al, 2013; Zhang et al, 2016; Marquis et al, 2020). Lastly, JA can be oxidised directly by JA OXIDASEs (JAOs) and JA-INDUCED OXYGENASEs (JOXs), yielding 12OH-JA without previously having been conjugated to Ile (Caarls et al, 2017; Smirnova et al, 2017).

Crosstalk between JA and other phytohormones is well characterised. While IAR3 and ILL6 have been discovered in the context of auxin signalling, they only facilitate one of multiple connection points between JA and auxin. Further major players include ETHYLENE RESPONSE FACTOR109 (ERF109) for lateral root formation as well as WRKY57, a transcription factor competitively up-regulated by auxin and down-regulated by JA, involved in leaf senescence (Cai et al, 2014; Jiang et al, 2014; Xu et al, 2020). There is also a complex interplay described between JA and the abscisic acid (ABA) pathway that seems largely synergistic (as reviewed in Delgado et al, 2021; Liu & Timko, 2021). An especially versatile connector, OCTADECANOID-RESPONSIVE APETALA 2/ERF-DOMAIN TRANSCRIPTION FACTOR 47 (ORA47), has been characterised as being involved in the biosynthesis and/or signalling of nine phytohormones, both activating and repressing genes, especially those involved in the JA and ABA pathways (Chen et al, 2016). In contrast to ABA, JA and salicylic acid (SA) interact in a generally antagonistic manner, crucially facilitated by MITOGEN-ACTIVATED PROTEIN KINASE 4 (MPK4) and GLUTAREDOXIN 480 (GRX480) (Brodersen et al, 2006; Zander et al, 2012). Further crosstalks in different contexts have been extensively reviewed (Yang et al, 2019; Delgado et al, 2021; Hewedy et al, 2023).

Flowering time phenotypes have long been observed for mutants of the JA pathway, such as in *coi1* mutants that flower early, whereas *jaz* mutants flower late. The mechanistic intricacies of how JA levels affect floral transition have been progressively elucidated in recent years and phytohormonal pathways are being crosslinked in more and more detail (as reviewed in Zhao et al, 2022; Huang et al, 2023). The DP, RB-like, E2F, and multi-vulval class B (MuvB)-core (DREAM) complex is a canonical transcriptional repressor featuring a constant core complex (MuvB) that is able to change its active interactors based on cell cycle state and phase, developmental stage, as well as environmental cues and stresses (Korenjak et al, 2004; Litovchick et al, 2007; Schmit et

al, 2007; Lang et al, 2021, 2023; Asthana et al, 2022; Koliopoulos et al, 2022). Its members ALWAYS EARLY (ALY, a LIN9 homologue), ABNORMAL CELL LINEAGE PROTEIN 37 (LIN37), LIN52, TESMIN/TSO1-LIKE CXC (TCX, a LIN54 homologue), and MULTICOPY SUPPRESSOR OF IRA (MSI, a RBBP4 homologue) comprise the MuvB-core complex, while its interactors, such as RETINOBLASTOMA-RELATED 1 (RBR1), DIMERIZATION PARTNER (DP), E2 PROMOTER BINDING FACTOR (E2F), and MYELOBLASTOMA 3R (MYB3R), facilitate the required specificity to initiate and maintain the appropriate transcriptional program (Kobayashi et al, 2015; Fischer & Müller, 2017). While there have been observations hinting at a role of the DREAM complex in flowering time regulation before (Bouveret et al, 2006; Ning et al, 2020), we were able to demonstrate this recently by characterising early-flowering phenotypes for LIN37 as well as the plant-specific DREAM interactors FLORAL INDUCTION CONTROLLER (FLIC) and FLORAL ANTICIPATION CONTROLLER (FLAC). We identified FLIC and FLAC based on tandem affinity purification (TAP) experiments using MuvB-core members and could show that they interact with the JUMONJI 14 (JMJ14)/NAM, ATAF1, and CUC1/CUC2 050 (NAC050)/NAC052 module (Lang et al, 2023), their absence leading to early flowering as well (Ning et al, 2015; Zhang et al, 2015c; Rodrigues et al, 2021). Strikingly, concomitant loss of *FLIC* and *FLAC* leads to severe defects in vegetative growth and fertility (Lang et al, 2023). Whether and how phytohormones are involved in this control, however, remained unclear.

In this study, we have analysed the transcriptome of *flic*, *flac*, and *flic flac* double mutants by mRNA-seq experiments to further investigate the causes of their phenotypes. We were thereby able to demonstrate a de-regulation of especially those genes that are part of the JA pathway. By investigating the response of *flic flac* mutants to pathogen attack, exogenous supply of MeJA, as well as by measuring JA levels directly, we could demonstrate that JA biosynthesis is constitutively up-regulated in these mutants, likely leading to resources being constantly diverted from vegetative growth towards bolstering defensive capabilities. The phenotypes we could observe stand in stark contrast to *coi1* mutants, which lack a functional JA response. Finally, we could highlight a developmental role of Zm*Flac*, the only homologue found in *Zea mays*.

Results

The transcriptome of *flic flac* double mutants reveals FLIC and FLAC as key regulators of JA metabolism

To further understand the cause behind the phenotypes that we could observe in *flic flac* double mutants (Lang et al, 2023), we isolated RNA from 9-d-old seedlings of wild-type, *flic* and *flac* single mutant, as well as *flic flac* double mutant plants and performed mRNA-seq experiments to identify differentially expressed genes (DEGs). Noticeably, a vast majority of genes is only de-regulated when both FLIC and FLAC are absent. While with thresholds of logfc > 0.7 and adjusted $P < 0.05$, 1 005 DEGs could be detected in the double mutant, only 8 and 52 were detected in the *flic* and *flac* single mutants, respectively (Fig 1A and Table S1). This indicates that these two homologues work in a transcriptionally highly redundant manner as we had expected from their high sequence identity of 47.2% (Lang et al, 2023). Further, 87.6% of DEGs in the *flic flac* double mutant were up-regulated, demonstrating the repressive nature of FLIC and FLAC. The only genes that we found up-regulated in all *flic*, *flac*, and *flic flac* mutants were *CRYPTOCHROME-INTERACTING BASIC-HELIX-LOOP-HELIX 1-LIKE 1* (*CIL1*), involved in flowering time regulation (Liu et al, 2013, 2018), as well as the uncharacterised *AT1G54890*.

We utilised the PANTHER Gene List Analysis tool (Thomas et al, 2022) to identify statistically overrepresented gene functions (applying Fisher's Exact test with Bonferroni correction) and centred our analysis on biological process gene ontology (GO) terms to gain insights into the potential causes of the *flic flac* phenotype (Lang et al, 2023). Strikingly, a large number of significantly overrepresented up-regulated biological processes in these mutants relate to phytohormonal signalling (Table S2), including “response to abscisic acid” (2.6-fold enrichment) and “response to salicylic acid” (4.3-fold enrichment), with multiple GO terms focusing on JA synthesis and signalling (“response to jasmonic acid” being 5.0-fold enriched) and its effects, such as secondary metabolite processes and pathogen defence (Cox, 2022). The only significantly overrepresented down-regulated biological process we found in *flic flac* mutant seedlings is “positive regulation of organ growth” (Table S3), which has been

demonstrated to be affected by JA before (Hyun et al, 2008; Uyehara et al, 2023). While we can observe DEGs in the entirety of JA biosynthesis (e.g., several 13-LOXs and OPCL1) and signalling (e.g., different JAZs, MYBs, and MYC2), there are also further up-regulated DEGs in the JA catabolism pathway (e.g., several CYP94s and ILL6) (Fig 1B and Table 1), making it highly likely that we observe at least partially also secondary effects. These findings strongly hint at FLIC and FLAC as repressors of JA metabolism. We could also determine that absence of both FLIC and FLAC is required for de-regulation of all but one gene with the GO term annotation "response to jasmonic acid", confirming a high redundancy in the context of JA metabolism (Fig 1A). Only JAZ6, which is up-regulated in *flic flac* mutant seedlings (logfc: 0.85; $P = 1.3 \times 10^{-6}$), is significantly down-regulated in *flac* mutant plants (logfc: −0.74; $P = 0.001$). However, the low logfc values as well as the minor significance in *flac* mutants might indicate its detection as a false positive.

JA and auxin levels are constitutively increased in *flic flac* mutants

Our observation of up-regulated genes in the JA biosynthesis pathway indicated that JA levels might be constitutively elevated in *flic flac* mutant plants. To analyse whether phytohormonal levels are indeed differing from the wildtype, we measured the levels of JA and other phytohormones in 9-d-old *flic flac* seedlings (Fig 2). Congruent with the mRNA-seq results we obtained, we could see significantly elevated levels of methyl jasmonate (MeJA) (wildtype: 47.1±5.3 MAU; *flic flac*: 63.8±2.2 MAU; $P = 0.044$), a metabolic derivative of JA. We could see a similar, though non-significant trend for epi-jasmonic acid (epi-JA) (wildtype: 11.6±4.6 MAU; *flic flac*: 36.1±12.6 MAU; $P = 0.142$), a naturally occurring epimer of JA (Wu et al, 2014; Shamsi & Akter, 2022). Interestingly, we could also observe levels of indole-3-acetic acid (IAA) (wildtype: 28.9±1.4 MAU; *flic flac*: 64.6±0.9 MAU; $P < 0.001$), the most common auxin class phytohormone in higher plants, that are more than double of what we measured in wild-type seedlings, despite none of the statistically overrepresented GO terms being related to auxin directly. These results provide direct evidence that FLIC and/or FLAC are necessary to properly regulate JA biosynthesis as well as auxin levels, and further indicate that the up-regulation of JA-catabolic genes is a secondary effect.

Absence of FLIC and FLAC confers phenotypes that contrast with those observed in *coi1* mutants

Being a central integrator of JA signalling, COI1 is of crucial importance for the ability to respond to JA-mediated cues (Fig 1B). Consequently, *coi1* mutants exhibit phenotypes that are representative of a disrupted JA response pathway and should stand in contrast to a constitutively active JA response, as we expect in a *flic flac* background. Hence, we decided to comparatively analyse *flic flac* and *coi1* mutant phenotypes.

As we have reported before, *flic flac* mutants exhibit a strong loss of apical dominance resulting in a bushy phenotype (Lang et al, 2023). This stands in contrast to a previously reported strengthening of apical dominance in *coi1* mutants in the Wassilewskija (WS) ecotype (Kim et al, 2013). Note that this could not yet be observed in the Columbia-0 (Col-0) ecotype used throughout this study. This being said, the *coi1* mutants we refer to hereafter all possess the Col-0 background.

It has been demonstrated before that JA pathway mutants react differently to when JA is supplied exogenously (Xu et al, 2002; Campos et al, 2016). To gauge the effects of a dys-regulation of JA signalling in *flic flac* mutants, we assessed their growth on medium containing MeJA (Fig 3A). When exposed to MeJA, we could observe that *flic flac* mutant roots were significantly shorter (1.68±0.12 cm; P = 0.041) than those of wild-type plants (2.27±0.12 cm), indicating that the high constitutive levels of JA in *flic flac* mutants prime them for down-regulating root growth more than in the wildtype once even more JA is present in the plant. This stands in contrast to the inability of *coi1* mutants to down-regulate root growth in these conditions (Xu et al, 2002).

We also followed plant development on media supplied with different amounts of boron (B), since it has been shown before that low B conditions activate JA biosynthesis. Consequently, *coi1* mutants are not able to down-regulate root growth as much as the wildtype upon B deficiency (Huang et al, 2021). When we analysed the root growth of *flic flac* mutants on modified Hoagland medium, either containing a high B (++B) or a low B (–B) concentration, root growth was not distinguishable from the wildtype in either case (Fig 3B). However, we could observe leaf and root phenotypes that did not appear in the wildtype (Fig 3C), including a

darkening of cotyledons and leaves, increased leaf epinasty, as well as an increased length of root hair. These are described phenotypes in response to B deficiency (Dell & Huang, 1997; Duran et al, 2018), that appear to occur only in *flic flac* mutants and not in the wildtype in our conditions, indicating that *flic flac* mutants are already primed to trigger a low B response due to their constitutively elevated JA levels. Since we could observe "cellular response to iron ion starvation" as a statistically enriched GO term, we also tested the response of *flic flac* mutants to medium containing different amounts of Fe, however, we could not detect any differences (Fig S1).

It has been demonstrated that the cortical microtubule array in *coi1* mutant root cells is less affected by oryzalin, a microtubule-destabilising drug, than in the wildtype (Yang et al, 2017). The authors reason that JA inhibits microtubule polymerisation via COI1 action. Thus, we analysed the response of *flic flac* mutants to oryzalin treatment (Fig 3D), employing *mitotic arrest-deficient 1* (*mad1*) mutants as a positive control (Komaki & Schnittger, 2017). Whereas a concentration of 150 nM oryzalin barely affects the wildtype (90.7±6.1%), *flic flac* mutants show a significant decrease in relative root length (74.0±1.8%; $P = 0.031$). This finding extends to the higher concentration of 200 nM oryzalin (wildtype: 70.6±4.3%; *flic flac*: 52.1±1.6%; $P = 0.014$). These results show that root growth in *flic flac* mutants with a constitutively active JA response is hypersensitive to a microtubule destabiliser, corroborating the theory that JA inhibits microtubule polymerisation.

Cortical microtubule organisation is dependent on the functionality of aurora kinases (Weimer et al, 2016). To check whether inhibition of aurora kinases would have an effect on *flic flac* mutants, we applied hesperadin, an aurora kinase inhibitor (Demidov et al, 2009), in the context of root growth assays (Fig 3E). Since this has – to the best of our knowledge – not been done before, we established a concentration of 3.5 µM as suitable, while again using *mad1* mutants as a positive control since we hypothesised spindle assembly checkpoint (SAC) components to be hypersensitive due to the observed reduced abundance of the SAC core component BUDDING UNINHIBITED BY BENZYMIDAZOL 1 (BUB1)/MAD3 FAMILY 3 (BMF3) upon hesperadin treatment (Lampou et al, 2023). We could observe that *flic flac* roots (0.76±0.03 cm; $P < 0.001$) were significantly shorter than the wildtype (0.99±0.03 cm) when exposed to

hesperadin, possibly providing further evidence for a microtubule-stabilising function of FLIC and FLAC.

Mutation of the only maize orthologue, ZmFLAC, leads to developmental retardation

To find out whether our findings are relevant in other plant species, we generated a CRISPR mutant in *Zea mays*. A similarity search for the AtFLIC and AtFLAC protein sequences in the A188 genome using BLAST yielded one orthologue, Zm00056aa025545, with 23.7% and 28.5% identity, respectively (Fig 4A). Hence, we will refer to this gene hereafter as Zm*Flac*. Targeting this gene close to the N-terminus led to the generation of a frameshift mutant that we designated Zm*flac-c1*, leading to the loss of at least the N-terminal half of the protein, when taking into account the possibility that transcription might also commence at the next available in-frame start codon near the centre of the coding sequence (Fig 4A, red dagger). The frameshift was caused by deletion of a single guanidine 19 bp after the transcriptional start of Zm*Flac*.

No striking phenotypic differences between genotypes could immediately be observed in a segregating Zm*flac-c1* population. However, analogous to our previous description of a role in flowering time regulation in *Arabidopsis thaliana* (Lang et al, 2023), we measured the time until the VT stage (visibility of all tassel branches) was reached. We found that Zm*flac-c1* mutants reach this stage significantly later (69.8±0.4 days after sowing [das]; P = 0.005) compared to the wildtype (67.8±0.4 das) and the heterozygous (67.8±0.3 das) sub-populations (Fig 4B). This result stands in contrast to what we could observe regarding flowering time in *Arabidopsis thaliana*, but demonstrates that ZmFLAC also plays a role in regulating the development of *Zea mays* in the line A188, possibly leading to developmental retardation due to high JA levels.

Discussion

Tight regulation of JA levels is of crucial importance for a plant to optimally divide its resources into growth and defence. Uncontrolled high levels of JA lead to a waste of energy into possibly unnecessary defensive capabilities, while insufficient levels cause susceptibility to pathogen attacks and/or abiotic stresses and eventual demise. In this study, we reveal FLIC and FLAC as essential repressors of JA biosynthesis.

Having analysed the transcriptome of *flic flac* mutant seedlings, a clear de-regulation could be seen throughout JA-related pathways, including biosynthesis, signalling, and catabolism (Fig 1). Whether the de-regulations we observed are direct or indirect cannot be concluded from our experiments. However, our previous findings of auto-activation in the context of yeast two-hybrid assays using BD-fused FLIC and FLAC constructs hint at an activity as a transcription factor (Causier & Davies, 2002; Lang et al, 2023). While they might directly bind promoters of genes involved in JA biosynthesis, we also found the mRNA of MYC2 and ORA47, two key regulators of JA biosynthesis (Chen et al, 2016; Van Moerkercke et al, 2019), significantly up-regulated, suggesting FLIC and FLAC might potentially control these regulators. Since a positive feedback loop has been described upon JA induction (Hickman et al, 2017), epistasis stays unclear at this point.

Strikingly, only very few genes could be detected as de-regulated in the single mutants compared to the double mutant background. This finding underlines the highly redundant activity of these homologues as evident in their phenotypes being relatively close to the wildtype compared to the double mutant (Lang et al, 2023). Since we reported a mild early-flowering phenotype for the *flac* single mutant, we also analysed our mRNA-seq data for flowering time genes by comparing the DEGs to genes listed by the Flowering Interactive Database (FLOR-ID) (Bouché et al, 2016). We detected the *FLOWERING LOCUS C* (*FLC*) homologue *MADS AFFECTING FLOWERING 5* (*MAF5*) as the only gene de-regulated in both *flac* and *flic flac* mutants, however, manual curation also revealed *CIL1* as up-regulated in both genotypes (Fig S2). It has been demonstrated that *CIL1* overexpression promotes flowering and its homologues interact with CONSTANS (CO) to bind the *FLOWERING LOCUS T* (*FT*) promoter (Liu et al, 2013, 2018). In contrast, while *maf5* mutants do not flower early by themselves,

MAF5 overexpression leads to repression of floral transition (Ratcliffe et al, 2003; Kim & Sung, 2010). Further known flowering genes are de-regulated in the *flic flac* double mutant (Fig S2), however, no clear picture can be drawn without further experiments that go beyond the scope of this study. Possibly counteracting JA as a flowering repressor (as reviewed in Zhao et al, 2022), we could measure elevated levels of auxin (Fig 2), which is a flowering promoter (as reviewed in Cucinotta et al, 2021). Auxin biosynthesis is induced by JA (Uppalapati et al, 2005; Sun et al, 2009; Hentrich et al, 2013), but conversely, we could not see any statistically enriched GO terms directly related to auxin (Tables S2 and S3), and we also could not detect any significant de-regulation of ERF109 or WRKY57 in our mRNA-seq data (Table S1). Thus, it appears plausible that the high auxin levels do not result in a hyper-active auxin signalling downstream. Nevertheless, we found ABA and SA responses as statistically enriched GO terms in the *flic flac* double mutants (Table S2) which promote flowering as well (as reviewed in Campos-Rivero et al, 2017) and might therefore explain the early-flowering phenotype. While exogenous ABA application can delay flowering, ABA has been found to promote flowering especially under stress conditions (Izawa, 2021), which might be simulated in a plant constitutively shifting resources into defensive capabilities, such as *flic flac* mutants. Lastly, it should be noted that an mRNA-seq experiment closer to the time point of floral transition might reveal more relevant data regarding regulation of flowering.

We could further demonstrate that JA levels in *flic flac* mutants are constitutively increased by direct measurement of MeJA and epi-JA (Fig 2). This indicates that the main function of FLIC and FLAC is the suppression of inappropriate JA biosynthesis. The resulting high JA levels in *flic flac* plants appear to consequently hyper-activate JA signalling and response, which is further corroborated by the fact that exogenous application of MeJA causes reduced root growth (Fig 3A) comparable to what has been described for *jaz* mutants, that fail to counteract transcription factors involved in the JA response (Campos et al, 2016). However, MeJA levels were only around 1.4-fold elevated in *flic flac* mutants and we could detect not more than a trend for epi-JA (for which levels seem roughly 3.1-fold increased). Thus, it would be highly revealing to measure the levels of JA-Ile, the most bioactive JA derivative (Fonseca et al, 2009; Yan et al, 2009; Wasternack & Strnad, 2016), since, according to

our mRNA-seq data, the JA response seems to be up-regulated as well. In the absence of FLIC and FLAC, higher levels of JA-Ile are hence to be expected. These results taken together suggest that JA biosynthesis is de-repressed in the absence of FLIC and FLAC, while JA signalling and response are then reacting to the elevated JA levels. JA catabolism might be up-regulated as a secondary consequence.

It would be interesting to determine whether *flic flac* mutants exhibit an altered resistance against herbivore and/or pathogen insult as a result, since such effects can be observed in *coi1* and *jaz* mutants (Ralhan et al, 2012; Guo et al, 2018; Liu et al, 2021). There also seems to be an extensive crosstalk between phytohormonal pathways in *flic flac* mutants since we could see "response to abscisic acid" and "response to salicylic acid" as statistically enriched GO terms (Table S2). While it is not clear why we could not consequently measure increased SA levels, but rather detected elevated auxin concentrations (Fig 2) without any directly related GO term being enriched, these findings pose a mystery as of now that is waiting to be unravelled in future studies.

Our findings are further corroborated by the plethora of phenotypes of *flic flac* mutants that contrast those found in *coi1* mutants (Fig 3). We demonstrated that *flic flac* root growth upon MeJA treatment is shorter, resembling *jaz* mutants (Campos et al, 2016), whereas in *coi1* mutants it is longer than in the wildtype (Xu et al, 2002). Apical dominance is severely weakened (Lang et al, 2023), whereas *coi1* mutants gain apical dominance in the WS ecotype (Kim et al, 2013). While this has not been observed in the Col-0 ecotype used as a background for the *flic flac* mutant, apical dominance is dependent on a multitude of factors (as reviewed in Beveridge et al, 2023), possibly masking COI1's role in this process in certain ecotypes.

Whereas *coi1* mutants are unable to down-regulate root growth in low B conditions (Huang et al, 2021), *flic flac* mutants exhibit a darkening of cotyledons and leaves, increased leaf epinasty, as well as an increased root hair length earlier than the wildtype (Fig 3C), which are typical responses to B deficiency (Dell & Huang, 1997; Duran et al, 2018). Especially root hair elongation has been substantially linked to elevated JA levels (as reviewed in Han et al, 2023). These findings demonstrate another contrasting response and agree with the results of exogenous MeJA application since low B conditions up-regulate JA levels endogenously. Interestingly,

this appears to be facilitated by ORA47 up-regulation (Huang et al, 2021), which we could also observe constitutively in *flic flac* mutants (Fig 1).

Finally, we could show that *flic flac* plants are hyper-sensitive to oryzalin and hesperadin (Fig 3D and E), corroborating the finding that JA de-stabilises microtubules in a COI1-dependent manner (Yang et al, 2017). The results of our hesperadin treatment seem to indicate that this is further dependent on aurora kinase activity. In the light of a recent publication demonstrating that aurora kinases are repressed by the DREAM complex in humans (Duan et al, 2022), one might speculate that a similar regulation is happening in Arabidopsis, possibly including FLIC and FLAC. Further, it has recently been shown that JA biosynthesis and chromosome condensation and segregation co-ordination are co-regulated by H_2O_2 levels (Zhang et al, 2022). However, besides this weak potential link, connecting these two processes is a thus far untapped avenue of research.

Mutating the only At*FLIC*/At*FLAC* orthologue in the *Zea mays* inbred line A188, Zm*Flac*, yielded a developmentally delayed plant (Fig 4). Although this phenotype is much less severe than what we could observe in *flic flac* mutants in *Arabidopsis thaliana*, growth retardation is a major response to elevated JA levels also in monocots as more resources are diverted towards defensive capabilities (Yan et al, 2014; Borrego & Kolomiets, 2016; Ma et al, 2023). Assuming Zm*Flac* has a comparable function to its Arabidopsis orthologues, the differences in phenotype and especially severity could potentially be explained by a (partial) divergence in function regarding core components of the JA pathway between dicots and monocots (as reviewed in Wan & Xin, 2022). While the overall functionality of JA signalling is conserved, the cross-talk, fine-tuning, and dependencies on single factors is distinct, potentially resulting in the absence of Zm*Flac* having less of an impact in regulating JA biosynthesis. Further experiments with maize will determine how far Zm*Flac*'s functionality overlaps with that of its Arabidopsis orthologues and whether controlling the JA response by modification of Zm*Flac* expression might be of agronomical benefit.

How FLIC and FLAC integrate exactly into the described JA pathway is thus far concealed. In our AP-MS analyses, we found only one recent connection, CROWDED NUCLEI 4 (CRWN4), as prey of FLIC (Lang et al, 2023). CRWNs are considered structural

homologues to vertebrate lamins, and Arabidopsis possesses four CRWN homologues (CRWN1–4), with CRWN4 being the most distinct (Dittmer et al, 2007; Dittmer & Richards, 2008). Recently, they have been shown to regulate pathogen defences negatively, and mutants exhibit elevated JA levels similar to *flic flac* mutants as well as increased SA levels, which we could not observe despite "response to SA" being a statistically enriched GO term (Table S2 and Fig 2) (Guo et al, 2017; Choi et al, 2019; Jarad et al, 2019; Groves et al, 2020). Genes responsible for glucosinolate biosynthesis, secondary metabolites contributing in pathogen defence, are up-regulated in *flic flac* mutants (Table S2). This has long been demonstrated as a JA-dependent process (Brader et al, 2001; Guo et al, 2013; Zhou & Memelink, 2016; Frerigmann et al, 2021) and *crwn* mutants have been investigated in this regard. However, the effect of CRWN absence on glucosinolate synthesis is unclear. While Choi et al report that glucosinolate synthesis is down-regulated in *crwn1* and *crwn4* mutants (Choi et al, 2019), Jarad et al seem to detect an up-regulation, at least in the *crwn1* mutant they analysed (Jarad et al, 2019). Unfortunately, none of them directly measured glucosinolate levels, so it remains shrouded for now in which direction glucosinolate biosynthesis is de-regulated in *crwn* mutants. CRWNs further interfere with ABA signalling (Zhao et al, 2016), whereas we detected "response to ABA" as an up-regulated GO term in *flic flac* mutants (Table S2), hinting at the possibility of counteracting functions despite regulating JA levels and the SA response in a similar direction. Future experiments will determine the exact nature of the relationship of FLIC, FLAC, and CRWN4 and will sort them into the characterised JA network.

Furthermore, it will be interesting to characterise the regulation of FLIC and FLAC themselves. It has been determined that the FLIC promoter is bound by MYC2 (Li et al, 2020), making a feedback loop likely. It is also bound by AGAMOUS-LIKE 15 (AGL15) (Yilmaz et al, 2011), a transcription factor involved in several phytohormonal pathways and likely being controlled by COI1 (Kim et al, 2013; Jibran et al, 2017). It is also a repressor of floral transition (Adamczyk et al, 2007). Additionally, AGL15 has an ERF-associated amphiphilic repression (EAR) motif, a sequence common in proteins involved in phytohormonal control (as reviewed in Chow et al, 2023). EAR motifs have been described as essential for the repressive activity of ERF4 as well as the protein-protein interaction between JAZ8 and TPL, both in the context of JA signalling

(McGrath et al, 2005; Shyu et al, 2012). In fact, AGL15 itself has been found to interact with TPL as well (Causier et al, 2012; Joshi et al, 2021). The FLAC promoter, on the other hand, is bound by SEPALLATA3 (SEP3) which is involved in the control of flowering time and hormone biosynthesis (Kaufmann et al, 2009). SEP3 also interacts with AGL15 (Immink et al, 2009). Noteworthily, FLIC itself has an intact EAR motif, whereas it appears degenerated in AtFLAC and ZmFLAC (Fig 4, golden box). Whether and how this plays a role in FLIC's functionality remains to be determined.

Taken together, we could demonstrate a clear implication of FLIC and FLAC in the JA biosynthesis. Since we previously characterised them as components of the plant DREAM complex (Lang et al, 2021, 2023), it will be highly interesting to unravel a potential involvement of the other complex members in phytohormonal regulation and/or responses. It has become clear that the plant DREAM complex as well as FLIC and FLAC are involved in a plethora of processes not only in plant development but also in response to different environmental cues and stresses.

Material and Methods

Plant materials and growth conditions

The *Arabidopsis thaliana* accession Columbia-0 (Col-0) was used as the wildtype reference. All mutants and transgenic lines used in this study were in the Col-0 background. The mutant lines *flic-1*, *flac-1*, and *mad1-2* have been described previously (Bao et al, 2014; Lang et al, 2023). If not stated otherwise, plants were germinated and grown on vertical plates containing ½ MS medium under long day conditions (16 h light, 8 h dark) at 21°C.

For experiments with *Zea mays*, the inbred line A188 was used as the wild-type reference, and the mutant line *flac-c1* was generated by CRISPR/Cas9 (s. below). Seeds were directly germinated on soil and grown in a greenhouse with 16 h of light at around 24°C followed by 8 h of dark at around 22°C. For developmental quantification, plants were distributed randomly within the same chamber, and the VT stage was scored blindly once the last tassel branch was visible.

Transcriptome analysis

Total RNAs were extracted using the RNeasy Plant Mini Kit (QIAGEN, Germany) from whole seedlings according to the manufacturer's instructions. Total RNAs from wild-type, *flic*, *flac*, and *flic flac* mutant plants at 9 d after germination were used for construction of cDNA libraries using the TruSeq RNA Library Preparation Kit v2 (Illumina, United States) according to the manufacturer's protocol. For transcriptome profiling in wild-type, *flic*, *flac*, and *flic flac* mutant plants, we analysed three biological replicates for statistical analysis. The libraries were sequenced using the NextSeq500 sequencer (Illumina, United States). Raw reads containing adaptor sequences were trimmed using bcl2fastq (Illumina, United States), and nucleotides with low-quality (QV < 25) were masked by *N* using the original script. Reads shorter than 50 bp were discarded, and the remaining reads were mapped to the cDNA reference using Bowtie with the following parameters: "–all–best–strata" (Langmead et al, 2009). The reads were counted by transcript models. Differentially expressed

genes were selected based on the adjusted *P*-value calculated using edgeR (version 3.20.9) with default settings (Robinson et al, 2010).

Extraction of metabolites

The extraction of metabolites from 9-d-old *Arabidopsis thaliana* seedlings was conducted as previously described (Liu et al, 2020). Briefly, 50 mg samples were measured and resuspended by vortex with 250 µL of precooled 80% (*v*/*v*) methanol containing 0.1% (*v*/*v*) formic acid. The samples were chilled on ice for 5 min and then centrifuged at 15 000 rpm for 5 min at 4°C. 200 µL of the supernatants were transferred to new tubes and diluted to a 53% (*v*/*v*) methanol concentration using water. Subsequently, the samples were centrifuged at 15 000 rpm at 4°C for 10 min. The supernatants were transferred to vials for UHPLC.

UHPLC-MS/MS analysis

An Ultimate 3000 UHPLC system (Thermo Fisher Scientific, San Jose, CA, USA) coupled with Orbitrap Q Exactive Plus (Thermo Fisher Scientific, San Jose, CA, USA) was used to analyse the metabolites. The separation of metabolites using UHPLC conditions was as follows: mobile phase A contained 0.1% (*v*/*v*) formic acid and 5 mM ammonium acetate at pH 9.0 in water, while mobile phase B comprised 99.7% methanol. The extraction solutions were injected into the reverse phase column, Hypersil GoldColumn (100 × 2.1 mm with 1.9 µm particle size). The injection volume was 10 µL, the flow rate was 0.25 mL/min, and the column temperature was 20°C. The gradient conditions were as follows: 0 min, 98% A and 2% B; 1.5 min, 98% A and 2% B; 12 min, 0% A and 100% B; 14 min 0% A and 100% B; 14.1 min 98% A and 2% B; 17 min 98% A and 2% B. The Orbitrap Q Exactive Plus mass spectrometer was operated in positive polarity mode with 3.2 kV of spray voltage. The capillary temperature was 320°C; the temperature of the autosampler was 10°C; 35 arb and 10 arb were the sheath gas flow rate and auxiliary gas flow rate, respectively (Liu et al, 2020).

Analysis of metabolome data

Compound discoverer v.3.1 (CD 3.1, Thermo Scientific, San Jose, CA, USA) was used for mass spectrometry data acquisition (Liu et al, 2020). The settings were as follows: 5 ppm mass tolerance, 30 signal of intensity tolerance, and 1 000 000 of minimum peak intensity (Scarpone et al, 2020). The annotations of metabolites were generated using the ChemSpider (www.chemspider.com) database, which consisted of integrating data from the Aracyc, Biocyc, KEGG pathways, mzVault, and mzCloud databases. Differentially accumulated metabolites by chemical treatments were selected with *P*-value < 0.05, fold change ≥ 1.5 and ≤ 0.667.

Seedling assays

To analyse their response to exogenous supplementation of MeJA, oryzalin, and hesperadin, plants were germinated and grown on vertical plates containing ½ MS medium supplemented with the indicated concentration of each chemical under long day conditions (16 h light, 8 h dark) at 21°C for 12 d, 6 d, or 7 d, respectively.

Analysis of growth on medium containing different levels of B or Fe was performed under the same conditions on (modified) Hoagland medium instead. Plants were germinated and pre-grown on vertical plates containing Hoagland medium for 5 d. They were then transferred to plates containing unmodified (control) or modified Hoagland medium and grown for 3 d. The pre-growth and control medium contained 46 µM B and 34 µM Fe. Low and high B (-B/++B) medium contained 0.1 µM B and 3 000 µM B instead, respectively. Low and high Fe (-Fe/++Fe) medium contained 4 µM Fe and 160 µM Fe instead, respectively.

Afterwards, plates were scanned and root length was measured digitally using the Simple Neurite Tracer plugin (Longair et al, 2011) for ImageJ. In the case of growth on control Hoagland and -B medium, pictures of seedlings were taken through binoculars using a Samsung Galaxy S20 with a Samsung S5K2LD sensor.

Multiple sequence alignments

Alignments were generated using the MUSCLE algorithm using default settings (Edgar, 2004). Structural predictions were generated by AlphaFold (Varadi et al, 2022). Data visualisation was done using ESPript 3 (Robert & Gouet, 2014).

Genomic editing of *Zea mays* by CRISPR/Cas9

To generate mutant alleles for Zm*Flac* (Zm00056aa025545), a CRISPR/Cas9 system was utilised. CRISPR-P 2.0 (He et al, 2021) was used for the design of sgRNAs (Table S5). They were first cloned into the *pENTR4-sgRNA5* entry vector (Zhou et al, 2014) and subsequently by Gateway LR reaction into the *p7oM-LH-GW* destination vector. The *Agrobacterium tumefaciens* strain LBA4404, which harbours additional *virB* and *virG* genes from *pTiBo542* (Komari et al, 1986), was transformed with the expression clones by electroporation.

Subsequent Agrobacterium-mediated transformation of the *Zea mays* inbred line A188 was performed as previously described (Ishida et al, 2007; Raji et al, 2018), with several modifications (Ono et al, in preparation) utilising a BASTA selection system featuring the *bar* gene. Briefly, we followed Raji et al (2018) for medium compositions, however, 25 mg/L of Meropenem trihydrate (Fujifilm Wako Chemicals) were supplied instead of carbenicillin, cefotaxime, and vancomycin. Immature embryos from A188 wildtype plants at 11 d after pollination, ranging from 0.8 mm to 1.5 mm in length, were isolated and used for Agrobacterium inoculation according to Ishida et al (2007), but without heat treatment of embryos, and embryos were co-cultured with Agrobacterium for 3 d. Afterwards, inoculated embryos were cultured on resting medium (without selective reagent) for 10 d and transferred onto the selection medium every 2 weeks with gradually increased selective reagent concentration, i.e. 1.5 mg/L and 3 mg/L of BASTA (Bayer Crop Science) for the first and second selection and 10 mg/L of glufosinate-ammonium (Sigma) for the third selection, respectively. After 6 weeks of selection, well-developed and enlarged positive calli were cut into smaller pieces (about 4–7 mm in diameter) and transferred to regeneration medium containing 4 mg/L of BASTA. Regeneration medium were refreshed after 10 d once, and after a total of 21 d of regeneration, the resultant

shoots were transferred to rooting medium with 2.5 mg/L of BASTA in sterile grass containers, further culturing them for 2 weeks. The regenerated T0 shoots with well-developed roots were transplanted into soil in trays with 8 cm diameter cells and allowed to be acclimated in a greenhouse with 26°C constant temperature and 14/10 h of light/dark. After 4–5 weeks of cultivation, selected plants were further cultivated in bigger pots (25.9 cm diameter and 20.6 cm height) at the same conditions as above. Induced mutations were screened by PCR amplification and Sanger sequencing.

Conflict of Interests

No competing interests declared.

Figures

Figure 1. DEGs detected by mRNA-seq in *flic*, *flac*, and *flic flac* mutants.

Details can be found in Tables 1 and S1–S3. **(A)** Venn diagram showing the overlap of DEGs with logfc > 0.7 and adjusted $P < 0.05$ in *flic*, *flac*, and *flic flac* mutant seedlings, the latter split by DEGs with and without the GO term annotation "response to jasmonic acid". **(B)** Overview of the JA pathway with its biosynthetic, signalling, and catabolic sections, demonstrating up-regulated DEGs in *flic flac* mutant seedlings. Solid green borders highlight up-regulated processes, the dashed green border indicates that JA catabolism appears up-regulated potentially as a secondary effect. Proteins of up-regulated genes are shown in green. Solid arrows signify described conversion or activation/repression processes. Dashed arrows indicate ORA47's positive feedback loop that has not been characterised in molecular detail. The dotted arrow designates 12OH-JA-Ile's minor bioactivity compared to JA-Ile. Modified and extended after Delgado et al, 2021 by incorporation of complementing information taken from various sources (Koo et al, 2006; Kienow et al, 2008; Pauwels & Goossens, 2011; Zhang et al, 2012; Wasternack & Hause, 2013; Chen et al, 2016; Caarls et al, 2017; Smirnova et al, 2017).

Figure 2. Direct measurement of hormone levels in *flic flac* mutants and analysis of their response to exogenous MeJA.

MeJA and IAA levels are elevated in *flic flac* mutant seedlings, and supplementation of exogenous MeJA leads to reduced root growth compared to the wildtype. Analysis of different phytohormone contents by LC-MS in wild-type and *flic flac* mutant seedlings. Quantification of three replicates. Significances are indicated above the boxes as determined by Student's *t*-test (ns, not significant; *, $P < 0.05$; ***, $P < 0.001$).

Figure 3. Analysis of the reaction of *flic flac* mutant seedlings to different JA-related stresses.

Absence of FLIC and FLAC leads to phenotypic responses to exogenous MeJA supplementation, B deficiency, as well as the presence of the microtubule

destabiliser oryzalin and the aurora kinase inhibitor hesperadin. **(A)** Root length of wild-type and *flic flac* mutant seedlings after 12 d on medium containing either 0 µM or 200 µM MeJA. Quantification of one replicate with 17–19 roots per genotype and condition. Significant differences as determined by ANOVA and Tukey post hoc test ($P < 0.05$). **(B)** Root growth of wild-type and *flic flac* mutant seedlings after 3 d on standard Hoagland (46 µM B), -B (0.1 µM B), and ++B (3 000 µM B) medium. Quantification of one replicate with 7–10 roots per genotype and condition. No significant differences between the wildtype and *flic flac* mutants could be determined by ANOVA and Tukey post hoc test ($P < 0.05$). **(C)** Representative pictures of wild-type and *flic flac* mutant seedlings on standard Hoagland and -B medium. In the absence of FLIC and FLAC, leaves are darker, show increased epinasty, and roots exhibit longer root hairs on B deficiency medium. **(D)** Root length of wild-type, *mad1*, and *flic flac* mutant seedlings normalised to each genotype's control root growth after 6 d on medium containing either 0 nM, 150 nM, or 200 nM oryzalin (each containing an equal final concentration of 0.002% DMSO). Quantification of averages of four replicates with 29–45 roots in each replicate per genotype and condition. Significant differences as determined by ANOVA and Tukey post hoc test ($P < 0.05$). **(E)** Root length of wild-type, *mad1*, and *flic flac* mutant seedlings after 7 d on medium containing either 0 µM or 3.5 µM hesperadin (each containing an equal final concentration of 0.035% DMSO). Quantification of three replicates with 16–20 roots in each replicate per genotype and condition. Significant differences as determined by Welch test and Dunnett T3 post hoc test ($P < 0.05$).

Figure 4. Comparison of Zm*Flac* to its *Arabidopsis thaliana* homologues and developmental analysis of its absence.

(A) Multiple sequence alignment of AtFLAC, AtFLIC, and ZmFLAC protein sequences. Structural predictions for AtFLAC and ZmFLAC are indicated above and below the sequences, respectively. The location and effect on the resulting protein of the Zm*flac-c1* mutation compared to the wildtype protein is described, with differing amino acids highlighted in red and an asterisk symbolising a stop codon. The EAR motif of AtFLIC and the aligned sequence in the other homologues are highlighted by a golden box. A red dagger marks the first location of an in-frame start

codon of Zm*Flac* after the mutation in Zm*flac-c1*. **(B)** Time until VT stage is reached by wild-type, Zm*Flac*/*flac-c1*, and *flac-c1* mutant plants. Quantification of 8–15 plants per genotype. Significant differences as determined by ANOVA and Tukey post hoc test ($P < 0.05$). das, days after sowing.

Tables

Table 1.

Significant DEGs (adjusted $P < 0.05$) categorised under the GO term “response to jasmonic acid” (GO:0009753) in *flic flac* mutant seedlings and their logfc.

Supplementary Figures

Figure S1. Analysis of *flic flac* mutant seedlings on different Fe concentrations.

Absence of FLIC and FLAC does not seem to have an effect on root growth on different Fe concentrations. Root growth of wild-type and *flic flac* mutant seedlings after 3 d on standard Hoagland (34 µM Fe), -Fe (4 µM Fe), and ++Fe (160 µM Fe) medium. Quantification of one replicate with 6–10 roots per genotype and condition. No significant differences between the wildtype and *flic flac* mutants in the same conditions could be determined by ANOVA and Tukey post hoc test ($P < 0.05$).

Figure S2. DEGs related to flowering time regulation detected by mRNA-seq in *flac* and *flic flac* mutants.

Venn diagram showing the overlap of DEGs with logfc > 0.7 and adjusted $P < 0.05$ related to flowering time regulation according to Flowering Interactive Database (FLOR-ID) in *flac* and *flic flac* mutant seedlings (Bouché et al, 2016). Details can be found in Table S4.

Supplementary Tables

Table S1.

DEGs with logfc > 0.7 and adjusted *P* < 0.05 in *flic*, *flac*, and *flic flac* mutant seedlings. adj_pvalue, adjusted *P*-value.

Table S2.

PANTHER Gene List Analysis (Thomas et al, 2022) to identify statistically overrepresented and underrepresented up-regulated biological process GO terms (applying Fisher's Exact test with Bonferroni correction) in *flic flac* mutant seedlings.

Table S3.

PANTHER Gene List Analysis (Thomas et al, 2022) to identify statistically overrepresented and underrepresented down-regulated biological process GO terms (applying Fisher's Exact test with Bonferroni correction) in *flic flac* mutant seedlings.

Table S4.

DEGs with logfc > 0.7 and adjusted *P* < 0.05 in *flac* and *flic flac* mutants related to flowering time regulation according to the Flowering Interactive Database (FLOR-ID) (Bouché et al, 2016). Additionally, CIL1 has been manually curated (Liu et al, 2013, 2018). The effect of overexpression (OE) and/or mutation of these genes on flowering is shown (Lee et al, 2000; Ratcliffe et al, 2003; Liu et al, 2007; Castillejo & Pelaz, 2008; Mathieu et al, 2009; Kim & Sung, 2010; Gillmor et al, 2014; Gomez et al, 2020; Yan et al, 2020; Nasim et al, 2022). ns, not significantly de-regulated.

Table S5.

List of oligonucleotides used in this study.

References

Adamczyk BJ, Lehti-Shiu MD, Fernandez DE (2007) The MADS domain factors AGL15 and AGL18 act redundantly as repressors of the floral transition in Arabidopsis. *Plant J* 50: 1007–1019.

Arnold MD, Gruber C, Floková K, Miersch O, Strnad M, Novák O, Wasternack C, Hause B (2016) The Recently Identified Isoleucine Conjugate of cis-12-Oxo-Phytodienoic Acid Is Partially Active in cis-12-Oxo-Phytodienoic Acid-Specific Gene Expression of Arabidopsis thaliana. *PLoS One* 11: e0162829.

Asthana A, Ramanan P, Hirschi A, Guiley KZ, Wijeratne TU, Shelansky R, Doody MJ, Narasimhan H, Boeger H, Tripathi S *et al* (2022) The MuvB complex binds and stabilizes nucleosomes downstream of the transcription start site of cell-cycle dependent genes. *Nat Commun* 13: 526.

Aubert Y, Widemann E, Miesch L, Pinot F, Heitz T (2015) CYP94-mediated jasmonoyl-isoleucine hormone oxidation shapes jasmonate profiles and attenuates defence responses to Botrytis cinerea infection. *J Exp Bot* 66: 3879–3892.

Bao Z, Zhang N, Hua J (2014) Endopolyploidization and flowering time are antagonistically regulated by checkpoint component MAD1 and immunity modulator MOS1. *Nat Commun* 5: 5628.

Beveridge CA, Rameau C, Wijerathna-Yapa A (2023) Lessons from a century of apical dominance research. *J Exp Bot* 74: 3903–3922.

Bömer M, O'Brien JA, Pérez-Salamó I, Krasauskas J, Finch P, Briones A, Daudi A, Souda P, Tsui T-L, Whitelegge JP *et al* (2018) COI1-dependent jasmonate signalling affects growth, metabolite production and cell wall protein composition in arabidopsis. *Ann Bot* 122: 1117–1129.

Borrego EJ, Kolomiets MV (2016) Synthesis and Functions of Jasmonates in Maize. *Plants* 5. doi:10.3390/plants5040041.

Bouché F, Lobet G, Tocquin P, Périlleux C (2016) FLOR-ID: an interactive database of flowering-time gene networks in Arabidopsis thaliana. *Nucleic Acids Res* 44: D1167–D1171.

Bouveret R, Schönrock N, Gruissem W, Hennig L (2006) Regulation of flowering time by Arabidopsis MSI1. *Development* 133: 1693–1702.

Brader G, Tas E, Palva ET (2001) Jasmonate-dependent induction of indole glucosinolates in Arabidopsis by culture filtrates of the nonspecific pathogen Erwinia carotovora. *Plant Physiol* 126: 849–860.

Brodersen P, Petersen M, Bjørn Nielsen H, Zhu S, Newman M-A, Shokat KM, Rietz S, Parker J, Mundy J (2006) Arabidopsis MAP kinase 4 regulates salicylic acid- and jasmonic acid/ethylene-dependent responses via EDS1 and PAD4. *Plant J* 47: 532–546.

Browse J (2009) Jasmonate passes muster: a receptor and targets for the defense hormone. *Annu Rev Plant Biol* 60: 183–205.

Bruckhoff V, Haroth S, Feussner K, König S, Brodhun F, Feussner I (2016) Functional Characterization of CYP94-Genes and Identification of a Novel Jasmonate Catabolite in Flowers. *PLoS One* 11: e0159875.

Caarls L, Elberse J, Awwanah M, Ludwig NR, de Vries M, Zeilmaker T, Van Wees SCM, Schuurink RC, Van den Ackerveken G (2017) JASMONATE-INDUCED OXYGENASES down-regulate plant immunity by hydroxylation and inactivation of the hormone jasmonic acid. *Proc Natl Acad Sci U S A* 114: 6388–6393.

Cai X-T, Xu P, Zhao P-X, Liu R, Yu L-H, Xiang C-B (2014) Arabidopsis ERF109 mediates cross-talk between jasmonic acid and auxin biosynthesis during lateral root formation. *Nat Commun* 5: 5833.

Campos ML, Yoshida Y, Major IT, de Oliveira Ferreira D, Weraduwage SM, Froehlich JE, Johnson BF, Kramer DM, Jander G, Sharkey TD *et al* (2016) Rewiring of jasmonate and phytochrome B signalling uncouples plant growth-defense tradeoffs. *Nat Commun* 7: 12570.

Campos-Rivero G, Osorio-Montalvo P, Sánchez-Borges R, Us-Camas R, Duarte-Aké F, De-la-Peña C (2017) Plant hormone signaling in flowering: An epigenetic point of view. *J Plant Physiol* 214: 16–27.

Castillejo C, Pelaz S (2008) The balance between CONSTANS and TEMPRANILLO activities determines FT expression to trigger flowering. *Curr Biol* 18: 1338–1343.

Causier B, Ashworth M, Guo W, Davies B (2012) The TOPLESS interactome: a framework for gene repression in Arabidopsis. *Plant Physiol* 158: 423–438.

Causier B, Davies B (2002) Analysing protein-protein interactions with the yeast two-hybrid system. *Plant Mol Biol* 50: 855–870.

Chen H-Y, Hsieh E-J, Cheng M-C, Chen C-Y, Hwang S-Y, Lin T-P (2016) ORA47 (octadecanoid-responsive AP2/ERF-domain transcription factor 47) regulates jasmonic acid and abscisic acid biosynthesis and signaling through binding to a novel cis-element. *New Phytol* 211: 599–613.

Chini A, Fonseca S, Chico JM, Fernández-Calvo P, Solano R (2009) The ZIM domain mediates homo- and heteromeric interactions between Arabidopsis JAZ proteins. *Plant J* 59: 77–87.

Chini A, Fonseca S, Fernández G, Adie B, Chico JM, Lorenzo O, García-Casado G, López-Vidriero I, Lozano FM, Ponce MR *et al* (2007) The JAZ family of repressors is the missing link in jasmonate signalling. *Nature* 448: 666–671.

Choi J, Strickler SR, Richards EJ (2019) Loss of CRWN Nuclear Proteins Induces Cell Death and Salicylic Acid Defense Signaling. *Plant Physiol* 179: 1315–1329.

Chow V, Kirzinger MW, Kagale S (2023) Lend Me Your EARs: A Systematic Review of the Broad Functions of EAR Motif-Containing Transcriptional Repressors in Plants. *Genes* 14. doi:10.3390/genes14020270.

Chung HS, Koo AJK, Gao X, Jayanty S, Thines B, Jones AD, Howe GA (2008) Regulation and function of Arabidopsis JASMONATE ZIM-domain genes in response to wounding and herbivory. *Plant Physiol* 146: 952–964.

Cox KL (2022) Stronger together: Ethylene, jasmonic acid, and MAPK signaling pathways synergistically induce camalexin synthesis for plant disease resistance. *Plant Cell* 34: 2829–2830.

Cucinotta M, Cavalleri A, Chandler JW, Colombo L (2021) Auxin and Flower Development: A Blossoming Field. *Cold Spring Harb Perspect Biol* 13. doi:10.1101/cshperspect.a039974.

Delgado C, Mora-Poblete F, Ahmar S, Chen J-T, Figueroa CR (2021) Jasmonates and Plant Salt Stress: Molecular Players, Physiological Effects, and Improving Tolerance by Using Genome-Associated Tools. *Int J Mol Sci* 22. doi:10.3390/ijms22063082.

Dell B, Huang L (1997) Physiological response of plants to low boron. *Plant and Soil* 193: 103–120.

Demidov D, Hesse S, Tewes A, Rutten T, Fuchs J, Ashtiyani RK, Lein S, Fischer A, Reuter G, Houben A (2009) Aurora1 phosphorylation activity on histone H3 and its cross-talk with other post-translational histone modifications in Arabidopsis. *Plant J* 59: 221–230.

Devoto A, Nieto-Rostro M, Xie D, Ellis C, Harmston R, Patrick E, Davis J, Sherratt L, Coleman M, Turner JG (2002) COI1 links jasmonate signalling and fertility to the SCF ubiquitin-ligase complex in Arabidopsis. *Plant J* 32: 457–466.

Dittmer TA, Richards EJ (2008) Role of LINC proteins in plant nuclear morphology. *Plant Signal Behav* 3: 485–487.

Dittmer TA, Stacey NJ, Sugimoto-Shirasu K, Richards EJ (2007) LITTLE NUCLEI genes affecting nuclear morphology in Arabidopsis thaliana. *Plant Cell* 19: 2793–2803.

Duan L, Perez RE, Calhoun S, Maki CG (2022) RBL2/DREAM-mediated repression of the Aurora kinase A/B pathway determines therapy responsiveness and outcome in p53 WT NSCLC. *Sci Rep* 12: 1049.

Duran C, Arce-Johnson P, Aquea F (2018) Methylboronic acid fertilization alleviates boron deficiency symptoms in Arabidopsis thaliana. *Planta* 248: 221–229.

Edgar RC (2004) MUSCLE: multiple sequence alignment with high accuracy and high throughput. *Nucleic Acids Res* 32: 1792–1797.

Feussner I, Wasternack C (2002) The lipoxygenase pathway. *Annu Rev Plant Biol* 53: 275–297.

Feys B, Benedetti CE, Penfold CN, Turner JG (1994) Arabidopsis Mutants Selected for Resistance to the Phytotoxin Coronatine Are Male Sterile, Insensitive to Methyl Jasmonate, and Resistant to a Bacterial Pathogen. *Plant Cell* 6: 751–759.

Fischer M, Müller GA (2017) Cell cycle transcription control: DREAM/MuvB and RB-E2F complexes. *Crit Rev Biochem Mol Biol* 52: 638–662.

Floková K, Feussner K, Herrfurth C, Miersch O, Mik V, Tarkowská D, Strnad M, Feussner I, Wasternack C, Novák O (2016) A previously undescribed jasmonate compound in flowering Arabidopsis thaliana - The identification of cis-(+)-OPDA-Ile. *Phytochemistry* 122: 230–237.

Fonseca S, Chini A, Hamberg M, Adie B, Porzel A, Kramell R, Miersch O, Wasternack C, Solano R (2009) (+)-7-iso-Jasmonoyl-L-isoleucine is the endogenous bioactive jasmonate. *Nat Chem Biol* 5: 344–350.

Frerigmann H, Hoecker U, Gigolashvili T (2021) New Insights on the Regulation of Glucosinolate Biosynthesis COP1 and DELLA Proteins in. *Front Plant Sci* 12: 680255.

Gillmor CS, Silva-Ortega CO, Willmann MR, Buendía-Monreal M, Poethig RS (2014) The Arabidopsis Mediator CDK8 module genes CCT (MED12) and GCT (MED13) are global regulators of developmental phase transitions. *Development* 141: 4580–4589.

Glauser G, Grata E, Dubugnon L, Rudaz S, Farmer EE, Wolfender J-L (2008) Spatial and temporal dynamics of jasmonate synthesis and accumulation in Arabidopsis in response to wounding. *J Biol Chem* 283: 16400–16407.

Gomez MD, Barro-Trastoy D, Fuster-Almunia C, Tornero P, Alonso JM, Perez-Amador MA (2020) Gibberellin-mediated RGA-LIKE1 degradation regulates embryo sac development in Arabidopsis. *J Exp Bot* 71: 7059–7072.

Groves NR, Biel A, Moser M, Mendes T, Amstutz K, Meier I (2020) Recent advances in understanding the biological roles of the plant nuclear envelope. *Nucleus* 11: 330–346.

Guo Q, Yoshida Y, Major IT, Wang K, Sugimoto K, Kapali G, Havko NE, Benning C, Howe GA (2018) JAZ repressors of metabolic defense promote growth and reproductive fitness in. *Proc Natl Acad Sci U S A* 115: E10768–E10777.

Guo R, Shen W, Qian H, Zhang M, Liu L, Wang Q (2013) Jasmonic acid and glucose synergistically modulate the accumulation of glucosinolates in Arabidopsis thaliana. *J Exp Bot* 64: 5707–5719.

Guo T, Mao X, Zhang H, Zhang Y, Fu M, Sun Z, Kuai P, Lou Y, Fang Y (2017) Lamin-like Proteins Negatively Regulate Plant Immunity through NAC WITH TRANSMEMBRANE MOTIF1-LIKE9 and NONEXPRESSOR OF PR GENES1 in Arabidopsis thaliana. *Mol Plant* 10: 1334–1348.

Han X, Kui M, He K, Yang M, Du J, Jiang Y, Hu Y (2023) Jasmonate-regulated root growth inhibition and root hair elongation. *J Exp Bot* 74: 1176–1185.

He C, Liu H, Chen D, Xie W-Z, Wang M, Li Y, Gong X, Yan W, Chen L-L (2021) CRISPR-Cereal: a guide RNA design tool integrating regulome and genomic variation for wheat, maize and rice. *Plant Biotechnol J* 19: 2141–2143.

Heitz T, Smirnova E, Marquis V, Poirier L (2019) Metabolic Control within the Jasmonate Biochemical Pathway. *Plant Cell Physiol* 60: 2621–2628.

Heitz T, Widemann E, Lugan R, Miesch L, Ullmann P, Désaubry L, Holder E, Grausem B, Kandel S, Miesch M *et al* (2012) Cytochromes P450 CYP94C1 and CYP94B3 catalyze two successive oxidation steps of plant hormone Jasmonoyl-isoleucine for catabolic turnover. *J Biol Chem* 287: 6296–6306.

Hentrich M, Böttcher C, Düchting P, Cheng Y, Zhao Y, Berkowitz O, Masle J, Medina J, Pollmann S (2013) The jasmonic acid signaling pathway is linked to auxin homeostasis through the modulation of YUCCA8 and YUCCA9 gene expression. *Plant J* 74: 626–637.

Hewedy OA, Elsheery NI, Karkour AM, Elhamouly N, Arafa RA, Mahmoud GA-E, Dawood MF-A, Hussein WE, Mansour A, Amin DH *et al* (2023) Jasmonic acid regulates plant development and orchestrates stress response during tough times. *Environ Exp Bot* 208: 105260.

Hickman R, Van Verk MC, Van Dijken AJH, Mendes MP, Vroegop-Vos IA, Caarls L, Steenbergen M, Van der Nagel I, Wesselink GJ, Jironkin A *et al* (2017) Architecture and Dynamics of the Jasmonic Acid Gene Regulatory Network. *Plant Cell* 29: 2086–2105.

Huang H, Chen Y, Wang S, Qi T, Song S (2023) Jasmonate action and crosstalk in flower development and fertility. *J Exp Bot* 74: 1186–1197.

Huang Y, Wang S, Wang C, Ding G, Cai H, Shi L, Xu F (2021) Induction of jasmonic acid biosynthetic genes inhibits Arabidopsis growth in response to low boron. *J Integr Plant Biol* 63: 937–948.

Hyun Y, Choi S, Hwang H-J, Yu J, Nam S-J, Ko J, Park J-Y, Seo YS, Kim EY, Ryu SB *et al* (2008) Cooperation and functional diversification of two closely related galactolipase genes for jasmonate biosynthesis. *Dev Cell* 14: 183–192.

Immink RGH, Tonaco IAN, de Folter S, Shchennikova A, van Dijk ADJ, Busscher-Lange J, Borst JW, Angenent GC (2009) SEPALLATA3: the 'glue' for MADS box transcription factor complex formation. *Genome Biol* 10: R24.

Ishida Y, Hiei Y, Komari T (2007) Agrobacterium-mediated transformation of maize. *Nat Protoc* 2: 1614–1621.

Izawa T (2021) What is going on with the hormonal control of flowering in plants? *Plant J* 105: 431–445.

Jarad M, Mariappan K, Almeida-Trapp M, Mette MF, Mithöfer A, Rayapuram N, Hirt H (2019) The Lamin-Like LITTLE NUCLEI 1 (LINC1) Regulates Pattern-Triggered Immunity and Jasmonic Acid Signaling. *Front Plant Sci* 10: 1639.

Jiang Y, Liang G, Yang S, Yu D (2014) Arabidopsis WRKY57 functions as a node of convergence for jasmonic acid- and auxin-mediated signaling in jasmonic acid-induced leaf senescence. *Plant Cell* 26: 230–245.

Jibran R, Tahir J, Cooney J, Hunter DA, Dijkwel PP (2017) Arabidopsis AGAMOUS Regulates Sepal Senescence by Driving Jasmonate Production. *Front Plant Sci* 8: 2101.

Jimenez Aleman GH, Thirumalaikumar VP, Jander G, Fernie AR, Skirycz A (2022) OPDA, more than just a jasmonate precursor. *Phytochemistry* 204: 113432.

Joshi S, Keller C, Perry SE (2021) The EAR Motif in the MADS Transcription Factor AGAMOUS-Like 15 Is Not Necessary to Promote Somatic Embryogenesis. *Plants* 10. doi:10.3390/plants10040758.

Kaufmann K, Muiño JM, Jauregui R, Airoldi CA, Smaczniak C, Krajewski P, Angenent GC (2009) Target genes of the MADS transcription factor SEPALLATA3: integration of developmental and hormonal pathways in the Arabidopsis flower. *PLoS Biol* 7: e1000090.

Kienow L, Schneider K, Bartsch M, Stuible H-P, Weng H, Miersch O, Wasternack C, Kombrink E (2008) Jasmonates meet fatty acids: functional analysis of a new acyl-coenzyme A synthetase family from Arabidopsis thaliana. *J Exp Bot* 59: 403–419.

Kim D-H, Sung S (2010) The Plant Homeo Domain finger protein, VIN3-LIKE 2, is necessary for photoperiod-mediated epigenetic regulation of the floral repressor, MAF5. *Proc Natl Acad Sci U S A* 107: 17029–17034.

Kim J, Dotson B, Rey C, Lindsey J, Bleecker AB, Binder BM, Patterson SE (2013) New clothes for the jasmonic acid receptor COI1: delayed abscission, meristem arrest and apical dominance. *PLoS One* 8: e60505.

Kobayashi K, Suzuki T, Iwata E, Nakamichi N, Suzuki T, Chen P, Ohtani M, Ishida T, Hosoya H, Müller S *et al* (2015) Transcriptional repression by MYB3R proteins regulates plant organ growth. *EMBO J* 34: 1992–2007.

Koliopoulos MG, Muhammad R, Roumeliotis TI, Beuron F, Choudhary JS, Alfieri C (2022) Structure of a nucleosome-bound MuvB transcription factor complex reveals DNA remodelling. *Nat Commun* 13: 5075.

Komaki S, Schnittger A (2017) The Spindle Assembly Checkpoint in Arabidopsis Is Rapidly Shut Off during Severe Stress. *Dev Cell* 43: 172–185.e5.

Komari T, Halperin W, Nester EW (1986) Physical and functional map of supervirulent Agrobacterium tumefaciens tumor-inducing plasmid pTiBo542. *J Bacteriol* 166: 88–94.

Kombrink E (2012) Chemical and genetic exploration of jasmonate biosynthesis and signaling paths. *Planta* 236: 1351–1366.

Koo AJK, Chung HS, Kobayashi Y, Howe GA (2006) Identification of a peroxisomal acyl-activating enzyme involved in the biosynthesis of jasmonic acid in Arabidopsis. *J Biol Chem* 281: 33511–33520.

Koo AJK, Cooke TF, Howe GA (2011) Cytochrome P450 CYP94B3 mediates catabolism and inactivation of the plant hormone jasmonoyl-L-isoleucine. *Proc Natl Acad Sci U S A* 108: 9298–9303.

Koo AJK, Gao X, Jones AD, Howe GA (2009) A rapid wound signal activates the systemic synthesis of bioactive jasmonates in Arabidopsis. *Plant J* 59: 974–986.

Koo AJ, Thireault C, Zemelis S, Poudel AN, Zhang T, Kitaoka N, Brandizzi F, Matsuura H, Howe GA (2014) Endoplasmic reticulum-associated inactivation of the hormone jasmonoyl-L-isoleucine by multiple members of the cytochrome P450 94 family in Arabidopsis. *J Biol Chem* 289: 29728–29738.

Koo YJ, Yoon ES, Seo JS, Kim J-K, Choi YD (2013) Characterization of a methyl jasmonate specific esterase in arabidopsis. *Hanguk Ungyong Saengmyong Hwahakhoe Chi* 56: 27–33.

Korenjak M, Taylor-Harding B, Binné UK, Satterlee JS, Stevaux O, Aasland R, White-Cooper H, Dyson N, Brehm A (2004) Native E2F/RBF complexes contain Myb-interacting proteins and repress transcription of developmentally controlled E2F target genes. *Cell* 119: 181–193.

Lampou K, Böwer F, Komaki S, Köhler M, Schnittger A (2023) A cytological and functional framework of the meiotic spindle assembly checkpoint in*Arabidopsis thaliana*.

Lang L, Böwer F, Tunçay Elbaşı H, Eeckhout D, Marschlich N, de Jaeger G, Heese M, Schnittger A (2023) The two plant-specific DREAM components FLIC and FLAC repress floral transition in *Arabidopsis*.

Lang L, Pettkó-Szandtner A, Tunçay Elbaşı H, Takatsuka H, Nomoto Y, Zaki A, Dorokhov S, De Jaeger G, Eeckhout D, Ito M *et al* (2021) The DREAM complex represses growth in response to DNA damage in. *Life Sci Alliance* 4. doi:10.26508/lsa.202101141.

Langmead B, Trapnell C, Pop M, Salzberg SL (2009) Ultrafast and memory-efficient alignment of short DNA sequences to the human genome. *Genome Biol* 10: R25.

Lee H, Suh SS, Park E, Cho E, Ahn JH, Kim SG, Lee JS, Kwon YM, Lee I (2000) The AGAMOUS-LIKE 20 MADS domain protein integrates floral inductive pathways in Arabidopsis. *Genes Dev* 14: 2366–2376.

Li C, Xu M, Cai X, Han Z, Si J, Chen D (2022) Jasmonate Signaling Pathway Modulates Plant Defense, Growth, and Their Trade-Offs. *Int J Mol Sci* 23. doi:10.3390/ijms23073945.

Lin Y-T, Chen L-J, Herrfurth C, Feussner I, Li H-M (2016) Reduced Biosynthesis of Digalactosyldiacylglycerol, a Major Chloroplast Membrane Lipid, Leads to Oxylipin Overproduction and Phloem Cap Lignification in Arabidopsis. *Plant Cell* 28: 219–232.

Litovchick L, Sadasivam S, Florens L, Zhu X, Swanson SK, Velmurugan S, Chen R, Washburn MP, Liu XS, DeCaprio JA (2007) Evolutionarily conserved multisubunit RBL2/p130 and E2F4 protein complex represses human cell cycle-dependent genes in quiescence. *Mol Cell* 26: 539–551.

Liu B, Seong K, Pang S, Song J, Gao H, Wang C, Zhai J, Zhang Y, Gao S, Li X *et al* (2021) Functional specificity, diversity, and redundancy of Arabidopsis JAZ family repressors in jasmonate and COI1-regulated growth, development, and defense. *New Phytol* 231: 1525–1545.

Liu H, Timko MP (2021) Jasmonic Acid Signaling and Molecular Crosstalk with Other Phytohormones. *Int J Mol Sci* 22. doi:10.3390/ijms22062914.

Liu S, Yu Y, Ruan Y, Meyer D, Wolff M, Xu L, Wang N, Steinmetz A, Shen W-H (2007) Plant SET- and RING-associated domain proteins in heterochromatinization. *Plant J* 52: 914–926.

Liu Y, Kong Z, Liu J, Zhang P, Wang Q, Huan X, Li L, Qin P (2020) Non-targeted metabolomics of quinoa seed filling period based on liquid chromatography-mass spectrometry. *Food Res Int* 137: 109743.

Liu Y, Li X, Li K, Liu H, Lin C (2013) Multiple bHLH proteins form heterodimers to mediate CRY2-dependent regulation of flowering-time in Arabidopsis. *PLoS Genet* 9: e1003861.

Liu Y, Li X, Ma D, Chen Z, Wang J-W, Liu H (2018) CIB1 and CO interact to mediate CRY2-dependent regulation of flowering. *EMBO Rep* 19. doi:10.15252/embr.201845762.

Li Z, Zhang Y, Zou D, Zhao Y, Wang H-L, Zhang Y, Xia X, Luo J, Guo H, Zhang Z (2020) LSD 3.0: a comprehensive resource for the leaf senescence research community. *Nucleic Acids Res* 48: D1069–D1075.

Longair MH, Baker DA, Armstrong JD (2011) Simple Neurite Tracer: open source software for reconstruction, visualization and analysis of neuronal processes. *Bioinformatics* 27: 2453–2454.

Ma C, Li R, Sun Y, Zhang M, Li S, Xu Y, Song J, Li J, Qi J, Wang L *et al* (2023) ZmMYC2s play important roles in maize responses to simulated herbivory and jasmonate. *J Integr Plant Biol* 65: 1041–1058.

Marquis V, Smirnova E, Poirier L, Zumsteg J, Schweizer F, Reymond P, Heitz T (2020) Stress- and pathway-specific impacts of impaired jasmonoyl-isoleucine (JA-Ile) catabolism on defense signalling and biotic stress resistance. *Plant Cell Environ* 43: 1558–1570.

Mathieu J, Yant LJ, Mürdter F, Küttner F, Schmid M (2009) Repression of flowering by the miR172 target SMZ. *PLoS Biol* 7: e1000148.

McGrath KC, Dombrecht B, Manners JM, Schenk PM, Edgar CI, Maclean DJ, Scheible W-R, Udvardi MK, Kazan K (2005) Repressor- and activator-type ethylene response factors functioning in jasmonate signaling and disease resistance identified via a genome-wide screen of Arabidopsis transcription factor gene expression. *Plant Physiol* 139: 949–959.

Monte I, Caballero J, Zamarreño AM, Fernández-Barbero G, García-Mina JM, Solano R (2022) JAZ is essential for ligand specificity of the COI1/JAZ co-receptor. *Proc Natl Acad Sci U S A* 119: e2212155119.

Monte I, Kneeshaw S, Franco-Zorrilla JM, Chini A, Zamarreño AM, García-Mina JM, Solano R (2020) An Ancient COI1-Independent Function for Reactive Electrophilic Oxylipins in Thermotolerance. *Curr Biol* 30: 962–971.e3.

Nasim Z, Susila H, Jin S, Youn G, Ahn JH (2022) Polymerase II-Associated Factor 1 Complex-Regulated -Clade Genes Repress Flowering in Response to Chilling. *Front Plant Sci* 13: 817356.

Nilsson AK, Fahlberg P, Ellerström M, Andersson MX (2012) Oxo-phytodienoic acid (OPDA) is formed on fatty acids esterified to galactolipids after tissue disruption in Arabidopsis thaliana. *FEBS Lett* 586: 2483–2487.

Ning Y-Q, Liu N, Lan K-K, Su Y-N, Li L, Chen S, He X-J (2020) DREAM complex suppresses DNA methylation maintenance genes and precludes DNA hypermethylation. *Nat Plants* 6: 942–956.

Ning Y-Q, Ma Z-Y, Huang H-W, Mo H, Zhao T-T, Li L, Cai T, Chen S, Ma L, He X-J (2015) Two novel NAC transcription factors regulate gene expression and flowering time by associating with the histone demethylase JMJ14. *Nucleic Acids Res* 43: 1469–1484.

Pauwels L, Barbero GF, Geerinck J, Tilleman S, Grunewald W, Pérez AC, Chico JM, Bossche RV, Sewell J, Gil E *et al* (2010) NINJA connects the co-repressor TOPLESS to jasmonate signalling. *Nature* 464: 788–791.

Pauwels L, Goossens A (2011) The JAZ proteins: a crucial interface in the jasmonate signaling cascade. *Plant Cell* 23: 3089–3100.

Poudel AN, Zhang T, Kwasniewski M, Nakabayashi R, Saito K, Koo AJ (2016) Mutations in jasmonoyl-L-isoleucine-12-hydroxylases suppress multiple JA-dependent wound responses in Arabidopsis thaliana. *Biochim Biophys Acta* 1861: 1396–1408.

Pratiwi P, Tanaka G, Takahashi T, Xie X, Yoneyama K, Matsuura H, Takahashi K (2017) Identification of Jasmonic Acid and Jasmonoyl-Isoleucine, and Characterization of AOS, AOC, OPR and JAR1 in the Model Lycophyte Selaginella moellendorffii. *Plant Cell Physiol* 58: 789–801.

Raji JA, Frame B, Little D, Santoso TJ, Wang K (2018) Agrobacterium- and Biolistic-Mediated Transformation of Maize B104 Inbred. *Methods Mol Biol* 1676: 15–40.

Ralhan A, Schöttle S, Thurow C, Iven T, Feussner I, Polle A, Gatz C (2012) The vascular pathogen Verticillium longisporum requires a jasmonic acid-independent COI1 function in roots to elicit disease symptoms in Arabidopsis shoots. *Plant Physiol* 159: 1192–1203.

Ratcliffe OJ, Kumimoto RW, Wong BJ, Riechmann JL (2003) Analysis of the Arabidopsis MADS AFFECTING FLOWERING gene family: MAF2 prevents vernalization by short periods of cold. *Plant Cell* 15: 1159–1169.

Ren C, Pan J, Peng W, Genschik P, Hobbie L, Hellmann H, Estelle M, Gao B, Peng J, Sun C *et al* (2005) Point mutations in Arabidopsis Cullin1 reveal its essential role in jasmonate response. *Plant J* 42: 514–524.

Robert X, Gouet P (2014) Deciphering key features in protein structures with the new ENDscript server. *Nucleic Acids Res* 42: W320–W324.

Robinson MD, McCarthy DJ, Smyth GK (2010) edgeR: a Bioconductor package for differential expression analysis of digital gene expression data. *Bioinformatics* 26: 139–140.

Rodrigues VL, Dolde U, Sun B, Blaakmeer A, Straub D, Eguen T, Botterweg-Paredes E, Hong S, Graeff M, Li M-W *et al* (2021) A microProtein repressor complex in the shoot meristem controls the transition to flowering. *Plant Physiol* 187: 187–202.

Scarpone R, Rosato R, Chiumiento F, Cipolletti C, Sergi M, Compagnone D (2020) Preliminary study to develop an alternative method for the non-targeted determination of xenobiotics in food by means of ultra high performance liquid chromatography coupled to high resolution and accuracy mass spectrometry. *Food Anal Methods* 13: 1099–1110.

Schaller A, Stintzi A (2009) Enzymes in jasmonate biosynthesis - structure, function, regulation. *Phytochemistry* 70: 1532–1538.

Schmit F, Korenjak M, Mannefeld M, Schmitt K, Franke C, von Eyss B, Gagrica S, Hänel F, Brehm A, Gaubatz S (2007) LINC, a human complex that is related to pRB-containing complexes in invertebrates regulates the expression of G2/M genes. *Cell Cycle* 6: 1903–1913.

Sembdner G, Parthier B (1993) The biochemistry and the physiological and molecular actions of jasmonates. *Annu Rev Plant Physiol Plant Mol Biol* 44: 569–589.

Seo HS, Song JT, Cheong JJ, Lee YH, Lee YW, Hwang I, Lee JS, Choi YD (2001) Jasmonic acid carboxyl methyltransferase: a key enzyme for jasmonate-regulated plant responses. *Proc Natl Acad Sci U S A* 98: 4788–4793.

Shamsi SA, Akter F (2022) Capillary Electrophoresis Mass Spectrometry: Developments and Applications for Enantioselective Analysis from 2011-2020. *Molecules* 27. doi:10.3390/molecules27134126.

Shi R, Yu J, Chang X, Qiao L, Liu X, Lu L (2023) Recent advances in research into jasmonate biosynthesis and signaling pathways in agricultural crops and products. *Processes (Basel)* 11: 736.

Shyu C, Figueroa P, Depew CL, Cooke TF, Sheard LB, Moreno JE, Katsir L, Zheng N, Browse J, Howe GA (2012) JAZ8 lacks a canonical degron and has an EAR motif that mediates transcriptional repression of jasmonate responses in Arabidopsis. *Plant Cell* 24: 536–550.

Smirnova E, Marquis V, Poirier L, Aubert Y, Zumsteg J, Ménard R, Miesch L, Heitz T (2017) Jasmonic Acid Oxidase 2 Hydroxylates Jasmonic Acid and Represses Basal Defense and Resistance Responses against Botrytis cinerea Infection. *Mol Plant* 10: 1159–1173.

Stenzel I, Hause B, Miersch O, Kurz T, Maucher H, Weichert H, Ziegler J, Feussner I, Wasternack C (2003) Jasmonate biosynthesis and the allene oxide cyclase family of Arabidopsis thaliana. *Plant Mol Biol* 51: 895–911.

Sun J, Xu Y, Ye S, Jiang H, Chen Q, Liu F, Zhou W, Chen R, Li X, Tietz O *et al* (2009) Arabidopsis ASA1 is important for jasmonate-mediated regulation of auxin biosynthesis and transport during lateral root formation. *Plant Cell* 21: 1495–1511.

Taki N, Sasaki-Sekimoto Y, Obayashi T, Kikuta A, Kobayashi K, Ainai T, Yagi K, Sakurai N, Suzuki H, Masuda T *et al* (2005) 12-oxo-phytodienoic acid triggers expression of a distinct set of genes and plays a role in wound-induced gene expression in Arabidopsis. *Plant Physiol* 139: 1268–1283.

Thines B, Katsir L, Melotto M, Niu Y, Mandaokar A, Liu G, Nomura K, He SY, Howe GA, Browse J (2007) JAZ repressor proteins are targets of the SCF(COI1) complex during jasmonate signalling. *Nature* 448: 661–665.

Thomas PD, Ebert D, Muruganujan A, Mushayahama T, Albou L-P, Mi H (2022) PANTHER: Making genome-scale phylogenetics accessible to all. *Protein Sci* 31: 8–22.

Uppalapati SR, Ayoubi P, Weng H, Palmer DA, Mitchell RE, Jones W, Bender CL (2005) The phytotoxin coronatine and methyl jasmonate impact multiple phytohormone pathways in tomato. *Plant J* 42: 201–217.

Uyehara AN, Del Valle-Echevarria AR, Hunter CT, Nelissen H, Demuynck K, Cahill JF, Gorman Z, Jander G, Muszynski MG (2023) Cytokinin Promotes Jasmonic Acid Accumulation in the Control of Maize Leaf Growth. *Plants* 12. doi:10.3390/plants12163014.

Van Moerkercke A, Duncan O, Zander M, Šimura J, Broda M, Vanden Bossche R, Lewsey MG, Lama S, Singh KB, Ljung K *et al* (2019) A MYC2/MYC3/MYC4-dependent transcription factor network regulates water spray-responsive gene expression and jasmonate levels. *Proc Natl Acad Sci U S A* 116: 23345–23356.

Varadi M, Anyango S, Deshpande M, Nair S, Natassia C, Yordanova G, Yuan D, Stroe O, Wood G, Laydon A *et al* (2022) AlphaFold Protein Structure Database: massively expanding the structural coverage of protein-sequence space with high-accuracy models. *Nucleic Acids Res* 50: D439–D444.

Vick BA, Zimmerman DC (1983) The biosynthesis of jasmonic acid: a physiological role for plant lipoxygenase. *Biochem Biophys Res Commun* 111: 470–477.

Wan S, Xin X-F (2022) Regulation and integration of plant jasmonate signaling: a comparative view of monocot and dicot. *J Genet Genomics* 49: 704–714.

Wasternack C, Hause B (2013) Jasmonates: biosynthesis, perception, signal transduction and action in plant stress response, growth and development. An update to the 2007 review in Annals of Botany. *Ann Bot* 111: 1021–1058.

Wasternack C, Song S (2017) Jasmonates: biosynthesis, metabolism, and signaling by proteins activating and repressing transcription. *J Exp Bot* 68: 1303–1321.

Wasternack C, Strnad M (2016) Jasmonate signaling in plant stress responses and development - active and inactive compounds. *N Biotechnol* 33: 604–613.

Wasternack C, Strnad M (2018) Jasmonates: News on Occurrence, Biosynthesis, Metabolism and Action of an Ancient Group of Signaling Compounds. *Int J Mol Sci* 19. doi:10.3390/ijms19092539.

Weimer AK, Demidov D, Lermontova I, Beeckman T, Van Damme D (2016) Aurora Kinases Throughout Plant Development. *Trends Plant Sci* 21: 69–79.

Widemann E, Miesch L, Lugan R, Holder E, Heinrich C, Aubert Y, Miesch M, Pinot F, Heitz T (2013) The amidohydrolases IAR3 and ILL6 contribute to jasmonoyl-isoleucine hormone turnover and generate 12-hydroxyjasmonic acid upon wounding in Arabidopsis leaves. *J Biol Chem* 288: 31701–31714.

Woldemariam MG, Onkokesung N, Baldwin IT, Galis I (2012) Jasmonoyl-L-isoleucine hydrolase 1 (JIH1) regulates jasmonoyl-L-isoleucine levels and attenuates plant defenses against herbivores. *Plant J* 72: 758–767.

Wu T, Liang Y, Zhu X, Zhao M, Liu H (2014) Separation and quantification of four isomers of indole-3-acetyl-myo-inositol in plant tissues using high-performance liquid chromatography coupled with quadrupole time-of-flight tandem mass spectrometry. *Anal Bioanal Chem* 406: 3239–3247.

Xie DX, Feys BF, James S, Nieto-Rostro M, Turner JG (1998) COI1: an Arabidopsis gene required for jasmonate-regulated defense and fertility. *Science* 280: 1091–1094.

Xu L, Liu F, Lechner E, Genschik P, Crosby WL, Ma H, Peng W, Huang D, Xie D (2002) The SCF(COI1) ubiquitin-ligase complexes are required for jasmonate response in Arabidopsis. *Plant Cell* 14: 1919–1935.

Xu P, Zhao P-X, Cai X-T, Mao J-L, Miao Z-Q, Xiang C-B (2020) Integration of Jasmonic Acid and Ethylene Into Auxin Signaling in Root Development. *Front Plant Sci* 11: 271.

Yang D-L, Yao J, Mei C-S, Tong X-H, Zeng L-J, Li Q, Xiao L-T, Sun T-P, Li J, Deng X-W *et al* (2012) Plant hormone jasmonate prioritizes defense over growth by interfering with gibberellin signaling cascade. *Proc Natl Acad Sci U S A* 109: E1192–E1200.

Yang J, Duan G, Li C, Liu L, Han G, Zhang Y, Wang C (2019) The Crosstalks Between Jasmonic Acid and Other Plant Hormone Signaling Highlight the Involvement of Jasmonic Acid as a Core Component in Plant Response to Biotic and Abiotic Stresses. *Front Plant Sci* 10: 1349.

Yang Z-B, He C, Ma Y, Herde M, Ding Z (2017) Jasmonic Acid Enhances Al-Induced Root Growth Inhibition. *Plant Physiol* 173: 1420–1433.

Yan J, Li X, Zeng B, Zhong M, Yang J, Yang P, Li X, He C, Lin J, Liu X *et al* (2020) FKF1 F-box protein promotes flowering in part by negatively regulating DELLA protein stability under long-day photoperiod in Arabidopsis. *J Integr Plant Biol* 62: 1717–1740.

Yan J, Zhang C, Gu M, Bai Z, Zhang W, Qi T, Cheng Z, Peng W, Luo H, Nan F *et al* (2009) The Arabidopsis CORONATINE INSENSITIVE1 protein is a jasmonate receptor. *Plant Cell* 21: 2220–2236.

Yan Y, Huang P-C, Borrego E, Kolomiets M (2014) New perspectives into jasmonate roles in maize. *Plant Signal Behav* 9: e970442.

Yan Y, Stolz S, Chételat A, Reymond P, Pagni M, Dubugnon L, Farmer EE (2007) A downstream mediator in the growth repression limb of the jasmonate pathway. *Plant Cell* 19: 2470–2483.

Yilmaz A, Mejia-Guerra MK, Kurz K, Liang X, Welch L, Grotewold E (2011) AGRIS: the Arabidopsis Gene Regulatory Information Server, an update. *Nucleic Acids Res* 39: D1118–D1122.

Yu C-W, Lin Y-T, Li H-M (2020) Increased ratio of galactolipid MGDG : DGDG induces jasmonic acid overproduction and changes chloroplast shape. *New Phytol* 228: 1327–1335.

Zander M, Chen S, Imkampe J, Thurow C, Gatz C (2012) Repression of the Arabidopsis thaliana jasmonic acid/ethylene-induced defense pathway by TGA-interacting glutaredoxins depends on their C-terminal ALWL motif. *Mol Plant* 5: 831–840.

Zhai Q, Yan C, Li L, Xie D, Li C (2017) Jasmonates. In Hormone Metabolism and Signaling in Plants, (Elsevier), pp. 243–272.

Zhang B, Wang L, Zeng L, Zhang C, Ma H (2015a) Arabidopsis TOE proteins convey a photoperiodic signal to antagonize CONSTANS and regulate flowering time. *Genes Dev* 29: 975–987.

Zhang F, Yao J, Ke J, Zhang L, Lam VQ, Xin X-F, Zhou XE, Chen J, Brunzelle J, Griffin PR *et al* (2015b) Structural basis of JAZ repression of MYC transcription factors in jasmonate signalling. *Nature* 525: 269–273.

Zhang Q, Dai X, Wang H, Wang F, Tang D, Jiang C, Zhang X, Guo W, Lei Y, Ma C *et al* (2022) Transcriptomic Profiling Provides Molecular Insights Into Hydrogen Peroxide-Enhanced Growth and Its Salt Tolerance. *Front Plant Sci* 13: 866063.

Zhang S, Zhou B, Kang Y, Cui X, Liu A, Deleris A, Greenberg MVC, Cui X, Qiu Q, Lu F *et al* (2015c) C-terminal domains of a histone demethylase interact with a pair of transcription factors and mediate specific chromatin association. *Cell Discov* 1: 15003 – .

Zhang T, Poudel AN, Jewell JB, Kitaoka N, Staswick P, Matsuura H, Koo AJ (2016) Hormone crosstalk in wound stress response: wound-inducible amidohydrolases can simultaneously regulate jasmonate and auxin homeostasis in Arabidopsis thaliana. *J Exp Bot* 67: 2107–2120.

Zhang X, Wu Q, Ren J, Qian W, He S, Huang K, Yu X, Gao Y, Huang P, An C (2012) Two novel RING-type ubiquitin ligases, RGLG3 and RGLG4, are essential for jasmonate-mediated responses in Arabidopsis. *Plant Physiol* 160: 808–822.

Zhao L, Li X, Chen W, Xu Z, Chen M, Wang H, Yu D (2022) The emerging role of jasmonate in the control of flowering time. *J Exp Bot* 73: 11–21.

Zhao W, Guan C, Feng J, Liang Y, Zhan N, Zuo J, Ren B (2016) The Arabidopsis CROWDED NUCLEI genes regulate seed germination by modulating degradation of ABI5 protein. *J Integr Plant Biol* 58: 669–678.

Zhou H, Liu B, Weeks DP, Spalding MH, Yang B (2014) Large chromosomal deletions and heritable small genetic changes induced by CRISPR/Cas9 in rice. *Nucleic Acids Res* 42: 10903–10914.

Zhou M, Memelink J (2016) Jasmonate-responsive transcription factors regulating plant secondary metabolism. *Biotechnol Adv* 34: 441–449.

Figure 1

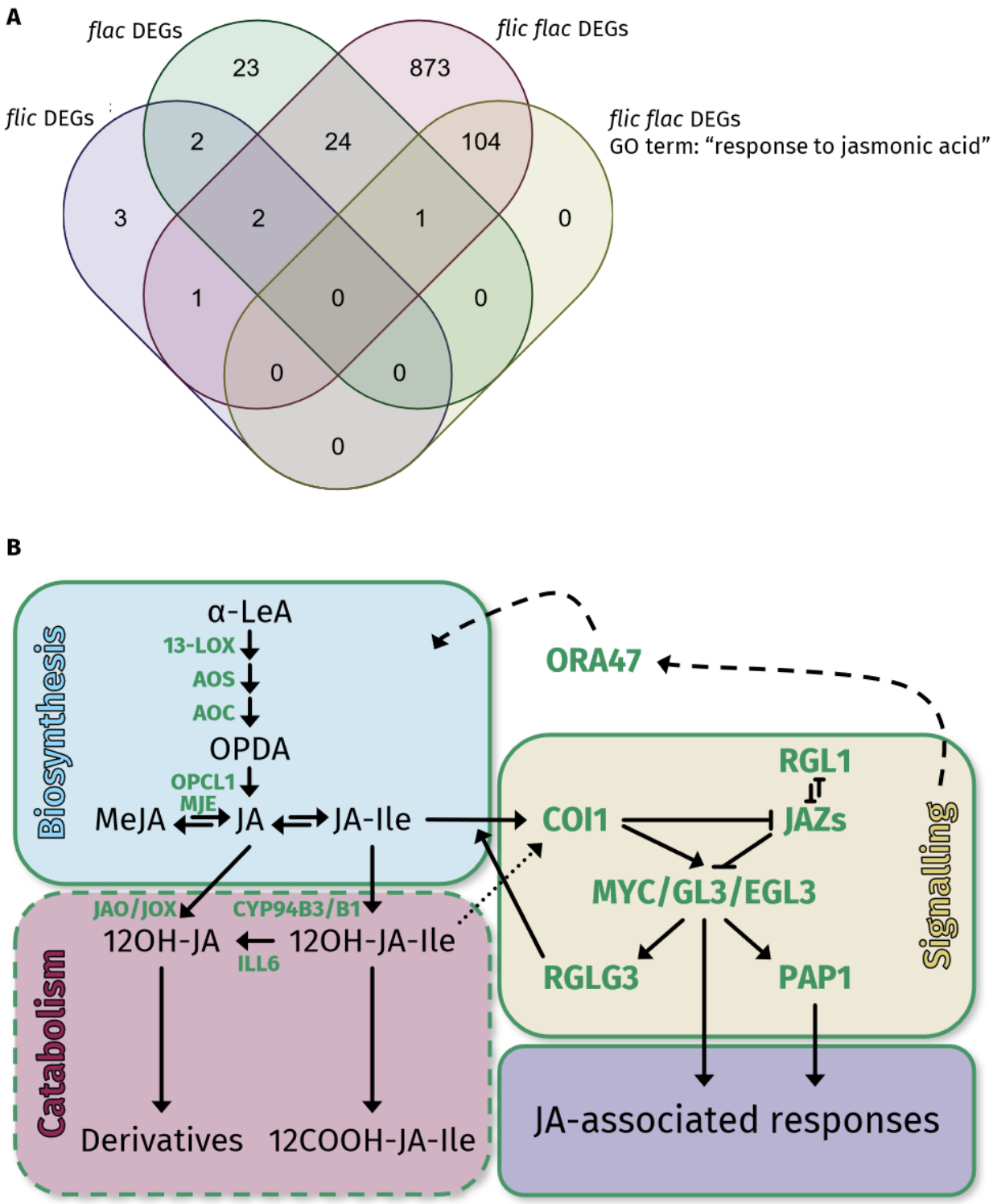
A
flac DEGs
flic flac DEGs
flic DEGs
flic flac DEGs
GO term: "response to jasmonic acid"
23
873
2
24
104
3
2
1
0
1
0
0
0
0
0
B
Biosynthesis
α-LeA
13-LOX
AOS
AOC
OPDA
OPCL1
MJE
MeJA
JA
JA-Ile
ORA47
RGL1
COI1
JAZs
MYC/GL3/EGL3
RGLG3
PAP1
Signalling
JAO/JOX
CYP94B3/B1
12OH-JA
12OH-JA-Ile
ILL6
Catabolism
Derivatives
12COOH-JA-Ile
JA-associated responses

Figure 2

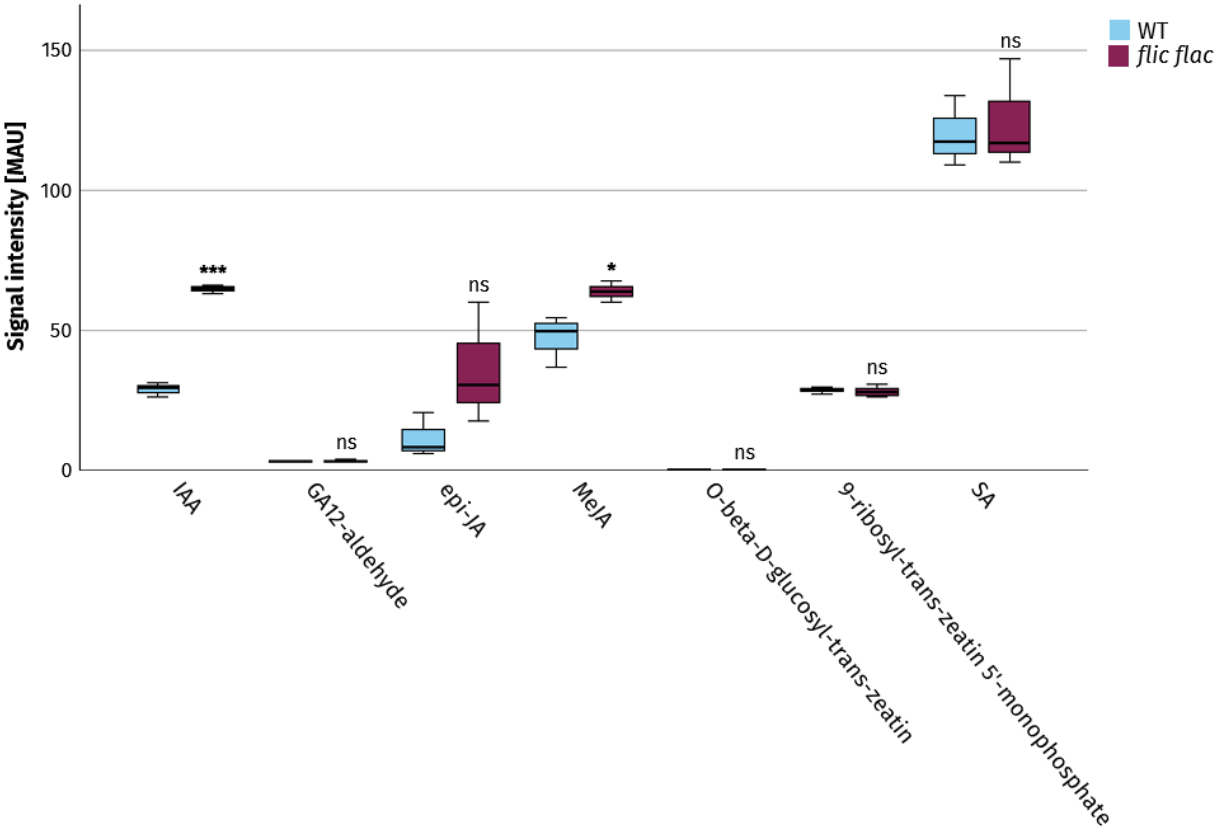
WT
flic flac
Signal intensity [MAU]
150
100
50
0
***
ns
ns
*
ns
ns
ns
IAA
GA12-aldehyde
epi-JA
MeJA
O-beta-D-glucosyl-trans-zeatin
9-ribosyl-trans-zeatin 5'-monophosphate
SA

Figure 3

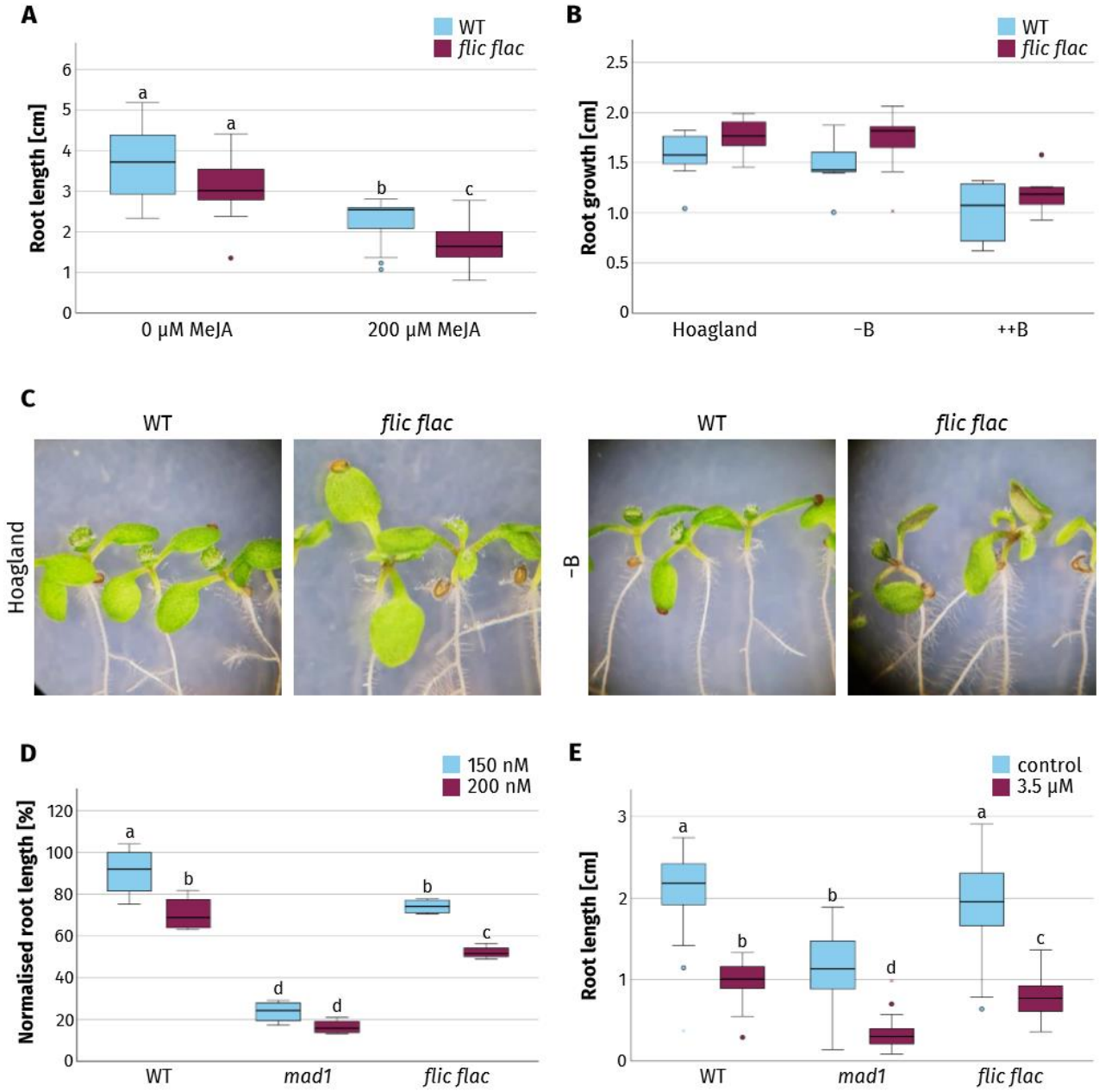
A
WT
flic flac
Root length [cm]
0 µM MeJA
200 µM MeJA
B
WT
flic flac
Root growth [cm]
Hoagland
−B
++B
C
WT
flic flac
Hoagland
−B
D
150 nM
200 nM
Normalised root length [%]
WT
mad1
flic flac
E
control
3.5 µM
Root length [cm]
WT
mad1
flic flac

Figure 4

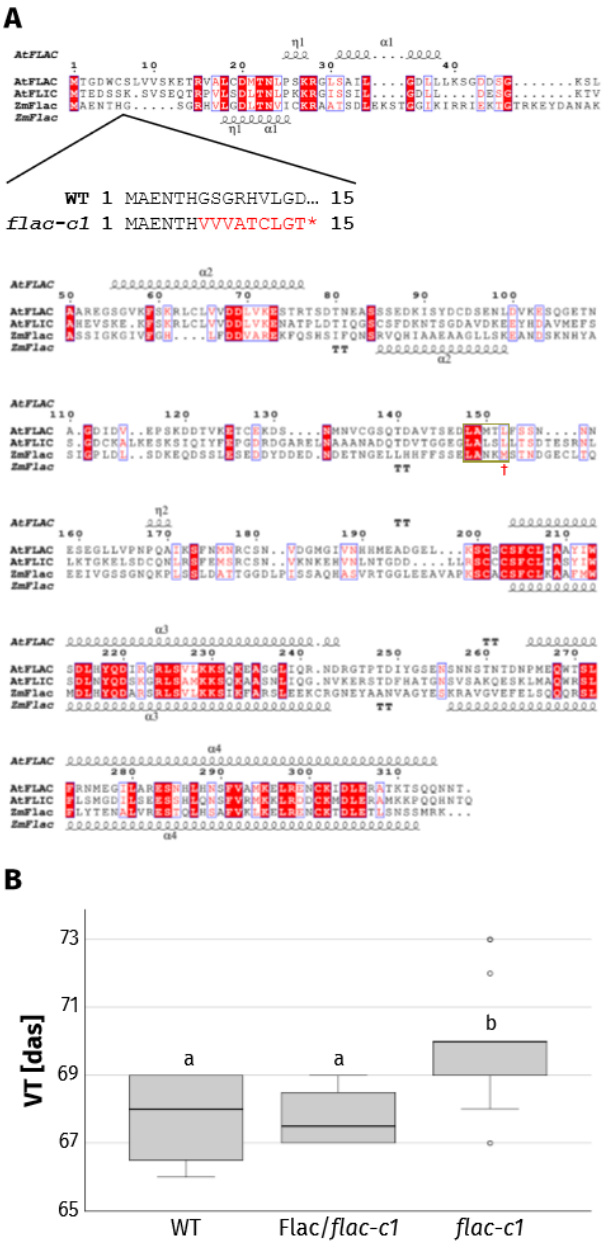
A
WT 1 MAENTHGSGRHVLGD… 15
flac-c1 1 MAENTHVVVATCLGT* 15
B
VT [das]
73
71
69
67
65
a
a
b
WT
Flac/flac-c1
flac-c1

Figure S1

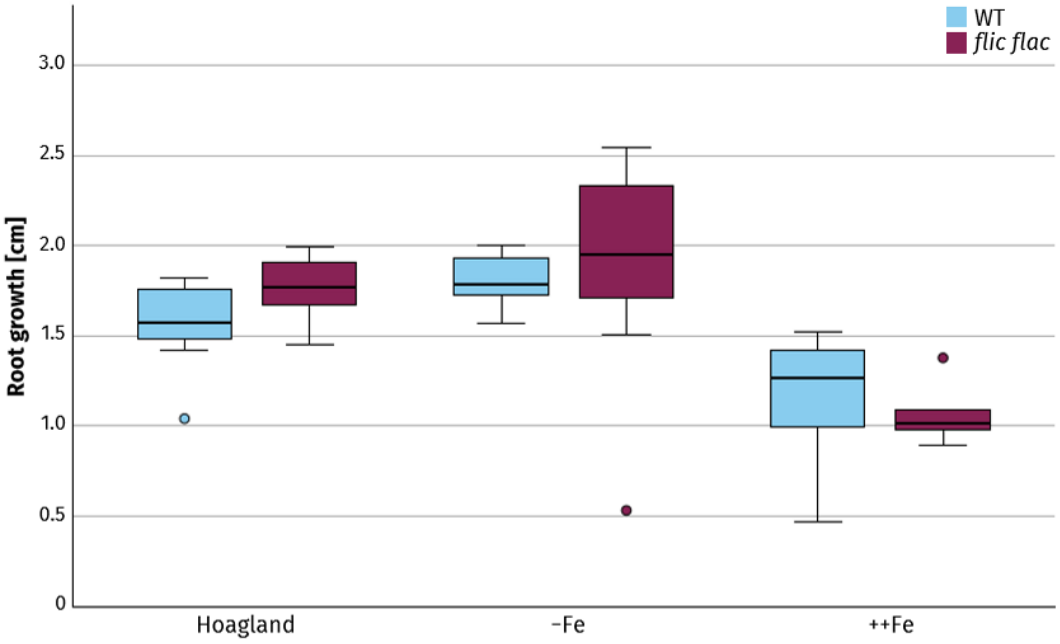

Figure S2

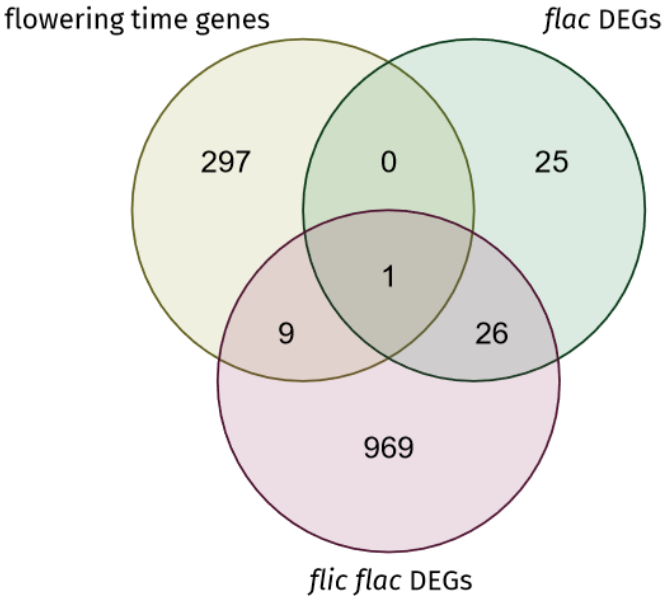
flowering time genes
flac DEGs
297
0
25
1
9
26
969
flic flac DEGs

Table 1. Significant DEGs ($P < 0.05$) categorised under the GO term "response to jasmonic acid" (GO:0009753) in *flic flac* mutant seedlings and their logfc.

Locus Identifier	Primary Gene Symbol	logfc (*flic flac*)
AT1G72260	THIONIN 2.1 (THI2.1)	6.91
AT1G61120	TERPENE SYNTHASE 04 (TPS04)	6.37
AT5G24780	VEGETATIVE STORAGE PROTEIN 1 (VSP1)	5.96
AT1G54020		5.55
AT2G39030	N-ACETYLTRANSFERASE ACTIVITY 1 (NATA1)	5.01
AT5G22545		4.91
AT3G28220		4.75
AT5G24770	VEGETATIVE STORAGE PROTEIN 2 (VSP2)	4.52
AT5G21960	ETHYLENE RESPONSE FACTOR 016 (ERF016)	4.32
AT1G52000		3.37
AT3G22275	JASMONATE ZIM-DOMAIN PROTEIN 13 (JAZ13)	3.34
AT1G66100		3.32
AT2G24850	TYROSINE AMINOTRANSFERASE 3 (TAT3)	2.95
AT1G17380	JASMONATE-ZIM-DOMAIN PROTEIN 5 (JAZ5)	2.84
AT1G65890	ACYL ACTIVATING ENZYME 12 (AAE12)	2.80
AT2G34810	(ATBBE16)	2.35
AT5G44420	PLANT DEFENSIN 1.2 (PDF1.2)	2.32
AT1G73325		2.13
AT3G50280		2.10
AT4G29780		2.05
AT3G50770	CALMODULIN-LIKE 41 (CML41)	2.04
AT3G15500	NAC DOMAIN CONTAINING PROTEIN 3 (NAC3)	2.03
AT4G22610		2.01
AT4G13310	CYTOCHROME P450, FAMILY 71, SUBFAMILY A, POLYPEPTIDE 20 (CYP71A20)	1.98
AT1G44350	IAA-LEUCINE RESISTANT (ILR)-LIKE GENE 6 (ILL6)	1.85
AT4G28703		1.81
AT1G73540	NUDIX HYDROLASE HOMOLOG 21 (NUDT21)	1.80
AT3G16470	JASMONATE RESPONSIVE 1 (JR1)	1.78
AT4G21840	METHIONINE SULFOXIDE REDUCTASE B8 (MSRB8)	1.78
AT1G56650	PRODUCTION OF ANTHOCYANIN PIGMENT 1 (PAP1)	1.70
AT1G20310		1.69
AT1G55020	LIPOXYGENASE 1 (LOX1)	1.64
AT1G58270	(ZW9)	1.63
AT2G27830		1.62
AT3G45140	LIPOXYGENASE 2 (LOX2)	1.59
AT4G13395	ROTUNDIFOLIA LIKE 12 (RTFL12)	1.56
AT1G60260	BETA GLUCOSIDASE 5 (BGLU5)	1.52
AT1G63720		1.51
AT1G32640	(MYC2)	1.51
AT4G29700		1.50
AT1G23710		1.49
AT1G61340	F-BOX STRESS INDUCED 1 (FBS1)	1.48
AT1G54040	EPITHIOSPECIFIER PROTEIN (ESP)	1.48
AT4G24340		1.47
AT3G51450		1.44
AT1G18300	NUDIX HYDROLASE HOMOLOG 4 (NUDT4)	1.40
AT5G47220	ETHYLENE RESPONSIVE ELEMENT BINDING FACTOR 2 (ERF2)	1.39
AT1G64200	VACUOLAR H+-ATPASE SUBUNIT E ISOFORM 3 (VHA-E3)	1.38
AT4G11280	1-AMINOCYCLOPROPANE-1-CARBOXYLIC ACID (ACC) SYNTHASE 6 (ACS6)	1.38
AT4G28085		1.37
AT1G70700	JASMONATE-ZIM-DOMAIN PROTEIN 9 (JAZ9)	1.33
AT5G41315		1.31
AT3G48360	BTB AND TAZ DOMAIN PROTEIN 2 (bt2)	1.29
AT1G60270	BETA GLUCOSIDASE 6 (BGLU6)	1.29
AT1G19180	JASMONATE-ZIM-DOMAIN PROTEIN 1 (JAZ1)	1.28
AT1G61065		1.22
AT2G32140		1.21
AT2G28400	(ATS40.4)	1.18
AT1G54010	GDSL-LIKE LIPASE 23 (GLL23)	1.16
AT1G06620		1.16
AT5G08240		1.10
AT1G23850		1.09
AT2G18210		1.08
AT1G24145		1.08
AT5G13220	(PW220)	1.03
AT2G39420	(MAGL8)	1.01
AT5G42650	ALLENE OXIDE SYNTHASE (AOS)	0.99
AT3G09940	MONODEHYDROASCORBATE REDUCTASE 3 (MDAR3)	0.99
AT2G44230		0.97
AT1G54000	GDSL LIPASE-LIKE PROTEIN 22 (GLL22)	0.97
AT2G27310		0.94
AT1G66350	RGA-LIKE 1 (RGL1)	0.94
AT2G36650		0.94
AT4G34710	ARGININE DECARBOXYLASE 2 (ADC2)	0.93
AT1G65820		0.93
AT1G63650	ENHANCER OF GLABRA 3 (EGL3)	0.92
AT5G41120	(ELT4)	0.91
AT5G02940	PLASTID ENVELOPE ION CHANNELS 1 (PEC1)	0.91
AT1G67340		0.91
AT5G61290		0.91
AT4G23600	CORONATINE INDUCED 1 (CORI3)	0.90
AT4G17480		0.90
AT1G03940		0.88
AT4G36500		0.87
AT1G17750	PEP1 RECEPTOR 2 (PEPR2)	0.86
AT1G72450	JASMONATE-ZIM-DOMAIN PROTEIN 6 (JAZ6)	0.85
AT3G25600	CALMODULIN LIKE 16 (CML16)	0.85
AT1G62810	COPPER AMINE OXIDASE1 (CUAO1)	0.84
AT1G74430	MYB DOMAIN PROTEIN 95 (MYB95)	0.84
AT3G15760		0.84
AT2G43550		0.83
AT1G19570	DEHYDROASCORBATE REDUCTASE (DHAR1)	0.82
AT1G20510	OPC-8:0 COA LIGASE1 (OPCL1)	0.80
AT1G52080	(AR791)	0.78
AT5G18130		0.78
AT3G43270	PECTIN METHYL ESTERASE INHIBITOR-PECTIN METHYLESTERASE 32 (PMEI-PME32)	0.78
AT5G18860	NUCLEOSIDE HYDROLASE 3 (NSH3)	0.75
AT3G15210	ETHYLENE RESPONSIVE ELEMENT BINDING FACTOR 4 (ERF4)	0.73
AT1G52720		0.73
AT5G63970	RING DOMAIN LIGASE 3 (RGLG3)	0.72
AT3G56880		0.71
AT5G08790	(ATAF2)	0.71
AT1G11050		0.70
AT1G55840		0.70
AT1G22890	(STMP2)	0.70

Declaration of contributions

I hereby declare that all results shown in this thesis were obtained by myself, except the ones indicated in the respective figure legends and in this list. Here, I summarise the contributions from collaborators.

Chapter 1

- Fig 1 was created based on data generated by G De Jaeger, D Eeckhout, M Heese and A Schnittger.
- Fig 2 was created based on data generated by A Pettkó-Szandtner.
- Fig 3 partly contains data that were generated by H Tunçay-Elbaşı.
- Fig 4 presents data and images generated by H Tunçay-Elbaşı.
- Fig 5 presents data and images generated by H Tunçay-Elbaşı.
- Fig 6 partly contains data and images generated by H Takatsuka and Y Nomoto and was created based on these.
- Fig 7 presents data and images generated by H Takatsuka and Y Nomoto and was created based on these.
- Fig 8 presents data and images generated by Z Magyar.
- Fig 9 presents data and images generated by A Zaki and was created based on these.
- Table 1 was created by M Heese.
- Fig S1 was created by M Heese.
- Fig S2 was created based on data generated by S Dorokhov.
- Fig S3 was created by M Heese.
- Fig S4 presents data and images generated by H Tunçay-Elbaşı.
- Fig S5 was created by M Heese.
- Fig S7 was created by and partly contains data that were generated by H Tunçay-Elbaşı.
- Fig S9 presents data and images generated by A Zaki and was created based on these.
- Fig S10 presents data and images generated by A Zaki and was created based on these.
- Table S1 was created based on data generated by G De Jaeger and D Eeckhout.
- Table S2 was created by G De Jaeger and D Eeckhout.
- Table S3 was created by S Dorokhov.
- Table S4 was created by A Pettkó-Szandtner.

Chapter 2

- Fig 1 was created based on data provided by D Eeckhout and G De Jaeger.
- Fig 2 partly contains data that were generated by H Tunçay-Elbaşı and N Marschlich.
- Fig 3 partly contains data that were generated by F Böwer.
- Fig 5 partly contains data that were generated by H Tunçay-Elbaşı.
- Fig 6 contains a graphical contribution by F Böwer.
- Fig S2 partly contains data that were generated by H Tunçay-Elbaşı and N Marschlich.

Chapter 3

- The transformation and growth of *Zea mays* to create the Zm*flac-c1* line were performed by Seijiro Ono and Misato Ono (both University of Hamburg).
- Fig 1A was created based on data provided by Masaki Ito (Kanazawa University).
- Fig 1B was created based on Delgado et al, 2021, as referenced.
- Fig 2 was created based on data provided by Takumi Nishiuchi (Nagoya University).
- Table 1 was created based on data provided by Masaki Ito (Kanazawa University).
- Table S1 was created based on data provided by Masaki Ito (Kanazawa University).
- Table S2 was created based on data provided by Masaki Ito (Kanazawa University).
- Table S3 was created based on data provided by Masaki Ito (Kanazawa University).
- Table S4 was created based on data provided by Masaki Ito (Kanazawa University).

Appendix

Sup Tables of Chapter 3 are provided here. Due to space constraints, gene annotations in Table S1 are omitted.

Table S1. DEGs with logfc > 0.7 and *P* < 0.05 in *flic*, *flac*, and *flic flac* mutant seedlings. adj_pvalue, adjusted *P*-value.

	***flic* / wildtype**		***flac* / wildtype**		***flic flac* / wildtype**	
AGI locus	**logfc**	**adj_pvalue**	**logfc**	**adj_pvalue**	**logfc**	**adj_pvalue**
AT2G41240	1.92	1	1.90	1	8.87	1.35E-05
AT3G25180	6.02	0.224520278	0.00	1	7.86	3.99E-05
AT3G21500	3.97	0.77936201	1.44	1	7.13	3.61E-05
AT1G72260	0.84	1	-1.82	1	6.91	6.65E-06
AT4G16590	0.00	1	0.00	1	6.60	0.001705153
AT4G19690	0.05	1	0.08	1	6.40	0.000230234
AT1G61120	4.63	0.075252855	-1.50	1	6.37	1.15E-05
AT5G24780	2.66	0.097947049	-1.66	0.564105009	5.96	7.38E-12
AT1G58050	0.00	1	3.23	1	5.89	0.014765626
AT2G16367	2.71	1	0.00	1	5.66	0.01176813
AT1G54020	2.05	0.580294586	-0.76	1	5.55	3.40E-12
AT5G04150	-1.84	1	-1.82	1	5.26	0.004536607
AT1G52040	1.73	0.245619639	-1.05	0.7226658	5.24	3.17E-16
AT3G56970	-4.07	1	-4.04	0.866556072	5.15	0.000507576
AT3G56980	0.25	1	-1.89	1	5.06	0.000726998
AT4G37990	3.02	0.834319663	1.02	1	5.03	0.000775152
AT1G52030	1.13	1	-0.71	0.974691946	5.02	7.21E-15
AT2G39030	2.77	0.708006931	-2.13	0.676921461	5.01	0.000239544
AT1G67220	2.68	1	4.02	0.193832151	5.00	0.000493506
AT1G14250	1.74	0.479193814	0.12	1	4.96	1.20E-13
AT5G22545	4.35	1	0.00	1	4.91	0.040256061
AT4G10250	3.87	1	3.60	0.9316272	4.91	0.015835725
AT5G65130	1.90	1	5.23	0.07069974	4.90	0.022185126
AT4G26260	4.66	0.787215437	4.56	0.507344147	4.90	0.034258802
AT1G53620	3.20	1	0.00	1	4.77	0.029136865
AT2G30766	-0.95	1	-1.07	1	4.76	0.000293154
AT3G28220	1.83	0.350843536	0.48	1	4.75	3.40E-12
AT1G30140	3.20	1	3.22	1	4.62	0.049545242
AT5G24770	1.22	0.949548096	-0.89	0.877084714	4.52	6.03E-12
AT3G55970	2.79	0.812941514	-1.54	1	4.34	0.002068193
AT5G21960	-1.85	1	0.09	1	4.32	0.000470005
AT5G57550	2.82	1	0.87	1	4.17	0.007003786
AT1G13609	-1.94	1	-0.05	1	4.16	0.004174816
AT4G08093	4.08	0.494561457	-1.83	1	4.15	0.018022225
AT1G20750	0.84	1	0.90	1	4.14	0.013708064
AT5G28237	2.52	1	-1.83	1	3.98	0.00636473
AT1G67855	0.95	1	1.31	1	3.83	0.001561254
AT3G49620	1.83	0.712453441	-1.49	0.635600974	3.80	1.01E-05
AT1G52400	1.00	0.224520278	-0.31	1	3.79	2.31E-28
AT4G37850	1.74	1	1.77	1	3.46	0.025199454
AT4G17470	0.73	1	-0.39	1	3.46	2.43E-13
AT5G52720	1.35	1	2.08	1	3.44	0.023556603
AT1G52000	0.60	1	-0.63	0.638922215	3.37	4.15E-25
AT3G22275	2.29	1	1.38	1	3.34	0.041307773
AT2G27120	-0.34	1	-0.29	1	3.33	4.38E-05

AT1G66100	-0.18	1	-0.65	1	3.32	3.29E-06
AT1G53885	0.48	1	-0.45	1	3.32	2.91E-11
AT1G53903	0.48	1	-0.45	1	3.32	2.92E-11
AT2G39330	1.18	0.857038284	-1.46	0.239068076	3.31	1.65E-08
AT4G36700	0.30	1	0.91	1	3.30	0.001290417
AT1G67856	-0.23	1	0.60	1	3.29	0.000256706
AT1G54560	2.23	0.841843293	2.86	0.077815842	3.28	0.000290679
AT3G09870	1.73	1	3.50	0.177180934	3.26	0.039326038
AT2G18720	1.10	1	2.46	0.082284929	3.25	8.77E-05
AT5G05340	1.28	1	0.16	1	3.24	0.002085898
AT1G65680	1.70	1	0.62	1	3.22	0.009632555
AT5G24420	1.44	1	-0.27	1	3.17	6.29E-05
AT5G42580	1.60	1	0.12	1	3.15	0.001403287
AT4G03620	0.84	1	2.31	0.936972187	3.13	0.046597391
AT1G47400	-0.13	1	-0.03	1	3.11	0.001067476
AT1G67980	0.53	1	0.79	1	3.07	0.017632871
AT3G28300	0.50	1	-0.16	1	3.05	1.21E-08
AT3G28290	0.50	1	-0.16	1	3.05	1.21E-08
AT1G30190	1.37	1	1.87	0.817099086	3.04	0.000557038
AT5G44430	2.08	0.769247165	-1.49	0.77146117	3.02	0.003691479
AT1G27730	0.81	0.723159154	1.09	0.060013671	3.02	3.44E-20
AT2G33080	1.24	1	0.61	1	3.00	0.013423225
AT4G37140	1.24	1	0.61	1	2.99	0.007383276
AT1G67000	1.05	1	0.35	1	2.97	1.43E-05
AT2G24850	2.16	0.723159154	-0.85	1	2.95	0.005558856
AT1G06100	1.57	0.503485459	1.41	0.327282182	2.92	4.23E-09
AT1G49570	2.41	0.022473793	1.14	0.762172163	2.91	7.75E-06
AT1G17380	1.68	0.075252855	-0.56	1	2.84	9.10E-10
AT1G65890	0.40	1	-0.46	1	2.80	2.28E-07
AT4G11911	1.06	1	-0.80	1	2.78	0.000418404
AT5G60610	1.12	1	3.16	2.34E-06	2.74	2.85E-05
AT1G09500	1.50	0.972224539	1.02	0.944447747	2.73	0.000550098
AT1G35210	1.05	1	0.61	1	2.73	1.64E-07
AT1G61610	0.71	1	-0.41	1	2.70	1.97E-07
AT1G63910	1.14	1	1.56	0.669883655	2.69	0.000109609
AT5G55420	0.43	1	-1.22	1	2.65	0.04540731
AT1G47395	-0.72	1	-0.47	1	2.64	0.003311093
AT5G54490	1.19	0.179435717	0.91	0.386285657	2.61	3.00E-17
AT2G37870	0.32	1	-1.02	1	2.60	0.001142915
AT1G18710	1.07	1	-0.05	1	2.59	9.00E-07
AT4G24570	0.73	0.877534751	0.77	0.425966298	2.59	1.44E-15
AT1G52410	0.46	1	-0.51	0.614004966	2.57	3.36E-24
AT2G29350	0.27	1	-0.73	0.972578282	2.56	0.000180723
AT1G74930	-0.86	1	-1.18	0.744775131	2.50	9.25E-08
AT2G33020	1.68	1	-4.02	0.711911827	2.46	0.005656445
AT3G60140	-0.43	1	-0.79	1	2.46	0.003843884
AT2G40000	0.56	1	0.84	0.177180934	2.46	7.39E-17
AT1G56600	-0.41	1	-0.24	1	2.46	1.89E-08
AT5G11210	1.81	1	1.36	0.987475489	2.45	0.03884323
AT3G10930	0.44	1	0.31	1	2.44	5.20E-07
AT1G65880	0.27	1	0.41	1	2.42	3.52E-06
AT1G07135	0.49	1	0.76	0.75145122	2.41	1.24E-07
AT4G15440	0.48	1	-0.50	1	2.37	1.07E-06
AT2G34810	0.55	1	-0.51	0.809663907	2.35	7.21E-15
AT3G57260	1.25	1	-0.68	1	2.35	0.034521996
AT5G44420	1.40	0.932146044	-1.56	0.422828454	2.32	0.00295233
AT4G10910	0.87	1	2.16	0.330234396	2.31	0.018702178
AT1G53100	-1.06	1	-0.63	1	2.30	0.010923267
AT1G66370	0.30	1	-2.54	0.338918184	2.29	0.003009691
AT1G66860	-1.02	1	-0.97	1	2.29	0.02446268
AT1G21890	-0.05	1	1.39	0.757210493	2.28	0.010743576

AT1G63710	0.54	1	0.23	1	2.27	3.92E-17
AT5G37478	1.47	1	1.08	1	2.27	0.014710431
AT5G03010	0.06	1	1.73	0.892827511	2.24	0.049074194
AT5G59820	0.66	1	0.92	0.199936454	2.24	9.34E-16
AT5G05250	-0.20	1	-0.56	0.989603012	2.23	2.22E-05
AT3G30120	0.68	1	0.86	0.986606105	2.23	0.002589767
AT2G22880	0.87	1	-0.30	1	2.23	0.010239363
AT1G64360	-0.30	1	-0.30	1	2.22	0.000133993
AT4G23590	1.21	1	1.21	0.91138183	2.22	0.014291204
AT5G02170	1.25	1	1.45	0.606123778	2.20	0.000939726
AT5G05600	0.89	0.764678878	-0.80	0.593891746	2.20	1.05E-08
AT4G17490	0.61	1	0.30	1	2.19	1.30E-07
AT5G61600	0.60	1	1.06	0.02634133	2.18	1.59E-13
AT2G44840	1.30	0.870998097	-0.24	1	2.18	0.00057418
AT1G61810	-0.39	1	-0.29	1	2.17	0.013202164
AT1G52120	-0.01	1	-0.59	1	2.17	0.009749582
AT5G01900	0.76	1	-1.43	0.916516884	2.16	0.031378851
AT2G18050	-0.30	1	-0.56	0.967821949	2.15	5.65E-06
AT1G66090	0.57	1	-0.18	1	2.14	7.51E-05
AT1G73325	0.02	1	-1.55	0.4516522	2.13	0.001651688
AT1G62760	0.00	1	-0.48	1	2.11	0.010299801
AT3G50280	0.14	1	-1.00	0.561085301	2.10	1.65E-08
AT1G12030	-0.03	1	-0.51	1	2.09	0.001775507
AT5G64190	-0.32	1	1.17	0.940109064	2.07	0.018707042
AT2G26530	0.33	1	-0.03	1	2.07	8.99E-08
AT3G44260	0.40	1	0.74	0.290106249	2.06	6.79E-13
AT1G64660	0.28	1	-0.04	1	2.06	8.46E-06
AT4G29780	0.48	1	0.27	1	2.05	2.00E-09
AT1G60470	-0.07	1	-0.89	0.980551636	2.04	0.003209342
AT3G50770	0.82	1	0.00	1	2.04	0.001759829
AT3G15500	-0.10	1	-0.24	1	2.03	0.005579993
AT4G27280	0.53	1	0.81	0.117244131	2.03	2.21E-14
AT1G19510	-0.23	1	0.36	1	2.02	0.029288979
AT1G51760	0.17	1	3.08	7.38E-20	2.02	3.64E-09
AT1G66800	0.68	1	0.44	1	2.01	0.001611964
AT4G22610	0.90	1	-0.24	1	2.01	0.000310449
AT4G33720	0.12	1	-1.19	0.509924774	1.99	0.001207326
AT1G76955	0.83	1	-0.10	1	1.98	1.53E-05
AT4G13310	0.94	1	0.10	1	1.98	0.00373577
AT5G21940	0.68	0.0105184	1.38	6.25E-18	1.96	4.86E-38
AT2G25200	0.75	0.986087473	1.08	0.087093365	1.96	1.55E-10
AT5G51190	0.76	1	0.83	0.560230663	1.95	3.33E-06
AT1G65150	0.32	1	0.97	0.217247121	1.94	1.04E-07
AT1G62540	0.30	1	-0.42	0.763146585	1.94	6.54E-17
AT4G17500	0.54	1	0.11	1	1.94	4.12E-09
AT5G04340	0.37	1	0.20	1	1.94	1.67E-15
AT3G45130	0.04	1	-0.45	1	1.93	0.047214797
AT5G13080	0.96	1	-0.11	1	1.93	0.006585628
AT2G25440	1.35	1	0.90	1	1.92	0.013127216
AT4G21926	0.56	1	0.47	1	1.91	0.018863476
AT1G28370	0.24	1	0.07	1	1.91	7.35E-07
AT5G16410	0.16	1	0.30	1	1.90	0.006683755
AT4G37610	0.33	1	1.03	0.000353972	1.89	5.89E-19
AT1G07985	0.40	1	0.88	0.94757449	1.88	0.008052508
AT1G24070	0.36	1	0.25	1	1.88	4.09E-10
AT2G43530	0.27	1	-0.87	0.304126929	1.87	1.71E-07
AT1G68620	0.08	1	-0.77	0.929310122	1.86	0.001173754
AT1G59590	0.27	1	0.49	0.92393022	1.86	5.74E-08
AT1G80840	1.00	0.986087473	-0.21	1	1.85	0.000627426
AT1G44350	0.68	0.552990946	0.01	1	1.85	5.58E-15
AT1G60190	-0.50	1	-0.79	1	1.84	0.000226895

AT1G14120	0.50	1	-0.44	1	1.84	1.35E-06
AT1G22340	0.84	1	-0.16	1	1.83	0.00373577
AT4G37150	0.75	1	0.86	0.745044134	1.83	0.000412495
AT3G48650	0.15	1	-0.30	1	1.82	0.047068312
AT1G67865	-0.02	1	0.10	1	1.81	1.74E-07
AT4G28703	0.32	1	-0.19	1	1.81	0.005979388
AT1G73540	0.17	1	0.64	0.393549619	1.80	8.88E-12
AT3G61190	0.08	1	0.22	1	1.79	0.000598607
AT3G16470	0.50	1	-0.23	1	1.78	1.22E-12
AT4G21840	1.24	0.896625621	0.02	1	1.78	0.009281868
AT5G24140	0.93	1	0.39	1	1.78	0.032264987
AT3G50800	0.23	1	0.58	0.795374502	1.76	8.65E-08
AT5G38020	0.19	1	-0.70	0.663207583	1.76	2.03E-07
AT5G05490	-0.38	1	0.25	1	1.76	0.011729369
AT1G52270	-0.66	1	0.54	0.970664812	1.76	0.000227865
AT1G68920	1.69	2.34E-42	1.67	8.08E-41	1.76	1.58E-47
AT5G56550	0.50	1	0.89	0.028907472	1.76	2.27E-13
AT3G06160	1.24	0.992820763	0.97	0.899633545	1.75	0.012960976
AT5G27420	0.60	1	-0.01	1	1.75	0.000682198
AT4G25470	-0.12	1	0.56	1	1.73	0.003495331
AT1G72920	0.52	1	0.12	1	1.73	1.16E-07
AT3G18773	0.46	1	1.29	0.01158977	1.73	2.87E-07
AT1G19670	0.50	1	-0.89	0.160053618	1.73	7.87E-08
AT4G18170	0.93	1	0.59	1	1.72	0.000170993
AT1G68360	0.07	1	0.84	0.929310122	1.71	0.003797295
AT1G53163	1.26	1	0.83	1	1.71	0.015633814
AT5G56544	0.07	1	0.43	1	1.70	0.006786239
AT1G23730	-0.24	1	-1.19	0.135156959	1.70	6.95E-05
AT1G56650	-0.03	1	-1.09	0.44593646	1.70	0.000586816
AT1G25400	0.33	1	0.27	1	1.70	4.83E-09
AT1G66760	0.19	1	-0.10	1	1.70	4.39E-07
AT1G20310	0.44	1	-0.83	1	1.69	0.035828805
AT2G46400	0.85	0.647307586	-0.47	0.949943143	1.67	9.67E-07
AT2G29460	0.44	1	-1.37	0.394320424	1.67	0.009192389
AT2G43570	0.34	1	-0.51	0.975096268	1.67	0.00038323
AT4G27657	-0.05	1	0.82	0.550749516	1.67	8.63E-06
AT3G18610	0.32	1	1.49	0.051312798	1.67	0.000612062
AT1G49920	-0.41	1	1.60	0.031247052	1.67	0.00090431
AT3G22740	0.77	1	-0.63	0.866556072	1.66	3.83E-05
AT1G61415	0.84	1	0.65	0.953902203	1.66	0.000507576
AT4G16260	0.60	0.90392689	-0.34	0.969167547	1.66	1.21E-08
AT3G29000	0.99	1	-0.90	0.931411753	1.66	0.012581927
AT4G21640	0.41	1	0.52	0.953902203	1.65	2.46E-06
AT1G05575	0.61	1	0.09	1	1.65	0.001795734
AT2G39240	0.90	1	1.34	0.670635955	1.65	0.030739383
AT1G18870	-0.01	1	-0.16	1	1.64	1.44E-06
AT4G21830	1.13	0.774531886	-0.03	1	1.64	0.00272126
AT1G55020	0.10	1	-0.13	1	1.64	1.12E-08
AT4G03130	1.33	0.224520278	1.23	0.22958635	1.63	0.000468366
AT1G58270	0.21	1	-0.15	1	1.63	2.17E-08
AT3G44770	0.44	1	1.52	0.03607896	1.62	0.000402247
AT2G27830	0.23	1	0.67	0.053592171	1.62	2.11E-17
AT5G57560	0.32	1	0.31	1	1.62	4.78E-07
AT1G66700	-0.01	1	-0.53	1	1.61	0.024822814
AT2G33380	0.07	1	-0.67	0.785986284	1.61	7.12E-05
AT1G07430	-0.42	1	0.59	1	1.61	0.025070215
AT1G80440	0.09	1	0.76	0.036402705	1.61	5.75E-14
AT1G57990	0.08	1	0.33	1	1.61	5.72E-05
AT5G40800	0.42	1	-0.10	1	1.61	0.012973349
AT5G22555	0.60	1	0.47	1	1.60	0.004229439
AT3G15450	0.19	1	1.08	0.000117469	1.60	1.54E-12

AT3G01960	0.85	1	1.37	0.470955515	1.60	0.023308425
AT3G45140	0.16	1	-0.76	0.084435487	1.59	1.43E-10
AT3G46090	0.16	1	0.34	1	1.58	0.01489666
AT2G37900	-0.60	1	-0.62	1	1.57	0.000613323
AT5G06870	0.34	1	-0.43	0.945235781	1.56	4.39E-06
AT1G71380	0.64	1	0.12	1	1.56	0.028816661
AT1G32928	0.57	1	1.19	0.050146586	1.56	2.57E-05
AT1G66460	0.33	1	0.06	1	1.56	0.006245703
AT1G66380	-0.56	1	-2.15	0.624397976	1.56	0.036441459
AT4G13395	-0.16	1	0.06	1	1.56	1.91E-05
AT3G10320	0.26	1	0.12	1	1.54	0.009448858
AT1G52342	0.44	1	0.35	1	1.53	0.001518342
AT5G46830	0.07	1	0.44	1	1.53	0.011993065
AT2G36780	0.60	1	0.13	1	1.53	0.007591149
AT2G23010	0.62	1	-0.58	0.768640778	1.52	7.26E-06
AT1G52100	-0.06	1	-0.01	1	1.52	1.48E-05
AT5G12340	0.22	1	-0.45	1	1.52	0.010600064
AT1G58420	0.23	1	0.22	1	1.52	3.11E-05
AT1G60260	0.02	1	0.22	1	1.52	5.52E-12
AT1G67970	0.23	1	0.05	1	1.52	3.73E-06
AT1G66280	0.83	0.616289086	0.24	1	1.51	1.59E-05
AT5G27060	1.10	0.552990946	-0.53	0.998066744	1.51	0.000619638
AT1G63720	0.39	1	-0.09	1	1.51	0.000494752
AT1G32640	0.27	1	-0.43	0.389504003	1.51	4.31E-19
AT1G76590	0.10	1	-0.33	1	1.51	1.18E-06
AT5G48000	0.77	0.932146044	-0.16	1	1.51	0.000150645
AT4G29700	0.09	1	-0.46	0.684497784	1.50	6.40E-10
AT5G47230	0.34	1	0.38	0.931241992	1.50	4.61E-08
AT2G32660	0.98	1	0.37	1	1.50	0.004988234
AT1G62420	-0.74	1	-0.44	1	1.50	0.036318237
AT1G23710	0.27	1	0.36	0.762745759	1.49	8.94E-16
AT1G73500	0.38	1	0.29	0.901193572	1.48	2.22E-15
AT1G61340	0.39	1	0.36	1	1.48	2.02E-06
AT1G54040	0.06	1	-0.15	1	1.48	1.39E-07
AT1G23390	-0.14	1	0.83	0.08898053	1.48	8.65E-08
AT4G24340	0.60	1	-0.08	1	1.47	0.006017367
AT1G71280	0.37	1	0.71	0.989603012	1.46	0.032089276
AT5G61070	-0.23	1	2.17	1.13E-07	1.45	0.000631404
AT1G62660	0.39	1	0.17	1	1.44	1.60E-11
AT1G32920	0.28	1	0.57	0.199936454	1.44	3.34E-13
AT3G51450	0.39	1	-0.61	0.81534682	1.44	0.000203882
AT1G76600	0.25	1	-0.03	1	1.43	2.99E-10
AT5G66650	0.40	1	0.50	0.686795277	1.43	3.39E-08
AT2G25735	0.41	1	0.63	0.908980303	1.43	0.002981135
AT1G61440	0.26	1	0.31	1	1.42	0.026451422
AT1G04330	0.09	1	0.26	1	1.41	0.042482075
AT5G02780	0.22	1	-0.45	1	1.41	0.019813837
AT1G18300	0.30	1	0.53	0.760849959	1.40	5.45E-06
AT4G22960	0.96	1	1.53	0.08898053	1.40	0.020391529
AT5G47220	0.20	1	-0.67	0.526724234	1.39	2.02E-05
AT5G62020	0.29	1	0.41	0.639245346	1.39	4.26E-15
AT1G73260	0.22	1	-0.28	1	1.39	0.003011618
AT1G64065	-0.18	1	0.03	1	1.38	0.004962609
AT1G64200	0.02	1	-0.13	1	1.38	6.98E-11
AT3G04640	0.22	1	-0.13	1	1.38	0.000631853
AT4G11280	0.49	1	0.21	1	1.38	9.05E-07
AT3G55980	0.40	1	0.24	1	1.38	3.99E-06
AT4G28085	0.34	1	0.33	1	1.37	0.027770472
AT3G48520	0.68	1	0.96	0.686795277	1.37	0.018033432
AT1G61560	0.38	1	0.16	1	1.37	1.06E-05
AT1G65690	0.03	1	-0.08	1	1.36	0.000115361

AT1G72940	0.24	1	-0.02	1	1.36	7.85E-09
AT2G32030	0.16	1	-0.52	1	1.35	0.000293956
AT5G37990	0.11	1	-0.53	0.9316272	1.35	0.001483768
AT1G26290	1.01	0.828258936	0.90	0.596517272	1.35	0.004566066
AT3G25770	0.09	1	-1.04	0.039758137	1.34	3.74E-05
AT2G28420	0.07	1	0.21	1	1.34	0.048203251
AT1G05490	0.25	1	1.35	0.077815842	1.34	0.007045054
AT1G33030	-0.11	1	-1.52	0.362923819	1.34	0.048121403
AT1G70700	0.51	1	-0.53	0.593891746	1.33	1.16E-06
AT1G66270	0.71	0.165216428	0.36	0.815882644	1.33	2.67E-09
AT1G54890	1.00	0.020360851	0.86	0.047427274	1.33	1.96E-07
AT1G28190	0.23	1	-0.05	1	1.32	0.001423027
AT4G21650	0.20	1	0.35	0.793590232	1.32	9.31E-11
AT3G14440	0.44	1	-0.20	1	1.32	0.00332967
AT1G66500	0.46	1	0.37	0.941750686	1.32	6.81E-07
AT1G68290	0.33	1	-0.57	1	1.32	0.001815312
AT1G65370	0.07	1	0.33	0.981753649	1.32	1.57E-05
AT5G41315	1.02	0.454045982	0.99	0.217247121	1.31	0.000619334
AT1G65860	0.35	1	-0.17	1	1.31	3.87E-12
AT5G38710	0.17	1	-0.16	1	1.31	0.014035717
AT5G53450	-0.15	1	-0.09	1	1.31	1.27E-05
AT3G50930	0.72	0.867921938	-0.12	1	1.30	0.000264962
AT5G23840	1.26	0.723159154	0.26	1	1.30	0.049074194
AT1G56550	0.59	1	0.17	1	1.30	1.98E-05
AT3G26125	1.05	0.841843293	1.20	0.324225065	1.30	0.018579326
AT1G56170	0.04	1	0.03	1	1.30	1.19E-07
AT1G22275	0.65	1	0.61	0.934218573	1.30	0.001236481
AT1G64625	0.40	1	0.12	1	1.29	1.59E-05
AT3G48360	0.19	1	0.74	0.343238529	1.29	7.29E-05
AT1G60270	0.22	1	-0.01	1	1.29	5.25E-07
AT1G66400	0.31	1	0.46	0.725774443	1.29	1.97E-08
AT1G64260	0.09	1	0.42	1	1.29	0.011906562
AT1G69890	0.36	1	0.04	1	1.29	0.0001198
AT1G56250	0.84	1	-0.19	1	1.29	0.037238663
AT3G56360	-0.30	1	-0.33	0.924234656	1.29	1.71E-07
AT2G42540	-0.02	1	-0.22	1	1.28	1.12E-06
AT1G61470	0.45	1	0.35	1	1.28	0.009480467
AT1G19180	0.27	1	-0.93	0.079929519	1.28	1.92E-05
AT1G63295	0.39	1	0.24	1	1.27	0.000115184
AT5G42900	-0.15	1	0.41	0.94757449	1.26	0.000140631
AT1G66810	0.69	1	0.36	1	1.26	0.007336734
AT1G57560	0.74	0.998677096	0.20	1	1.25	0.000886686
AT1G62990	0.29	1	0.11	1	1.25	3.82E-07
AT1G10560	0.75	1	0.89	0.731608073	1.25	0.034270939
AT5G22570	0.64	1	-0.42	1	1.25	0.01651859
AT1G52640	0.51	1	0.38	1	1.24	0.008704347
AT1G56430	-0.08	1	0.15	1	1.24	0.004215708
AT5G22250	0.54	1	0.01	1	1.24	2.30E-05
AT5G17350	-0.03	1	0.29	1	1.24	0.003797199
AT4G33550	-0.09	1	-0.24	1	1.23	0.011590584
AT5G48010	1.00	0.106026466	-0.01	1	1.23	0.000103325
AT3G11000	0.57	1	0.88	0.598272118	1.23	0.016413307
AT1G23560	0.78	1	1.25	0.228606202	1.23	0.034520622
AT5G47240	-0.23	1	-0.49	0.747649273	1.23	6.19E-06
AT3G24982	0.73	0.106026466	0.10	1	1.22	1.10E-08
AT5G47990	0.63	1	-0.27	1	1.22	0.016476353
AT1G02670	0.11	1	0.69	0.864031911	1.22	0.019343293
AT2G38470	0.36	1	0.04	1	1.22	0.000367211
AT2G43510	-0.05	1	-0.48	0.905366221	1.22	0.000846758
AT3G53980	-0.08	1	-0.05	1	1.22	0.000198109
AT5G41750	0.88	1	-0.07	1	1.22	0.045262623

AT1G11080	0.04	1	0.88	0.263769943	1.22	0.000671863
AT1G61065	0.10	1	-0.01	1	1.22	0.000323722
AT4G17380	0.56	1	0.80	0.709226663	1.22	0.013005976
AT2G32140	0.23	1	-0.95	0.830640985	1.21	0.019625003
AT1G60030	0.60	1	0.73	0.732144029	1.20	0.009613354
AT1G67650	0.18	1	0.34	0.957531745	1.20	1.49E-05
AT5G07660	0.21	1	0.95	0.12613245	1.20	0.000402952
AT3G56710	0.46	1	-0.29	1	1.20	0.01339735
AT3G28340	0.45	1	0.51	0.930751253	1.20	0.002882177
AT3G04720	0.18	1	-0.71	0.388597887	1.19	0.000293508
AT1G18810	0.32	1	0.20	1	1.19	2.81E-05
AT1G56240	-0.26	1	-0.12	1	1.19	0.035984989
AT2G28400	0.14	1	-0.13	1	1.18	0.01489051
AT3G46600	0.30	0.896625621	0.35	0.314648285	1.18	6.61E-20
AT1G61840	0.10	1	0.04	1	1.18	0.02989179
AT1G07050	0.06	1	0.50	0.993682216	1.18	0.031994226
AT5G45850	0.58	1	0.59	0.910580407	1.17	0.008331599
AT5G46350	0.01	1	-1.00	0.705945113	1.17	0.013247823
AT2G40140	0.34	1	0.14	1	1.17	7.19E-09
AT1G64710	0.00	1	-0.18	1	1.17	1.60E-06
AT4G38780	0.05	1	0.72	0.476831709	1.17	0.001223817
AT1G34180	0.29	1	-0.17	1	1.16	0.0008966
AT4G15320	0.45	1	0.66	0.892827511	1.16	0.019832956
AT1G54010	0.22	1	-0.19	1	1.16	2.67E-09
AT3G16690	0.07	1	-0.31	1	1.16	0.003812321
AT1G60730	0.02	1	-0.04	1	1.16	1.72E-06
AT4G24350	0.45	1	-0.52	0.712335703	1.16	0.000213391
AT1G17020	-0.25	1	-0.60	0.889861493	1.16	0.015018066
AT1G06620	0.38	1	-0.34	0.921759992	1.16	3.33E-06
AT1G54050	0.04	1	-0.07	1	1.15	5.36E-06
AT3G23550	0.16	1	-0.65	0.643069831	1.15	0.002273121
AT1G61480	0.41	1	-0.40	1	1.15	0.014035717
AT2G14247	-0.04	1	-0.18	1	1.15	0.0113339
AT5G07380	1.33	0.215724802	0.90	0.699823932	1.14	0.030759036
AT5G56490	0.46	1	-0.27	1	1.13	0.048602628
AT1G52450	0.01	1	0.05	1	1.13	0.000102356
AT5G24200	0.51	1	-0.12	1	1.13	0.041462049
AT1G17744	0.17	1	-0.39	0.894801071	1.12	6.70E-05
AT1G61590	0.24	1	0.25	1	1.12	0.000114546
AT1G56690	0.56	0.833207765	0.51	0.60316752	1.12	6.60E-06
AT3G46620	0.38	1	0.47	0.327501232	1.12	2.49E-09
AT3G16650	0.04	1	1.46	2.64E-06	1.11	0.000190102
AT5G26920	0.37	1	-0.36	1	1.11	0.047322842
AT3G19580	0.43	1	0.08	1	1.11	0.005318084
AT1G64970	0.23	1	0.06	1	1.11	7.98E-10
AT1G76790	0.29	1	-0.26	1	1.11	9.11E-05
AT1G67860	-0.32	1	-0.23	1	1.11	0.000167561
AT1G71030	-0.20	1	0.47	0.91138183	1.10	0.003363151
AT2G44130	0.13	1	0.57	0.252770871	1.10	3.13E-07
AT2G20670	0.20	1	0.87	0.04316275	1.10	5.42E-05
AT5G33370	0.43	1	0.22	1	1.10	4.48E-05
AT5G59550	0.24	1	0.10	1	1.10	3.90E-10
AT4G32480	0.04	1	0.18	1	1.10	7.37E-08
AT3G07350	0.14	1	0.06	1	1.10	5.65E-06
AT2G36770	0.39	1	-0.25	1	1.10	0.048204453
AT5G08240	0.47	1	-0.01	1	1.10	0.000500224
AT3G19030	0.32	1	0.51	0.270671385	1.10	4.27E-08
AT1G23850	0.32	1	-0.46	0.884668901	1.09	6.24E-05
AT5G64870	0.60	1	0.29	1	1.09	0.005261616
AT5G37940	0.00	1	-0.56	0.959053559	1.09	0.007949787
AT1G56300	-0.32	1	0.06	1	1.09	1.68E-06

AT1G68050	-0.30	1	-0.11	1	1.09	0.000564469
AT3G09405	0.23	1	0.20	1	1.09	0.018420852
AT5G23830	0.72	0.479193814	-0.05	1	1.08	0.000107912
AT2G18210	0.66	1	0.07	1	1.08	0.012568938
AT1G62975	0.32	1	0.01	1	1.08	6.97E-05
AT1G55920	0.05	1	-0.03	1	1.08	1.77E-06
AT1G47655	0.24	1	0.87	0.531407133	1.08	0.01754516
AT1G67050	-0.15	1	0.05	1	1.08	0.000105078
AT4G37410	0.41	1	-0.09	1	1.08	5.88E-06
AT1G24145	0.38	1	-0.77	0.778758063	1.08	0.039834124
AT4G29030	0.67	0.787215437	0.96	0.048961337	1.08	0.000666571
AT4G37409	0.43	1	-0.08	1	1.08	1.06E-05
AT1G67520	0.08	1	-0.37	1	1.07	0.025394231
AT3G18290	-0.09	1	0.05	1	1.07	2.52E-05
AT1G65180	0.42	1	0.06	1	1.07	0.002624867
AT1G52565	0.28	1	0.40	1	1.07	0.029078796
AT5G61440	0.36	0.885103286	0.71	0.000673339	1.07	8.86E-12
AT1G26800	-0.21	1	0.12	1	1.06	3.00E-05
AT1G17745	0.19	1	-0.43	0.717893798	1.06	3.27E-05
AT1G55110	0.14	1	-0.05	1	1.06	2.18E-05
AT5G66080	-0.06	1	0.66	0.686795277	1.06	0.003456697
AT2G33830	-0.45	1	-0.26	1	1.06	0.000212414
AT1G64405	0.27	1	0.00	1	1.05	0.001254241
AT1G62560	0.11	1	-0.08	1	1.05	5.36E-11
AT1G63440	0.14	1	0.24	1	1.05	6.56E-06
AT1G67850	0.16	1	0.02	1	1.05	4.09E-05
AT1G60360	0.55	1	0.65	0.855186193	1.05	0.02147833
AT1G54540	0.42	1	0.58	0.81534682	1.05	0.005922823
AT2G17040	0.36	1	-0.26	1	1.05	0.016329505
AT1G63390	-0.06	1	0.32	1	1.05	0.038292272
AT5G45340	0.28	1	0.20	1	1.05	3.45E-05
AT2G24550	0.17	1	0.24	0.940109064	1.04	2.39E-09
AT1G64610	0.14	1	-0.09	1	1.04	0.001330269
AT5G58610	0.71	1	0.91	0.393549619	1.04	0.019719627
AT1G74590	0.02	1	-0.36	1	1.04	0.017563759
AT1G72120	-0.01	1	-0.47	0.971589332	1.04	0.009910205
AT1G64300	0.14	1	0.32	1	1.04	0.005826888
AT5G25450	0.13	1	0.48	0.939828525	1.03	0.002832161
AT1G54030	0.13	1	-0.21	1	1.03	3.45E-07
AT1G59640	0.06	1	-0.01	1	1.03	0.009865257
AT2G30360	0.22	1	0.31	0.99940659	1.03	0.000256485
AT1G64060	0.21	1	0.18	1	1.03	1.07E-06
AT1G51840	0.44	1	0.36	0.983380541	1.03	0.00098666
AT5G13220	0.21	1	-0.10	1	1.03	0.018579326
AT1G54570	0.10	1	0.08	1	1.03	0.000416725
AT1G63350	-0.08	1	-0.62	0.764600188	1.02	0.008940076
AT1G77520	0.23	1	0.10	1	1.02	0.00967024
AT3G27200	0.69	0.106026466	0.44	0.560230663	1.02	3.24E-07
AT4G01390	0.07	1	0.21	1	1.02	4.38E-05
AT1G53830	0.74	0.812941514	0.44	0.944218942	1.01	0.006786239
AT2G39420	0.36	1	-0.08	1	1.01	6.64E-06
AT5G38000	0.18	1	-0.37	0.994559775	1.01	0.003466938
AT2G38790	-0.20	1	-0.47	0.924549626	1.01	0.002396463
AT1G66990	-0.22	1	0.12	1	1.01	0.003718341
AT1G67300	0.11	1	-0.01	1	1.01	4.30E-09
AT3G48390	0.00	1	0.59	0.829508139	1.01	0.01017157
AT1G61820	0.05	1	-0.06	1	1.01	0.000241774
AT1G55850	0.00	1	-0.17	1	1.00	7.58E-10
AT1G67880	0.06	1	0.16	1	1.00	3.79E-07
AT2G38995	0.32	1	0.35	0.957999922	1.00	0.000527153
AT4G22753	0.20	1	-0.17	1	1.00	8.18E-06

AT1G62440	0.47	1	0.02	1	1.00	0.012749217
AT5G42650	0.07	1	-0.73	0.126638969	0.99	0.000192078
AT3G09940	0.74	0.589055797	0.07	1	0.99	0.001920125
AT2G23620	0.79	0.552990946	0.36	1	0.99	0.002716629
AT1G64583	0.33	1	-0.13	1	0.98	0.012908094
AT1G60740	0.19	1	-0.02	1	0.98	0.002851251
AT1G67810	-0.20	1	-0.64	0.527200573	0.98	0.001934329
AT3G28270	0.57	1	0.77	0.606123778	0.98	0.043060023
AT3G09520	0.36	1	0.23	1	0.98	0.002212227
AT1G02205	0.23	1	0.38	0.731879306	0.98	1.17E-05
AT1G10070	-0.16	1	-1.04	0.274840655	0.98	0.036441459
AT1G02940	0.67	0.834319663	-0.85	0.416123601	0.98	0.003078035
AT1G56423	0.13	1	0.12	1	0.98	1.50E-05
AT1G61400	0.22	1	0.27	1	0.98	0.000278454
AT3G09020	0.00	1	-0.11	1	0.98	0.010699736
AT1G65610	0.49	1	0.15	1	0.98	0.013058534
AT1G57820	0.46	0.650792567	0.52	0.196140745	0.98	2.87E-07
AT1G30260	0.04	1	0.30	1	0.98	0.00186906
AT1G56710	0.07	1	-0.11	1	0.98	0.042348837
AT1G62310	0.10	1	0.04	1	0.98	6.10E-05
AT1G55915	0.43	1	0.01	1	0.97	0.000588745
AT1G51860	0.30	1	0.18	1	0.97	0.00055355
AT4G13572	0.47	1	0.09	1	0.97	0.034708846
AT2G44230	0.13	1	0.28	0.953902203	0.97	9.02E-06
AT1G54000	0.63	0.075252855	0.29	0.787165854	0.97	8.23E-08
AT1G53840	0.07	1	0.05	1	0.96	7.15E-08
AT1G68020	0.05	1	0.00	1	0.96	2.99E-06
AT5G06320	0.14	1	0.03	1	0.96	1.30E-05
AT1G54740	0.02	1	-0.02	1	0.96	4.29E-06
AT1G14640	0.30	1	0.57	0.693610145	0.96	0.005015662
AT1G53110	0.13	1	-0.04	1	0.95	7.06E-05
AT3G48350	0.02	1	-0.16	1	0.95	1.12E-05
AT1G61420	0.36	1	-0.02	1	0.95	0.004488402
AT2G35930	0.33	1	0.12	1	0.95	0.000168732
AT1G66880	0.30	1	-0.12	1	0.95	0.000191209
AT1G64980	-0.03	1	-0.04	1	0.95	5.36E-05
AT1G55205	0.55	1	0.31	1	0.95	0.001096839
AT2G27310	0.20	1	-0.24	1	0.94	9.70E-05
AT1G70420	0.17	1	0.36	0.949548835	0.94	0.001352173
AT1G55820	0.37	1	0.44	0.564034478	0.94	1.77E-05
AT1G67900	-0.17	1	-0.09	1	0.94	9.07E-05
AT2G41640	0.45	1	0.14	1	0.94	0.02004796
AT2G45660	-0.29	1	-0.16	1	0.94	0.000224673
AT5G19120	0.12	1	0.45	0.38751365	0.94	1.93E-06
AT1G66350	-0.17	1	-0.37	0.911019157	0.94	0.000758901
AT2G36650	0.78	0.884213831	0.23	1	0.94	0.02591395
AT1G63830	0.05	1	-0.04	1	0.94	3.07E-09
AT1G66140	-0.05	1	0.17	1	0.93	4.66E-06
AT1G66480	0.16	1	-0.01	1	0.93	0.002021234
AT1G55510	0.08	1	0.26	0.969167547	0.93	2.10E-05
AT4G34710	0.17	1	-0.16	1	0.93	1.10E-05
AT1G67510	0.05	1	0.09	1	0.93	1.74E-05
AT4G11360	0.16	1	0.23	0.907855232	0.93	4.11E-10
AT1G65820	-0.02	1	-0.19	1	0.93	1.16E-06
AT1G58200	-0.14	1	-0.14	1	0.93	9.38E-09
AT1G53320	-0.08	1	-0.05	1	0.92	2.65E-09
AT1G67530	0.15	1	0.14	1	0.92	2.04E-05
AT1G28330	-0.33	1	0.04	1	0.92	1.49E-05
AT1G24320	0.15	1	0.01	1	0.92	0.00295233
AT1G60620	0.23	1	0.10	1	0.92	5.70E-06
AT2G15080	0.02	1	-0.24	1	0.92	0.005939043

AT1G63650	0.29	1	0.38	0.9316272	0.92	0.002746534
AT5G65690	0.89	0.148969621	0.48	0.846130715	0.91	0.002353439
AT5G41120	0.03	1	0.12	1	0.91	2.03E-07
AT5G02940	0.13	1	-0.27	0.830640985	0.91	7.67E-08
AT1G54660	-0.04	1	-0.18	1	0.91	0.00018286
AT5G59530	0.24	1	0.19	1	0.91	0.006505135
AT2G30550	-0.05	1	0.02	1	0.91	0.000500224
AT1G67400	-0.24	1	0.13	1	0.91	0.000180703
AT1G67340	0.04	1	0.20	0.953902203	0.91	9.66E-10
AT3G03190	0.37	1	0.02	1	0.91	0.000960053
AT1G65580	0.04	1	0.07	1	0.91	1.46E-08
AT5G61290	-0.04	1	-0.06	1	0.91	0.012960976
AT4G11211	-0.06	1	0.09	1	0.90	0.000671863
AT4G23600	0.05	1	-0.88	0.236422531	0.90	0.022632867
AT1G62260	0.26	1	0.26	1	0.90	0.002735647
AT1G67820	0.24	1	0.11	1	0.90	0.002739986
AT4G17480	-0.02	1	-0.25	1	0.90	0.006063492
AT4G36040	-0.13	1	0.29	0.91138183	0.90	3.00E-05
AT3G16720	0.04	1	0.18	1	0.90	8.65E-08
AT4G18470	0.49	1	0.66	0.394320424	0.90	0.003020446
AT2G27740	0.61	1	0.79	0.497804799	0.90	0.042408176
AT3G54990	0.50	1	0.51	0.576960509	0.90	0.000497433
AT1G59860	-0.38	1	0.44	0.979394862	0.90	0.044345117
AT1G64890	0.03	1	-0.07	1	0.89	0.001363327
AT1G67470	-0.17	1	-0.31	0.908980303	0.89	2.16E-05
AT1G53345	0.36	1	0.30	1	0.89	0.009830165
AT1G61660	0.26	1	0.18	1	0.89	1.87E-06
AT1G67630	0.36	1	0.27	1	0.89	0.00098418
AT1G64470	0.20	1	0.08	1	0.89	0.00015593
AT1G64105	0.04	1	0.12	1	0.89	0.00091716
AT1G66920	0.09	1	-0.16	1	0.89	0.001330269
AT4G29930	0.39	1	0.00	1	0.89	0.004436777
AT1G45145	0.13	1	-0.16	1	0.89	0.00050157
AT1G64690	-0.19	1	0.00	1	0.89	0.008983066
AT5G13740	0.10	1	0.08	1	0.89	0.00023858
AT1G58470	0.30	1	0.53	0.734534133	0.89	0.01035194
AT1G63840	0.19	1	0.07	1	0.89	2.81E-05
AT1G02660	0.08	1	0.12	1	0.88	0.016800971
AT1G67310	0.03	1	0.06	1	0.88	1.10E-07
AT1G59620	-0.09	1	-0.11	1	0.88	0.000901792
AT5G19890	0.41	1	-0.34	0.988171686	0.88	0.006122737
AT1G62300	0.17	1	0.13	1	0.88	0.001489159
AT5G60680	0.09	1	0.66	0.001223883	0.88	1.73E-08
AT1G55730	0.19	1	0.15	1	0.88	2.45E-06
AT5G50950	0.29	1	-0.13	1	0.88	0.000195756
AT1G62430	0.01	1	0.08	1	0.88	1.77E-05
AT1G61600	0.05	1	-0.08	1	0.88	0.000818009
AT1G59870	-0.02	1	-0.26	1	0.88	0.001736545
AT1G65032	0.25	1	-0.04	1	0.88	0.00050157
AT2G40435	-0.14	1	-0.57	0.625023037	0.88	0.005336629
AT1G53430	-0.08	1	-0.04	1	0.88	1.74E-05
AT1G67560	-0.02	1	-0.06	1	0.88	3.20E-05
AT1G67780	0.43	1	0.38	1	0.88	0.047026909
AT1G03940	0.57	1	0.05	1	0.88	0.015411887
AT5G24160	0.02	1	-0.38	0.701782357	0.87	7.44E-05
AT4G08870	-0.01	1	-0.82	0.063733144	0.87	0.002048565
AT1G68330	-0.02	1	-0.01	1	0.87	0.001083303
AT2G20340	0.13	1	0.40	0.854577482	0.87	0.002244845
AT1G68150	0.43	1	0.04	1	0.87	0.009060485
AT2G32100	0.22	1	0.39	0.98828024	0.87	0.030041424
AT1G67410	0.02	1	-0.06	1	0.87	0.000165893

AT4G36500	0.25	1	0.01	1	0.87	0.030000311
AT1G65790	0.19	1	-0.37	0.945235781	0.87	0.007494655
AT3G10190	0.28	1	0.31	0.8667198	0.87	1.68E-05
AT4G16370	-0.14	1	-0.09	1	0.87	3.89E-05
AT1G68440	0.09	1	0.12	1	0.87	8.94E-08
AT1G56130	0.36	1	0.14	1	0.87	0.004613014
AT1G65800	-0.03	1	-0.26	0.945235781	0.87	6.37E-05
AT1G55750	0.13	1	0.26	0.830640985	0.86	5.28E-08
AT1G53025	0.21	1	0.16	1	0.86	0.000178176
AT1G67920	-0.40	1	-0.83	0.551522511	0.86	0.040611276
AT1G64370	-0.07	1	-0.11	1	0.86	1.92E-05
AT4G37260	0.26	1	0.38	0.217247121	0.86	2.20E-10
AT1G64080	-0.11	1	-0.04	1	0.86	0.001638052
AT1G54100	-0.07	1	-0.31	0.928536367	0.86	0.000512867
AT1G25560	0.18	1	0.48	0.214338912	0.86	2.91E-06
AT1G56460	0.03	1	-0.09	1	0.86	3.12E-07
AT1G52880	-0.19	1	-0.20	1	0.86	0.000920607
AT1G79890	0.74	0.706111499	0.53	0.76894186	0.86	0.014710431
AT1G22190	0.27	1	0.44	0.051312798	0.86	7.38E-12
AT1G14190	0.23	1	0.53	0.686795277	0.86	0.005838894
AT1G19020	0.16	1	-0.35	1	0.86	0.017891775
AT1G17750	0.62	0.971479608	-0.04	1	0.86	0.013577319
AT3G16490	0.67	0.996909825	1.05	0.04398734	0.85	0.023796231
AT3G02020	0.28	1	-0.23	0.884668901	0.85	8.24E-08
AT3G49570	-0.10	1	-0.33	1	0.85	0.047579514
AT1G62045	0.23	1	0.41	0.980905969	0.85	0.037856217
AT1G63740	0.19	1	0.01	1	0.85	2.48E-05
AT1G73330	-0.21	1	-0.42	0.561085301	0.85	0.000114215
AT2G38390	0.16	1	-0.03	1	0.85	0.001026014
AT1G63300	0.40	1	0.26	0.947719054	0.85	9.47E-05
AT1G15310	0.34	1	0.44	0.744320241	0.85	0.002465718
AT3G16450	0.29	1	-0.20	1	0.85	1.38E-05
AT4G23880	0.10	1	0.11	1	0.85	0.005354021
AT1G68840	0.10	1	0.60	0.013003683	0.85	2.71E-07
AT1G72450	-0.06	1	-0.74	0.00104999	0.85	1.27E-06
AT1G61460	0.11	1	-0.04	1	0.85	0.012123833
AT1G53790	-0.36	1	-0.26	1	0.85	0.01009313
AT3G25600	0.09	1	0.29	0.864031911	0.85	5.79E-06
AT1G64940	0.15	1	0.20	1	0.85	0.00418407
AT1G60430	0.01	1	0.25	0.989603012	0.84	0.000187213
AT4G28500	0.33	1	0.60	0.745044134	0.84	0.027512044
AT1G62810	0.09	1	-0.17	1	0.84	4.65E-06
AT1G64570	0.11	1	0.18	1	0.84	0.00013374
AT1G61170	0.12	1	0.08	1	0.84	0.00686657
AT1G74430	0.06	1	-0.17	1	0.84	0.023629265
AT1G15125	-0.17	1	-0.55	0.649828124	0.84	0.01426435
AT3G15760	0.47	1	0.38	0.817099086	0.84	0.000428121
AT3G57520	0.35	1	0.27	0.998066744	0.84	0.002643505
AT2G32150	0.03	1	-0.02	1	0.84	0.001453765
AT1G53170	-0.27	1	-0.22	0.966966721	0.84	4.25E-06
AT1G62422	-0.14	1	-0.23	1	0.84	0.000682198
AT5G59130	0.12	1	0.32	0.862876031	0.84	5.09E-05
AT1G67940	-0.17	1	-0.11	1	0.83	9.23E-06
AT1G64620	-0.22	1	0.03	1	0.83	0.001509292
AT1G13260	0.01	1	0.40	0.236422531	0.83	2.33E-08
AT2G43550	0.19	1	-0.23	1	0.83	0.001474016
AT1G67320	0.28	1	0.16	1	0.83	0.005508788
AT5G37980	-0.02	1	-0.14	1	0.83	0.032625317
AT1G65120	0.39	1	0.02	1	0.83	0.015732254
AT1G60010	0.01	1	0.05	1	0.83	3.35E-07
AT1G54790	0.03	1	-0.18	1	0.83	0.016723689

AT4G05070	-0.01	1	0.34	0.478653345	0.83	9.65E-08
AT2G38750	0.02	1	-0.31	1	0.83	0.017246331
AT5G52320	0.26	1	-0.55	0.344267893	0.83	0.000475263
AT1G67120	0.22	1	0.25	1	0.83	0.003258735
AT1G53165	0.14	1	0.12	1	0.83	5.89E-07
AT1G58360	0.05	1	-0.05	1	0.83	4.56E-06
AT1G55530	0.08	1	-0.06	1	0.83	1.17E-05
AT1G55325	0.20	1	0.23	0.969167547	0.82	3.15E-05
AT1G68080	0.25	1	0.18	1	0.82	0.000735126
AT2G47180	0.10	1	0.15	1	0.82	7.61E-05
AT1G03820	0.32	1	0.05	1	0.82	0.000971932
AT1G71140	0.12	1	-0.06	1	0.82	0.044076828
AT3G49790	-0.03	1	0.14	1	0.82	0.000208989
AT5G06860	0.41	1	0.11	1	0.82	0.00046027
AT1G63310	0.36	1	0.34	0.911690613	0.82	0.001727866
AT1G18860	0.59	1	-0.10	1	0.82	0.049443688
AT1G54340	-0.04	1	-0.01	1	0.82	1.71E-07
AT5G26220	-0.37	1	-0.40	0.901193572	0.82	0.01087744
AT1G59780	0.67	0.717831097	0.18	1	0.82	0.009887282
AT1G62730	0.22	1	0.18	1	0.82	2.80E-05
AT1G19570	0.00	1	-0.50	0.188423414	0.82	1.93E-05
AT3G47640	0.11	1	-0.06	1	0.82	0.008404127
AT2G39050	0.12	1	-0.24	1	0.81	0.004856072
AT2G46750	0.38	1	0.07	1	0.81	0.00141899
AT1G56290	0.22	1	0.16	1	0.81	3.10E-05
AT1G24625	0.20	1	0.01	1	0.81	4.27E-07
AT1G66750	0.17	1	-0.01	1	0.81	1.74E-05
AT1G60590	-0.08	1	-0.09	1	0.81	0.003668809
AT1G66910	0.00	1	0.05	1	0.81	2.73E-06
AT4G20320	0.11	1	0.22	1	0.81	0.003312398
AT3G55710	-0.25	1	0.39	0.763146585	0.81	0.000974518
AT1G63160	0.40	1	0.45	0.560230663	0.81	0.000550192
AT2G33850	0.23	1	0.10	1	0.81	0.000120905
AT1G61000	0.22	1	0.31	0.899633545	0.81	0.000235935
AT1G65660	0.04	1	0.02	1	0.81	7.70E-06
AT1G19550	0.02	1	-0.52	0.225228542	0.81	5.44E-05
AT1G63430	0.07	1	0.08	1	0.81	5.25E-07
AT5G55970	-0.02	1	-0.08	1	0.81	0.005542551
AT3G58160	0.09	1	0.84	0.00766606	0.81	0.000858475
AT3G59940	-0.12	1	0.53	0.090010372	0.80	8.63E-06
AT1G53440	0.01	1	-0.04	1	0.80	1.36E-06
AT1G20510	0.19	1	-0.51	0.29841081	0.80	0.000188563
AT1G53900	0.07	1	0.18	1	0.80	1.42E-06
AT1G53880	0.07	1	0.18	1	0.80	1.42E-06
AT1G55880	0.05	1	0.04	1	0.80	1.12E-05
AT1G65190	0.04	1	-0.08	1	0.80	3.38E-06
AT3G26840	-0.18	1	-0.60	0.404801837	0.80	0.005359178
AT5G50090	0.55	1	0.58	0.61292428	0.80	0.018965131
AT1G65440	0.15	1	0.22	0.944218942	0.80	5.24E-06
AT3G25780	0.56	1	-0.12	1	0.79	0.0215723
AT2G23000	0.56	0.552990946	0.13	1	0.79	0.000584248
AT5G23820	0.19	1	-0.20	1	0.79	6.11E-05
AT1G65710	0.53	0.812941514	0.51	0.472310581	0.79	0.001796436
AT4G10390	0.39	1	0.21	1	0.79	0.000697961
AT1G56220	-0.30	0.828258936	-0.28	0.541749885	0.79	1.29E-09
AT1G61490	0.04	1	0.16	1	0.79	0.025791836
AT5G54690	0.20	1	0.26	1	0.79	0.006377148
AT4G24010	-0.11	1	0.12	1	0.79	0.039326038
AT1G63010	0.08	1	-0.16	1	0.79	7.95E-05
AT1G55590	0.11	1	0.11	1	0.79	7.13E-06
AT1G62970	0.23	1	0.15	1	0.79	6.93E-05

AT1G55265	-0.36	1	0.02	1	0.79	0.015809425
AT1G62120	0.19	1	0.21	1	0.79	0.000208465
AT1G51830	0.27	1	0.30	0.971074376	0.79	0.005245473
AT1G68600	-0.18	1	-0.16	1	0.79	0.007703457
AT1G65900	0.06	1	0.09	1	0.79	0.000534346
AT1G63480	0.18	1	0.29	0.880553137	0.78	7.95E-05
AT1G53590	0.01	1	0.08	1	0.78	2.33E-07
AT1G52080	0.01	1	0.01	1	0.78	0.001572359
AT3G26510	0.04	1	0.39	0.178955849	0.78	9.46E-09
AT5G59570	0.03	1	0.18	1	0.78	0.002103158
AT1G57870	-0.04	1	-0.01	1	0.78	1.23E-05
AT2G01610	-0.09	1	0.02	1	0.78	0.017071669
AT5G18130	-0.16	1	-0.34	0.878315967	0.78	0.001238364
AT3G44720	0.05	1	-0.15	1	0.78	0.000949189
AT1G53785	-0.07	1	0.15	1	0.78	0.000682198
AT3G43270	0.34	0.844934289	-0.05	1	0.78	5.18E-07
AT1G55610	0.05	1	0.15	1	0.78	1.19E-05
AT5G67190	0.04	1	0.32	0.990962542	0.78	0.009540543
AT1G64780	0.33	1	0.43	0.654892639	0.78	0.001796436
AT1G54160	-0.33	1	-0.30	1	0.78	0.01743922
AT1G67590	0.22	1	0.34	0.757210493	0.78	0.000214564
AT1G53035	-0.24	1	-0.21	1	0.78	0.000369859
AT1G65970	-0.11	1	0.00	1	0.78	0.006786239
AT5G23235	-0.53	0.986087473	-0.28	1	0.78	0.007420289
AT1G61240	-0.01	1	0.12	1	0.78	9.75E-05
AT5G17420	0.33	0.90392689	0.41	0.245879736	0.78	5.24E-07
AT1G55180	0.06	1	0.13	1	0.78	0.000637981
AT1G12570	0.13	1	0.21	1	0.78	0.010640852
AT1G66345	-0.04	1	-0.05	1	0.78	0.01524183
AT1G65985	0.21	1	0.24	1	0.77	0.004596552
AT1G03495	0.53	1	0.00	1	0.77	0.024376639
AT1G61180	0.13	1	0.06	1	0.77	9.36E-06
AT1G19770	0.02	1	0.25	0.518616363	0.77	7.38E-12
AT1G64280	0.02	1	0.02	1	0.77	3.08E-06
AT1G60490	0.01	1	-0.02	1	0.77	3.20E-06
AT1G63220	0.09	1	0.14	1	0.77	0.003421838
AT2G39650	0.36	1	-0.03	1	0.77	0.000701782
AT1G61250	0.14	1	-0.08	1	0.77	8.12E-07
AT1G59910	0.02	1	0.09	1	0.77	0.001144117
AT1G56090	-0.27	1	-0.21	1	0.77	0.000150697
AT1G08920	0.11	1	0.00	1	0.77	0.00101593
AT1G53070	0.07	1	-0.05	1	0.77	0.000505951
AT1G55152	-0.30	1	0.06	1	0.77	0.012648054
AT1G63120	0.18	1	0.13	1	0.77	0.000168192
AT1G56140	0.24	1	0.08	1	0.77	0.001013303
AT4G21910	0.23	1	-0.15	1	0.77	0.000234129
AT1G52260	0.10	1	-0.08	1	0.76	4.98E-05
AT1G57790	0.04	1	-0.42	0.915971788	0.76	0.021933756
AT1G23120	-0.16	1	0.11	1	0.76	0.015732254
AT1G53050	0.17	1	0.12	1	0.76	9.05E-06
AT1G66980	-0.05	1	0.00	1	0.76	4.11E-05
AT1G67580	0.06	1	0.12	1	0.76	9.49E-06
AT1G66890	0.00	1	-0.03	1	0.76	0.000503768
AT1G62880	-0.01	1	-0.01	1	0.76	0.00048291
AT3G13100	0.27	1	-0.03	1	0.76	0.030337552
AT3G12145	0.29	1	-0.14	1	0.76	8.18E-06
AT1G53710	0.08	1	0.03	1	0.76	3.89E-06
AT2G22330	0.44	0.812941514	-0.20	1	0.76	0.000254261
AT1G58030	-0.05	1	0.06	1	0.76	7.52E-06
AT2G36220	0.23	1	0.29	0.787897161	0.76	1.17E-05
AT1G63110	0.10	1	0.03	1	0.76	2.35E-08

AT1G01640	0.14	1	0.40	0.712335703	0.76	0.000671764
AT5G17700	0.09	1	-0.05	1	0.76	9.10E-05
AT1G61140	0.11	1	-0.03	1	0.76	6.99E-05
AT5G10520	0.42	0.946833287	0.23	1	0.75	0.000335879
AT5G18860	0.50	0.532805909	0.44	0.425061081	0.75	0.000181954
AT1G64385	0.06	1	-0.07	1	0.75	1.49E-05
AT1G52760	0.06	1	-0.05	1	0.75	7.90E-05
AT5G11920	0.09	1	-0.06	1	0.75	0.012915525
AT1G21100	0.07	1	-0.23	1	0.75	0.005543742
AT1G64170	-0.35	1	-0.24	1	0.75	0.003109522
AT1G63180	-0.27	1	0.34	0.921759992	0.75	0.005529752
AT1G64760	0.20	1	0.30	0.857665809	0.75	0.000209658
AT4G31020	0.65	0.503485459	0.65	0.229407054	0.75	0.004652808
AT1G56230	0.02	1	-0.01	1	0.75	8.19E-06
AT1G53200	0.00	1	-0.22	1	0.75	0.003068722
AT1G61620	-0.05	1	-0.08	1	0.75	5.68E-05
AT1G55550	0.04	1	-0.13	1	0.75	0.005558856
AT2G39310	0.16	1	-0.15	1	0.75	2.01E-05
AT1G52320	-0.06	1	-0.03	1	0.74	0.000105078
AT1G55260	-0.07	1	-0.05	1	0.74	1.74E-05
AT1G35260	0.08	1	-0.11	1	0.74	0.000533098
AT1G28230	-0.16	1	-0.66	0.344267893	0.74	0.010781157
AT1G80820	0.30	1	0.10	1	0.74	0.036283306
AT1G59820	0.06	1	0.05	1	0.74	0.00037587
AT1G60200	0.09	1	0.18	0.968761914	0.74	1.53E-06
AT1G61690	0.00	1	-0.01	1	0.74	4.83E-05
AT1G56580	-0.02	1	-0.04	1	0.74	0.001246243
AT1G67140	0.11	1	0.15	1	0.74	9.63E-05
AT1G60420	-0.10	1	-0.08	1	0.74	8.01E-05
AT5G23240	-0.61	0.867921938	-0.35	0.952075942	0.74	0.024164101
AT1G52150	0.13	1	0.17	1	0.74	3.67E-05
AT4G30180	0.46	1	0.23	1	0.74	0.015976163
AT1G55860	0.09	1	0.19	1	0.74	0.002685824
AT1G60995	0.00	1	-0.04	1	0.74	2.16E-05
AT1G59660	0.16	1	0.19	1	0.74	0.000494752
AT1G66730	-0.01	1	0.04	1	0.74	0.000174473
AT1G76780	0.14	1	0.76	0.10370414	0.74	0.012749217
AT1G54150	0.05	1	-0.18	1	0.74	0.000163825
AT3G16400	0.17	1	-0.13	1	0.74	1.04E-05
AT3G15210	0.05	1	-0.03	1	0.73	2.94E-06
AT1G67750	-0.04	1	0.03	1	0.73	0.000212414
AT4G34230	0.02	1	-0.19	1	0.73	0.023796231
AT4G11650	-0.03	1	-0.30	0.933716682	0.73	0.00470064
AT1G61010	0.07	1	0.07	1	0.73	3.25E-06
AT3G50060	-0.19	1	0.12	1	0.73	0.000153441
AT1G52720	0.01	1	0.03	1	0.73	2.53E-05
AT4G19460	0.13	1	0.47	0.717893798	0.73	0.009872717
AT1G68220	0.04	1	0.03	1	0.73	4.38E-05
AT1G54990	0.13	1	-0.12	1	0.73	1.48E-05
AT1G61310	0.11	1	0.12	1	0.73	6.24E-07
AT1G59610	0.05	1	0.09	1	0.73	2.53E-05
AT1G53650	0.17	1	0.07	1	0.73	0.000553538
AT1G67550	0.08	1	0.06	1	0.73	2.00E-06
AT1G63360	0.03	1	-0.01	1	0.73	1.95E-06
AT1G54730	-0.03	1	-0.13	1	0.73	0.003215821
AT1G66900	-0.02	1	-0.09	1	0.72	5.61E-07
AT5G58350	0.13	1	-0.08	1	0.72	0.000255337
AT3G15630	-0.07	1	0.39	0.632998514	0.72	0.000627426
AT1G66080	0.00	1	0.15	1	0.72	0.003754056
AT1G56420	-0.17	1	-0.41	0.86398275	0.72	0.003883904
AT1G67330	0.34	1	0.13	1	0.72	0.001518342

AT1G67060	0.11	1	0.15	1	0.72	0.001813091
AT1G55350	0.12	1	0.22	0.963604818	0.72	0.000240067
AT1G58100	0.17	1	0.15	1	0.72	3.48E-06
AT1G63770	0.07	1	0.12	1	0.72	2.58E-07
AT5G02490	0.29	1	0.26	1	0.72	0.018292121
AT1G03850	0.13	1	0.14	1	0.72	0.000681628
AT3G16410	0.19	1	-0.09	1	0.72	8.11E-06
AT5G44005	-0.13	1	-0.45	0.686795277	0.72	0.003384877
AT5G63970	0.17	1	0.06	1	0.72	0.020715641
AT3G54880	0.14	1	-0.07	1	0.71	1.36E-05
AT1G61040	0.03	1	0.11	1	0.71	3.27E-05
AT1G52430	-0.20	1	-0.33	1	0.71	0.049225041
AT1G77210	-0.30	1	0.20	1	0.71	0.000738903
AT1G63460	0.06	1	-0.15	1	0.71	1.92E-05
AT1G64400	0.05	1	-0.12	1	0.71	1.62E-05
AT1G70290	-0.08	1	-0.21	1	0.71	0.001144117
AT1G52910	0.08	1	0.14	1	0.71	0.008107763
AT1G62020	0.08	1	0.09	1	0.71	7.86E-05
AT2G46600	0.06	1	-0.05	1	0.71	2.08E-07
AT3G14050	0.12	1	-0.32	0.830640985	0.71	0.000831844
AT1G63470	0.15	1	0.18	1	0.71	0.000102285
AT4G12545	0.91	0.075252855	0.13	1	0.71	0.021408209
AT1G53580	-0.04	1	-0.25	0.882077235	0.71	5.85E-05
AT3G11840	0.42	1	-0.51	0.801234278	0.71	0.043692567
AT1G57765	0.08	1	0.06	1	0.71	0.000207104
AT1G53230	-0.02	1	0.01	1	0.71	0.000472015
AT3G56880	0.18	1	0.29	0.662366822	0.71	9.57E-06
AT5G08790	0.29	1	-0.19	1	0.71	0.000275078
AT5G57630	0.00	1	-0.10	1	0.71	6.93E-05
AT1G56440	0.07	1	0.04	1	0.71	0.000399527
AT1G55190	0.07	1	0.09	1	0.71	6.35E-05
AT1G11050	0.02	1	-0.20	1	0.70	0.000254875
AT1G55840	-0.05	1	-0.15	1	0.70	4.25E-06
AT1G55130	0.14	1	0.04	1	0.70	0.00017026
AT1G54090	0.03	1	0.02	1	0.70	0.000518659
AT1G22890	0.16	1	-0.16	1	0.70	0.047577737
AT1G54200	-0.05	1	0.03	1	0.70	0.011246348
AT1G62050	0.04	1	0.10	1	0.70	0.000434274
AT4G27860	0.23	1	-0.20	0.911933658	0.70	1.10E-06
AT1G61190	0.16	1	0.01	1	0.70	5.41E-08
AT4G18880	0.14	1	-0.38	0.632576579	0.70	0.000326147
AT1G67490	0.07	1	-0.02	1	0.70	0.000189267
AT1G58210	-0.08	1	-0.31	0.945235781	0.70	0.004673427
AT2G36690	-0.33	1	0.00	1	-0.70	0.008037881
AT3G10280	-0.16	1	0.00	1	-0.72	0.048058034
AT5G27890	0.07	1	0.19	1	-0.73	0.009818641
AT3G55250	-0.21	1	-0.18	1	-0.73	9.02E-05
AT4G29150	0.01	1	0.29	0.830640985	-0.73	0.001784643
AT3G49410	-0.07	1	-0.03	1	-0.73	0.022776005
AT4G30250	0.02	1	0.12	1	-0.73	0.000177907
AT3G55500	-0.28	1	-0.05	1	-0.74	0.017013765
AT1G73830	-0.16	1	-0.05	1	-0.74	0.014896644
AT1G21460	-0.05	1	-0.34	0.857665809	-0.74	0.003343162
AT2G40300	0.07	1	0.16	1	-0.74	7.61E-05
AT2G46720	-0.03	1	-0.01	1	-0.75	0.008240032
AT1G75750	-0.04	1	0.34	0.593288552	-0.76	2.81E-05
AT3G05660	-0.12	1	-0.49	0.807266003	-0.76	0.045446539
AT5G65390	-0.22	1	-0.18	1	-0.76	2.22E-05
AT1G80080	0.06	1	0.16	1	-0.76	0.016147254
AT2G34060	-0.31	1	-0.18	1	-0.77	0.001561293
AT3G16660	-0.21	1	-0.06	1	-0.77	0.0010654

AT1G11850	-0.15	1	-0.06	1	-0.77	0.005748224
AT5G01600	0.12	1	0.00	1	-0.77	0.001030723
AT5G20410	-0.13	1	-0.16	1	-0.77	0.034480041
AT5G08565	0.01	1	-0.08	1	-0.77	0.002983715
AT4G24670	0.11	1	0.20	1	-0.78	0.000691088
AT1G34245	0.05	1	0.08	1	-0.78	0.047142874
AT4G21590	-0.33	1	-0.03	1	-0.78	0.017952443
AT3G60290	-0.13	1	-0.04	1	-0.78	0.005477002
AT5G05060	-0.05	1	-0.57	0.04316275	-0.78	1.50E-05
AT3G19850	-0.37	1	-0.04	1	-0.79	0.00091356
AT1G29770	-0.77	0.671755966	-0.42	0.922048501	-0.79	0.038653603
AT4G32460	-0.18	1	0.06	1	-0.79	0.010801774
AT5G55450	-0.23	1	-0.27	1	-0.79	0.007802735
AT4G21870	-0.28	1	0.13	1	-0.80	5.85E-05
AT1G29720	-0.23	1	-0.19	1	-0.80	0.001519983
AT1G04800	-0.13	1	-0.13	1	-0.80	0.000872739
AT1G70985	-0.25	1	-0.16	1	-0.81	0.016252778
AT2G41990	-0.22	1	0.44	0.744853918	-0.81	0.015544852
AT1G72070	-0.18	1	-0.45	0.735485198	-0.82	0.006108394
AT3G48700	0.18	1	0.17	1	-0.82	0.018863476
AT5G44130	-0.12	1	0.14	1	-0.83	0.002931749
AT1G28660	-0.30	0.895441288	-0.31	0.479156662	-0.83	7.19E-09
AT2G39980	0.17	1	-0.11	1	-0.85	0.010858376
AT1G19050	-0.21	1	-0.33	0.984083782	-0.85	0.015985042
AT1G27045	-0.24	1	-0.03	1	-0.87	0.006388333
AT3G06145	0.02	1	0.18	1	-0.88	0.023375578
AT5G53210	0.02	1	0.27	0.941568151	-0.89	0.000224327
AT5G02760	-0.34	1	-0.33	0.997247496	-0.89	0.010870599
AT1G26600	-0.11	1	-0.08	1	-0.89	0.041573893
AT3G22840	0.60	0.224520278	0.38	0.656275162	-0.92	1.57E-05
AT2G42870	-0.06	1	0.07	1	-0.94	0.016120505
AT3G49160	0.15	1	0.27	0.9316272	-0.96	1.72E-05
AT1G18400	-0.21	1	-0.31	0.918907485	-0.97	0.000141208
AT2G22140	0.13	1	0.11	1	-0.97	0.020669357
AT3G51750	-0.16	1	-0.35	0.977424494	-0.98	0.007652556
AT2G31320	0.13	1	-1.71	1.11E-05	-0.99	0.009258082
AT1G10060	-0.27	1	-0.24	0.929310122	-1.00	2.03E-07
AT3G44990	-0.18	1	-0.23	1	-1.01	0.001905724
AT3G16670	-0.56	1	-0.69	0.638922215	-1.02	0.01776381
AT2G42170	-0.30	1	-0.21	1	-1.03	0.000283664
AT1G24260	0.16	1	-0.12	1	-1.03	0.006734794
AT2G23130	-0.39	1	-0.22	1	-1.04	2.88E-05
AT4G19430	-0.51	1	-0.35	0.965171114	-1.04	0.001050899
AT2G43140	-0.18	1	-0.13	1	-1.05	0.000164648
AT5G57530	0.48	1	0.14	1	-1.05	0.038150254
AT3G14210	-0.51	0.833207765	-0.91	0.004524404	-1.05	1.44E-05
AT1G21540	-0.47	1	-0.20	1	-1.07	5.02E-05
AT4G11460	-0.17	1	0.10	1	-1.10	0.002877729
AT2G43870	-0.03	1	-0.48	0.908980303	-1.10	0.007949787
AT2G11810	-0.01	1	-0.17	1	-1.13	0.03833592
AT4G14690	0.73	0.385730602	0.31	0.972276088	-1.13	0.000113699
AT1G13430	-0.26	1	-0.26	1	-1.16	0.017456385
AT2G44970	-0.04	1	-2.14	2.61E-15	-1.17	2.63E-05
AT3G22750	-0.16	1	-0.28	0.823100139	-1.17	9.43E-11
AT5G39190	-0.56	0.833207765	0.46	0.660127912	-1.17	1.75E-05
AT5G39160	-0.57	0.834319663	0.48	0.617514225	-1.17	2.85E-05
AT5G03860	-0.66	1	-0.47	0.933716682	-1.17	0.006419629
AT1G50040	-0.53	1	-0.45	1	-1.18	0.027383389
AT5G44575	-0.13	1	-0.63	0.889628664	-1.19	0.022140891
AT5G09970	-0.60	1	-0.22	1	-1.20	0.009055848
AT1G03010	-1.20	0.65824893	-0.55	0.972276088	-1.21	0.043008634

AT5G57770	-0.34	1	-0.37	0.972276088	-1.23	0.000342799
AT5G09570	-0.22	1	-0.05	1	-1.23	0.000826805
AT5G57760	-0.39	1	-0.35	0.994559775	-1.28	0.00023858
AT2G05540	-0.75	0.986087473	-0.26	1	-1.30	0.002054542
AT3G09450	-0.13	1	0.03	1	-1.30	0.011269386
AT5G39130	-0.58	0.986087473	0.29	1	-1.30	4.27E-05
AT2G34210	-0.14	1	-0.16	1	-1.31	0.006499861
AT3G06120	-0.36	1	-0.25	1	-1.31	0.000753366
AT5G54070	-0.66	1	-1.09	0.377737692	-1.35	0.016800971
AT4G28530	0.03	1	-0.80	0.789667241	-1.41	0.022007911
AT3G58070	-0.09	1	-0.13	1	-1.43	7.07E-05
AT5G67060	-0.85	0.932146044	-0.62	0.866556072	-1.45	0.002336535
AT5G13170	-0.38	1	0.52	0.967659854	-1.47	0.003370785
AT1G23110	-0.09	1	-0.33	1	-1.51	0.006302958
AT5G65080	-0.42	1	-2.13	0.041296033	-1.52	0.034096614
AT1G21320	-0.42	1	-0.26	1	-1.56	0.000538428
AT4G12470	-0.28	1	-0.40	1	-1.60	0.000684006
AT3G59900	-0.51	1	-0.36	1	-1.61	2.21E-05
AT2G45135	0.02	1	0.17	1	-1.62	0.000267557
AT2G41230	-0.20	1	-0.55	0.971942217	-1.63	0.002212227
AT2G40670	-0.37	1	-0.17	1	-1.63	3.76E-07
AT4G28850	-0.03	1	-0.03	1	-1.71	0.018702178
AT4G25750	-0.19	1	-0.07	1	-1.76	2.12E-11
AT2G36540	-0.60	1	-0.62	1	-1.82	0.027164874
AT5G05290	-0.25	1	-2.40	0.028233437	-1.85	0.012943726
AT5G08030	0.16	1	-0.27	1	-1.86	0.002668025
AT3G27940	0.07	1	-0.11	1	-1.93	0.023151586
AT2G41231	-0.46	1	-0.58	0.985559055	-1.96	0.00082343
AT5G46890	0.61	1	0.07	1	-1.99	0.000178618
AT5G46900	0.62	1	0.18	1	-2.00	0.000365106
AT5G50790	-0.89	1	-0.70	0.882077235	-2.03	0.000124406
AT2G29370	-0.36	1	0.42	0.958739684	-2.09	2.21E-05
AT1G04660	-0.34	1	-0.14	1	-2.20	0.005045871
AT3G62760	-0.25	1	-0.17	1	-2.29	1.45E-06
AT5G40320	0.15	1	-0.26	1	-2.40	0.035771011
AT5G41730	0.07	1	-0.63	1	-2.40	0.046354421
AT5G35770	-0.68	1	-0.77	1	-2.40	0.043910487
AT3G09922	-0.47	1	-0.44	1	-2.53	2.44E-05
AT1G20400	-0.26	1	-0.24	1	-2.58	0.000287295
AT3G46340	-0.77	1	-0.47	1	-2.64	0.046918304
AT4G36350	-0.53	1	-0.75	1	-2.64	0.044076828
AT5G15725	-0.96	1	-1.32	0.91138183	-2.89	0.042724559
AT5G55690	0.26	1	-0.58	1	-3.50	0.018143773
AT5G54190	-2.08	0.626487174	-0.67	1	-4.40	0.000293154
AT2G36190	0.34	1	-0.69	1	-4.66	0.04726036

Table S2. PANTHER Gene List Analysis (Thomas et al, 2022) to identify statistically overrepresented and underrepresented up-regulated biological process GO terms (applying Fisher's Exact test with Bonferroni correction) in *flic flac* mutant seedlings.

Analysis Type:	PANTHER Overrepresentation Test (Released 20231017)
Annotation Version and Release Date:	GO Ontology database DOI: 10.5281/zenodo.7942786 Released 2023-01-05
Analyzed List:	Client Text Box Input (Arabidopsis thaliana)
Reference List:	Arabidopsis thaliana (all genes in database)
Test Type:	FISHER
Correction:	BONFERRONI
Bonferroni count:	2976

GO biological process complete	***Arabidopsis thaliana* - REFLIST (27436)**	**Client Text Box Input (852)**	**Client Text Box Input (expected)**	**Client Text Box Input (over/ under)**	**Client Text Box Input (fold Enrichment)**	**Client Text Box Input (*P*-value)**
cellular response to iron ion starvation (GO:0010106)	8	6	0.25	+	24.15	5.33E-03
indole glucosinolate metabolic process (GO:0042343)	39	10	1.21	+	8.26	4.92E-03
cellular response to hypoxia (GO:0071456)	237	54	7.36	+	7.34	1.29E-23
cellular response to decreased oxygen levels (GO:0036294)	239	54	7.42	+	7.28	1.83E-23
cellular response to oxygen levels (GO:0071453)	240	54	7.45	+	7.25	2.18E-23
jasmonic acid metabolic process (GO:0009694)	49	11	1.52	+	7.23	4.60E-03
regulation of jasmonic acid mediated signaling pathway (GO:2000022)	45	10	1.4	+	7.16	1.49E-02
sulfur compound catabolic process (GO:0044273)	41	9	1.27	+	7.07	4.81E-02
long-chain fatty acid metabolic process (GO:0001676)	60	12	1.86	+	6.44	4.49E-03
response to hypoxia (GO:0001666)	341	59	10.59	+	5.57	1.30E-20
jasmonic acid mediated signaling pathway (GO:0009867)	146	25	4.53	+	5.51	2.09E-07
response to decreased oxygen levels (GO:0036293)	351	59	10.9	+	5.41	4.74E-20
response to oxygen levels (GO:0070482)	353	59	10.96	+	5.38	6.10E-20
cellular response to fatty acid (GO:0071398)	186	31	5.78	+	5.37	2.07E-09
cellular response to jasmonic acid stimulus (GO:0071395)	180	30	5.59	+	5.37	4.86E-09
response to jasmonic acid (GO:0009753)	673	105	20.9	+	5.02	2.47E-35
response to wounding (GO:0009611)	940	145	29.19	+	4.97	6.08E-50
response to fatty acid (GO:0070542)	706	106	21.92	+	4.83	2.24E-34
aromatic amino acid metabolic process (GO:0009072)	153	22	4.75	+	4.63	5.03E-05
systemic acquired resistance (GO:0009627)	119	17	3.7	+	4.6	2.27E-03
indole-containing compound metabolic process (GO:0042430)	189	26	5.87	+	4.43	5.94E-06

glycosyl compound biosynthetic process (GO:1901659)	117	16	3.63	+	4.4	7.96E-03
cellular response to salicylic acid stimulus (GO:0071446)	125	17	3.88	+	4.38	4.18E-03
S-glycoside metabolic process (GO:0016143)	275	37	8.54	+	4.33	4.24E-09
glucosinolate metabolic process (GO:0019760)	275	37	8.54	+	4.33	4.24E-09
glycosinolate metabolic process (GO:0019757)	275	37	8.54	+	4.33	4.24E-09
regulation of cellular ketone metabolic process (GO:0010565)	149	20	4.63	+	4.32	6.10E-04
response to oxidative stress (GO:0006979)	740	99	22.98	+	4.31	3.37E-28
indole-containing compound biosynthetic process (GO:0042435)	120	16	3.73	+	4.29	1.07E-02
glycosyl compound metabolic process (GO:1901657)	316	42	9.81	+	4.28	1.87E-10
response to salicylic acid (GO:0009751)	417	55	12.95	+	4.25	3.03E-14
response to molecule of bacterial origin (GO:0002237)	160	21	4.97	+	4.23	4.28E-04
response to nutrient levels (GO:0031667)	280	36	8.7	+	4.14	2.77E-08
cellular response to nutrient levels (GO:0031669)	203	23	6.3	+	3.65	1.21E-03
response to extracellular stimulus (GO:0009991)	342	38	10.62	+	3.58	3.63E-07
regulation of small molecule metabolic process (GO:0062012)	208	23	6.46	+	3.56	1.78E-03
response to fungus (GO:0009620)	1183	124	36.74	+	3.38	7.61E-27
regulation of defense response (GO:0031347)	883	92	27.42	+	3.36	6.81E-19
secondary metabolite biosynthetic process (GO:0044550)	368	38	11.43	+	3.33	2.43E-06
amine metabolic process (GO:0009308)	233	23	7.24	+	3.18	1.05E-02
regulation of response to stress (GO:0080134)	1016	100	31.55	+	3.17	4.05E-19
defense response to fungus (GO:0050832)	927	90	28.79	+	3.13	1.48E-16
cellular response to extracellular stimulus (GO:0031668)	259	25	8.04	+	3.11	5.78E-03
secondary metabolic process (GO:0019748)	788	76	24.47	+	3.11	2.02E-13
response to starvation (GO:0042594)	222	21	6.89	+	3.05	4.96E-02
response to organic cyclic compound (GO:0014070)	963	91	29.91	+	3.04	4.62E-16
cellular response to external stimulus (GO:0071496)	265	25	8.23	+	3.04	8.42E-03
defense response to bacterium (GO:0042742)	1102	103	34.22	+	3.01	3.03E-18
alpha-amino acid metabolic process (GO:1901605)	409	38	12.7	+	2.99	3.45E-05
response to salt stress (GO:0009651)	711	66	22.08	+	2.99	1.29E-10
response to osmotic stress (GO:0006970)	1056	96	32.79	+	2.93	4.81E-16
cellular response to organic cyclic compound (GO:0071407)	297	27	9.22	+	2.93	6.52E-03
response to bacterium (GO:0009617)	1399	126	43.44	+	2.9	9.73E-22

amino acid metabolic process (GO:0006520)	604	54	18.76	+	2.88	1.06E-07
sulfur compound biosynthetic process (GO:0044272)	291	26	9.04	+	2.88	1.34E-02
sulfur compound metabolic process (GO:0006790)	642	57	19.94	+	2.86	3.81E-08
response to external biotic stimulus (GO:0043207)	2673	233	83.01	+	2.81	8.82E-43
response to other organism (GO:0051707)	2673	233	83.01	+	2.81	8.82E-43
response to biotic stimulus (GO:0009607)	2676	233	83.1	+	2.8	1.05E-42
biological process involved in interspecies interaction between organisms (GO:0044419)	2687	233	83.44	+	2.79	2.01E-42
cellular response to stress (GO:0033554)	1213	105	37.67	+	2.79	2.19E-16
response to water deprivation (GO:0009414)	1249	108	38.79	+	2.78	6.55E-17
response to external stimulus (GO:0009605)	3195	273	99.22	+	2.75	2.06E-50
response to water (GO:0009415)	1361	116	42.26	+	2.74	6.14E-18
response to acid chemical (GO:0001101)	1394	118	43.29	+	2.73	4.42E-18
regulation of response to stimulus (GO:0048583)	1475	123	45.8	+	2.69	2.16E-18
response to salt (GO:1902074)	1469	121	45.62	+	2.65	1.07E-17
defense response to other organism (GO:0098542)	2295	189	71.27	+	2.65	3.65E-30
response to cold (GO:0009409)	651	53	20.22	+	2.62	4.58E-06
cellular response to chemical stimulus (GO:0070887)	2126	173	66.02	+	2.62	1.80E-26
defense response (GO:0006952)	2615	212	81.21	+	2.61	1.05E-33
response to lipid (GO:0033993)	2753	223	85.49	+	2.61	8.20E-36
response to alcohol (GO:0097305)	1324	107	41.12	+	2.6	1.39E-14
response to abscisic acid (GO:0009737)	1181	95	36.67	+	2.59	1.75E-12
response to inorganic substance (GO:0010035)	2246	178	69.75	+	2.55	3.72E-26
response to hormone (GO:0009725)	2717	210	84.37	+	2.49	1.60E-30
response to endogenous stimulus (GO:0009719)	2748	212	85.34	+	2.48	8.76E-31
response to oxygen-containing compound (GO:1901700)	3432	260	106.58	+	2.44	3.12E-38
cellular response to hormone stimulus (GO:0032870)	1123	84	34.87	+	2.41	4.04E-09
cellular response to oxygen-containing compound (GO:1901701)	1257	94	39.03	+	2.41	1.25E-10
hormone-mediated signaling pathway (GO:0009755)	861	64	26.74	+	2.39	2.52E-06
cellular response to endogenous stimulus (GO:0071495)	1157	86	35.93	+	2.39	2.41E-09
response to stress (GO:0006950)	5749	427	178.53	+	2.39	1.45E-72
cellular response to lipid (GO:0071396)	836	62	25.96	+	2.39	5.18E-06
cellular response to organic substance (GO:0071310)	1646	117	51.12	+	2.29	2.62E-12
response to chemical (GO:0042221)	5308	369	164.84	+	2.24	1.31E-51
response to organic substance (GO:0010033)	4560	315	141.61	+	2.22	5.86E-41

oxoacid metabolic process (GO:0043436)	2053	138	63.75	+	2.16	2.81E-13
carboxylic acid metabolic process (GO:0019752)	1559	104	48.41	+	2.15	4.15E-09
organic acid metabolic process (GO:0006082)	2173	144	67.48	+	2.13	1.28E-13
cellular catabolic process (GO:0044248)	1081	67	33.57	+	2	9.96E-04
regulation of DNA-templated transcription (GO:0006355)	2445	151	75.93	+	1.99	8.24E-12
regulation of RNA biosynthetic process (GO:2001141)	2453	151	76.18	+	1.98	9.22E-12
cellular response to stimulus (GO:0051716)	3848	236	119.5	+	1.97	6.87E-21
regulation of macromolecule biosynthetic process (GO:0010556)	2675	160	83.07	+	1.93	1.07E-11
carbohydrate derivative metabolic process (GO:1901135)	1004	60	31.18	+	1.92	1.09E-02
response to temperature stimulus (GO:0009266)	1309	78	40.65	+	1.92	3.52E-04
regulation of biosynthetic process (GO:0009889)	3061	181	95.06	+	1.9	2.89E-13
positive regulation of cellular process (GO:0048522)	1038	61	32.23	+	1.89	1.55E-02
regulation of cellular biosynthetic process (GO:0031326)	2901	170	90.09	+	1.89	6.73E-12
regulation of RNA metabolic process (GO:0051252)	2717	157	84.37	+	1.86	3.86E-10
cell communication (GO:0007154)	2519	144	78.23	+	1.84	1.21E-08
response to abiotic stimulus (GO:0009628)	4732	268	146.95	+	1.82	1.18E-19
response to stimulus (GO:0050896)	9743	549	302.56	+	1.81	4.31E-60
small molecule metabolic process (GO:0044281)	3094	171	96.08	+	1.78	1.10E-09
signal transduction (GO:0007165)	2224	120	69.06	+	1.74	2.94E-05
regulation of nucleobase-containing compound metabolic process (GO:0019219)	3053	164	94.81	+	1.73	3.02E-08
signaling (GO:0023052)	2294	120	71.24	+	1.68	1.42E-04
regulation of cellular metabolic process (GO:0031323)	3679	191	114.25	+	1.67	5.65E-09
positive regulation of biological process (GO:0048518)	1611	83	50.03	+	1.66	3.94E-02
regulation of primary metabolic process (GO:0080090)	3784	185	117.51	+	1.57	2.28E-06
regulation of nitrogen compound metabolic process (GO:0051171)	3666	178	113.84	+	1.56	9.20E-06
regulation of gene expression (GO:0010468)	3823	180	118.72	+	1.52	5.74E-05
regulation of cellular process (GO:0050794)	6159	289	191.26	+	1.51	1.71E-10
regulation of metabolic process (GO:0019222)	4999	233	155.24	+	1.5	3.55E-07
regulation of macromolecule metabolic process (GO:0060255)	4279	194	132.88	+	1.46	2.41E-04
regulation of biological process (GO:0050789)	8236	357	255.76	+	1.4	1.51E-09
biological regulation (GO:0065007)	8659	366	268.9	+	1.36	2.05E-08
cellular process (GO:0009987)	15242	569	473.33	+	1.2	1.46E-07

nucleobase-containing compound metabolic process (GO:0006139)	3651	71	113.38	-	0.63	2.71E-02
nucleic acid metabolic process (GO:0090304)	3267	60	101.45	-	0.59	1.56E-02
Unclassified (UNCLASSIFIED)	1134	19	35.22	-	0.54	0.00E+00
RNA metabolic process (GO:0016070)	2812	46	87.32	-	0.53	2.41E-03
gene expression (GO:0010467)	1499	13	46.55	-	0.28	3.08E-05

Table S3. PANTHER Gene List Analysis (Thomas et al, 2022) to identify statistically overrepresented and underrepresented down-regulated biological process GO terms (applying Fisher's Exact test with Bonferroni correction) in *flic flac* mutant seedlings.

Analysis Type:	PANTHER Overrepresentation Test (Released 20231017)
Annotation Version and Release Date:	GO Ontology database DOI: 10.5281/zenodo.7942786 Released 2023-01-05
Analyzed List:	Client Text Box Input (Arabidopsis thaliana)
Reference List:	Arabidopsis thaliana (all genes in database)
Test Type:	FISHER
Correction:	BONFERRONI
Bonferroni count:	2976

GO biological process complete	***Arabidopsis thaliana* - REFLIST (27436)**	**Client Text Box Input (852)**	**Client Text Box Input (expected)**	**Client Text Box Input (over/ under)**	**Client Text Box Input (fold Enrichment)**	**Client Text Box Input (*P*-value)**
positive regulation of organ growth (GO:0046622)	6	3	0.03	+	> 100	1.98E-02
Unclassified (UNCLASSIFIED)	1134	7	4.96	+	1.41	0.00E+00

Table S4. DEGs with logfc > 0.7 and $P < 0.05$ in *flac* and *flic flac* mutants related to flowering time regulation according to the Flowering Interactive Database (FLOR-ID) (Bouché et al, 2016). Additionally, CIL1 has been manually curated (Liu et al, 2013, 2018). The effect of overexpression (OE) and/or mutation of these genes on flowering is shown (Lee et al, 2000; Ratcliffe et al, 2003; Liu et al, 2007; Castillejo & Pelaz, 2008; Mathieu et al, 2009; Kim & Sung, 2010; Gillmor et al, 2014; Gomez et al, 2020; Yan et al, 2020; Nasim et al, 2022). ns, not significantly de-regulated.

AGI locus	Primary Gene Symbol	logfc (*flac*)	logfc (*flic flac*)	Effect on flowering	Reference
AT1G68920	CIL1	1.67	1.76	OE promotes	Liu et al, 2013, 2018
AT1G68050	FKF1	ns	1.09	OE promotes	Yan et al, 2020
AT1G57820	VIM1	ns	0.98	OE represses	Liu et al, 2007
AT2G45660	AGL20	ns	0.94	OE promotes	Lee et al, 2000
AT1G66350	RGL1	ns	0.94	mutation represses	Gomez et al, 2020
AT3G54990	SMZ	ns	0.90	OE represses	Mathieu et al, 2009
AT1G25560	TEM1	ns	0.86	OE represses	Castillejo & Pelaz, 2008
AT1G68840	RAV2	< 0.7	0.85	OE represses	Castillejo & Pelaz, 2008
AT1G55325	GCT	ns	0.82	mutation represses	Gillmor et al, 2014
AT1G61040	VIP5	ns	0.71	mutation promotes	Nasim et al, 2022
AT5G65080	MAF5	-2.13	-1.52	mutation no effect/ OE represses	Ratcliffe et al, 2003; Kim & Sung, 2010

Table S5. List of oligonucleotides used in this study.

Purpose	Name	Sequence	Line
CRISPR	ZmTI3 CRISPR129 fw	TGTTGCGGAAAACACCCACGGTAG	Zm*flac-c1*
CRISPR	ZmTI3 CRISPR129 rv	AAACCTACCGTGGGTGTTTTCCGC	Zm*flac-c1*
Genotyping	ZmTI3 CR 69/129 fw	GCGCATGTACTTGTTTCCCTC	Zm*flac-c1*
Genotyping	ZmTI3 CR 69/129 rv	GTTCTTCGAGTCATTGGCTTCC	Zm*flac-c1*

Eidesstattliche Versicherung/Declaration On Oath

Hiermit erkläre ich an Eides statt, dass ich die vorliegende Dissertationsschrift selbst verfasst und keine anderen als die angegebenen Quellen und Hilfsmittel benutzt habe.

I hereby declare, on oath, that I have written the present dissertation by my own and have not used other than the acknowledged resources and aids.

Hamburg, den 21.11.2023 Unterschrift .....  .....

Confirmation of correct English

Hamburg, 21/11/2023

To whom it may concern,

I am writing to confirm that the thesis submitted by Lucas Lang has been written in correct English throughout its entire text.

Kind regards,

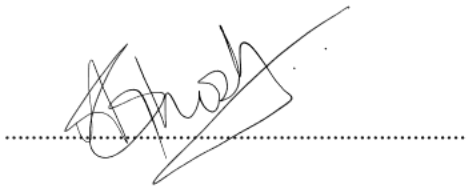

Ankit Ghosh

PhD student
Developmental Biology
Institute of Plant Science and Microbiology
University of Hamburg